Modelisation Intermediaire entre Equations Cinetiques et Limites hydrodynamiques : Derivation, Analyse et Simulations

Martin Parisot

N° ORDRE : 40591

École Doctorale Science Pour l'Ingénieur Lille Nord-de-France
Université Lille 1 Science et Technologie

Modélisation Intermédiaire entre Équations Cinétiques et Limites Hydrodynamiques : Dérivation, Analyse et Simulations

THÈSE

présentée et soutenue publiquement le 23 septembre 2011
pour l'obtention du

Doctorat de l'Université Lille 1

Spécialité Mathématiques appliquées

par

Martin Parisot

Composition du jury

Rapporteurs :	Nicolas Crouseilles,	Chargé de recherche, Irma, Strasbourg.
	Phillipe Villedieu,	Maître de recherche, Onera, Toulouse.
Directeurs :	Jean-François Clouët,	Directeur de recherche, Cea/Dam, Bruyères-le-Châtel.
	Thierry Goudon,	Directeur de recherche, Inria, Lille Nord-Europe.
Examinateurs :	Claire Chainais,	Professeur, Laboratoire P. Painlevé, Université Lille 1.
	Bruno Després,	Professeur, Laboratorie J.-L. Lions, Université Paris 6.
	Guy Schurtz,	Ingénieur-chercheur, CEA/CELIA, Bordeaux.

Équipe Simpaf (Inria Lille Nord-Europe) Laboratoire Paul Painlevé

Modélisation Intermédiaire entre Équations Cinétiques et Limites Hydrodynamiques: Dérivation, Analyse et Simulations

Résumé :

Ce travail est consacré à l'étude d'un problème issu de la physique des plasmas : le transfert thermique des électrons dans un plasma proche de l'équilibre Maxwellien.

Dans un premier temps, une étude dimensionnelle du système de Vlasov-Fokker-Planck-Maxwell est réalisée, permettant d'une part d'exhiber un paramètre de mise à l'échelle physiquement pertinent et d'autre part de définir mathématiquement les contours du cadre d'étude. Le régime asymptotique dit de Spitzer-Härm est étudié pour une classe d'opérateurs de collisions relativement générale. La suite de ce travail est consacrée à la dérivation et à l'étude de la limite hydrodynamique du système de Vlasov-Landau-Maxwell hors du cadre strictement asymptotique. Un modèle proposé par Schurtz et Nicolaï est alors situé dans ce contexte et analysé. La particularité de ce modèle réside dans l'application d'un opérateur de délocalisation sur le flux de chaleur. Le lien avec les modèles non-locaux de Luciani et Mora est établi, ainsi que des propriétés mathématiques comme le principe du maximum et la dissipation d'entropie.

Ensuite, une dérivation formelle à partir des équations de Vlasov, avec un opérateur de collisions simplifié, est proposée. La dérivation, inspirée par les récents travaux de D. Levermore, fait intervenir des méthodes de décomposition suivant les harmoniques sphériques et des méthodes de fermeture dite de diffusion. Une hiérarchie de modèles intermédiaires entre les équations cinétiques et la limite hydrodynamique est ainsi décrite. Notamment, un nouveau système hydrodynamique, de nature intégro-différentielle, est proposé. Le système de Schurtz et Nicolaï apparaît comme une simplification du système issu de la dérivation, si l'on suppose un flux de chaleur stationnaire. Les résultats précédents sont alors généralisés pour tenir compte de la dépendance en énergie interne qui apparaît naturellement au cours de la mise en équations. L'existence et l'unicité de la solution du système non stationnaire sont également établies dans un cadre simplifié.

La dernière partie est consacrée à la mise en œuvre d'un schéma numérique spécifique pour résoudre ces modèles. On propose une approche par volumes finis pouvant être efficace sur des maillages non-structurés. L'originalité du schéma réside dans la discrétisation de l'inconnue numérique comme valeur moyenne du flux de chaleur sur les faces des volumes de contrôle. La précision de ce schéma permet de capturer des effets spécifiques de nature cinétique, qui ne peuvent être reproduits par le modèle asymptotique de Spitzer–Härm, par exemple les effets de flux dit "d'anti-diffusion". La consistance de ce schéma avec celui de l'équation de Spitzer–Härm est mise en évidence ouvrant la voie à des stratégies de couplage entre les deux modélisations.

Mots-clé : Physique des plasmas, Équations cinétiques, Limite hydrodynamique, Régime de Spitzer-Härm, Modèles non-locaux, Schémas volumes finis, Maillages non structurés.

AMS Subject classification : 35B25, 35Q99, 65M08, 76M12, 76X05, 82C70, 82D10.

Intermediate Modeling between Kinetic Equations and Hydrodynamic Limits: Derivation, Analysis and Simulations

Abstract:

This work is dedicated study of a problem resulting from plasma physics: the thermal transfer of electrons in a plasma close to equilibrium Maxwellian.

Firstly, a dimensional study of the Vlasov-Fokker-Planck-Maxwell system is performed, allowing one hand to identify a physically relevant parameter of scale and also to define mathematically the contours of validity domain. The asymptotic regime called Spitzer-Harm is studied for a relatively general class of collision operator. The following part of this work is devoted to the derivation and study of the hydrodynamic limit of the system of Vlasov-Maxwell-Landau outside the strictly asymptotic. A model proposed by Schurtz and Nicolaï is located in this context and analyzed. The particularity of this model lies in the application of a delocalization operatior in the heat flux. The link with non-local models of Luciani and Mora is established, as well as mathematics properties as the principle of maximum and entropy dissipation.

Then, a formal derivation from the Vlasov equations, with a simplified collision operator, is proposed. The derivation, inspired by the recent work of D. Levermore, involves decomposition methods according to the spherical harmonics and methods of closing called diffusion methods. A hierarchy of intermediate models between the kinetic equations and the hydrodynamic limit is described. In particular, a new hydrodynamic system, integro-differential by nature, is proposed. The Schurtz and Nicolaï model appears as a simplification of the system resulting from the derivation, assuming a steady flow of heat. The above results are then generalized to account for the internal energy dependence which appears naturally in the equation establishment. The existence and uniqueness of the solution of the nonstationary system are established in a simplified framework.

The last part is devoted was the implementation of a specific numerical scheme to solve these models. We propose a finite volume approach can be effective on unstructured grids. The originality of the scheme lies in the discretization of the unknown as a digital average value of heat flux on faces of control volumes. The precision of this scheme to capture the specific effects, kinetic by nature, that can not be reproduced by the asymptotic Spitzer-Härm model, as for example the effects called "anti-diffusion" heat flux. The consistency of this pattern with that of Spitzer-Härm equation is highlighted, paving the way for a strategy of coupling the two models.

Key-words: Plasma physics, Kinetic equations, Hydrodynamic limit, Spitzer-Härm Regime, Non-local models, Finite volume scheme, Unstructured grids.

AMS Subject classification: 35B25, 35Q99, 65M08, 76M12, 76X05, 82C70, 82D10.

Remerciements

Je souhaite remercier tout particulièrement Thierry Goudon pour m'avoir guidé le long de ces trois années de thèse. J'ai bénéficié en plus de son expérience scientifique d'une grande attention morale. J'ai apprécié la façon dont il a dirigé mes recherches en apportant ses conseils tout en me laissant la liberté dans l'orientation de mes travaux. Je tiens à le remercier encore pour sa patience et sa volonté devant mes explications parfois obscures. Enfin je souhaiterai le remercier pour m'avoir encouragé à participer au Cemracs 2010 qui a été pour moi un été de recherche mais aussi de rencontres avec autant de personnes de grandes qualités scientifiques et sociales.

Toute ma gratitude se porte également à Jean-François Clouët, qui m'a acceuilli au sein de son équipe au Cea. Ses conseils et son expérience des plasmas ont été indispensables à la compréhension des phénomènes physiques modélisés, pour moi qui n'avait jamais travaillé sur de tels sujets.

Je remercie Nicolas Crouseilles et Phillipe Villedieu pour le temps qu'ils ont pris à rapporter ma thèse ainsi que pour les remarques qui ont permis l'amélioration de mon manuscript. L'ensemble du jury reçoit également les mêmes remerciements pour avoir témoigné de leur intérêt à mes travaux : Claire Chainais, Bruno Després et Guy Schurtz.

Au cours de ces années de recherche, j'ai été intégré à deux laboratoires distincts : à l'Inria Lille et au Cea de Bruyère-le-Châtel. Je suis reconnaissant aux administrations respectives de m'avoir permis de gérer mon temps entre ces deux laboratoires.

Je tiens à remercier tous ceux qui m'ont apporté leurs conseils, en particulier Caterina Calgaro, Jean-François Coulombel, Emmanuel Creusé et Dominique Deck sans qui je ne serai jamais parvenu à maîtriser les outils, à la fois d'analyse et numérique, qui ont été nécessaires à cette thèse.

Je remercie toute l'équipe Simpaf ainsi que tous ceux qui ont fait partie de mon quotidient : Antoine, Guillaume (je me suis senti obligé), Mathias, Ingrid, Sebastian et Stella pour avoir partagé quelques moments de détente ; Anne et Bénédicte pour avoir largement participé à l'ambiance, voir l'agitation du bureau ; Leon (fréro) et Chang pour l'entre aide que nous avons alimenté pour répondre à toutes nos questions ; Alexis, Benoit et Eric pour m'avoir montré la marche à suivre ; Aliu, Manuel et Yohan pour les discussions parfois difficiles à arrêter ; Damien et Laurent pour m'avoir guidé et accepté dans le couloir des doctorants du Cea; Benjamin, Thomas, Stéphane et Lucille pour les verres que nous avons pris ensemble.

Je n'oublie pas tous les participants du Cemracs de l'été 2010 en commençant bien entendu par Claudia Negulescu, Fabrice Deluzet et Jacek Narski qui m'ont accepté et guidé dans leur sujet de recherche. Je salue également Dario Maldarella qui participait au même titre que moi à cette aventure.

Je remercie au passage mes compagnons de foot, de coinche et de vadrouilles dans les calanques, bien entendu Li-Ma, Romain, Rémi, Jérémie, Aubin, George, Thomas, Frédérique et Marc. J'attends avec impatience notre prochaine rencontre.

Enfin je remercie également toute ma famille et mes amis pour les relectures et le support affectif qu'ils m'ont témoignés. À mes parents pour s'être intéressés à un sujet

qui ne les intéressait pas. À mes frères pour m'avoir questionné sur mes motivations et donc permis de les comprendre. Leurs participations à ma thèse est d'une autre nature mais je suis persuadé que mes travaux ne seraient pas les mêmes sans leur présence, malgrè l'éloignement.

Mes derniers remerciements sont pour Lise qui m'a particulièrement soutenu en étant pour moi un abri aux doutes et un échappatoire au monde scientifique grâce aux merveilleux week end qu'elle organisait pour nous.

Je ne sais pas où je vais, oh ça je l'ai jamais bien su.
Mais si jamais je le savais, je crois bien que je n'irai plus.
- La rue Kétanou -

Table des matières

Chapitre I :

Introduction générale

Ce travail est consacré à l'établissement d'une description macroscopique d'un plasma lorsque les effets collectifs de collisions sont prépondérants.

Un plasma est un gaz constitué de particules chargées, les électrons et les ions, placées dans des conditions telles que les forces d'interactions binaires, liant les électrons aux ions dans une structure atomique, deviennent négligeables devant les forces électromagnétiques de longue portée. Ces conditions peuvent être obtenues par deux stratégies.

La première consiste à augmenter la température du milieu. De la même manière qu'un solide passe à l'état liquide et qu'un liquide passe à l'état gazeux lorsque leurs températures augmentent, un gaz passe à l'état de plasma pour une température suffisamment élevée. Pour cette raison, le plasma est parfois désigné comme le quatrième état de la matière. On notera toutefois la différence avec les autres changements d'état qui se font à température et densité constantes, jusqu'à avoir reçu l'énergie nécessaire dite chaleur latente. Le passage de gaz à plasma est quand à lui progressif et un plasma peut n'être que partiellement ionisé. Au-dessus d'une température de 100 000 K, toute matière, quelque soit sa composition, est ionisée et on obtient alors un plasma. Le cœur des étoiles est ionisé à cause de l'importante température qui y règne (de l'ordre du million de kelvins).

La seconde stratégie consiste à provoquer la ionisation de la matière à très faible densité, grâce à des collisions ou grâce à un intense champ électromagnétique. Les plasmas en haute atmosphère (ionosphère) sont dûs à la faible présence de particules à partir de 60 km d'altitude. La plupart des plasmas produits en laboratoire sont créés suivant cette stratégie.

Bien que la matière existe en majorité sous l'état de plasma dans l'univers, la découverte des plasmas et de leurs applications est très récente. Le terme de plasma est utilisé pour la première fois par le physicien Irving Langmuir en 1928 pour décrire l'analogie entre un écoulement de gaz ionisé et le plasma sanguin. L'étude des plasmas permet notamment de comprendre plus en détail des phénomènes physiques courants, comme la foudre ou les perturbations des télécommunications dans l'ionosphère. Les applications sont aujourd'hui diverses et présentes dans la vie quotidienne comme par exemple les tubes néons ou la soudure par arc électrique.

Cependant l'application majeure de la physique des plasmas reste la fusion thermonucléaire contrôlée qui a pour but de produire une énergie propre et pratiquement inépuisable. La fusion est un processus où deux noyaux atomiques, aussi appelés ions, s'assemblent pour en former un autre, plus lourd. Cette application cherche à reproduire les conditions présentes dans le coeur des étoiles, où les particules composant la matière à l'état de plasma atteignent des vitesses leur permettant de vaincre les forces de répulsion électrique et de fusionner. Il s'ensuit un dégagement d'énergie suivant la relation bien connue d'Einstein ($E = mc^2$), dû à la différence de masse entre les réactifs et les produits de la réaction de fusion.

Parmis les réactions de fusion ayant lieu au sein des étoiles, la plus simple à reproduire, parce qu'elle met en jeu des espèces de faible masse, est la fusion du Deutérium avec le Tritium. L'essentiel de la recherche se porte donc sur cette réaction. Le Deutérium (composé d'un proton et d'un neutron) et le Tritium (composé d'un proton et de deux neutrons) sont deux isotopes de l'Hydrogène (composé d'un proton). Le Tritium est un élément radioactif, d'une durée de demi-vie d'environ douze ans. Il émet un rayonnement bêta ($\beta-$) qui est simplement arrêté par le plastique ou le verre. Il peut être produit par surrégénération du Lithium, présent à l'état naturel dans la croûte terrestre. Le Deutérium, non-radioactif, est présent dans les océans sous forme d'eau lourde. La proportion d'eau lourde dans l'eau naturelle est de 0.03 %. Cependant 70 % de la surface de la terre est recouverte d'eau. L'enrichissement de l'eau en eau lourde pour obtenir du Deutérium se fait généralement par électrolyse.

Ces éléments sont uniformément répartis sur la Terre et en quantité pratiquement illimitée. Le produit de la réaction de fusion, l'Hélium, est le deuxième élément le plus présent dans l'Univers. C'est un gaz rare et par conséquent il est particulièrement stable. La réaction de fusion thermonucléaire met ainsi en jeu des éléments moins dangereux pour l'homme que la réaction de fission actuellement utilisée dans les centrales, qui produit des déchets radioactifs de demi-vie nettement plus longue. De plus elle produit trois à quatre fois plus d'énergie, pour la même masse de réactif, que la fission nucléaire. Pour illustrer son potentiel énergétique, on estime qu'un litre d'eau serait équivalent sur ce plan à 300 litres de pétrole, une fois la réaction de fusion maîtrisée. De plus, à cause des conditions très strictes nécessaires à la réalisation de la fusion, il n'y a pas de risque d'emballement, c'est-à-dire de réaction en chaîne, possible.

Pour que deux noyaux puissent fusionner, il faut qu'ils se trouvent très proches l'un de l'autre afin que leur collision soit possible. Cependant la force électromagnétique, ou force de Lorentz, induite par leur charge, tend à les éloigner. Pour qu'une réaction nucléaire ait lieu, il faut, par principe d'inertie liée à la masse des particules, que leurs énergies cinétiques soit suffisantes pour vaincre les forces de répulsion.

Il faut donc pouvoir apporter de l'énergie aux particules tout en les empêchant de s'éloigner. On parle alors de confinement du plasma. Pour se faire, deux approches ont été imaginées. La première et la plus connue consiste à forcer les particules à suivre une trajectoire fermée sur elle–même à l'aide d'un champ magnétique très intense. On apporte ensuite suffisamment d'énergie pour mettre le plasma dans les conditions nécessaires aux réactions de fusion thermonucléaire. Cette méthode dite de confinement magnétique est réalisable dans des structures particulières notamment les tokamaks. Elle présente certains avantages. Par exemple la grande quantité de matière fusible mise en jeu permet de réaliser des réactions auto-entretenues. Cependant de nombreux points

sont encore à l'étude. En particulier, la simulation de la dynamique d'un plasma soumis à un fort champ magnétique n'est pas complètement maîtrisée.

La seconde approche consiste à produire une boule de mélange fusible, appelée cible, parfaitement sphérique puis à la comprimer en tirant sur elle un laser très puissant uniformément réparti sur toute sa surface. La matière ainsi condensée atteint la densité et la température nécessaires aux réactions de fusion thermonucléaire. Cette méthode dite de confinement inertiel présente certains avantages, par exemple les infrastructures nécessaires à sa mise en œuvre sont modulaires et moins volumineuses. Ainsi il est plus facile de les faire évoluer au fur et à mesure des nouvelles découvertes scientifiques. De plus, la faible quantité de mélange fusible présent dans la chambre de combustion rend le dispositif plus sûr et plus facile à décontaminer.

Il est donc important, pour reproduire les conditions nécessaires à la fusion thermonucléaire de mettre en place des modèles tenant compte à la fois du transport, des collisions et de la force de Lorentz. Trois échelles de modélisation sont alors décrites, suivant les lois de la physique classique.

La première échelle, dite particulaire, cherche à décrire la position de chaque particule du plasma. Les équations régissant le mouvement des particules sont alors données par le principe fondamental de la dynamique ou loi de Newton

$$\partial_t x_p = v_p, \qquad m_p \partial_t v_p = R\left(t, x_p, v_p\right)$$

où $t \geq 0$ représente le temps, m_p la masse de la particule, $x_p \in \mathbb{R}^3$ la position et $v_p \in \mathbb{R}^3$ la vitesse de la particule. La résultante des forces R est la combinaison des éventuelles forces extérieures avec la force de Lorentz F, données par

$$F(t, x_p, v_p) = \frac{q_p}{m_p}\left(E\left(t, x_p\right) + v_p \wedge B\left(t, x_p\right)\right),$$

où q_p représente la charge de la particule. Le champ électrique autoconsistant $E\left(t, x\right)$ et le champ magnétique autoconsistant $B\left(t, x\right)$ sont les solutions des équations de Maxwell

$$\begin{cases} \partial_t E - c^2 \nabla_x \times B = -\dfrac{J}{\varepsilon_0}, \\ \partial_t B + \nabla_x E = 0, \\ \nabla_x \cdot E = \dfrac{\rho}{\varepsilon_0}, \qquad \nabla_x \cdot B = 0. \end{cases}$$

Dans ces équations, c désigne la vitesse de la lumière dans le vide, ε_0 la permittivité diélectrique du vide, $\rho\left(t, x\right)$ et $J\left(t, x\right)$ sont les variables hydrodynamiques représentant respectivement la densité de charge et le courant de l'ensemble des particules chargées du plasma. Cette modélisation des plasmas ne permet pas des simulations pour des applications industrielles, telles que les réacteurs thermonucléaires. En effet le nombre de particules mises en jeu (de l'ordre de 10^{20} particules) dépasse largement les moyens de simulation actuellement disponibles.

La seconde échelle, dite microscopique, traduit un écoulement global de particules. La population de chaque espèce, p, est représentée par sa fonction de distribution, f_p. L'évolution statistique au cours du temps de la fonction de distribution dérive de l'échelle

particulaire sous certaines hypothèses, en particulier le nombre de particules doit être suffisamment élevé. Elle est alors traduite par l'équation cinétique de Vlasov

$$C\left(f_p\right) = \frac{\mathrm{d}}{\mathrm{d}t} f_p = \partial_t f_p + v \cdot \nabla_x f_p + F \cdot \nabla_v f_p,$$

où $C\left(f_p\right)$ modélise les collisions entre les particules p avec l'ensemble des particules présentes dans le plasma. Plusieurs opérateurs de collision sont décrits dans la littérature, notamment les opérateurs de collision de Boltzmann, de Landau, de Fokker-Planck ou de Bhatnagar-Gross-Krook (BGK). Ces opérateurs sont de nature différente, intégro-différentielle, différentielle ou de relaxation, mais possèdent certaines propriétés essentielles en commun. Boltzmann montre en 1872, qu'il existe une fonction évoluant de façon monotone au cours du temps, lorsqu'un gaz relaxe vers un état d'équilibre. L'existence de cette fonction, appelée entropie, est une importante propriété nécessaire à la description des collisions entre particules. De plus, ces opérateurs conservent globalement certains moments de la fonction de distribution. Pour l'ensemble des particules, on a

$$\sum_p \int_{\mathbb{R}^3} \begin{pmatrix} 1 \\ v \\ |v|^2 \end{pmatrix} C\left(f_p\right) \mathrm{d}v = 0.$$

Plus spécifiquement, il est classique de supposer que la masse et l'énergie sont conservées par l'opérateur de collision pour chaque espèce, pour f_p suffisamment régulier,

$$\int_{\mathbb{R}^3} \begin{pmatrix} 1 \\ |v|^2 \end{pmatrix} C\left(f_p\right) \mathrm{d}v = 0.$$

La quantité de mouvement peut être transmise d'une espèce à l'autre au cours des collisions. Remarquons que la conservation de la masse implique que les réactions thermonucléaires ne sont pas prises en compte par l'équation de Vlasov. L'étude est ainsi limitée aux plasmas d'inition, c'est-à-dire avant les réactions thermonucléaires. Cependant cette étape est indispensable pour comprendre les mécanismes nécessaires à l'initialisation des réactions nucléaires. Cette modélisation est largement utilisée pour l'étude des plasmas de fusion [12], dans un cadre théorique. Cependant, elle ne permet que des simulations limitées à un temps court et pour des configurations spatiales simples (en une ou deux dimensions sans géométrie complexe). En effet, à cause de la nature hyperbolique de l'équation, sa résolution numérique est soumise à une contrainte sur le pas de temps (CFL) très restrictive, de la forme

$$h_t < \frac{h_x}{v_{max}},$$

où h_t représente le pas de temps de simulation, h_x le pas d'espace et v_{max} la vitesse maximale des particules prise en compte. De plus, en régime fortement collisionel, le pas de temps est limité par le temps entre deux collisions.

La troisième échelle de modélisation des plasmas, dite macroscopique, repose sur les propriétés de conservation des grandeurs hydrodynamiques. Les variables hydrodynamiques sont définies comme les moments de la fonction de distribution relative à

chaque espèce, c'est-à-dire la densité de particules, la vitesse moyenne et la température de chaque espèce p, respectivement

$$\rho_p = \int_{\mathbb{R}^3} f_p \mathrm{d}v, \qquad \rho_p u_p = \int_{\mathbb{R}^3} v f_p \mathrm{d}v, \qquad 3\rho_p \frac{k_B \theta_p}{m_p} = \int_{\mathbb{R}^3} |v - u_p|^2 f_p \mathrm{d}v,$$

avec k_B la constante de Boltzmann. La densité de charge et le courant intervenant dans les équations de Maxwell sont alors définis à partir des variables hydrodynamiques par

$$\rho = \sum_p q_p \rho_p, \qquad J = \sum_p q_p \rho_p u_p,$$

avec q_p la charge de la particule p (négative pour les électrons). Ainsi les équations d'Euler traduisant l'évolution des grandeurs macroscopiques au cours du temps sont données en multipliant l'équation de Vlasov respectivement par $1, v$ et $|v|^2$,

$$\begin{cases} \partial_t \rho_p + \nabla_x \left(\rho_p u_p\right) = 0, \\ \rho_p \left(\partial_t u_p + u_p \cdot \nabla_x u_p\right) + \nabla_x P_p = \displaystyle\int_{\mathbb{R}^3} v C(F_p) \mathrm{d}v + \rho_p E, \\ \partial_t \left(3\rho_p \theta_p + \rho_p u_p^2\right) + 2\nabla_x \cdot Q_p + \nabla_x \cdot \left(3\rho_p \theta_p u_p + 2P_p u_p\right) = -2\rho_p E \cdot u_p - \nabla_x \cdot \left(\rho_p |u_p|^2 u_p\right), \end{cases}$$

avec $P_p = \int_{\mathbb{R}^3} (v - u_p) \otimes (v - u_p) f_p \mathrm{d}v$, le tenseur de pression et $Q_p = \int_{\mathbb{R}^3} |v - u_p|^2 (v - u_p) f_p \mathrm{d}v$ le flux thermique. Ces équations ne sont pas fermées tant que le tenseur de pression et le flux thermique ne sont pas définis en fonction des autres grandeurs hydrodynamiques. Pour ce faire, il est nécessaire de préciser le cadre de l'écoulement qui se caractérise essentiellement par deux paramètres.

La longeur de Debye λ_D représente la distance sous laquelle la séparation significative entre les charges positives et négatives ne peut avoir lieu. Autrement dit, pour un écoulement caractérisé par une longueur de référence suffisamment grande par rapport à la longueur de Debye, la répartition spatiale des charges électriques est la même pour les charges positives et négatives, on a ainsi $\rho = 0$. Le libre parcours moyen ℓ_p définit la distance moyenne que parcourt une particule p entre deux collisions, voir Figure I.1. Plus le plasma est dense, plus les particules sont proches les unes des autres et donc plus les collisions sont importantes. Dans le cadre d'un écoulement où le rapport entre le libre parcours moyen et la longueur caractéristique (L) à laquelle on regarde le plasma est suffisamment petit, il est possible de négliger certains phénomènes ayant peu d'influence à une échelle supérieure au libre parcours moyen. Ainsi Spitzer et Härm ont montré [14] qu'en régime très fortement collisionnel ($\varepsilon = \ell/L \ll 1$), la population de particules dans le plasma suit une loi de répartition gaussienne, généralement appelée maxwellienne dans le cadre de la physique des plasmas, c'est-à-dire

$$f_p = \frac{\rho_p}{\left(2\pi k_B \theta_p\right)^{3/2}} \exp\left(-\frac{m_p |v - u_p|^2}{2k_B \theta_p}\right) + \mathcal{O}(\varepsilon).$$

On ferme ainsi le système d'équations hydrodynamiques en reprenant les définitions du tenseur de pression et du flux thermique,

$$P_p^{SH} = \rho_p \frac{k_p \theta_p}{m_p} Id, \qquad Q_p^{SH} = -K \nabla_x \theta_p,$$

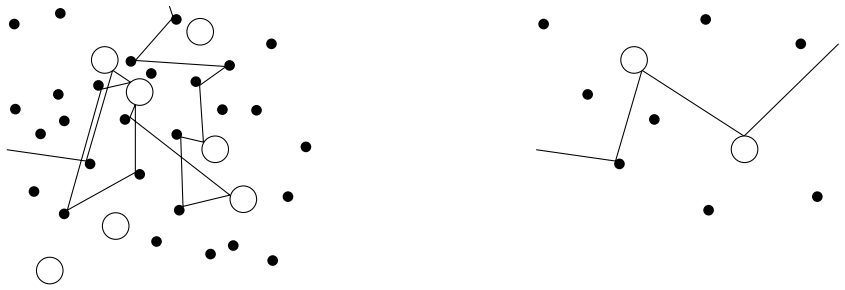

Plasma dense,
libre parcours moyen faible.

Plasma peu dense,
libre parcours moyen important.

Figure I.1: Parcours d'une particule dans un plasma.

avec $K(\theta_p) > 0$ le coefficient de diffusion thermique. Cette modélisation est bien adaptée aux simulations de problèmes industriels car elle permet d'utiliser des pas de discrétisation relativement élevés. Dans la plupart des applications, les collisions sont suffisamment importantes pour que cette modélisation soit représentative de la physique. Cependant pour certaines d'entre elles, le libre parcours moyen devient sensiblement plus important et des effets qui ne sont pas pris en compte à cette échelle se font ressentir. En particulier, la réaction de fusion thermonucléaire par confinement inertiel est initiée par un plasma peu dense et avec de forts gradients de température. Dans ces conditions, le libre parcours moyen est trop grand, et la modélisation du plasma par les équations d'Euler n'est pas valide [10]. Cependant, pour les raisons déjà énoncées, les simulations ne peuvent pas être effectuées à l'échelle microscopique. Il est donc nécessaire de mettre en place des modèles posés sur les variables hydrodynamiques ρ_p, u_p et θ_p, mais tenant compte de certains effets de l'échelle microscopique.

Pour simplifier l'étude, on ne s'intéresse qu'à la population d'électrons, en supposant les ions froids et fixes. Cette hypothèse est cohérente avec le contexte physique, c'est-à-dire la phase d'allumage, dite phase d'inition des réactions de fusion thermonucléaire par confinement inertiel. En effet les électrons sont plus légers que les ions et donc ils se mettent plus rapidement en mouvement. On suppose également que le plasma reste localement neutre, c'est-à-dire $\rho(t,x) = 0$. Cette hypothèse revient à considérer des écoulements où le rapport entre la longueur de Debye et la longueur caractéristique de l'étude est négligeable. Ces hypothèses peuvent être résumées en considérant que la vitesse moyenne des électrons est nulle. On remplace ainsi les équations de Maxwell par une hypothèse de courant nul. Le couplage entre l'équation de Vlasov-Fokker-Planck et l'hypothèse de courant nul est peu classique. Cependant, il est largement utilisé pour ce domaine d'application [12, 10, 11, 13].

Lorsque les collisions se font moins importantes, le libre parcours moyen augmente et donc certaines particules peuvent parcourir des distances significatives avant de rentrer en collision, et d'échanger ainsi une partie de leur énergie. Le flux thermique doit donc tenir compte de l'impact des particules provenant d'une région relativement éloignée. Plus précisément, pour un profil de température croissant convexe, l'intensité du flux thermique va être augmentée par le déplacement sans collision des particules sur des dis-

tances non négligeables. Cependant, pour les profils admettant un extrémum, l'intensité du flux thermique proche de cet extrémum peut être diminuée. D'après des simulations à partir de codes cinétiques, il est même possible que le flux thermique soit dans la même direction que le gradient de température. Une simple correction du coefficient de diffusion n'est donc pas satisfaisante. Le cas où le flux thermique et le gradient de température sont dans la même direction correspond à un coefficient de diffusion négatif et donc à une équation mal posée (chaleur rétrograde). A partir de cette remarque, Luciani et Mora décrivent dans une succession d'articles [10, 11], un ensemble de modèles où le flux thermique s'écrit sous la forme d'un flux délocalisé. Le flux thermique est définit comme un produit de convolution dans l'espace entre un certain noyau, dit de délocalisation, et le flux du régime asymptotique, décrit par le modèle de Spitzer-Härm. Pour être plus précis, le flux thermique est alors

$$Q_\varepsilon^{LM}(t,x) = W_\varepsilon(t,x) * Q^{SH}(t,x) = \int_{\mathbb{R}^3} W_\varepsilon(t,x) Q^{SH}(t,y-x)\mathrm{d}y,$$

avec $W_\varepsilon(t,x)$, le noyau de délocalisation. Plusieurs expressions de ce noyau sont proposées dans la littérature, notamment par Luciani et Mora. On remarque que ce noyau doit tendre vers une distribution de Dirac lorsque le libre parcours moyen devient infiniment petit. Ce modèle est intéressant car il rend bien compte du caractère non-local du flux. Cependant les produits de convolution sont coûteux à résoudre numériquement, en particulier pour les applications en trois dimensions.

Schurtz et Nicolaï remarquent [13] que le noyau de délocalisation est essentiellement un noyau de la chaleur. De plus, ils remarquent que l'opérateur de délocalisation dépend de la norme de la vitesse des particules. On retiendra que les particules ayant une vitesse plus élevée que la vitesse moyenne du plasma parcourent en général entre deux collisions des distances plus grandes que le libre parcours moyen. Inversement, les particules ayant une vitesse moins élevée parcourent en général entre deux collisions des distances moins grandes que le libre parcours moyen. Autrement dit, plus les particules vont vite par rapport à la vitesse moyenne des particules du plasma, plus elles ont tendance à parcourir de longs chemins avant de rentrer en collision avec d'autres particules. Ces auteurs introduisent ainsi le flux thermique généralisé solution d'une EDP elliptique largement étudiée de la forme

$$\mathcal{Q}_\varepsilon^{LM} - \varepsilon^2 \nu \Delta_x \mathcal{Q}_\varepsilon^{LM} = -\kappa \nabla_x \theta,$$

avec $\nu(t,x,|v|) > 0$ un paramètre de délocalisation et $\kappa(t,x,|v|)$ le coefficient de diffusion généralisé tel que $K = \int_{\mathbb{R}} \kappa \mathrm{d}|v|$. Le flux thermique est alors défini comme la somme des contributions des flux thermiques généralisés, c'est-à-dire

$$Q_\varepsilon^{LM} = \int_{\mathbb{R}} \mathcal{Q}_\varepsilon^{LM} \mathrm{d}|v|.$$

Les modèles délocalisés par Luciani et Mora ou par Schurtz et Nicolaï présentent cependant certains inconvénients de modélisation. En effet tels quels ils ne respectent à priori pas la contrainte de courant nul. De plus, le modèle de Schurtz et Nicolaï nécessite de considérer un coefficient de diffusion généralisé positif quelque soit la vitesse de la particule considérée. Cette hypothèse n'est pas cohérente avec l'expression du coefficient de diffusion généralisé obtenue par Spitzer et Härm à partir des équations de

Vlasov-Fokker-Planck. De plus elle s'oppose directement à l'hypothèse de courant nul, puisqu'elle implique que toutes les particules se déplacent dans le même sens.

On remarque que des équations similaires sont obtenues pour modéliser les interactions électrostatiques dans des processus biomoléculaires. Les interactions entre les protéines, essentiellement dûes aux forces électrostatiques, sont les principaux mécanismes sous-jacents à certains processus moléculaires dans l'eau. De ce fait, une description précise de ses mécanismes ainsi que leurs résolutions à l'aide d'outils numériques sont actuellement largement étudiées. De récents modèles présentés dans [7, 6] utilisent des opérateurs non locaux de même nature que ceux proposés par Schurtz et Nicolaï pour décrire les effets cinétiques à l'échelle macroscopique. Dans la dérivation de ces modèles, les auteurs proposent de tenir compte de la structure diélectrique des molécules d'eau.

Parallèlement, des travaux sont réalisés pour approcher l'équation de Vlasov-Fokker-Planck pour permettre de résoudre la numériquement. La fonction de distribution, solution de l'équation de Vlasov-Fokker-Planck, est une fonction du temps $t \in \mathbb{R}^+$, de l'espace $x \in \mathbb{R}^3$ et de la vitesse $v \in \mathbb{R}^3$. Ainsi la résolution numérique d'une telle équation nécessite une discrétisation de $\mathbb{R}^6$. Le nombre d'inconnues numériques est donc très important. De plus il est en général nécessaire de tronquer le domaine des vitesses par une vitesse maximale. Pour réduire le nombre d'inconnues, on utilise une décomposition de la fonction de distribution suivant les harmoniques sphériques. Les harmoniques sphériques sont une base des applications L^2 de la sphère dans $\mathbb{R}$. En supposant que la solution se décompose suivant un ensemble restreint d'harmoniques sphériques, l'équation de Vlasov-Fokker-Planck est décrite par les modèles P_n, largement utilisés pour la réalisation de codes numériques [2]. Plus récemment, Levermore revoit ce modèle [8] dans le cas de la dynamique des gaz neutres. Il apporte une correction des harmoniques sphériques tronquées pour les modèles P_n en supposant le libre parcours moyen suffisamment petit.

L'objectif de ce travail est de faire le lien entre l'équation de Vlasov-Fokker-Planck et les modèles intermédiaires proposés par Luciani-Mora et Schurtz-Nicolaï. Cette question est principalement motivée par une demande du Commissariat à l'Énergie Atomique et aux Énergies Alternatives (CEA) dont les applications, notamment le Laser Mégajoule, nécessitent de prendre en compte les effets cinétiques à l'échelle macroscopique. Une réponse est fournie en utilisant le procédé de fermeture proposé par Levermore. L'étude plus approfondie de la dérivation des équations permet de lever certains inconvénients des modèles proposés comme la troncature du coefficient de diffusion thermique généralisé, ceci afin d'être en accord avec la physique. De plus une résolution des modèles à l'aide d'outils numériques est mise en place en tenant compte des contraintes de l'application et dans l'optique d'être intégrée aux codes de calculs déjà existants. Ce travail est organisé de la manière suivante.

I.1 Chapitre II: On the Spitzer-Härm Regime and Non-Local approximations: modeling, analysis and numerical simulations

Dans ce chapitre, nous commençons par une analyse du régime asymptotique de Spitzer-Härm. L'équation de Vlasov-Fokker-Planck-Maxwell est d'abord adimensionnée et nous précisons la nature du régime en définissant les paramètres caractéristiques de l'écoulement. Nous voyons ainsi que l'écoulement est gouverné par le rapport entre la longueur de Debye et la longueur caractéristique ainsi que par le rapport entre le libre parcours moyen et la longueur caractéristique. Les équations de Maxwell dégénèrent alors en l'hypothèse de courant nul.

Ensuite dans le cadre où ces rapports sont infiniment petits, nous réécrivons un système équivalent posé sur les inconnues hydrodynamiques à l'aide d'un développement de Hilbert. La fonction de distribution, solution de l'équation de Vlasov-Fokker-Planck, est décrite par une série de puissance de ε, c'est-à-dire

$$f_\varepsilon(t,x,v) = \sum_j \varepsilon^j F_j(t,x,v),$$

avec F_j les termes de la série, indépendants de ε. Ces termes sont ensuite estimés en identifiant les termes de même puissance en ε dans l'équation de Vlasov-Fokker-Planck. Nous retrouvons ainsi les résultats énoncés par Spitzer-Härm et établissons que le régime est caractérisé par un coefficient de diffusion non-linéaire en $\theta^{5/2}$. Plus précisément le flux thermique s'écrit

$$Q^{SH} = -\tilde{K}\theta^{5/2}\nabla_x\theta,$$

avec $\tilde{K} > 0$. Le corollaire évident de ce résultat est que le modèle est bien posé et vérifie le principe du maximum, quelque soit l'opérateur de collision satisfaisant les hypothèses précédemment énoncées.

Nous nous intéressons ensuite au modèle non-local proposé par Schurtz et Nicolaï, sans tenir compte de sa dépendance au module de la vitesse des particules. Nous montrons (Théorème II.3.1) que sous certaines hypothèses simplificatrices, le modèle de Schurtz-Nicolaï est bien posé et vérifie le principe du maximum. La démonstration de ce théorème repose sur une transformation de Fourier qui nous permet d'identifier le noyau de délocalisation de Luciani-Mora relatif au modèle de Schurtz-Nicolaï. Les propriétés de ce noyau, positif et unitaire, permettent de conclure en utilisant un procédé itératif et limitant la dérivée du coefficient de diffusion ("cut-off") pour traiter sa non-linéarité. Enfin nous montrons que la solution reste bornée par les extréma de la condition initiale, validant ainsi la limitation de la variation du coefficient de diffusion. Nous montrons également (Proposition II.3.1) que l'énergie totale est conservée et qu'il existe une entropie qui se dissipe au cours du temps. Ce résultat se montre en appliquant l'opérateur de délocalisation à l'évolution de la température permettant ainsi de découpler les inconnues et de ne travailler que sur la température.

Enfin, un schéma numérique permettant de résoudre l'équation de Schurtz-Nicolaï est proposé à partir d'une approche Différences Finies. Le schéma est construit pour

satisfaire les équivalents numériques des propositions précédentes (Propositions II.4.1 et II.4.2). De plus, nous montrons (Théorème II.4.1) que la norme L^2 de la solution du schéma numérique est décroissante sous une condition liant le pas de temps et le pas d'espace. Nous montrons ainsi que la solution vérifie le principe de dissipation d'entropie, classique pour les problèmes physiques. Cette condition est moins restrictive que la condition classique des schémas numériques pour les équations paraboliques. Enfin nous montrons (Théorème II.4.2) que le schéma vérifie le principe du maximum sous une condition originale sur le pas de temps. Il est intéressant de noter que ce schéma permet de mettre en évidence certains effets cinétiques à l'échelle macroscopique par des simulations numériques. En particulier, nous illustrons la présence de flux "d'anti-diffusion" à partir de certains profils de température, tout en respectant les conditions nécessaires au principe du maximum.

I.2 Chapitre III: Non-Local Macroscopic Models based on Gaussian Closures for the Spitzer-Härm Regime

Ce chapitre est principalement consacré à la dérivation à partir de l'équation de Vlasov-Fokker-Planck d'une hiérarchie de modèles intermédiaires du transfert radiatif des électrons. Dans un premier temps, nous adaptons la décomposition proposée par Levermore pour décrire les gaz neutres à partir de l'équation de Vlasov-Fokker-Planck au cas d'un gaz de particules chargées. Cette dérivation fait intervenir les harmoniques sphériques et une étape de fermeture des équations à l'aide d'une approximation. La première approximation généralement utilisée pour écrire les codes numériques repose sur une troncature des harmoniques sphériques à partir d'un certain rang. Le nombre d'inconnues grandissant exponentiellement avec le nombre d'harmoniques sphériques prises en compte, il est rare de considérer plus de deux ou trois harmoniques sphériques. La seconde approximation proposée par Levermore repose sur une estimation des harmoniques sphériques négligées en ne conservant que les termes principaux dans un développement en puissance de ε. Cette approximation n'est donc valable qu'en régime fortement collisionnel. Dans ces modèles, le nombre d'inconnues croit toujours exponentiellement avec le nombre d'harmoniques sphériques considérées.

Le second niveau dans la hiérarchie est obtenu en remarquant que le terme principal de la fonction de distribution est une maxwellienne. Ainsi nous décrivons un plasma en régime fortement collisionel à l'aide de l'équation de Vlasov-Fokker-Planck linéarisée autour de la maxwellienne. L'inconnue de cette équation est alors une perturbation du terme principal. L'approximation de Levermore est ensuite effectuée permettant ainsi d'établir un modèle plus particulièrement adapté aux études de la variation du flux thermique.

L'intérêt de la linéarisation vient du fait que le terme principal de la perturbation est porté par la seconde harmonique sphérique. Cette harmonique sphérique est celle qui décrit les flux macroscopiques, notamment le flux thermique. Ainsi on écrit un modèle composé du minimum d'inconnues possible, soit une inconnue vectorielle, en considérant uniquement la seconde harmonique sphérique et en effectuant l'approximation

de Levermore sur les autres. On écrit ainsi le modèle qu'on nommera Spitzer-Härm généralisé, faisant intervenir trois équations couplées. La première traduit la conservation de la température (ou de l'énergie totale). La seconde est l'équation du flux thermique généralisé. Le flux thermique généralisé est à un changement de variable près la projection sur la seconde harmonique sphérique de la fonction de distribution. Il est donc remarquable de noter que l'hypothèse de courant nul peut s'écrire à l'aide de cette inconnue et composera ainsi la troisième équation du modèle. L'équation sur le flux thermique généralisé est une équation d'évolution de type réaction-advection-diffusion. Le terme de transport est estimé au régime asymptotique grâce à un développement de Hilbert. Le terme de diffusion est composé de l'opérateur de délocalisation, relativement proche de celui proposé par Schurtz et Nicolaï. On notera que la principale différence entre les modèles de flux délocalisé précédemment proposés et le modèle de Spitzer-Härm généralisé réside dans la dérivée temporelle du flux thermique ainsi que dans le terme de correction du champ moyen. Ainsi le modèle de Spitzer-Härm généralisé ne s'inscrit pas dans la famille des flux délocalisés puisqu'il ne peut pas être réécrit sous la forme d'un produit de convolution entre un certain noyau de délocalisation et le flux thermique de Spitzer-Härm.

La présence de cette dérivée temporelle permet d'inscrire le modèle dans le cadre des systèmes d'équations d'évolution. Ainsi nous montrons dans le principal résultat du chapitre (Théorème III.5.1) que le modèle linéarisé est bien posé à l'aide d'une analyse des valeurs propres sans effectuer de troncature sur le coefficient de diffusion généralisé. Cette démonstration est adaptée de la méthode proposée par Liu et Zeng dans leur étude des systèmes d'évolution [9]. L'équation de Spitzer-Härm généralisée permet ainsi de traiter la contrainte de courant nul et comble le principal inconvénient du modèle de Schurtz-Nicolaï. Enfin nous proposons un schéma numérique pour une résolution multi-dimensionelle du modèle de Spitzer-Härm généralisé grâce à la méthode proposée dans le chapitre précédent.

Le modèle de Schurtz-Nicolaï peut être vu comme une simplification du modèle de Spitzer-Härm généralisé, notamment sous l'hypothèse du flux de chaleur stationnaire. Nous mettons ainsi en évidence la dépendance en énergie interne ($\xi = \frac{|v|^2}{2\theta}$) des paramètres du modèle de Schurtz-Nicolaï. En annexe de ce chapitre, nous généralisons les résultats du chapitre précédent pour tenir compte de cette dépendance (Théorème III.A.1 et Proposition III.A.1). La démonstration de ces résultats fait intervenir une température généralisée qui peut être interprétée comme la contribution à l'évolution de la température du flux généralisé pour une certaine énergie interne fixée. Cette nouvelle inconnue permet notamment d'établir un schéma numérique performant dans le cas d'un opérateur de délocalisation simplifié.

I.3 Chapitre IV: Finite Volume Schemes on Unstructured Grids for Generalized Non-Local Spitzer-Härm Models

Ce chapitre est consacré à la résolution numérique de l'équation de Spitzer-Härm généralisée sur un maillage non cartésien avec des conditions limites de type Neumann homogène sur la température. A la différence des schémas présentés dans les chapitres précédents, la résolution proposée prend en compte l'opérateur de délocalisation complet, comme décrit par la dérivation du chapitre III.

Le schéma a été écrit pour satisfaire certains critères et être applicable dans le cadre d'applications complexes. Le schéma doit être suffisamment simple à résoudre pour pouvoir être couplé à d'autres équations traduisant notamment le mouvement des ions. En effet les applications sont largement multiphysiques. Une méthode de quadrature de Gauss-Laguerre généralisée est alors utilisée pour estimer les intégrales en énergie, limitant ainsi le nombre de points utilisés et représentant bien le domaine d'intégration.

Le schéma doit être suffisamment stable pour admettre des pas de temps relativement élevés. Plus précisemment, le schéma doit accepter des pas de temps comparables à ceux utilisés dans le cas de la résolution de l'équation classique de Spitzer-Härm. Ainsi nous utilisons une discrétisation en temps à l'aide d'un schéma de relaxation. Cette méthode consiste à introduire un paramètre numérique $0 \leq \tau \leq 1$ et à moyenner le schéma d'Euler progressif et Euler rétrograde respectivement par $1 - \tau$ et τ. Les schémas d'Euler progressif et rétrograde ainsi que la méthode de Crank-Nicolson sont des cas particuliers de la méthode de relaxation obtenus respectivement pour $\tau = 0$, $\tau = 1$ et $\tau = 1/2$. Sauf dans le cas particulier de la méthode d'Euler progressif, la méthode de relaxation est implicite en temps. Dans le cas linéaire et pour un coefficient de relaxation suffisamment grand ($\tau \geq 1/2$) la méthode semble inconditionnellement stable. Les non-linéarités sont estimées à l'aide d'un schéma de point fixe de Picard. C'est un procédé qui consiste à itérer à chaque pas de temps la résolution d'un système linéaire dont les coefficients sont réactualisés en tenant compte de la valeur de la solution intermédiaire précédemment estimée. Les résultats théoriques de cette méthode montrent qu'elle converge à l'ordre un, sous certaines hypothèses. D'autres méthodes comme la méthode de Newton sont plus efficaces pour traiter les non-linéarités mais nécessitent d'estimer la dérivée du système par rapport aux inconnues. La dépendance des coefficients de l'opérateur de délocalisation par rapport à la température n'est pas claire, comme décrite dans la dérivation proposée au chapitre (III). Ainsi la méthode du point fixe permet de modifier facilement ces coefficients sans modifier l'essentiel du schéma. En pratique, les calculs convergent au bout de quelques itérations.

Le schéma doit être écrit pour des maillages non-structurés sans contrainte géométrique. En effet, pour les applications, l'hypothèse des ions fixes est remplacée par une équation de quantité de mouvement. L'hypothèse de courant nul est toujours justifiée en considérant que le mouvement des électrons est largement plus rapide. La résolution du mouvement des ions est généralement réalisée à l'aide d'une méthode lagrangienne, où le maillage est déformé pour suivre le mouvement de la matière. On adopte alors un point de vue Volumes Finis avec un maillage primal triangulaire. Une généralisation aux maillages primals polygonaux quelconques est proposée, permettant

également de traiter le cas des maillages non-conformes.

Le schéma proposé doit également converger lorsque le libre parcours moyen devient infiniment petit, vers un schéma de l'équation de Spitzer-Härm. Cette propriété permet, en plus de valider la robustesse du schéma dans la variable ε, de coupler dans l'espace l'équation de Spitzer-Härm généralisée avec l'équation de Spitzer-Härm. En effet, dans les applications, l'équation de Spitzer-Härm est valide dans presque tout le domaine. Cependant les zones de non-validité de l'équation de Spitzer-Härm sont particulièrement importantes puisqu'elles sont le siège de l'apport d'énergie par le laser. La particularité de la méthode réside dans le choix de l'inconnue numérique. Pour des raisons de construction de l'opérateur de délocalisation, on utilise le flux thermique généralisé comme inconnue, discrétisé comme valeur moyenne sur une face des volumes de contrôle, et non pas sur un volume. On retrouve ainsi directement la variable nécessaire à la résolution de la conservation de la température. La construction de la version discrète de l'opérateur de délocalisation se fait ensuite en reconstruisant un gradient moyen sur les volumes de contrôle à l'aide d'une formule de Stokes. Puis, une reconstruction linéaire de ce gradient par éléments du maillage primal permet d'estimer les dérivées secondes du flux thermique généralisé. Enfin, la contrainte de courant nul est traité par une méthode de lagrangien augmenté, donnant ainsi une estimation de la correction du champ moyen.

Le schéma est ensuite validé par une série de cas tests mettant en évidence certains comportements. Dans un premier temps, des tests de convergence en espace sont réalisés à partir d'une solution analytique en régime stationnaire. Les résultats montrent une convergence d'ordre deux sur des maillages non-structurés. Ensuite, des tests de convergence en énergie interne sont réalisés. Les résultats semblent relativement proches ce qui confirme la discrétisation par méthode de quadrature. Cependant, le choix du poids de quadrature ainsi que la vitesse de convergence ne sont pas clairement identifiables à cause du faible nombre de points de discrétisation en énergie considéré. En effet, le nombre d'inconnues et le stencil de la matrice du système linéaire associé au schéma sont proportionels au nombre de points de discrétisation en énergie. Il est donc nécessaire pour pousser plus en avant les tests de convergence d'établir un schéma découplant les points de discrétisation en énergie. Ce découplage peut être réalisé à partir d'une méthode de Jacobi. Une dernière série de tests permet de mettre en évidence les effets de flux d'anti-diffusion précédemment introduits. Ainsi le modèle répond aux attentes en modélisant certains effets cinétiques qui n'étaient pas pris en compte à l'échelle macroscopique.

I.4 Chapitre V: Hybrid Model for the coupling of an Asymptotic Preserving Scheme with the Asymptotic Limit Model: the one dimension case

Ce chapitre est consacré à l'étude d'un autre problème lié à la physique des plasmas. La modélisation des plasmas soumis à un fort champ magnétique nécessite la résolution d'une équation elliptique fortement anisotrope. C'est par exemple le cas des plasmas ionosphériques à une latitude d'environ 60 $^\circ$ soumis au champ magnétique terrestre ainsi qu'aux plasmas expérimentaux obtenus pour l'étude de la fusion par confinement magnétique, dans les tokamaks. Ces plasmas sont généralement modélisés par l'équation

d'Euler-Lorentz dans le cadre de la "Drift Limit" [1, 5]. L'estimation de la composante de la vitesse dans la direction du champ magnétique nécessite la résolution d'une équation elliptique anisotropique avec des conditions limites de Neumann ou périodiques. Lorsque l'anisotropie devient infiniment forte, le modèle dégénère formellement vers une équation mal posée. Cependant, une intégration le long de la direction de l'anisotropie permet de mettre en évidence un système d'équations équivalent, dont la limite pour de fortes anisotropies est bien posée. Cette méthode est détaillée, et deux schémas numériques sont proposés [3, 4]. Le premier permet la résolution du problème limite alors que le second résoud le problème reformulé avec un conditionnement de la matrice du système linéaire indépendant du paramètre d'anisotropie. De tels schémas sont dit "asymptotic preserving".

Nous nous intéressons ici au couplage spatial entre ces deux modèles ainsi qu'à la résolution numérique de simulation mettant en scène une sous région où le schéma "asymptotic preserving" est nécessaire alors que le schéma du problème limite est suffisant dans le reste du domaine de simulation. Ce couplage est réalisé à l'aide d'une méthode de conditions d'interface de type Dirichlet-to-Neumann. Enfin, des simulations numériques valident la méthode.

Remarque : *Il est important de noter que ce manuscrit est composé d'un ensemble de publications réalisées au cours du doctorat. Les notations ne sont donc pas définies pour l'ensemble du document mais pour chaque chapitre. Nous rappelons ici la liste des réalisations scientifiques correspondant aux chapitres du manuscrit de thèse :*

Publications:

- Goudon, T., and Parisot, M.,
  On the Spitzer-Härm Regime and Non-Local Approximations: modeling, analysis and numerical simulations,
  SIAM Multiscale Model. Simul. 9(2) (2011), 568-600.

- Goudon, T., and Parisot, M.,
  Non-Local Macroscopic Models based on Gaussian Closures for the Spitzer-Härm regime,
  AIMS Kinet. Relat. Models 4(3) (2011), 735-766.

- Goudon, T., and Parisot, M.,
  Finite Volume Schemes on Unstructured Grids for Generalized Non-Local Spitzer-Härm Models,
  Soumis dans *J. Comput. Phys.*

Proceeding:

- Degond, P., Deluzet, F., Maldarella, D., Narski, J., Negulescu, C., Parisot, M.,
  Hybrid model for the coupling of an Asymptotic Preserving Scheme with the Asymptotic Limit Model: the one dimensional case,
  À paraître dans *ESAIM: Proceedings.*

Bibliographie

[1] Brull, S., Degond, P., and Deluzet, F. Degenerate anisotropic elliptic problems and magnetized plasma simulations. *Commun. Comput. Phys.* (2011). to appear.

[2] Deck, D. Documentation du code `fpelec`. Tech. rep., CEA/DAM, 2009.

[3] Degond, P., Deluzet, F., Lozinski, A., Narski, J., and Negulescu, C. Duality based Asymptotic-Preserving Method for highly anisotropic diffusion equations. *Commun. Math. Sci.* (2011). to appear.

[4] Degond, P., Deluzet, F., and Negulescu, C. An Asymptotic Preserving scheme for strongly anisotropic elliptic problems. *SIAM Multiscale Model. Simul. 8* (2010), 645–666.

[5] Degond, P., Deluzet, F., Sangam, A., and Vignal, M.-H. An asymptotic preserving scheme for the Euler equations in a strong magnetic field. *J. Comput. Phys. 228* (2009), 3540–3558.

[6] Hildebrandt, A., Blossey, R., Rjasanow, S., Kohlbacher, O., and Lenhof, H.-P. Novel formulation of nonlocal electrostatics. *Physical Review Letters 93* (2004). article 108104.

[7] Hildebrandt, A., Blossey, R., Rjasanow, S., Kohlbacher, O., and Lenhof, H.-P. Electrostatic potentials of proteins in water: a structured continuum approach. *Bioinformatics 23* (2007), e99–e103.

[8] Levermore, D. Boundary conditions for moment closures. *IPAM KT2009, UCLA, CA* (2009).

[9] Liu, T.-P., and Zeng, Y. Large time behavior of solutions for general quasilinear hyperbolic-parabolic systems of conservation laws. *Mem. Amer. Math. Soc. 125*, 599 (1997), viii+120.

[10] Luciani, J.-F., and Mora, P. Resummation methods of the Chapman-Enskog Expansion for a Strongly Inhomogeneous Plasma. *J. Stat. Phys. 43* (1986), 281–302.

[11] Luciani, J.-F., Mora, P., and Pellat, R. Quasistatic heat front and delocalized heat flux. *Phys. Fluids 28* (1985), 835–845.

[12] Nicolaï, P., Feugeas, J.-L., and Schurtz, G. A practical nonlocal model for heat transport in magnetized laser plasmas. *Phys. Plasmas 13* (2006), 032701+13.

[13] Schurtz, G. P., Nicolaï, P., and Busquet, M. A nonlocal electron conduction model for multidimensional radiation hydrodynamics codes. *Phys. Plasmas 7* (2000), 4238–4250.

[14] Spitzer, L., and Härm, R. Transport phenomena in a completely ionized gas. *Phys. Rev. 89* (1953), 977–981.

Chapitre II :

On the Spitzer-Härm Regime and Non-Local Approximations: modeling, analysis and numerical simulations

Résumé : Ce papier est consacré à la dérivation de la limite de Spitzer-Härm à partir du système d'EDP décrivant l'évolution des particules chargées et du champ électromagnétique engendré. Nous identifions un régime asymptotique pertinent conduisant à un système de diffusion non linéaire pour la température électronique. Nous discutons ensuite de certains régimes intermédiaires, qui reste de nature hydrodynamique mais non-locales en introduisant des intégrales ou des opérateurs pseudo-différentiels. En particulier, nous présentons d'importantes propriétés mathématiques du modèle introduit par Schurtz et Nicolaï comme le caractère bien posé et le principe du maximum. Enfin nous concevons un schéma numérique pour les modèles non-locaux dont nous analysons la consistance et la stabilité.

Abstract: This paper is devoted to the derivation of the Spitzer-Härm limit from the coupled system of PDEs describing the evolution of charged particles and electromagnetic fields. We identify a relevant asymptotic regime which leads to a non linear diffusion equation for the electron temperature. Then, we discuss some intermediate models, which remain of hydrodynamic nature but involve a nonlocal coupling through integral or pseudo-differential operators. In particular, we exhibit important mathematical properties of the so-called Schurtz-Nicolaï model like the well-posedness and the maximum principle. We also design numerical schemes for the non local models and analyze their consistency and stability properties.

Note: Ce chapitre à donné lieu a une publication dans *SIAM Multiscale Modeling and Simulation* en collaboration avec Thierry Goudon.

II.1 Introduction

We are concerned with the following equations

$$\partial_t f_k + \nabla_x \cdot (v f_k) \pm \frac{q\, Z_k}{m_k} \nabla_v \cdot \big((E + v \wedge B) f_k\big) = \sum_l C_{kl}(f_k, f_l) \tag{1.1}$$

where the unknowns $f_k(t, x, v)$ stand for the number density in phase space of charged particles within the species labelled by k. These quantities depend on the time variable $t \geq 0$, the space variable $x \in \mathbb{R}^3$ and the velocity variable $v \in \mathbb{R}^3$. The parameters q and m_k are the electron charge and the mass of the particles, respectively. In what follows the index $k = 0$ is used for electrons, and positive indices k are used for ions. Then, the sign $+$ in front of the acceleration term corresponds to positively charged particles, the sign $-$ corresponds to electrons. By convention we set $Z_0 = 1$ and Z_k is the ionization number for the ion specie $k > 0$. The right hand side in (1.1) describes interparticles interactions. Usually, in plasma physics, it is given by the Landau-Fokker-Planck operators

$$C_{kl}(f_k, f_l) = \Gamma_{kl} \nabla_v \cdot \left(\int_{\mathbb{R}^3} S_{k,\alpha}(v - v_\star) \big(\nabla_v - \frac{m_k}{m_l} \nabla_{v_\star} \big) f_l(v_\star) f_k(v) \mathrm{d}v_\star \right) \tag{1.2}$$

with

$$\Gamma_{kl} = \frac{4\pi Z_k^2 Z_l^2 q^4 \ln \Lambda}{\varepsilon_0^2 m_k^2},$$

$\ln \Lambda$ being the Coulomb logarithm, and ε_0 the vacuum permittivity. The kernel of the collision operator is given by

$$S_{k,\alpha}(z) = \left(\frac{k_B \Theta_k}{m_k z^2} \right)^{\frac{\alpha}{2}} \frac{\Pi_z}{|z|}, \qquad \Pi_z = \mathbb{I} - \frac{z \otimes z}{|z|^2},$$

with k_B the Boltzmann constant. The case $\alpha < -3$ is traditionally referred to as *hard potentials*, the case $\alpha = -3$ as *Maxwell molecules*, and the case $\alpha > -3$ as *soft potentials*. The most relevant case in plasma physics corresponds to the Coulombian interactions between charged particles where $\alpha = 0$. For further analysis it will be interesting to consider slightly different operators, like for example the Boltzmann and BGK models, having the same fundamental properties (conservation and dissipation). Here and below, we consider the densities, current densities and temperatures defined as velocity average of the microscopic unknowns

$$\rho_k(t, x) = \int_{\mathbb{R}^3} f_k(t, x, v) \mathrm{d}v, \qquad J_k(t, x) = Z_k q \rho_k u_k(t, x) = Z_k q \int_{\mathbb{R}^3} v f_k(t, x, v) \mathrm{d}v,$$

$$\rho_k |u_k|^2 + 3\rho_k \frac{k_B \Theta_k}{m_k} = \int_{\mathbb{R}^3} |v|^2 f_k \mathrm{d}v.$$

Finally, the particles are subject to a force field determined by the electromagnetic field (E, B), which is self-consistently defined by the Maxwell equations :

$$\begin{cases} \partial_t E - c^2 \mathrm{curl}_x B = \dfrac{1}{\varepsilon_0} \Big(J_0 - \displaystyle\sum_{k>0} J_k \Big), \\ \partial_t B + \mathrm{curl}_x E = 0, \\ \mathrm{div}_x E = \dfrac{q}{\varepsilon_0} \Big(\displaystyle\sum_{k>0} Z_k \rho_k - \rho_0 \Big), \\ \mathrm{div}_x B = 0, \end{cases} \tag{1.3}$$

with c the speed of light.

We refer to [2, 9] for an introduction to the physics background on the model. The mathematical theory on existence–uniqueness issues for Vlasov–Maxwell equations with collisional terms is not complete, depending on the complexity of the collision operator. Concerning weak solutions we refer to [13], but considering Boltzmann or Landau operators might lead to very weak notion of solutions [20, sp. Section IV]. Impressive progress have appeared recently dealing with classical solutions close to equilibrium, with proofs based on subtle energy estimates [17, 29, 30]. Here we will be interested in asymptotic questions. Due to the multiscale nature of the problem the cost of numerical simulations of the system becomes prohibitive in many practical situations. This motivates to seek reduced models. Therefore our goal is first to identify relevant parameters and asymptotic regimes, that can be embodied into a scaling term $0 < \varepsilon \ll 1$ and second to derive the corresponding limit equations. Then, having understood this behavior we seek intermediate models, depending on ε. These models will be of hydrodynamic type, that means describing the evolution of macroscopic quantities like the charge and current densities and the temperatures. As a typical example, the description of laser plasma interactions, as in the modeling of Inertial Confinement Fusion (ICF), is highly demanding in computational resources. Simulations of the fully microscopic model is not affordable at the scales of physical interest and usually this situation is modeled by fluid codes. It turns out that electron heat flow is a crucial aspect of laser fusion and it has been observed that these codes often produce overestimated heat fluxes compared to experiments. Comparisons to kinetic codes, available in very simplified geometries, have confirmed this drawback, which motivates that quest for more accurate macroscopic models.

Here, to start with, we adopt the following simplified framework:

- Ions reduce to one specie.
- The distribution of positive charge has already been thermalized, so that
$$f_i(t,x,v) = \frac{\rho_i}{(2\pi k_B\Theta_i/m_i)^{3/2}} \exp\Big(- \frac{|v-u_i|^2}{2k_B\Theta_i/m_i}\Big).$$
- The associated macroscopic quantities ρ_i, Θ_i only depend on the space variable and the current of the positive particles vanishes $u_i = 0$.

Therefore we are interested in the evolution of the distribution of electrons $f_e(t,x,v)$, driven by

$$\partial_t f_e + v\cdot\nabla_x f_e - \frac{q}{m_e}\nabla_v\cdot\big((E+v\wedge B)f_e\big) = C_{ee}(f_e) + C_{ei}(f_e).$$

Coming back to (1.2), the collision operators read

$$C_{ee}(f) = \Gamma_{ee}\nabla_v\cdot\left(\int S_{e,\alpha}(v-v_\star)\big(\nabla_v-\nabla_{v_\star}\big)f(v_\star)f(v)\mathrm{d}v_\star\right),$$
$$C_{ei}(f) = \frac{\rho_i}{(2\pi k_B\Theta_i/m_i)^{3/2}}\Gamma_{ei}$$
$$\nabla_v\cdot\left(\int S_{e,\alpha}(v-v_\star)\big(\nabla_v - \frac{m_e}{m_i}\nabla_{v_\star}\big)\exp\Big(-\frac{v_\star^2}{2k_B\Theta_i/m_i}\Big)\ f(v)\mathrm{d}v_\star\right).$$

The electromagnetic field satisfies

$$\begin{cases} \partial_t E - c^2 \mathrm{curl}_x B = \dfrac{J_e}{\varepsilon_0} = \dfrac{q}{\varepsilon_0} \displaystyle\int_{\mathbb{R}^3} v f_e \mathrm{d}v, \\ \partial_t B + \mathrm{curl}_x E = 0, \\ \mathrm{div}_x E = \dfrac{q}{\varepsilon_0} \left(Z_i \rho_i - \rho_e \right) = \dfrac{q}{\varepsilon_0} \left(Z_i \rho_i - \displaystyle\int_{\mathbb{R}^3} f_e \mathrm{d}v \right), \\ \mathrm{div}_x B = 0. \end{cases}$$

The paper is organized as follows. The next section is devoted to the asymptotic analysis of the problem. We start with the dimensional analysis of the equations, in order to identify a set of relevant dimensionless parameters (section II.2.1). A first approximation consists in simplifying the electron/ion collision term, based on the scaling $m_e/m_i \ll 1$ (section II.2.2). In particular, we bring out the fundamental properties of the approximate collision operator: charge and energy conservation, entropy dissipation. Then by using Hilbert expansions we are led to the so-called Spitzer-Härm regime where the dynamics is driven by a non linear diffusion equation for the electron temperature; we identify the diffusion coefficient which depends on the details of the collision operator (section II.2.3). The intermediate model which is discussed in section II.3 is derived on physical grounds and it is quite popular for the simulation of ICF experiments. There, the flux is obtained as a suitable convolution of the gradient of the temperature, which leads to a non local model. We shall establish some remarkable mathematical properties of the model. In section II.4.1 we design and analyze numerical schemes for the non local models. It is completed in section IV.4 by a set of commented numerical simulations. Eventually a conclusion summarizes the main contribution of the paper.

II.2 The Spitzer-Härm regime

II.2.1 Dimensional analysis

Let us write now the equations in dimensionless form. To this end, we introduce a particle reference density $\bar{\rho}_e$ and a reference temperature $\bar{\Theta}_e$. Then, $\sqrt{k_B \bar{\Theta}_e / m_e}$ defines the thermal velocity and $k_B \bar{\Theta}_e / q$ defines a reference potential. We also need time and length units, T and L respectively. Then we define dimensionless variables by setting

$$t = \mathrm{T}\ t', \qquad x = \mathrm{L}\ x', \qquad v = \sqrt{\frac{k_B \bar{\Theta}_e}{m_e}}\ v'.$$

Next, we define the dimensionless density by

$$f_e(t,x,v) = \frac{\bar{\rho}_e}{\mathrm{L}^3 \left(\dfrac{k_B \bar{\Theta}_e}{m_e} \right)^{3/2}}\ f'(t',x',v'),$$

while the electromagnetic field scales as follows

$$E(t,x) = \frac{k_B \bar{\Theta}_e}{q}\ \frac{1}{\mathrm{L}}\ E'(t',x'), \qquad B(t,x) = \frac{k_B \bar{\Theta}_e}{q}\ \frac{1}{\mathrm{T}c^2}\ B'(t',x').$$

Note that

$$\frac{k_B\bar\Theta_e}{q}\ \frac{1}{\mathrm{L}}\times\frac{q}{k_B\bar\Theta_e}\ \mathrm{T}c^2\sqrt{\frac{m_e}{k_B\bar\Theta_e}}=\frac{\mathrm{T}c^2}{\mathrm{L}}\sqrt{\frac{m_e}{k_B\bar\Theta_e}}$$

measures the ratio of the electric force over the magnetic force. We also set

$$\rho_i(x)=\frac{\bar\rho_i}{\mathrm{L}^3}\ \rho_i'(x'),\qquad \Theta_i(x)=\bar\Theta_i\ \Theta_i'(x'),$$

with $\bar\rho_i$ and $\bar\Theta_i$ reference values for the ion density and temperature respectively. Finally, typical length scales are defined by

$$\begin{aligned}&\text{Debye length:}\qquad \lambda_D=\sqrt{\frac{\varepsilon_0 k_B\bar\Theta_e\ \mathrm{L}^3}{q^2\bar\rho_e}},\\ &\text{electron mean free path:}\qquad \ell=\frac{\varepsilon_0^2\ k_B^2\bar\Theta_e^2\ \mathrm{L}^3}{4\pi\bar\rho_e q^4\ln\Lambda}.\end{aligned}$$

Up to a slight change of notation, the dimensionless equations read as follows:

$$\begin{aligned}&\partial_t f+\sqrt{\frac{k_B\bar\Theta_e}{m_e}}\ \frac{\mathrm{T}}{\mathrm{L}}\ v\cdot\nabla_x f-\sqrt{\frac{k_B\bar\Theta_e}{m_e}}\ \frac{\mathrm{T}}{\mathrm{L}}\ \nabla_v\cdot\Big(\big(E+\sqrt{\frac{m}{k_B\bar\Theta_e}}\frac{\mathrm{L}}{\mathrm{T}}\frac{k_B\bar\Theta_e}{mc^2}v\wedge B\big)f\Big)\\ &\qquad=\mathrm{T}\Gamma_{ee}\frac{\bar\rho_e}{\mathrm{L}^3}\left(\frac{m_e}{k_B\bar\Theta_e}\right)^{3/2}\Big(C_{ee}(f)+Z_iC_{ei}(f)\Big),\end{aligned}$$

with now

$$\begin{aligned}C_{ee}(f)&=\nabla_v\cdot\left(\int_{\mathbb{R}^3}\Theta_e^{\alpha/2}\frac{\Pi_{v-v_\star}}{|v-v_\star|^{\alpha+1}}\big(\nabla_v-\nabla_{v_\star}\big)f(v_\star)f(v)\mathrm{d}v_\star\right),\\ C_{ei}(f)&=\frac{Z_i\bar\rho_i}{\bar\rho_e}\ \left(\frac{m_i}{m_e}\frac{\bar\Theta_e}{\bar\Theta_i}\frac{1}{2\pi\Theta_i}\right)^{3/2}\rho_i\\ &\qquad\nabla_v\cdot\left(\int_{\mathbb{R}^3}\Theta_e^{\alpha/2}\frac{\Pi_{v-v_\star}}{|v-v_\star|^{\alpha+1}}\big(\nabla_v-\frac{m_e}{m_i}\nabla_{v_\star}\big)\exp\Big(-\frac{m_i}{m_e}\frac{\bar\Theta_e}{\bar\Theta_i}\ \frac{|v_\star|^2}{2\Theta_i}\Big)\ f(v)\mathrm{d}v_\star\right),\end{aligned}\tag{2.1}$$

coupled to the Maxwell system

$$\begin{aligned}&\partial_t E-\mathrm{curl}_x B=\frac{q^2\bar\rho_e T}{\varepsilon_0 L^2\sqrt{k_B\bar\Theta_e m_e}}\ \int_{\mathbb{R}^3}vf\mathrm{d}v,\\ &\left(\frac{\mathrm{L}}{\mathrm{T}c}\right)^2\partial_t B+\mathrm{curl}_x E=0,\\ &\nabla_x\cdot B=0,\\ &\nabla_x\cdot E=\frac{q^2\bar\rho_e}{\varepsilon_0 k_B\bar\Theta_e L}\left(\frac{Z_i\bar\rho_i}{\bar\rho_e}\rho_i-\int_{\mathbb{R}^3}f\mathrm{d}v\right).\end{aligned}$$

The dynamics is therefore governed by the dimensionless parameters

$$\frac{1}{\varepsilon}=\sqrt{\frac{k_B\bar\Theta_e}{m_e}}\ \frac{\mathrm{T}}{\mathrm{L}},\qquad \eta=\sqrt{\frac{k_B\bar\Theta_e}{m_e}}\ \frac{1}{c},$$

the ratio of the thermal velocity over the velocity unit defined by the time and length scales, and the ratio of the thermal velocity over the light speed, respectively;

$$\frac{\mathrm{L}}{\lambda_D}, \qquad \frac{\mathrm{T}}{\tau},$$

where the relaxation time

$$\tau = \frac{\ell}{\sqrt{\frac{k_B\bar{\Theta}_e}{m_e}}}$$

is the time necessary for the electron moving at speed $\sqrt{\frac{k_B\bar{\Theta}_e}{m_e}}$ to travel the distance ℓ and the mass ratio m_e/m_i, the temperature ratio $\bar{\Theta}_e/\bar{\Theta}_i$ and the density ratio $\bar{Z} = Z_i\bar{\rho}_i/\bar{\rho}_e$. Indeed, we have

$$\partial_t f + \frac{1}{\varepsilon}\, v\cdot\nabla_x f - \frac{1}{\varepsilon}\,\nabla_v\cdot\Big(\big(E+\varepsilon\,\eta^2\, v\wedge B\big)f\Big) = \frac{\mathrm{T}}{\tau}\Big(C_{ee}(f) + Z_i C_{ei}(f)\Big), \tag{2.2}$$

and

$$\begin{aligned}
&\partial_t E - \mathrm{curl}_x B = -\frac{1}{\varepsilon}\left(\frac{\mathrm{L}}{\lambda_D}\right)^2 \int_{\mathbb{R}^3} v f \mathrm{d}v,\\
&\varepsilon^2\eta^2\partial_t B + \mathrm{curl}_x E = 0,\\
&\nabla_x\cdot B = 0,\\
&\nabla_x\cdot E = \left(\frac{\mathrm{L}}{\lambda_D}\right)^2\left(\bar{Z}\rho_i - \int_{\mathbb{R}^3} f\mathrm{d}v\right).
\end{aligned} \tag{2.3}$$

Remark II.2.1 *It can be convenient to rewrite*

$$\lambda_D = \frac{1}{\omega_P}\sqrt{\frac{k_B\bar{\Theta}_e}{m_e}},$$

with

$$\omega_P = \sqrt{\frac{q^2\bar{\rho}_e}{\mathrm{L}^3 m_e\varepsilon_0}},$$

the plasma frequency, and

$$\ell = \lambda_D^2 \times \frac{1}{r_e} \times \frac{k_B\bar{\Theta}_e}{m_e\, c^2}$$

with $r_e = q^2/(\varepsilon_0 m_e c^2) \simeq 2.82.10^{-15}$ *m., the classical electron radius.*

II.2.2 Approximation of the electron/ion collision operator; Conserved quantities and entropy dissipation

Taking into account $m_e/m_i \ll 1$ and $\bar{\Theta}_e/\bar{\Theta}_i$ fixed to a positive constant, the electron/ion collision operator simplifies to

$$\widetilde{C}_{ei}(f_e)(v) = \bar{Z}\ \rho_i\ \nabla_v\cdot\Big(\Theta_e^{\alpha/2}\frac{\Pi_v}{|v|^{\alpha+1}}\nabla_v f(v)\Big), \tag{2.4}$$

see e. g. [24]. This approximation is often used in practice, and we adopt from now on to replace C_{ei} by $\widetilde{C}_{ei}$ in the kinetic equation (2.2). As a matter of fact, we observe that the system (2.2)- (2.3), with the approximate operator (2.4), conserves energy and dissipates the entropy.

Proposition II.2.1 *Let (f, E, B) be a (smooth enough) solution of (2.2)–(2.3) set on the whole space, with the approximate operator (2.4). Then, we have*

$$\frac{\mathrm{d}}{\mathrm{d}t}\left[\int_{\mathbb{R}^3}\int_{\mathbb{R}^3}\frac{|v|^2}{2}f\mathrm{d}v\mathrm{d}x+\frac{1}{2}\Big(\frac{\lambda_D}{\mathrm{L}}\Big)^2\int_{\mathbb{R}^3}\big(E^2+\varepsilon^2\eta^2B^2\big)\mathrm{d}x\right]=0,$$

and

$$\frac{\mathrm{d}}{\mathrm{d}t}\int_{\mathbb{R}^3}\int_{\mathbb{R}^3}f\ln(f)\mathrm{d}v\mathrm{d}x=\frac{\mathrm{T}}{\tau}\int_{\mathbb{R}^3}\big(C_{ee}(f)+Z_i\widetilde{C}_{ei}(f)\big)\ln(f)\mathrm{d}v\mathrm{d}x\leq 0.$$

This statement is a consequence of the following fundamental properties of the collision operators.

Lemma II.2.1 *Let C_{ee} and $\widetilde{C}_{ei}$ be defined by (2.1) and (2.4), respectively. We have*

$$\int_{\mathbb{R}^3}C_{ee}(f)\begin{pmatrix}1\\ v\\ |v|^2\end{pmatrix}\mathrm{d}v=0, \tag{2.5}$$

$$\int_{\mathbb{R}^3}\widetilde{C}_{ei}(f)\begin{pmatrix}1\\ |v|^2\end{pmatrix}\mathrm{d}v=0, \tag{2.6}$$

$$\begin{aligned}\int_{\mathbb{R}^3}C_{ee}(f)\ln(f)\mathrm{d}v &= -\int_{\mathbb{R}^3}\Theta_e^{\alpha/2}\frac{\Pi_{v-v_\star}}{|v-v_\star|^{\alpha+1}}\Big(\frac{\nabla_v f}{f}(v)-\frac{\nabla_{v_\star}f}{f}(v_\star)\Big)\\ &\qquad\cdot\Big(\frac{\nabla f}{f}(v)-\frac{\nabla f}{f}(v_\star)\Big)\ f(v_\star)f(v)\mathrm{d}v_\star\mathrm{d}v\\ &= -\int_{\mathbb{R}^3}\Big|\Pi_{v-v_\star}\Big(\nabla_v-\nabla_{v_\star}\Big)f(v)f(v_\star)\Big|^2\ \frac{\Theta_e^{\alpha/2}\mathrm{d}v_\star\mathrm{d}v}{|v-v_\star|^{\alpha+1}f(v)f(v_\star)}\\ &\leq 0,\end{aligned} \tag{2.7}$$

$$\begin{aligned}\int_{\mathbb{R}^3}\widetilde{C}_{ei}(f)\ \ln(f)\mathrm{d}v &= -4\bar{Z}\rho_i\int_{\mathbb{R}^3}\Theta_e^{\alpha/2}\frac{\Pi_v}{|v|^{\alpha+1}}\nabla_v\sqrt{f}\cdot\nabla_v\sqrt{f}\mathrm{d}v\\ &= -4\bar{Z}\rho_i\int_{\mathbb{R}^3}\frac{\Theta_e^{\alpha/2}}{|v|^{\alpha+1}}\ \big|\Pi_v\nabla_v\sqrt{f}\big|^2\mathrm{d}v\leq 0.\end{aligned} \tag{2.8}$$

More precisely the entropy dissipation vanishes in (2.7) if and only if the distribution function is a Maxwellian $f(v)=\rho(2\pi\Theta_e)^{-3/2}e^{-|v-u|^2/2\Theta_e}$ for some $\rho,\Theta_e\geq 0$ and $u\in\mathbb{R}^3$; and the entropy dissipation vanishes in (2.8) if and only if the distribution is isotropic: $f(v)=F(|v|)$. Actually, we observe that $\widetilde{C}_{ei}\big(\varphi(|v|)f(v)\big)=\varphi(|v|)\ \widetilde{C}_{ei}\big(f(v)\big)$.

Proof. The proof of (2.5)–(2.8) follows by direct evaluation, using integration by parts and the fact that $(\mathbb{I}-\frac{z\otimes z}{|z|^2})z=0$. Remark that the collision operator $C_{ee}+Z_i\widetilde{C}_{ei}$ does

not preserve the momentum, but it preserves only mass and energy. However we observe that

$$\int_{\mathbb{R}^3} \widetilde{C}_{ei}(f) v \mathrm{d}v = -\bar{Z}\rho_i \int_{\mathbb{R}^3} \Theta_e^{\alpha/2} \frac{\Pi_v}{|v|^{\alpha+1}} \nabla_v f \mathrm{d}v = -2\bar{n}\rho_i \Theta_e^{\alpha/2} \int_{\mathbb{R}^3} \frac{v}{|v|^{\alpha+3}} f \mathrm{d}v$$

which of course vanishes when f is isotropic. In the Maxwellian molecules case ($\alpha = -3$), the momentum variation is proportional to the current density :

$$\int_{\mathbb{R}^3} \widetilde{C}_{ei}(f) v \mathrm{d}v \Big|_{\alpha=-3} = -2\frac{\bar{Z}\rho_i}{\Theta_e^{3/2}} \int_{\mathbb{R}^3} v f \mathrm{d}v.$$

Clearly the collision operator C_{ee} (resp. C_{ei}) and the entropy dissipation vanish when f is a Maxwellian (resp. isotropic function). Let us prove the reverse implication. Saying that the entropy dissipation associated to the electron–electron collisions vanishes means that $\frac{1}{f(v)f(v_\star)}(\nabla_v - \nabla_{v_\star})f(v)f(v_\star) = \nabla_v \ln(f(v)) - \nabla_{v_\star} \ln(f(v_\star))$ is proportional to $v - v_\star$ (which means that it is equal to $\alpha(v, v_\star)(v - v_\star)$ for some scalar function α). Let us set $g(v) = \ln(f(v))$. Clearly any affine function $b \cdot v + c$, with $b \in \mathbb{R}^3$, $c \in \mathbb{R}$, satisfies this relation. Possibly at the price of adding such a function we assume from now on that $\nabla_v g(0) = 0$. In particular, we obtain $\nabla_v g(v) = \tilde{\alpha}(v)v$, $\tilde{\alpha}(v) \in \mathbb{R}$. Writing $g(v) = \tilde{g}(|v|^2/2, v/|v|)$ it implies that $\tilde{g}$ does not depend on the second argument, hence $g(v) = \tilde{g}(|v|^2/2)$ is radially symmetric. (By the way, it proves that the entropy dissipation of the electron–ion collision operator vanishes only if f is isotropic.) Therefore, we are led to $v\big(\alpha(v, v_\star) - \tilde{g}'(|v|^2/2)\big) - v_\star\big(\alpha(v, v_\star) - \tilde{g}'(|v_\star|^2/2)\big) = 0$. Up to the negligible set in $\mathbb{R}^3 \times \mathbb{R}^3$ where v and $v_\star$ are colinear, this relation implies that $\tilde{g}'(|v|^2/2) = \tilde{g}'(|v_\star|^2/2)$ is constant, hence $\tilde{g}(|v|^2/2) = a|v|^2$, $a \in \mathbb{R}$. We conclude that the functions that make the electron–electron entropy dissipation vanish are given by $f(v) = \exp(a|v|^2 + b \cdot v + c)$ (with $a < 0$ to guaranty integrability), which can be recast as $\rho(2\pi\Theta_e)^{-3/2} e^{-|v-u|^2/2\Theta_e}$, with a suitable relation $(a, b, c) \mapsto (\rho, u, \Theta_e)$. ∎

Based on (2.5) and (2.6), we can look at the first three moments of the equation (1.1). Using charge density, current density and temperature definition, we have :

$$\begin{cases} \partial_t \rho + \dfrac{1}{\varepsilon} \nabla_x \cdot (\rho u) = 0, \\ \rho \left(\partial_t u + \dfrac{1}{\varepsilon} (u \cdot \nabla_x) u \right) + \dfrac{1}{\varepsilon} \nabla_x \cdot \mathsf{P} = \dfrac{\mathrm{T}}{\tau} Z_i \displaystyle\int_{\mathbb{R}^3} v \widetilde{C}_{ei}(f) \mathrm{d}v - \dfrac{1}{\varepsilon} \rho \left(E + \varepsilon \eta^2 u \wedge B \right), \\ \partial_t \left(3\rho\Theta_e + \rho|u|^2 \right) + 2\nabla_x \cdot \mathsf{Q} + \dfrac{1}{\varepsilon} \nabla_x \cdot (3\rho\Theta_e u + 2\mathsf{P}u) = -2\rho E \cdot u - \nabla_x \cdot \left(\rho |u|^2 u \right), \end{cases} \tag{2.9}$$

coupled with equations (2.3). These equations are not closed since the pressure tensor P and the heat flux Q are defined by

$$\mathsf{P} = \int_{\mathbb{R}^3} (v - u) \otimes (v - u) f \mathrm{d}v, \qquad \mathsf{Q} = \frac{1}{2\varepsilon} \int_{\mathbb{R}^3} |v - u|^2 (v - u) f \mathrm{d}v$$

respectively. The system also involves the microscopic distribution function through the integral term $\int v \widetilde{C}_{ei}(f) \mathrm{d}v$. These terms in general cannot be expressed by means of the low order moments and the macroscopic quantities ρ, u, Θ_e.

II.2.3 Asymptotic regime: Hilbert expansion

The asymptotic regime we are interested in assumes

$$\varepsilon \ll 1, \qquad \lambda_\varepsilon = \frac{\lambda_D}{\mathrm{L}} \ll 1, \qquad \frac{\tau}{\mathrm{T}} \simeq \varepsilon^2 \ll 1,$$

while η, Z_i and $\bar{Z}$ are kept fixed. We are thus concerned with the behavior of the solutions of

$$\begin{aligned}
&\partial_t f + \frac{1}{\varepsilon}\, v\cdot\nabla_x f - \frac{1}{\varepsilon}\,\nabla_v\cdot\Big(\big(E+\varepsilon\,\eta^2\, v\wedge B\big)f\Big) = \frac{1}{\varepsilon^2}\Big(C_{ee}(f)+Z_i\widetilde{C}_{ei}(f)\Big),\\
&\partial_t E - \mathrm{curl}_x B = -\frac{1}{\varepsilon\lambda_\varepsilon^2}\int_{\mathbb{R}^3} v f \mathrm{d}v,\\
&\varepsilon^2\eta^2\partial_t B + \mathrm{curl}_x E = 0,\\
&\nabla_x\cdot B = 0,\\
&\nabla_x\cdot E = \frac{1}{\lambda_\varepsilon^2}\Big(\bar{Z}\rho_i - \int_{\mathbb{R}^3} f\mathrm{d}v\Big),
\end{aligned}$$

with $\varepsilon\to 0$ and $\lambda_\varepsilon\to 0$, the other parameters being fixed. As it will be detailed below, in this regime the system (2.9) reduces to

$$\rho = \bar{Z}\rho_i, \qquad \partial_t\Theta + \frac{2\nabla_x\cdot Q}{3\rho} = 0, \tag{2.10}$$

where the flux Q is proportional to the gradient of a certain power of Θ, hence a non linear diffusion equation for the electron temperature. Relevant intermediate models can be thought of as closure relations defining the flux Q by means of Θ.

Of course, we have in mind the Landau-Fokker-Planck operator (2.1) and the approximate operator (2.4) which are the most relevant for the application to plasma physics. But it is worth bringing out the key assumptions on the collisions operators which are needed to derive the asymptotic models, without specializing too much. The basic assumptions state as follows

A1) $C_{ee}(f)$ vanishes if and only if f is a Maxwellian, $\widetilde{C}_{ei}(f)$ vanishes if and only if f is isotropic, $(C_{ee}+Z_iC_{ei})(f)$ vanishes if and only if f makes the two vanish, which means that f is a centered Maxwellian,

A2) $\int_{\mathbb{R}^3} C_{ee}(f)\,(1,v,|v|^2)\mathrm{d}v = 0$, $\int_{\mathbb{R}^3}\widetilde{C}_{ei}(f)\,(1,|v|^2)\mathrm{d}v = 0$,

A3) $\int_{\mathbb{R}^3} C_{ee}(f)\ln(f)\mathrm{d}v \le 0$, $\int_{\mathbb{R}^3}\widetilde{C}_{ei}(f)\ln(f)\mathrm{d}v \le 0$.

Clearly, Proposition II.2.1 holds for any operators satisfying (A2)–(A3). We refer to Lemma II.2.1 for the case of (2.1) and (2.4). It is interesting to consider other operators like e. g.

- Boltzmann operator

$$C_{ee}^B(f) = \int_{\mathbb{R}^3\times\mathbb{S}^2} B\big(|v-v_\star|,(v-v_\star)\cdot\omega\big)\,\big(f(v'_\star)f(v') - f_\star(v_\star)f(v)\big)\mathrm{d}\omega\mathrm{d}v_\star,$$

  with $v' = v-\omega(v-v_\star)\cdot\omega$, $v'_\star = v_\star+\omega(v-v_\star)\cdot\omega$ and $\mathrm{d}\omega$ is the normalized mesure on $\mathbb{S}^2$.

- BGK operator

$$C_{ee}^{BGK}(f) = \frac{M[f] - f}{\tau_{ee}(\rho, \Theta)}, \qquad M[f](v) = \frac{\rho}{(2\pi\Theta)^{3/2}} e^{-|v-u|^2/2\Theta}$$

  with $(\rho, \rho u, \rho|u|^2 + 3\rho\Theta) = \int_{\mathbb{R}^3} (1, v, |v|^2)\, f \mathrm{d}v$.

- Fokker-Planck operator

$$C_{ee}^{FP}(f) = \nabla_v \cdot \big((v-u)f + \Theta \nabla_v f\big).$$

Similarly, the electron-ion operator (2.4) could be replaced by the following simplified Boltzmann operator

$$\widetilde{C}_{ei}^{R}(f)(v) = \frac{1}{\tau_{ei}(\rho, \Theta, |v|)} \Big(\int_{\mathbb{S}^2} f(|v|\omega) \mathrm{d}\omega - f(v) \Big),$$

where τ_{ei} is a positive function. This expression can be obtained from the Boltzmann operator for electron-ion collision in the asymptotic $m_e/m_i \ll 1$, see [10, 16].

We obtain (formally) the asymptotic equation by developing the solution in power series of ε:

$$f(t, x, v) = \sum_j \varepsilon^j F_j(t, x, v)$$

and identifying terms that arise in the equation with the same power of ε. At leading order we get

$$(C_{ee} + Z_i \widetilde{C}_{ei})(F_0) = 0.$$

Therefore, the leading term is a centered Maxwellian, by (A1). Moreover, by using $\lambda_\varepsilon \ll 1$, the Maxwell system leads to the quasi-neutrality relations

$$\rho = \int F_0 \mathrm{d}v = \bar{Z}\rho_i, \qquad J = \int v F_0 \mathrm{d}v = 0. \tag{2.11}$$

We conclude that

$$F_0(t, x, v) = \frac{\rho(x)}{(2\pi\Theta(t,x))^{3/2}} \exp\left(-\frac{|v|^2}{2\Theta(t,x)} \right), \qquad \rho = \bar{Z}\rho_i.$$

Hence the goal is to determine the evolution equation satisfied by the temperature Θ.

To this end, for ρ and Θ positive, we set $M_{\rho,\Theta}(v) = \frac{\rho}{(2\pi\Theta)^{3/2}} e^{-|v|^2/2\Theta}$ and we introduce the linearized operator

$$L_{\rho,\Theta} f(v) = \frac{\mathrm{d}}{\mathrm{d}z} (C_{ee} + Z_i \widetilde{C}_{ei})(M_{\rho,\Theta} + zf)(v) \Big|_{z=0}.$$

Owing to assumptions (A1)-(A3), we observe that the linearized operator satisfies

$$\int_{\mathbb{R}^3} \begin{pmatrix} 1 \\ |v|^2 \end{pmatrix} L_{\rho,\Theta} f(v) \mathrm{d}v = 0,$$

and

$$\int_{\mathbb{R}^3} \frac{f}{M_{\rho,\Theta}}\, L_{\rho,\Theta} f(v)\mathrm{d}v = \frac{1}{2}\frac{\mathrm{d}^2}{\mathrm{d}z^2}\int_{\mathbb{R}^3} (C_{ee} + Z_i\widetilde{C}_{ei})(M_{\rho,\Theta}+zf)\ln(M_{\rho,\Theta}+zf)\mathrm{d}v\Big|_{z=0} \leq 0.$$

Differentiating $(C_{ee}+Z_i\widetilde{C}_{ei})(M_{\rho,\Theta})=0$ with respect to ρ and Θ we observe that $L_{\rho,\Theta}\big(\big[\frac{\varrho}{\rho}+\frac{\theta}{2\Theta}\big(\frac{|v|^2}{\Theta}-\frac{3}{2}\big)\big]M_{\rho,\Theta}\big)=0$ for any ϱ and θ. We slightly strengthen these properties that follow from (A1-A3) by requiring

B1) $\qquad \mathrm{Ker}(L_{\rho,\Theta}) = \mathrm{Span}\big(M_{\rho,\Theta}, |v|^2 M_{\rho,\Theta}\big).$

It is satisfied by most of the classical collision operators, which furthermore are usually self-adjoint. For the Landau-Fokker-Planck operator (2.1) and (2.4) we have

$$\begin{aligned} L_{\rho,\Theta} f(v) \;&=\; \nabla_v \cdot \int \Theta^{\alpha/2} \frac{\Pi_{v-v_\star}}{|v-v_\star|^{\alpha+1}}\, M_{\rho,\Theta}(v) M_{\rho,\Theta}(v_\star) \\ &\qquad\qquad \times\Big(\nabla_v \frac{f}{M_{\rho,\Theta}}(v) - \nabla_{v_\star}\frac{f}{M_{\rho,\Theta}}(v_\star)\Big)\mathrm{d}v_\star \\ &\quad + Z_i\bar\rho\Theta^{\alpha/2}\nabla_v\cdot\Big(\frac{\Pi_v}{|v|^{\alpha+1}}\nabla_v f\Big). \end{aligned}$$

Observe that

$$\begin{aligned} &-\int \frac{f}{M_{\rho,\Theta}}\, L_{\rho,\Theta} f \mathrm{d}v \\ &\quad = \frac{\Theta^{\alpha/2}}{2}\int \Big|\Pi_{v-v_\star}\Big(\nabla_v\frac{f}{M_{\rho,\Theta}}(v) - \nabla_{v_\star}\frac{f}{M_{\rho,\Theta}}(v_\star)\Big)\Big|^2\, \frac{M_{\rho,\Theta}(v)M_{\rho,\Theta}(v_\star)\mathrm{d}v_\star\mathrm{d}v}{|v-v_\star|^{\alpha+1}} \\ &\qquad + Z_i\rho\Theta^{\alpha/2}\int \frac{\Pi_v}{|v|^{\alpha+1}}\nabla_v\frac{f}{M_{\rho,\Theta}}\cdot\nabla_v\frac{f}{M_{\rho,\Theta}}\mathrm{d}v. \end{aligned}$$

Coming back to the Hilbert expansion, we obtain

$$\begin{aligned} L_{\rho,\Theta}F_1 &= v\cdot\nabla_x F_0 - E\cdot\nabla_v F_0 \\ &= v\; F_0(t,x,v)\cdot\Big(\frac{\nabla_x\rho}{\rho} - \frac{3}{2}\frac{\nabla_x\Theta}{\Theta} + \frac{E}{\Theta}\Big) + v\frac{|v|^2}{2}\; F_0(t,x,v)\cdot\frac{\nabla_x\Theta}{\Theta^2}, \end{aligned} \tag{2.12}$$

with $F_0(t,x,v) = M_{\rho(x),\Theta(t,x)}(v)$. Bearing in mind (A2), we remark that the zeroth and second moments of $v\cdot\nabla_x F_0 - E\cdot\nabla_v F_0$ vanish so that (2.12) makes sense. We need further assumptions:

B2) For any Φ verifying $\int_{\mathbb{R}^3}\Phi\mathrm{d}v = \int_{\mathbb{R}^3}|v|^2\Phi\mathrm{d}v = 0$, there exists a unique Γ such that $L_{\rho,\Theta}\Gamma = \Phi$ with the constraints $\int_{\mathbb{R}^3}\Gamma\mathrm{d}v = \int_{\mathbb{R}^3}|v|^2\Gamma\mathrm{d}v = 0$.

This assumption has the flavor of the Fredholm alternative that would identify the range $\mathrm{Ran}(L_{\rho,\Theta})$ to the orthogonal to the kernel $\mathrm{Span}(M_{\rho,\Theta}, |v|^2M_{\rho,\Theta})$. Note however that proving that $\mathrm{Ran}(L_{\rho,\Theta})$ is closed depends on the collision kernels. It is satisfied when the collision operator satisfies the following spectral gap inequality: there exists $\lambda_{\rho,\Theta}>0$ such that

$$-\int_{\mathbb{R}^3} L_{\rho,\Theta}F\;\frac{F}{M_{\rho,\Theta}}\mathrm{d}v \geq \lambda_{\rho,\Theta}\;\int_{\mathbb{R}^3}\frac{|F|^2}{M_{\rho,\Theta}}\mathrm{d}v \tag{2.13}$$

holds for any F verifying $\int_{\mathbb{R}^3} F\mathrm{d}v = \int_{\mathbb{R}^3} |v|^2 F\mathrm{d}v = 0$. Typically it holds for the BGK operator or the Boltzmann operator in the case of Maxwell molecules or hard potentials with an angular cutoff, see [7], and we refer to [11] for the Landau-Fokker-Planck operator. The case of soft potentials imposes to work with suitable weighted spaces and the proofs involve quite intricate arguments, see [15]. In appendix II.A.1, we detail the arguments for the Landau-Fokker-Planck operator by using the fine estimates derived in [1, 17, 25]. For the time being, we do not detail the functional difficulties associated to (B2). The useful consequence of (B2) relies on the fact that there exist (vector valued) functions $G_{\rho,\Theta}$ and $H_{\rho,\Theta}$ verifying $L_{\rho,\Theta}G_{\rho,\Theta} = vM_{\rho,\Theta}(v)$ and $L_{\rho,\Theta}H_{\rho,\Theta} = v|v|^2 M_{\rho,\Theta}(v)$. As a matter of fact, we observe that the matrices $\int v \otimes G_{\rho,\Theta}\mathrm{d}v$ and $\int v|v|^2 \otimes H_{\rho,\Theta}\mathrm{d}v$ are negative definite, since we can rewrite

$$\int v \otimes G_{\rho,\Theta}\mathrm{d}v = \int L_{\rho,\Theta}(G_{\rho,\Theta}) \otimes G_{\rho,\Theta}\frac{\mathrm{d}v}{M_{\rho,\Theta}}$$

and

$$\int v|v|^2 \otimes H_{\rho,\Theta}\mathrm{d}v = \int L_{\rho,\Theta}(H_{\rho,\Theta}) \otimes H_{\rho,\Theta}\frac{\mathrm{d}v}{M_{\rho,\Theta}}$$

which are negative matrices by virtue of the dissipation properties (2.7) and (2.8). Furthermore, using symmetry and homogeneity arguments, we can derive simpler formulae.

Lemma II.2.2 *We suppose that the collision operator satisfies the following properties:*

i) $L_{\rho,\Theta}f = \rho L_{1,\Theta}f$,

ii) denoting τ_Θ *the application defined by* $\tau_\Theta f(v) = f(\sqrt{\Theta}v)$, *we have* $\tau_\Theta\big(L_{1,\Theta}(f)\big) = \frac{1}{\Theta^{3/2}}L_{1,1}\big(\tau_\Theta f\big)$,

iii) for any isometry $R \in O(\mathbb{R}^3)$, *we have* $L_{1,\Theta}(f \circ R) = L_{1,\Theta}(f) \circ R$.

Then, there exists functions $g, h : \mathbb{R}^+ \to \mathbb{R}$ *such that*

$$G_{\rho,\Theta}(v) = g\Big(\frac{|v|}{\sqrt{\Theta}}\Big)\ v\ e^{-|v|^2/2\Theta},$$

and

$$H_{\rho,\Theta}(v) = \Theta\ h(|v|/\sqrt{\Theta})\ v\ e^{-|v|^2/2\Theta}. \tag{2.14}$$

Consequently, there exists some constants q_1, q_2, q_3, q_4, *with* $q_1 > 0$, $q_4 > 0$ *such that*

$$\int v \otimes G_{\rho,\Theta}\mathrm{d}v = -q_1\Theta^{5/2}\ \mathbb{I}, \quad \int v|v|^2 \otimes G_{\rho,\Theta}\mathrm{d}v = -q_2\Theta^{7/2}\ \mathbb{I},$$
$$\int v \otimes H_{\rho,\Theta}\mathrm{d}v = -q_3\Theta^{7/2}\ \mathbb{I}, \quad \int v|v|^2 \otimes H_{\rho,\Theta}\mathrm{d}v = -q_4\Theta^{9/2}\ \mathbb{I}.$$

Proof. By i), the equation defining $G_{\rho,\Theta}$ becomes $L_{1,\Theta}G_{\rho,\Theta} = vM_{1,\Theta}(v)$. We deduce that it does not depend on ρ. Next, ii) yields $L_{1,1}\big(\frac{1}{\sqrt{\Theta}}\tau_\Theta G_{\rho,\Theta}\big)(v) = vM_{1,1}(v)$ which means

$G_{\rho,\Theta}(v) = \sqrt{\Theta}G_{1,1}(v/\sqrt{\Theta})$. Eventually, repeating the arguments in [12, Lemma 3], iii) implies $G_{1,1}(v) = vg(|v|)M_{1,1}(v)$. Similar reasoning applies for $H_{\rho,\Theta}$. Now, we compute

$$\begin{aligned}
\int v\otimes G_{\rho,\Theta}\mathrm{d}v &= \int v\otimes v\ g\Big(\frac{|v|}{\sqrt{\Theta}}\Big)e^{-|v|^2/2\Theta}\mathrm{d}v = \Theta^{5/2}\int v\otimes v\ g(|v|)e^{-|v|^2/2}\mathrm{d}v,\\
\int v|v|^2\otimes G_{\rho,\Theta}\mathrm{d}v &= \Theta^{7/2}\int v\otimes v\ |v|^2\ g(|v|)e^{-|v|^2/2}\mathrm{d}v,\\
\int v\otimes H_{\rho,\Theta}\mathrm{d}v &= \Theta^{7/2}\int v\otimes v\ h(|v|)e^{-|v|^2/2}\mathrm{d}v,\\
\int v|v|^2\otimes H_{\rho,\Theta}\mathrm{d}v &= \Theta^{9/2}\int v\otimes v\ |v|^2\ h(|v|)e^{-|v|^2/2}\mathrm{d}v.
\end{aligned}$$

The matrices in the right hand side are clearly diagonal and we set $q_1 = -\frac{1}{3}\int |v|^2 g(|v|)e^{-|v|^2/2}\mathrm{d}v$, $q_2 = -\frac{1}{3}\int |v|^4 g(|v|)e^{-|v|^2/2}\mathrm{d}v$, $q_3 = -\frac{1}{3}\int |v|^2 h(|v|)e^{-|v|^2/2}\mathrm{d}v$ and $q_4 = -\frac{1}{3}\int |v|^4 g(|v|)e^{-|v|^2/2}\mathrm{d}v$. As discussed above, q_1 and q_4 are positive as a consequence of the dissipation properties of the collision operator. ∎

We postpone to appendix II.A.2 the proof of the following claim which makes the previous statement relevant for our purpose.

Lemma II.2.3 *The assumptions of Lemma II.2.2 hold for the operators* (2.1) *and* (2.4).

Having disposed of these preliminaries, we go back to the equation (2.12). We remind that $F_0(t,x,v) = M_{\rho(x),\Theta(t,x)}$ is the Maxwellian with density $\rho(x)$ and temperature $\Theta(t,x)$. The functions G and H we consider are actually parameterized by t, x. Therefore, we get

$$F_1(t,x,v) = G_{\rho,\Theta}(t,x,v)\cdot\Big(\frac{\nabla_x\rho}{\rho} - \frac{3}{2}\frac{\nabla_x\Theta}{\Theta} + \frac{E}{\Theta}\Big)(t,x) + H_{\rho,\Theta}(t,x,v)\cdot\frac{\nabla_x\Theta}{\Theta^2}(t,x).$$

Now the electric field has to be determined by the constraint of vanishing current. Indeed, the Maxwell equation tells us that

$$\begin{aligned}
\lambda_\varepsilon^2\Big(\partial_t E - \mathrm{curl}_x B\Big) &= \mathcal{O}(\lambda_\varepsilon^2)\\
&= -\int\frac{v}{\varepsilon}f\mathrm{d}v \simeq -\int vF_1\mathrm{d}v.
\end{aligned}$$

Hence, we impose

$$\int vF_1\mathrm{d}v = 0$$

which yields the following definition of the asymptotic electric field

$$\begin{aligned}
E(t,x) = -\Theta(t,x)\Bigg(&\Big(\frac{\nabla_x\rho}{\rho} - \frac{3}{2}\frac{\nabla_x\Theta}{\Theta}\Big)(t,x)\\
&+\Big(\int v\otimes G_{\rho,\Theta}(t,x,v)\mathrm{d}v\Big)^{-1}\int v\otimes H_{\rho,\Theta}(t,x,v)\mathrm{d}v\frac{\nabla_x\Theta}{\Theta^2}(t,x)\Bigg).
\end{aligned}$$

Having obtained the expression of the corrector F_1, we use the compatibility condition for the relation

$$L_{\rho,\Theta}F_2 + R_{ee}(F_1) = \partial_t F_0 + v\cdot\nabla_x F_1 - E\cdot\nabla_v F_1$$

with R_{ee} the second derivative of C_{ee} evaluated at $M_{\rho,\Theta}$. (The magnetic field effect disappears at this order.)
The energy conservation leads to the evolution equation for the temperature. Indeed, we have

$$\partial_t \int |v|^2 F_0 \mathrm{d}v = -\nabla_x \cdot \int v|v|^2 F_1 \mathrm{d}v,$$

which recasts as

$$\begin{aligned} 3\rho\partial_t\Theta &= \nabla_x\cdot\Big[-\int v|v|^2\otimes G_{\rho,\Theta}(t,x,v)\mathrm{d}v\Big(\frac{\nabla_x\rho}{\rho}-\frac{3}{2}\frac{\nabla_x\Theta}{\Theta}+\frac{E}{\Theta}\Big) \\ &\qquad -\int v|v|^2\otimes H_{\rho,\Theta}(t,x,v)\mathrm{d}v\frac{\nabla_x\Theta}{\Theta^2}\Big] \\ &= \nabla_x\cdot\Big[\int v|v|^2\otimes G_{\rho,\Theta}(t,x,v)\mathrm{d}v\left(\int v\otimes G_{\rho,\Theta}(t,x,v)\mathrm{d}v\right)^{-1} \\ &\qquad\qquad \times\int v\otimes H_{\rho,\Theta}(t,x,v)\mathrm{d}v\frac{\nabla_x\Theta}{\Theta^2} \\ &\qquad -\int v|v|^2\otimes H_{\rho,\Theta}(t,x,v)\mathrm{d}v\frac{\nabla_x\Theta}{\Theta^2}.\Big] \end{aligned}$$

Owing to Lemma II.2.2 and II.2.3 we arrive at the following non linear diffusion equation

$$\partial_t\Theta = \frac{1}{3\rho}\nabla_x\cdot\Big[\Big(q_4-\frac{q_2q_3}{q_1}\Big)\Theta^{5/2}\nabla_x\Theta\Big].$$

This heat flux

$$Q_{SH} = -\frac{\bar q}{2}\Theta^{5/2}\nabla_x\Theta, \tag{2.15}$$

with $\bar q = q_4 - \frac{q_2q_3}{q_1}$ corresponds to the so-called Spitzer-Härm heat flux, see [28].

Written in this way, it is not clear that the flux is defined with a positive coefficient. There is a alternative way to obtain the diffusion coefficient. Indeed, multiplying (2.12) by v and integrating, we obtain the following expression for the electric field

$$E = \Theta\left(\int_{\mathbb{R}^3} v\otimes vF_0\mathrm{d}v\right)^{-1}\left[\int_{\mathbb{R}^3} vL_{\rho,\Theta}F_1\mathrm{d}v - \int_{\mathbb{R}^3} v\otimes v\frac{|v|^2}{2}F_0\mathrm{d}v\frac{\nabla_x\Theta}{\Theta^2}\right]+\frac{3}{2}\nabla_x\Theta-\Theta\frac{\nabla_x\rho}{\rho}.$$

It recasts as

$$\begin{aligned} E &= \frac{\Theta}{\rho\Theta}\left(\int_{\mathbb{R}^3} vL_{\rho,\Theta}F_1\mathrm{d}v - \frac{5}{2}\rho\Theta^2\frac{\nabla_x\Theta}{\Theta^2}\right)+\frac{3}{2}\nabla_x\Theta-\Theta\frac{\nabla_x\rho}{\rho} \\ &= \frac{1}{\rho}\int_{\mathbb{R}^3} vL_{\rho,\Theta}F_1\mathrm{d}v - \nabla_x\Theta-\Theta\frac{\nabla_x\rho}{\rho}. \end{aligned}$$

Therefore, (2.12) becomes

$$\mathcal{L}_{\rho,\Theta}F_1 = \frac{v}{2\Theta}\Big(\frac{|v|^2}{\Theta}-5\Big)F_0\cdot\nabla_x\Theta,$$

where we have set

$$\mathcal{L}_{\rho,\Theta}F = L_{\rho,\Theta}F - \frac{vF_0}{\rho\Theta}\int_{\mathbb{R}^3} v_\star L_{\rho,\Theta}F(v_\star)\mathrm{d}v_\star.$$

In particular we observe that

$$\int_{\mathbb{R}^3}\begin{pmatrix}1\\ v\\ |v|^2\end{pmatrix}\mathcal{L}_{\rho,\Theta}F\mathrm{d}v = 0, \qquad \int_{\mathbb{R}^3}\begin{pmatrix}1\\ v\\ |v|^2\end{pmatrix}\frac{v}{2\Theta}\Big(\frac{|v|^2}{\Theta}-5\Big)F_0\mathrm{d}v = 0.$$

We assume the following analog of (B2) for the modified operator:

B3) For any Φ verifying $\int_{\mathbb{R}^3}\Phi\mathrm{d}v = \int_{\mathbb{R}^3}|v|^2\Phi\mathrm{d}v = 0$ and $\int_{\mathbb{R}^3} v\Phi\mathrm{d}v = 0$, there exists a unique Γ such that $\mathcal{L}_{\rho,\Theta}\Gamma = \Phi$ with the constraints $\int_{\mathbb{R}^3}\Gamma\mathrm{d}v = \int_{\mathbb{R}^3}|v|^2\Gamma\mathrm{d}v = 0$ and $\int_{\mathbb{R}^3} v\Gamma\mathrm{d}v = 0$.

Clearly it holds when the estimate (2.13) is satisfied. We can define χ as the solution of

$$\mathcal{L}_{1,1}\chi = \frac{v}{2}(|v|^2-5)\frac{e^{-|v|^2/2}}{(2\pi)^{3/2}}, \qquad \int_{\mathbb{R}^3}\begin{pmatrix}1\\ v\\ |v|^2\end{pmatrix}\chi(v)\mathrm{d}v = 0$$

and, reasoning as in Lemma II.2.2, we get

$$\mathcal{L}_{\rho,\Theta}\Big[\frac{1}{\sqrt{\Theta(t,x)}}\chi\Big(\frac{\cdot}{\sqrt{\Theta(t,x)}}\Big)\Big](v) = \frac{1}{\sqrt{\Theta(t,x)}}\,\frac{v}{2\sqrt{\Theta}}\Big(\frac{|v|^2}{\Theta}-5\Big)\frac{\rho}{(2\pi\Theta)^{3/2}}e^{-|v|^2/(2\Theta)},$$

and accordingly

$$F_1(t,x,v) = \frac{1}{\sqrt{\Theta(t,x)}}\chi\Big(\frac{v}{\sqrt{\Theta(t,x)}}\Big)\cdot\nabla_x\Theta(t,x).$$

Finally, we obtain (using the fact that the flux $\int vF_1\mathrm{d}v$ vanishes)

$$\begin{aligned}\int_{\mathbb{R}^3} v|v|^2F_1\mathrm{d}v &= 2\Theta^{3/2}\int_{\mathbb{R}^3}\frac{v}{2\sqrt{\Theta}}\Big(\frac{|v|^2}{\Theta}-5\Big)\otimes\frac{1}{\sqrt{\Theta(t,x)}}\chi\Big(\frac{v}{\sqrt{\Theta(t,x)}}\Big)\mathrm{d}v\nabla_x\Theta\\ &= 2\Theta^{5/2}\int_{\mathbb{R}^3}\frac{v}{2}(|v|^2-5)\otimes\chi(v)\mathrm{d}v\nabla_x\Theta.\end{aligned}$$

We observe that the matrix

$$\int_{\mathbb{R}^3}\frac{v}{2}(|v|^2-5)\otimes\chi(v)\mathrm{d}v = \int_{\mathbb{R}^3}\mathcal{L}_{1,1}\chi\otimes\chi(v)\mathrm{d}v$$

is non negative. Indeed, for any $\xi\in\mathbb{R}^3\setminus\{0\}$, we have

$$\begin{aligned}\int_{\mathbb{R}^3}\mathcal{L}_{1,1}\chi\otimes\chi(v)\mathrm{d}v\xi\cdot\xi &= \int_{\mathbb{R}^3}\mathcal{L}_{1,1}(\chi\cdot\xi)(\chi\cdot\xi)(v)\mathrm{d}v\\ &= \int_{\mathbb{R}^3}L_{1,1}(\chi\cdot\xi)(\chi\cdot\xi)(v)\mathrm{d}v - \int_{\mathbb{R}^3}v\chi\cdot\xi\mathrm{d}v\int_{\mathbb{R}^3}vL_{1,1}(\chi\cdot\xi)\mathrm{d}v\\ &= \int_{\mathbb{R}^3}L_{1,1}(\chi\cdot\xi)(\chi\cdot\xi)(v)\mathrm{d}v \geq 0.\end{aligned}$$

Actually, as observed in Lemma II.2.2, see iii), it can be expressed as a mere scalar matrix since we have $\chi(v) = v\Xi(|v|)e^{-|v|^2/2}$, with $Z : \mathbb{R} \to \mathbb{R}$.

For some collision operators, we can explicitly solve the equations that define the corrector F_1 and in turn, we get an explicit formula for the diffusion coefficient. For example, consider the following combination :

$$\begin{aligned} C_{ee}(f)(v) &= \frac{1}{\tau_e}(M[f] - f)(v), \\ C_{ei}(f)(v) &= \frac{\bar{Z}\rho_i}{\tau_i}\left(\int_{\mathbb{S}^2} f(|v|\omega)\mathrm{d}\omega - f(v)\right), \end{aligned}$$

with $\tau_e \in \mathbb{R}$ and $\tau_i \in \mathbb{R}$. The linearized operator then reads

$$L_{\rho,\Theta}f = \frac{1}{\tau_e}\big(\mathbf{P}(f/M_{\rho,\Theta})M_{\rho,\Theta} - f\big) + Z_i\frac{\bar{Z}\rho_i}{\tau_i}\left(\int_{\mathbb{S}^2} f(|v|\omega)\mathrm{d}\omega - f(v)\right)$$

where $\mathbf{P}$ is the orthogonal projection of $L^2(M_{\rho,\Theta}\mathrm{d}v)$ on $\mathrm{Span}\{1, v, |v|^2\}$:

$$\mathbf{P}g = \frac{\tilde{\rho}}{\rho} + \frac{v\cdot\tilde{u}}{\Theta} + \frac{\tilde{\theta}}{2\Theta}\Big(\frac{|v|^2}{\Theta} - 3\Big)$$

with

$$\begin{pmatrix} \tilde{\rho} \\ \rho\tilde{u} \\ 3\tilde{\rho}\Theta + 3\rho\tilde{\theta} \end{pmatrix} = \int_{\mathbb{R}^3} \begin{pmatrix} 1 \\ v \\ |v|^2 \end{pmatrix} gM_{\rho,\Theta}\mathrm{d}v.$$

Then we obtain

$$\chi(v) = -\frac{\tau_e}{2}\frac{v(|v|^2 - 5)}{1 + Z_i\tau_e/\tau_i}\frac{e^{-|v|^2/2}}{(2\pi)^{3/2}},$$

and thus

$$\begin{aligned} E &= -\Theta\left(\nabla_x \ln\rho + \nabla_x \ln\Theta\right), \\ \bar{q} &= \frac{16\sqrt{2}}{3\sqrt{\pi}}\frac{\tau_e}{1 + Z_i\tau_e/\tau_i}\int_0^\infty \xi^{5/2}\left(\xi - \frac{5}{2}\right)e^{-\xi}\mathrm{d}\xi = 80\sqrt{2}\frac{\tau_e}{1 + Z_i\tau_e/\tau_i}. \end{aligned}$$

For a general collision operator however there is no such explicit formula and the numerical evaluation of the coefficient might remain a difficulty. Continuing the Hilbert expansion at a higher order usually leads to an ill-posed problem. A rigorous proof of the asymptotic regime is certainly a tough piece of analysis; we refer for related problems to [5, 6]. We are now going to discuss an ε-dependent macroscopic model that can be found in the physics literature.

II.3 An asymptotic nonlocal model : the Schurtz-Nicolaï model

For some applications in plasma physics, we need a more precise model of conduction, retaining more of the microscopic features. Let us describe here the derivation of an

intermediate model, which is widely used in several plasma physics codes. According to experimental results, the idea consists in expressing the heat flux as a space convolution of the Spitzer-Härm heat flux, with a kernel $W_\varepsilon(x, x')$ that tends to a Dirac function as ε goes to 0:

$$Q(t,x) = \int_{\mathbb{R}^3} W_\varepsilon\left(x, x'\right) Q_{SH}(t, x')\mathrm{d}x'$$

This expression is inserted in (2.3) to close the equation, Q_{SH} being still defined by (2.15). This approach dates back to Luciani and Mora [21] and it has been revisited since then by many authors [14, 22, 23, 27]. The point is precisely to propose a relevant definition of the kernel W_ε. In what follows, we present a derivation inspired from the work of Schurtz and Nicolaï [27]: the idea is to describe the heat flux as the result of the transport of the energy associated to the solution of (2.12). We set $\Omega = \frac{v}{|v|}$ and $r = |v|$ and we introduce $\mathcal{E}_{t,r}(x, \Omega)$, solution of

$$\mathcal{E} + \varepsilon\Omega \cdot \nabla_x \mathcal{E} = r^2 F_1(t, x, r\Omega). \tag{3.1}$$

Here r^2F_1/ε is seen as a source of energy and $\mathcal{E}$ can be interpreted as the radiative intensity associated to this source, subject to a damping of order $1/\varepsilon$. As a matter of fact, when $\varepsilon = 0$, $\mathcal{E}$ coincides to r^2F_1. The nonlocal heat flux is defined by

$$Q(t,x) = \frac{1}{2}\int_{\mathbb{R}^3} v\mathcal{E}\mathrm{d}v = \frac{1}{2}\int_0^\infty \int_{\mathbb{S}^2} r^3\mathcal{E}\mathrm{d}r\ \Omega\mathrm{d}\Omega.$$

The solution of (3.1) can be obtained by using the method of characteristics and we get

$$\mathcal{E}_{t,r}(x,\Omega) = \int_0^\infty \frac{e^{-\frac{s}{\varepsilon}}}{\varepsilon} F_1(t, x - s\Omega, r\Omega)\ r^2\mathrm{d}s.$$

Remark that according Lemma II.2.2, there exists a (isotropic) vector $\bar{F}_1(t, x, r)$ satisfying $F_1(t, x, r\Omega) = \Omega \cdot \bar{F}_1(t, x, r)$. Accordingly, we can write :

$$Q(t,x) = \int_0^\infty \int_{\mathbb{S}^2} \frac{e^{-\frac{s}{\varepsilon}}}{\varepsilon s^2} \int_0^\infty \frac{r^5}{2}\bar{F}_1(t, x - s\Omega, r)\mathrm{d}r\mathrm{d}\Omega\ s^2\mathrm{d}s.$$

The expression of the Spitzer-Härm heat flux is obtained from F_1; we remind that

$$\int_0^\infty \frac{r^5}{2}\bar{F}_1(t, x, r)\mathrm{d}r = \frac{3}{4\pi}Q_{SH}(t, x).$$

We set $x' = s\Omega$, $\mathrm{d}x' = s^2\mathrm{d}s\mathrm{d}\Omega$. The nonlocal heat flux can be defined by the following convolution formula

$$Q(t,x) = \frac{3}{4\pi\varepsilon}\int_{\mathbb{R}^3} \frac{e^{-\frac{|x'|}{\varepsilon}}}{|x'|^2}\ Q_{SH}(t, x - x')\mathrm{d}x'.$$

This expression makes a link between Schurtz-Nicolaï's approach [27] and the seminal work of Luciani-Mora [21].

It turns out that a useful approximate formula can be derived for the non local

heat flux. We set $q_t(x,\Omega) = \int_0^\infty \frac{r^3}{2}\mathcal{E}_{t,r}(x,\Omega)\mathrm{d}r$. Multiply (3.1) by $\frac{r^3}{2}$ and integrate. It yields

$$q_t(x,\Omega) + \varepsilon\Omega\cdot\nabla_x q_t(x,\Omega) = \Omega\cdot\int_0^\infty \frac{r^5}{2}\bar{F}_1(t,x,r)\mathrm{d}r = \frac{3}{4\pi}\Omega\cdot Q_{SH}(t,x).$$

Thus we can write the following moments system

$$\begin{aligned}
&\int_{\mathbb{S}^2}\Omega\ q_t(x,\Omega)\mathrm{d}\Omega + \varepsilon\nabla_x\cdot\int_{\mathbb{S}^2}\Omega\otimes\Omega\ q_t(x,\Omega)\mathrm{d}\Omega = \frac{3}{4\pi}\int_{\mathbb{S}^2}\Omega\otimes\Omega\mathrm{d}\Omega\ Q_{SH}(t,x)\\
&\int_{\mathbb{S}^2}\Omega\otimes\Omega\ q_t(x,\Omega)\mathrm{d}\Omega + \varepsilon\int_{\mathbb{S}^2}\Omega\otimes\Omega\ \nabla_x\cdot(\Omega q_t(x,\Omega))\,\mathrm{d}\Omega = 0.
\end{aligned}$$

We now make a new approximation in order to close this system. For small ε's it is natural to expect that $\Omega q_t(x,\Omega)$ becomes isotropic which motivates the approximation $\Omega q_t(x,\Omega) \approx \frac{3}{4\pi}\Omega\otimes\Omega\int_{\mathbb{S}^2}\Omega' q_t(x,\Omega')\mathrm{d}\Omega'$. Inserting this approximation in the moment system leads to

$$\begin{aligned}
\int_{\mathbb{S}^2}\Omega q_t(x,\Omega)\mathrm{d}\Omega - \varepsilon^2\frac{3}{4\pi}\nabla_x\cdot\int_{\mathbb{S}^2}(\Omega\otimes\Omega)\,(\Omega\otimes\Omega) : \nabla_x\int_{\mathbb{S}^2}\Omega' q_t(x,\Omega')\mathrm{d}\Omega'\mathrm{d}\Omega\\
= \frac{3}{4\pi}\int_{\mathbb{S}^2}\Omega\otimes\Omega\mathrm{d}\Omega\ Q_{SH}(t,x).
\end{aligned}$$

Then, the nonlocal heat flux is defined, within this approximation, by the elliptic equation

$$Q - \frac{\varepsilon^2}{3}\Delta_x Q = Q_{SH}, \tag{3.2}$$

coupled with equations (2.3) and (2.15). This simplified model, or variant of it, appears in several simulation codes. It is worth mentioning that similar equations have been derived in the modeling of electrostatic interactions in biomolecular processes, [19, 18]. We also refer to [3] for a similar derivation applied to radiative transfer problems. We can establish the following statement which provides a rigorous basis to the non local model.

Theorem II.3.1 *Let $\bar{q} > 0$ and suppose $\rho(x) \geq \underline{\rho} > 0$. Let $\Theta_0 \in L^\infty(\mathbb{R}^3)$ be a non negative function such that $\rho\Theta_0 \in L^1(\mathbb{R}^3)$. There exists a unique function such that $\rho\Theta \in C^1\left([0,+\infty[; L^1(\mathbb{R}^3)\right)$ solution of the system (2.3), (2.15), (3.2) with Θ_0 as initial condition. In addition, Θ satisfies the maximum principle: for any $t \geq 0$ and a.e. $x \in \mathbb{R}^3$,*

$$0 \leq \min_{z\in\mathbb{R}^3}\Theta_0(z) \leq \Theta(t,x) \leq \max_{z\in\mathbb{R}^3}\Theta_0(z). \tag{3.3}$$

Proof. We denote by $\mathcal{F}$ the Fourier transform, by $\mathcal{F}^{-1}$ the inverse Fourier transform

$$\mathcal{F}(\psi)(w) = \int_{\mathbb{R}^3}\psi(x)e^{-ix\cdot w}\mathrm{d}x, \qquad \mathcal{F}^{-1}(\phi)(x) = \left(\frac{1}{2\pi}\right)^3\int_{\mathbb{R}^3}\phi(w)e^{ix\cdot w}\mathrm{d}w,$$

with w the Fourier space variable. We start by rewriting the system (3.2) in the Fourier space. Since

$$\mathcal{F}Q(w) = \frac{1}{1+\varepsilon^2 w^2/3}\mathcal{F}Q_{SH}(w),$$

we get

$$\frac{3}{2}\partial_t \mathcal{F}\left(\rho\Theta\right) = -\mathcal{F}(\nabla_x \cdot Q) = iw\mathcal{F}Q = -\frac{3\bar{q}}{7\varepsilon^2}\left(1 - \frac{1}{1+\varepsilon^2 w^2/3}\right)\mathcal{F}\left(\Theta^{7/2}\right).$$

Back to the real space, it becomes:

$$\rho\partial_t\Theta = -\frac{2\bar{q}}{7\varepsilon^2}\ \left(\Theta^{7/2} - W_\varepsilon \star \Theta^{7/2}\right),$$

with

$$W_\varepsilon = \mathcal{F}^{-1}\left(\frac{1}{1+\varepsilon^2 w^2/3}\right).$$

We have the following expression for the convolution kernel, see [4, Section 6.5] ,

$$W_\varepsilon(x) = \frac{3}{4\pi\varepsilon^2|x|}\ e^{-\sqrt{3}|x|/\varepsilon}.$$

This kernel is positive and unitary in the sense that

$$W_\varepsilon \geq 0 \qquad \text{and} \qquad W_\varepsilon \star 1 = \frac{3}{4\pi\varepsilon^2}\int_{\mathbb{R}^3}\frac{e^{-\sqrt{3}|x|/\varepsilon}}{|x|}\mathrm{d}x = \frac{3}{\varepsilon^2}\int_0^\infty z\ e^{-\sqrt{3}z/\varepsilon}\mathrm{d}z = 1$$

holds. It is also worth pointing out that

$$\frac{1}{\varepsilon^2}\left(1 - \frac{1}{1+\varepsilon^2 w^2/3}\right) \to \frac{w^2}{3}$$

as ε goes to 0, so that the operator $\frac{1}{\varepsilon^2}(I - W_\varepsilon\star)$ tends to $\frac{\Delta_x}{3}$, which is another way to check that the non local model is formally consistent with the Spitzer–Härm limit.
For proving Theorem II.3.1, we introduce a cut-off of the non-linearity: the L^∞ estimate will show that the cut-off is actually not relevant. We set $M = \max\Theta_0 > 0$ (bearing in mind that Θ_0 is non negative). Then we define

$$f_M(\psi) = \frac{2\bar{q}}{7}\left|\begin{array}{ll}\psi^{7/2}, & \text{if } \psi \leq M,\\ \dfrac{7}{2}M^{5/2}\psi - \dfrac{5}{2}M^{7/2} & \text{else.}\end{array}\right.$$

The function $\psi \mapsto f_M(\psi)$ is non-decreasing and ($L = \bar{q}M^{5/2}$)-Lipschitzian. Let us consider the auxiliary problem

$$\left\{\begin{array}{l}\rho\partial_t u + f_M(u) = g,\\ \qquad u(t=0) = \Theta_0,\end{array}\right. \tag{3.4}$$

with $\rho g \in C^0\left([0,+\infty[;L^1(\mathbb{R}^3)\right)$. With a standard contraction argument, we show that there exists a unique solution u of (1.4) with $\rho u \in C^1\left([0,+\infty[;L^1(\mathbb{R}^3)\right)$. Observe also that $u \geq 0$ when $g \geq 0$ and $\Theta_0 \geq 0$. Let $\left(u_n\right)_{n\in\mathbb{N}}$ be the sequence defined by $u_0(t,x) = \Theta_0(x)$ and

$$\left\{\begin{array}{l}\rho\partial_t u_{n+1} + f_M(u_{n+1}) = W_\varepsilon \star f_M(u_n),\\ \qquad u_{n+1}(t=0,x) = \Theta_0(x).\end{array}\right. \tag{3.5}$$

This sequence is well-defined because u_{n+1} is solution of (1.4) with $g = W_\varepsilon \star f_M(u_n)$. So, we have, for any n, $\rho u_n \in C^1\left([0,+\infty[; L^1(\mathbb{R}^3)\right)$.

We have

$$\rho\partial_t\left(u_{n+1}-u_n\right)+f_M(u_{n+1})-f_M(u_n)=W_\varepsilon\star f_M(u_n)-W_\varepsilon\star f_M(u_{n-1}).$$

We set

$$\mathrm{sg}(x)=\left|\begin{array}{ll}1 & \text{if } x\geq 0,\\ -1 & \text{else.}\end{array}\right.$$

Then we get

$$\begin{aligned}\rho\partial_t\left(u_{n+1}-u_n\right)\mathrm{sg}\left(u_{n+1}-u_n\right)+\left(f_M(u_{n+1})-f_M(u_n)\right)\mathrm{sg}\left(u_{n+1}-u_n\right)&\\ =\left(W_\varepsilon\star f_M(u_n)-W_\varepsilon\star f_M(u_{n-1})\right)\mathrm{sg}\left(u_{n+1}-u_n\right).&\end{aligned}$$

Since f_M is non decreasing, we have $\left(f_M(u_{n+1})-f_M(u_n)\right)\mathrm{sg}\left(u_{n+1}-u_n\right)\geq 0$, and, since W_ε is non negative and unitary, we get

$$\begin{aligned}\int_{\mathbb{R}^3}\left|\left(W_\varepsilon\star f_M(u_n)-W_\varepsilon\star f_M(u_{n-1})\right)\mathrm{sg}\left(u_{n+1}-u_n\right)\right|\mathrm{d}x &\leq \int_{\mathbb{R}^3} W_\varepsilon\star\left(L|u_n-u_{n-1}|\right)\mathrm{d}x\\ &\leq L\int_{\mathbb{R}^3}|u_n-u_{n-1}|\mathrm{d}x.\end{aligned}$$

It follows that

$$\int_{\mathbb{R}^3}\rho|u_{n+1}-u_n|(t,x)\mathrm{d}x\leq\frac{L}{\underline{\rho}}\int_0^t\int_{\mathbb{R}^3}\rho|u_n-u_{n-1}|(s,x)\mathrm{d}x\mathrm{d}s.$$

We deduce that

$$\|\rho(u_{n+1}-u_n)(t,\cdot)\|_{L^1(\mathbb{R}^3)}\leq\frac{(Lt/\underline{\rho})^{n+1}}{(n+1)!}\sup_{s\in[0,t]}\|\rho(u_1-u_0)(s,\cdot)\|_{L^2(\mathbb{R}^3)}$$

holds. Since the series $\sum_n\frac{(Lt/\underline{\rho})^{n+1}}{(n+1)!}$ converges, it implies that the sequence $\left(u_n\right)_{n\in\mathbb{N}}$ satisfies the Cauchy criterion and thus it has a limit Θ with $\rho\Theta\in C^0\left([0,+\infty[; L^1(\mathbb{R}^3)\right)$. Passing to the limit in (1.5) we observe that Θ satisfies

$$\rho\partial_t\Theta+f_M(\Theta)=W_\varepsilon\star f_M(\Theta),$$

with initial data Θ_0. It remains to discuss the L^∞ estimate.
Of course, the initial guess verifies $u_0(t,x)=\Theta_0(x)\leq M$. Let us now assume that $\max_{x\in\mathbb{R}^3}\ u_n(t,x)\leq M$ holds. Since W_ε is unitary, we have $W_\varepsilon\star f_M\left(M\right)=f_M\left(M\right)$. Therefore, we can write

$$\rho\partial_t\left(u_{n+1}-M\right)+f_M(u_{n+1})-f_M\left(M\right)=W_\varepsilon\star f_M(u_n)-W_\varepsilon\star f_M\left(M\right).$$

We use the function

$$(\psi)_+=\left|\begin{array}{ll}\psi & \text{if } \psi>0,\\ 0 & \text{else.}\end{array}\right.$$

Then we have

$$\rho\partial_t \left(u_{n+1} - M\right)\left(u_{n+1} - M\right)_+ + \left(f_M(u_{n+1}) - f_M(M)\right)\left(u_{n+1} - M\right)_+ \\ = \left(W_\varepsilon \star f_M(u_n) - W_\varepsilon \star f_M(M)\right)\left(u_{n+1} - M\right)_+ .$$

Since f_M is non decreasing, we observe that

$$\left(f_M(u_{n+1}) - f_M(M)\right)\left(u_{n+1} - M\right)_+ \geq 0,$$

and, since W_ε is non negative, we get

$$W_\varepsilon \star \left(f_M(u_n) - f_M(M)\right)\left(u_{n+1} - M\right)_+ \leq 0.$$

It follows that

$$\frac{\mathrm{d}}{\mathrm{d}t}\int_{\mathbb{R}^3} \rho \left(u_{n+1} - M\right)_+^2 (t,x)\mathrm{d}x \leq 0.$$

Since initially $(u_{n+1}(0,x) - M) = (\Theta_0(x) - M) \leq 0$, we conclude that $u_{n+1}(t,x) \leq M$. With similar arguments, we treat the bound from below and we finally obtain, for any $n \in \mathbb{N}$,

$$\min_{z\in\mathbb{R}^3} \Theta_0(z) \leq u_n(t,x) \leq \max_{z\in\mathbb{R}^3} \Theta_0(z).$$

In particular, we have

$$f_M(u_n(x,t)) = \frac{2\bar{q}}{7} u_n(x,t)^{7/2}.$$

Therefore, u_n converges to the solution Θ of the system (2.3), (2.15), (3.2) and it satisfies (1.2). ∎

In addition, it is worth pointing conservation and dissipation properties of the model.

Proposition II.3.1 *The total energy is conserved*

$$\frac{\mathrm{d}}{\mathrm{d}t}\int_{\mathbb{R}^3} \rho\Theta\mathrm{d}x = 0. \tag{3.6}$$

Suppose furthermore that $\rho = \rho_\star > 0$ is constant. Then, the following entropy dissipation holds

$$\frac{\mathrm{d}}{\mathrm{d}t}\left(\int_{\mathbb{R}^3} \rho_\star|\Theta|^2\mathrm{d}x + \frac{\varepsilon^2}{3}\int_{\mathbb{R}^3} \rho_\star|\nabla_x\Theta|^2\mathrm{d}x\right) \leq 0 \tag{3.7}$$

Proof. The energy conservation follows directly by integration of equation (2.3). Next, we apply the operator $\left(Id - \frac{\varepsilon^2}{3}\Delta_x\right)$ to (2.3). Then we use (3.2) to make the Spitzer-Härm heat flux appear. We obtain

$$\left[Id - \frac{\varepsilon^2}{3}\Delta_x\right]\partial_t\Theta = \frac{2}{3\rho_\star}\nabla_x \cdot \left(\kappa\nabla_x\Theta\right).$$

Multiply by Θ, and integrate with respect to the space variable. Using several integrations by part we obtain

$$\frac{\mathrm{d}}{\mathrm{d}t}\left(\int_{\mathbb{R}^3} |\Theta|^2\mathrm{d}x + \frac{\varepsilon^2}{3}\int_{\mathbb{R}^3} |\nabla_x\Theta|^2\mathrm{d}x\right) = -\frac{4}{3\rho_\star}\int_{\mathbb{R}^3} \kappa|\nabla_x\Theta|^2\mathrm{d}x \leq 0.$$

■

In the next section, we propose a numerical scheme to solve efficiently the system (2.3), (2.15), (3.2), and preserving the properties in Proposition II.3.1 and the maximum principle (1.2).

II.4 Numerical analysis

II.4.1 A numerical scheme for the Schurtz-Nicolaï model

For the sake of simplicity we discuss the numerical issues by restricting ourselves to the one-dimension framework. However, we consider models slightly more general than equation (3.2) derived above. Precisely let us consider two (smooth) positive functions $\nu : \mathbb{R} \to (0, \infty)$ and $\kappa : \mathbb{R} \to (0, \infty)$. We are concerned with the numerical approximation of the system

$$\partial_t \Theta = -\frac{2}{3\rho} \partial_x Q, \tag{4.1}$$

$$Q - \varepsilon^2 \nu(\Theta) \partial_x^2 Q \ = -\kappa(\Theta) \partial_x \Theta, \tag{4.2}$$

with a prescribed initial data $\Theta(t = 0, x) = \Theta_{Init}(x)$. For the time being we neglect the question of the boundary condition and we consider the problem as set on the whole line $x \in \mathbb{R}$ (see Remark II.4.3 below). The function κ is related to the definition of the Spitzer-Härm flux and relies on the identification of the coefficient in (2.15). The additional function ν has been introduced as a tuning parameter to fit the results with kinetic simulations, see [21, 22, 23, 27]. Our goal is to derive and analyze a numerical scheme for (4.1)–(4.2).

Let $h_t > 0$ and $h_x > 0$ stand for time and space steps, respectively. The scheme is based on the approximation of the following integrated form of (4.1), at the point jh_x

$$\Theta((n+1)h_t, jh_x) = \Theta(nh_t, jh_x) - \frac{2}{3\rho(jh_x)} \left(\partial_x \Big(\int_{nh_t}^{(n+1)h_t} Q(s, x) \mathrm{d}s \Big) \right)_{x = jh_x}$$

together with (4.2). We adopt a Finite Difference viewpoint but temperature and fluxes will be evaluated on staggered grids, see Figure II.1. The numerical unknown Θ_j^n, with $n \in \mathbb{N}$ and $j \in \mathbb{Z}$, is intended to be an approximation of $\Theta(nh_t, jh_x)$. We denote $\rho_j = \rho(jh_x)$, with $\rho : \mathbb{R} \to (0, \infty)$ a given function. We define the scheme by

$$\Theta_j^{n+1} = \Theta_j^n - h_t \frac{2}{3\rho_j} \left(\nabla^D \cdot \mathcal{Q}^{n,n+1} \right)_j$$

where we are left with the task of defining the numerical flux $\mathcal{Q}_{j+1/2}^{n,n+1}$ intended to approximate the flux

$$\frac{1}{h_t} \int_{nh_t}^{(n+1)h_t} Q(s, (j + 1/2)h_x) \mathrm{d}s,$$

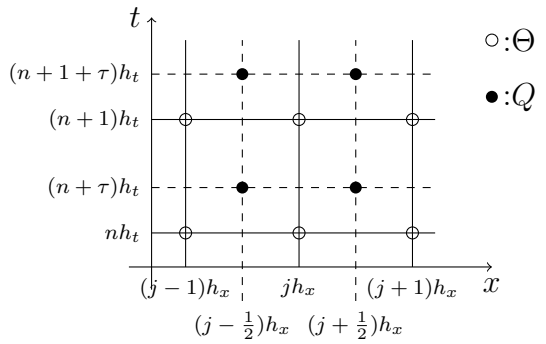

Figure II.1: Staggered grids

and the numerical operator $\nabla^D \cdot \bullet$ intended to be a discrete version of the derivative $\partial_x \bullet$.

For further purposes it is convenient to introduce the following operators

$$\begin{aligned}
\nabla^D : &\quad \big(\Theta_j\big)_{j\in\mathbb{Z}} &\longmapsto &\quad \Big((\nabla^D\Theta)_{j+1/2} = \frac{\Theta_{j+1}-\Theta_j}{h_x}\Big)_{j\in\mathbb{Z}},\\
\nabla^D\cdot : &\quad \big(Q_{j+1/2}\big)_{j\in\mathbb{Z}} &\longmapsto &\quad \Big((\nabla^D\cdot Q)_j = \frac{Q_{j+1/2}-Q_{j-1/2}}{h_x}\Big)_{j\in\mathbb{Z}},\\
\Delta^D : &\quad \big(\Theta_j\big)_{j\in\mathbb{Z}} &\longmapsto &\quad \Big((\Delta^D\Theta)_j = \frac{\Theta_{j+1}-2\Theta_j+\Theta_{j-1}}{h_x^2}\Big)_{j\in\mathbb{Z}}.
\end{aligned}$$

Note that $(\nabla^D\cdot)\circ\nabla^D = \Delta^D$. We shall also use the following definition, with a slight abuse of notation,

$$\Delta^D : \big(Q_{j+1/2}\big)_{j\in\mathbb{Z}} \longmapsto \Big((\Delta^D Q)_{j+1/2} = \frac{Q_{j+3/2}-2Q_{j+1/2}+Q_{j-1/2}}{h_x^2}\Big)_{j\in\mathbb{Z}}.$$

A naive approach consists in using an explicit discretization: we set $\mathcal{Q}^{n,n+1}_{j+1/2} = Q^n_{j+1/2}$, intended to be an approximation of $Q(nh_t,(j+1/2)h_x)$, where the approximation of (4.2) yields

$$Q^n_{j+1/2} - \varepsilon^2\nu^n_{j+1/2}\Delta^D Q^n_{j+1/2} = -\kappa^n_{j+1/2}(\nabla^D\Theta^n)_{j+1/2}.$$

Here, for the nonlinear terms we use

$$\nu^n_{j+1/2} = \nu\Big(\frac{\Theta^n_{j+1}+\Theta^n_j}{2}\Big), \qquad \kappa^n_{j+1/2} = \kappa\Big(\frac{\Theta^n_{j+1}+\Theta^n_j}{2}\Big).$$

But for $\varepsilon = 0$ the problem reduces to a nonlinear heat equation and the scheme we are writing is nothing but a mere explicit scheme for the heat equation. In particular it will be certainly constrained by a parabolic CFL condition where the time step h_t should be proportional to h_x^2. Such a condition induces a prohibitive numerical cost and in particular the computation will not be affordable for any extension to multi-dimensional problems. This remark motivates to seek an implicit definition of the numerical fluxes. The scheme we propose is based on the observation that (II.4.1) can be approached by $Q((n+\tau)h_t,(j+1/2)h_x)$ for $0\le\tau\le 1$. Hence pick $0\le\tau\le 1$; we define the

numerical flux $\mathcal{Q}_{j+1/2}^{n,n+1} = Q_{j+1/2}^{n+\tau}$ which has to be thought of as an approximation of the flux $Q((n+\tau)h_t, (j+1/2)h_x)$. It leads to the following discrete version of (4.2)

$$Q_{j+1/2}^{n+\tau} - \varepsilon^2 \nu_{j+1/2}^{n+\tau} \Delta^D Q_{j+1/2}^{n+\tau} = -\kappa_{j+1/2}^{n+\tau} \Big(\tau \big(\nabla^D \Theta^{n+1}\big)_{j+1/2} + (1-\tau)\big(\nabla^D \Theta^n\big)_{j+1/2} \Big). \quad (4.3)$$

It is coupled to

$$\Theta_j^{n+1} = \Theta_j^n - h_t \frac{2}{3\rho_j} \frac{Q_{j+1/2}^{n+\tau} - Q_{j-1/2}^{n+\tau}}{h_x} = \Theta_j^n - h_t \frac{2}{3\rho_j} (\nabla^D \cdot Q^{n+\tau})_j. \quad (4.4)$$

Inserting (4.4) into (4.3) yields

$$Q_{j+1/2}^{n+\tau} - \varepsilon^2 \nu_{j+1/2}^{n+\tau} \Delta^D Q_{j+1/2}^{n+\tau} - \frac{2\tau h_t}{3} \kappa_{j+1/2}^{n+\tau} \nabla^D \Big(\frac{1}{\rho} \nabla^D \cdot Q^{n+\tau} \Big)_{j+1/2} = -\kappa_{j+1/2}^{n+\tau} (\nabla^D \Theta^n)_{j+1/2}.$$

The detailed expression of the third term in the left side is

$$\nabla^D \Big(\frac{1}{\rho} \nabla^D \cdot Q^{n+\tau} \Big)_{j+1/2} = \frac{1}{h_x^2} \Big(\frac{Q_{j+3/2}^{n+\tau} - Q_{j+1/2}^{n+\tau}}{\rho_{j+1}} - \frac{Q_{j+1/2}^{n+\tau} - Q_{j-1/2}^{n+\tau}}{\rho_j} \Big).$$

Finally, the nonlinearities are defined as follows

$$\begin{aligned} \nu_{j+1/2}^{n+\tau} &= \nu \Big(\tau \frac{\Theta_{j+1}^{n+1} + \Theta_j^{n+1}}{2} + (1-\tau) \frac{\Theta_{j+1}^n + \Theta_j^n}{2} \Big), \\ \kappa_{j+1/2}^{n+\tau} &= \kappa \Big(\tau \frac{\Theta_{j+1}^{n+1} + \Theta_j^{n+1}}{2} + (1-\tau) \frac{\Theta_{j+1}^n + \Theta_j^n}{2} \Big). \end{aligned}$$

In order to solve the non linear system (4.3)–(4.4) that defines the pair $(\Theta_j^{n+1}, Q_{j+1/2}^{n+\tau})$ we proceed as follows. We set $\tilde{\Theta}_j^{n,0} = \Theta_j^n$. Then, we define the iteration process

$$\begin{cases} \tilde{\nu}_{j+1/2}^{n,r} = \nu \Big(\tau \dfrac{\tilde{\Theta}_{j+1}^{n,r} + \tilde{\Theta}_j^{n,r}}{2} + (1-\tau) \dfrac{\Theta_{j+1}^n + \Theta_j^n}{2} \Big), \\ \kappa_{j+1/2}^{n,r} = \kappa \Big(\tau \dfrac{\tilde{\Theta}_{j+1}^{n,r} + \tilde{\Theta}_j^{n,r}}{2} + (1-\tau) \dfrac{\Theta_{j+1}^n + \Theta_j^n}{2} \Big), \\ \tilde{Q}_{j+1/2}^{n,r+1} - \varepsilon^2 \tilde{\nu}_{j+1/2}^{n,r} \Delta^D Q_{j+1/2}^{n,r+1} - \dfrac{2\tau h_t}{3} \tilde{\kappa}_{j+1/2}^{n,r} \nabla^D \Big(\dfrac{1}{\rho} \nabla^D \cdot \tilde{Q}^{n,r+1} \Big)_{j+1/2} \\ \qquad\qquad = -\tilde{\kappa}_{j+1/2}^{n,r} (\nabla^D \Theta^n)_{j+1/2}, \\ \tilde{\Theta}_j^{n,r+1} = \Theta_j^n - h_t \dfrac{2}{3\rho_j} (\nabla^D \cdot \tilde{Q}^{n,r+1})_j. \end{cases} \quad (4.5)$$

The solution $(\Theta_j^{n+1}, Q_{j+1/2}^{n+\tau})$ is seen as the limit $\lim_{r\to\infty} (\tilde{\Theta}_j^{n,r}, \tilde{Q}_{j+1/2}^{n,r})$. In practice, we stop the iteration when the relative error becomes smaller than a given (small) threshold, and a few iterations are usually enough to construct the fixed point. As a matter of fact, it is worth remarking that the first step of the iteration corresponds to a quite natural semi-implicit discretization (only nonlinear terms are defined explicitly) and it already produces satisfactory results.

For the analysis of the scheme, the following manipulation will be useful: we apply the operator $\rho \bullet - \nabla^D \cdot \Big(\varepsilon^2 \tilde{\nu}^{n,r} \nabla^D (\rho \bullet) + \dfrac{2\tau h_t}{3} \tilde{\kappa}^{n,r} \nabla^D \bullet \Big)$ to the fourth equation in (4.5). We obtain

$$\begin{aligned}
&\rho_j \tilde{\Theta}_j^{n,r+1} - \nabla^D \cdot \Big(\varepsilon^2 \tilde{\nu}^{n,r} \nabla^D (\rho \tilde{\Theta}^{n,r+1}) + \frac{2\tau h_t}{3} \tilde{\kappa}^{n,r} \nabla^D \tilde{\Theta}^{n,r+1} \Big)_j \\
&\quad = \rho_j \tilde{\Theta}_j^{n} - \nabla^D \cdot \Big(\varepsilon^2 \tilde{\nu}^{n,r} \nabla^D (\rho \Theta^{n}) + \frac{2\tau h_t}{3} \tilde{\kappa}^{n,r} \nabla^D \Theta^{n} \Big)_j \\
&\qquad - \frac{2h_t}{3} \nabla^D \cdot \Big(\tilde{Q}^{n,r} - \varepsilon^2 \tilde{\nu}^{n,r} \Delta^D \tilde{Q}^{n,r+1} - \frac{2\tau h_t}{3} \tilde{\kappa}^{n,r} \nabla^D \Big(\frac{1}{\rho} \nabla^D \cdot \tilde{Q}^{n,r+1} \Big) \Big)_j .
\end{aligned}$$

The last term can be rewritten by using the third equation in (4.5). We are led to the following formula

$$\begin{aligned}
&\rho_j \tilde{\Theta}_j^{n,r+1} - \nabla^D \cdot \Big(\varepsilon^2 \tilde{\nu}^{n,r} \nabla^D (\rho \tilde{\Theta}^{n,r+1}) + \frac{2\tau h_t}{3} \tilde{\kappa}^{n,r} \nabla^D \tilde{\Theta}^{n,r+1} \Big)_j \\
&\quad = \rho_j \Theta_j^{n} - \nabla^D \cdot \Big(\varepsilon^2 \tilde{\nu}^{n,r} \nabla^D (\rho \Theta^{n}) + \frac{2(\tau-1) h_t}{3} \tilde{\kappa}^{n,r} \nabla^D \Theta^{n} \Big)_j .
\end{aligned} \tag{4.6}$$

Let us perform the numerical analysis of the scheme neglecting for the sake of simplicity any boundary terms. Namely, we consider the unknown as being defined for any $j \in \mathbb{Z}$. See Remark II.4.3 for details on the boundary conditions.

Theorem II.4.1 (Von Neumann stability) *Let us suppose that the coefficients are constant: $\rho = \rho_\star > 0$, $\nu = \nu_\star > 0$, $\kappa = \kappa_\star > 0$. We assume that*

$$1 - 2\tau - \frac{3\rho_\star \nu_\star}{\kappa_\star} \frac{\varepsilon^2}{h_t} \leq \frac{3\rho_\star h_x^2}{2\kappa_\star h_t} \tag{4.7}$$

holds. Then, the scheme (4.5) (or (4.6)) is L^2-stable.

Remark II.4.1 *In particular the scheme is unconditionally (L^2-)stable for $1/2 \leq \tau \leq 1$ and it can be expected to reach second order accuracy with respect to h_t and h_x in the Crank-Nicolson case ($\tau = 1/2$). Anyway, the scheme is stable under the standard parabolic CFL condition $\frac{2h_t}{h_x^2} \leq 1$.*

Proof. We associate to a sequence $\big(u_j\big)_{j\in\mathbb{Z}}$ the Fourier series $\mathcal{F}_D(u)(\xi) = \sum_{j\in\mathbb{Z}} u_j e^{2i\pi j\xi}$. The amplification factor of the scheme (4.6) reads

$$\frac{\mathcal{F}_D(\tilde{\Theta}^{n,r})}{\mathcal{F}_D(\Theta^n)}(\xi) = \frac{1 - \dfrac{2}{h_x^2} \left(\varepsilon^2 \nu_\star + \dfrac{2\,(\tau-1)\, h_t \kappa_\star}{3\rho_\star} \right) (1 - \cos\xi)}{1 - \dfrac{2}{h_x^2} \left(\varepsilon^2 \nu_\star + \dfrac{2\tau h_t \kappa_\star}{3\rho_\star} \right) (1 - \cos\xi)}.$$

The amplification factor satisfies $\Big| \frac{\mathcal{F}_D(\Theta^{n+1})}{\mathcal{F}_D(\Theta^n)}(\xi) \Big| \leq 1$ iff the condition (4.7) holds. A similar stability analysis appeared in [3]. ∎

Theorem II.4.2 (Maximum principle) *We suppose that $\rho = \rho_\star > 0$ is constant and that $0 < \underline{\nu} \le \nu(z) \le \overline{\nu}$, $0 < \underline{\kappa} \le \kappa(z) \le \overline{\kappa}$ holds for any $z \ge 0$. Assume that*

$$\frac{3\varepsilon^2\rho_\star\overline{\nu}}{2(1-\tau)\underline{\kappa}} \le h_t \le \frac{3\rho_\star}{4(1-\tau)\overline{\kappa}}\,(h_x^2 + 2\varepsilon^2\underline{\nu}). \tag{4.8}$$

Initially the data is required to satisfy $0 < \underline{\Theta} \le \Theta_j^0 \le \bar{\Theta}$. Then, the solution of the scheme (4.6)) satisfies the same inequality.

Proof. Assuming that $\rho_j = \rho_\star$, we rewrite the scheme (4.6) as follows

$$(1+a_j)\tilde{\Theta}_j^{n,r+1} = a_j^+\tilde{\Theta}_{j+1}^{n,r+1} + a_j^-\tilde{\Theta}_{j-1}^{n,r+1} + (1+\gamma_j)\Theta_j^n + b_j^+\Theta_{j+1}^n + b_j^-\Theta_{j-1}^n \tag{4.9}$$

where we use the shorthand notation

$$\begin{aligned}
a_j &= \frac{2\tau h_t}{3\rho_\star h_x^2}(\tilde{\kappa}_{j+1/2}^{n,r} + \tilde{\kappa}_{j-1/2}^{n,r}) + \frac{\varepsilon^2}{h_x^2}(\tilde{\nu}_{j+1/2}^{n,r} + \tilde{\nu}_{j-1/2}^{n,r}),\\
a_j^\pm &= \frac{2\tau h_t}{3\rho_\star h_x^2}\tilde{\kappa}_{j\pm1/2}^{n,r} + \frac{\varepsilon^2}{h_x^2}\tilde{\nu}_{j\pm1/2}^{n,r},\\
\gamma_j &= -\frac{2(1-\tau)h_t}{3\rho_\star h_x^2}(\tilde{\kappa}_{j+1/2}^{n,r} + \tilde{\kappa}_{j-1/2}^{n,r}) + \frac{\varepsilon^2}{h_x^2}(\tilde{\nu}_{j+1/2}^{n,r} + \tilde{\nu}_{j-1/2}^{n,r}),\\
b_j^\pm &= \frac{2(1-\tau)h_t}{3\rho_\star h_x^2}\tilde{\kappa}_{j\pm1/2}^{n,r} - \frac{\varepsilon^2}{h_x^2}\tilde{\nu}_{j\pm1/2}^{n,r}.
\end{aligned}$$

The condition (4.8), implies that the coefficients satisfy

$$a_j \ge 0, \qquad a_j^\pm \ge 0, \qquad b_j^\pm \ge 0, \qquad 1+\gamma_j \ge 0$$

with furthermore

$$1 + \gamma_j + b_j^+ + b_j^- = 1, \qquad a_j = a_j^+ + a_j^-.$$

Let us denote $\mu^n = \sup_{j\in\mathbb{Z}} \Theta_j^n$ and $\mu^{n,r+1} = \sup_{j\in\mathbb{Z}} \tilde{\Theta}_j^{n,r+1}$. Since the coefficients in the right hand side of (4.9) are non negative, we have

$$\tilde{\Theta}_j^{n,r+1} \le \frac{\mu^{n,r+1}(a_j^+ + a_j^-) + \mu^n}{1+a_j}.$$

We argue by contradiction: let us assume that there exists $0 < \eta < 1$ such that $\mu^n = (1-\eta)\mu^{n,r+1} < \mu^{n,r+1}$. Since the a_j's are bounded (uniformly with respect to j),

$$0 \le a_j \le \frac{4\tau h_t}{3\rho_\star h_x^2}\overline{\kappa} + \frac{2\varepsilon^2}{h_x^2}\overline{\nu} = M,$$

the previous inequality becomes

$$\tilde{\Theta}_j^{n,r+1} \le \mu^{n,r+1}\Big(1 - \frac{\eta}{1+M}\Big),$$

which would contradict the definition of $\mu^{n,r+1}$. ∎

Remark II.4.2 *Note that the condition* (4.8) *is consistent when* $\varepsilon = 0$ *with the usual condition, which makes a proportionality constraint between* h_t *and* h_x^2 *appear, for proving the maximum principle (see [26, Theorem 2.2]).*

Proposition II.4.1 (Energy conservation) *The solution of the scheme satisfies the discrete analog of property* ((H1))*:*

$$\sum_{j\in\mathbb{Z}} \rho_j \Theta_j^n = \sum_{i\in\mathbb{Z}} \rho_j \Theta_j^0.$$

Proof. Assume this equality is true at iteration n. Using (4.5), we have

$$\sum_{j\in\mathbb{Z}} \rho_j \tilde{\Theta}_j^{n,r} = \sum_{j\in\mathbb{Z}} \rho_j \Theta_j^n - \frac{2h_t}{h_x}\left(\sum_{j\in\mathbb{Z}} \tilde{Q}_{j+1/2}^{n,r} - \sum_{j\in\mathbb{Z}} \tilde{Q}_{j-1/2}^{n,r}\right) = \sum_{j\in\mathbb{Z}} \rho_j \Theta_j^n.$$

■

Proposition II.4.2 (Entropy dissipation) *Let* $\tau = 1/2$*, and assume that* $\rho = \rho_\star > 0$ *is constant. The solution of the scheme satisfies the discrete analog of property* (1.6)*:*

$$\sum_{j\in\mathbb{Z}} \left(\tilde{\Theta}_j^{n,r+1}\right)^2 + \varepsilon^2 \sum_{j\in\mathbb{Z}} \left(\tilde{\nu}_{j+1/2}^{n,r} |(\nabla^D \tilde{\Theta}^{n,r+1})_{j+1/2}|^2\right) \leq \sum_{j\in\mathbb{Z}} \left(\Theta_j^n\right)^2 + \varepsilon^2 \sum_{j\in\mathbb{Z}} \left(\tilde{\nu}_{j+1/2}^{n,r} |(\nabla^D \tilde{\Theta}^n)_{j+1/2}|^2\right).$$

Proof. First, we make some general observation. Let $(A_j)_{j\in\mathbb{Z}}, (B_j)_{j\in\mathbb{Z}}$ and $\left(\alpha_{j+1/2}\right)_{j\in\mathbb{Z}}$ be given sequences. Remark that we have

$$\begin{aligned}\sum_{j\in\mathbb{Z}} A_j \nabla^D \cdot \left(\alpha \nabla^D B\right)_j &= \sum_{j\in\mathbb{Z}} \frac{\alpha_{j+1/2}}{h_x^2}\left(A_{j+1}B_j + A_j B_{j+1} - A_j B_j - A_{j+1}B_{j+1}\right) \\ &= -\sum_{j\in\mathbb{Z}} \alpha_{j+1/2}\left(\nabla^D A\right)_{j+1/2}\left(\nabla^D B\right)_{j+1/2}\end{aligned} \tag{4.10}$$

Therefore, we multiply (4.6) by $\left(\tilde{\Theta}_j^{n,r+1} + \Theta_j^n\right)$ and we write the result as follows

$$\begin{aligned}&\left(\tilde{\Theta}_j^{n,r+1} + \Theta_j^n\right)\left(\tilde{\Theta}_j^{n,r+1} - \Theta_j^n\right) - \varepsilon^2\left(\tilde{\Theta}_j^{n,r+1} + \Theta_j^n\right)\nabla^D \cdot \left(\tilde{\nu}^{n,r}\nabla^D(\tilde{\Theta}^{n,r+1} - \Theta^n)\right)_j \\ &\quad = \frac{2h_t}{3\rho_\star}\left(\tilde{\Theta}_j^{n,r+1} + \Theta_j^n\right)\nabla^D \cdot \left(\tilde{\kappa}^{n,r}\nabla^D\left(\tau\tilde{\Theta}^{n,r+1} + (1-\tau)\,\Theta^n\right)\right)_j.\end{aligned}$$

Then using (4.10), we have

$$\begin{aligned}&\sum_{j\in\mathbb{Z}}\left(\left(\tilde{\Theta}_j^{n,r+1}\right)^2 - \left(\Theta_j^n\right)^2\right) + \varepsilon^2\sum_{j\in\mathbb{Z}}\left(\tilde{\nu}_{j+1/2}^{n,r}\left(|(\nabla^D\tilde{\Theta}^{n,r+1})_{j+1/2}|^2 - |(\nabla^D\Theta^n)_{j+1/2}|^2\right)\right) \\ &\quad = -\frac{2h_t}{3\rho_\star}\sum_{j\in\mathbb{Z}}\tilde{\kappa}_{j+1/2}^{n,r}\Big(\tau|\left(\nabla^D\Theta^{n,r+1}\right)_{j+1/2}|^2 + (1-\tau)\,|\left(\nabla^D\Theta^n\right)_{j+1/2}|^2 \\ &\qquad\qquad + \left(\nabla^D\Theta^{n,r}\right)_{j+1/2}\left(\nabla^D\Theta^n\right)_{j+1/2}\Big).\end{aligned}$$

For $\tau = 1/2$, we conclude by factorization that

$$\sum_{j\in\mathbb{Z}} \left(\left(\tilde{\Theta}_j^{n,r+1}\right)^2 - \left(\Theta_j^n\right)^2 \right) + \varepsilon^2 \sum_{j\in\mathbb{Z}} \left(\tilde{\nu}_{j+1/2}^{n,r} \left(|(\nabla^D \tilde{\Theta}^{n,r+1})_{j+1/2}|^2 - |(\nabla^D \Theta^n)_{j+1/2}|^2 \right) \right)$$
$$= -\frac{4h_t}{3\rho_\star} \sum_{j\in\mathbb{Z}} \tilde{\kappa}_{j+1/2}^{n,r} \left| \left(\nabla^D \frac{\tilde{\Theta}^{n,r} + \Theta^n}{2} \right)_{j+1/2} \right|^2 \leq 0$$

holds. ∎

Remark II.4.3 *The previous discussion does not account for boundary conditions. In practice of course the index j lies in a bounded domain, say $j \in \{1, ..., J\}$. The scheme involves "ghost" points with indices out of this range, the values of which need to be prescribed by boundary conditions. It turns out that the formulation* (4.5) *is well adapted to Neumann–like conditions where the flux Q is prescribed at the boundary: we impose the values of $Q_{1/2}$ and $Q_{J+1/2}$ by using the prescribed flux. The formulation* (4.6) *is well adapated to Dirichlet conditions where the unknown Θ is imposed at the boundary: the value of Θ_0 and Θ_{J+1} is given by the Dirichlet conditions. The adaptation of Theorems II.4.1 and II.4.2, and Propositions II.4.1 and II.4.2 to these contexts is straightforward, with energy and entropy inequalities involving the prescribed boundary terms.*

II.4.2 Numerical results

A key features of ICF simulations is the possible occurrence of "antidiffusive effects", see e. g. [14], such that the heat flux follows the direction of the temperature gradient. We illustrate this fact in Figure II.2. This figure has been obtained by using the kinetic code `fpelec` developed at the Atomic Energy Commission [8]. In fact the code works on a simplified version of the Landau-Fokker-Planck equation considered here, based on a truncated expansion on spherical harmonics, together with the constraint of vanishing current. The boundary condition guarantees the conservation of energy. This model is more easily amenable to a numerical treatment but it preserves the main features of the original equation. The simulation is performed with a atomic number $Z_i = 4$, and a density constant equal to 2.5×10^{21} $g.cm^{-3}$. The size of the domain is 10^{-2} cm. We plot the temperature $\Theta(t, x)$ for several times, as well as the product of the heat flux Q by the temperature gradient $\partial_x\Theta$. The antidiffusion is characterized by regions where the product $\mathsf{Q}\partial_x\Theta$ takes positive values (see Figure II.2(b)). The Spitzer-Härm model completely misses such a phenomena since, by definition, we have $Q_{SH} \cdot \partial_x\Theta = -\frac{\bar{q}}{2}\Theta^{5/2}|\partial_x\Theta|^2 < 0$.
We illustrate the ability of the asymptotic model (4.1)-(4.2) in capturing the anti-diffusive effect, see Figure II.3. The comparison with the kinetic simulation cannot be fair since we do not have access to all physical data, nevertheless we can bring out the main features of the nonlocal model. We consider the normalized space domain $(0, 1)$ and the initial data reads

$$\Theta_{init}(x) = (1 - (0.3 - 1) \times 2x)\, \mathbb{1}_{[0,0.5]}(x) + (1 - (0.3 - 1) \times 2(x - 0.5))\, \mathbb{1}_{]0.5,1]}(x),$$

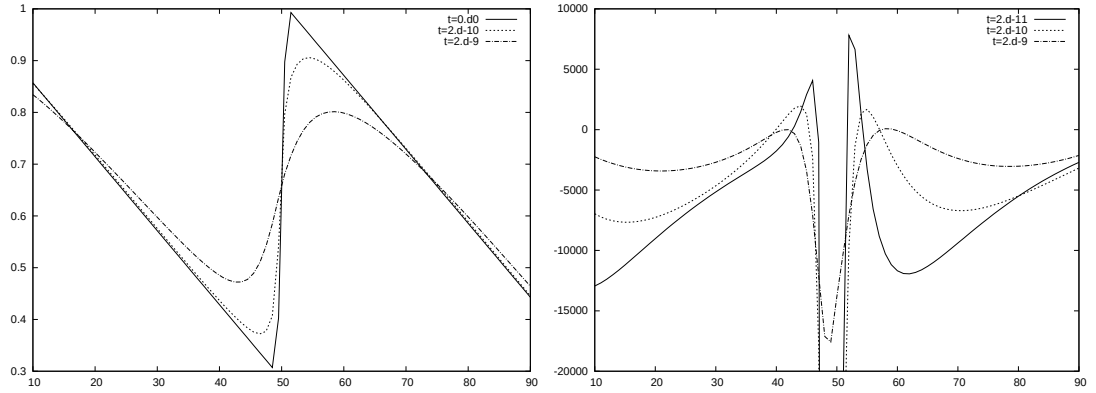

(a) Heat distribution $\Theta(t,x)$ (b) Heat flux $\times$ temperature gradient: $\mathsf{Q}\times\partial_x\Theta$

Figure II.2: Kinetic results: Simulation of a kinetic model (`fpelec` code from CEA)

see Figure II.3(a). We use the scheme (4.5). Of course, with $\varepsilon = 0$ it also provides a scheme for the Spitzer-Härm equation. We perform simulations for several values of the scaling parameter ε. The simulations are performed with $\tau = 1/2$, $h_x = 1/100$, and $j \in [\![1, 99]\!]$. In order to conserve the total energy, we impose that the boundary fluxes vanish ($Q_{1/2} = Q_{99+1/2} = 0$). The (common) time step is chosen so that the stability condition (4.8) for the maximum principle is satisfied. We remind that ν is a phenomenological nonlinearity introduced in many hydrodynamic codes to fit with kinetic simulations. Here we restrict to the simple case $\nu = 1$. As expected the smaller ε, the smoother the temperature profile, see Figures II.3(c) and II.3(e). In Figures 4.10, II.3(d) and II.3(f), we can observe the antidiffusive effects for positive values of ε, with quite sharp profiles for the largest ε's. This effect reduces as time grows, as observed with the kinetic results. We point out that running the hydrodynamic code is very fast. This aspect is particularly important since for ICF simulation the computation of the electronic temperature is a small piece of a large hydrodynamic code involving coupled systems of PDEs.

Conclusion

We have derived precisely the non linear diffusion equation for the electron temperature which arises in the Spitzer-Härm regime. The derivation starts from collisional models accounting for both electron-electron and electron-ion collisions. Due to the latter the collision operator preserves charge and energy only. The kinetic equation for the electron distribution is coupled to the Maxwell system. We discuss in details the scaling issues. The quasi-neutral regime implies that the asymptotic solution has a vanishing current, which can be interpreted as a constraint on the electric field. We identify, depending on the collision operator, the diffusion coefficient of the limit equation. Next, we revisit the Schurtz-Nicolaï model, which is a non local macroscopic approximation of the kinetic model. In particular we justify the well-posedness of the non local model and prove the maximum principle. We design a specific numerical scheme for the Schurtz-Nicolaï system and perform the stability analysis. Finally, we check numerically the ability of

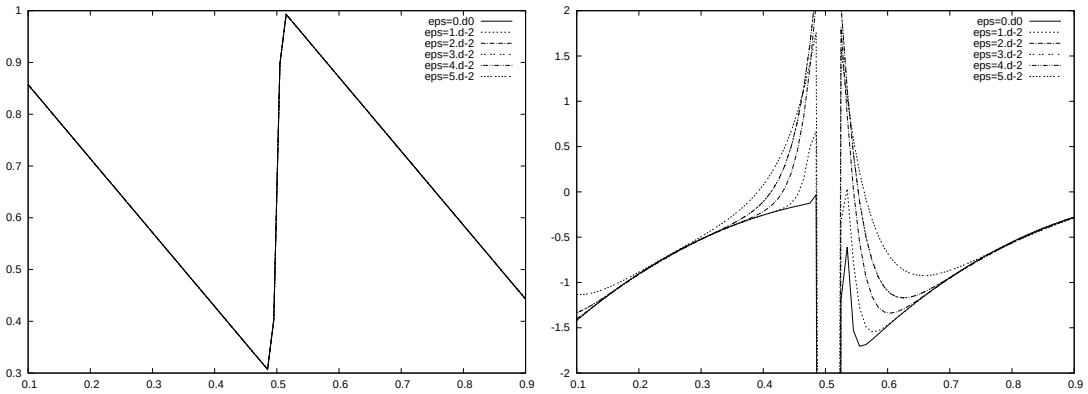

(a) Initial heat distribution

(b) $Q \times \partial_x \Theta$ at $t = 0$

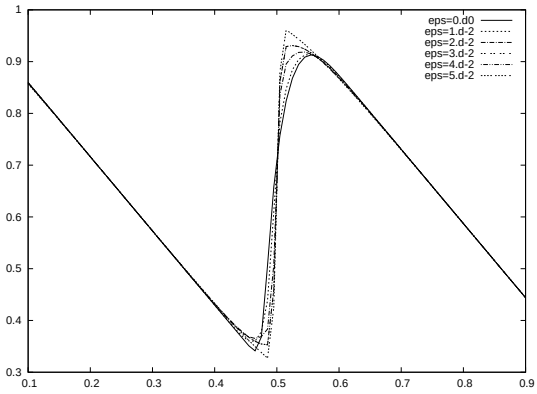

(c) Heat distribution at $t = 10h_t$

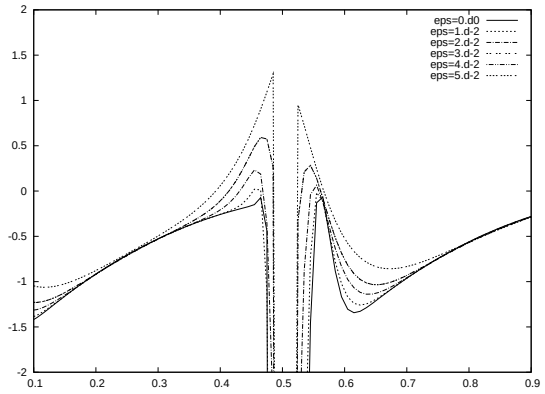

(d) $Q \times \partial_x \Theta$ at $t = 10h_t$

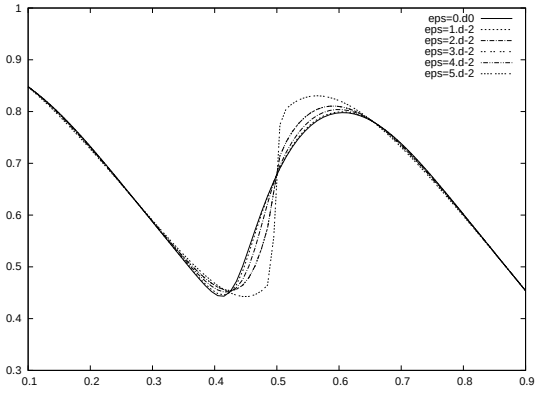

(e) Heat distribution at $t = 100h_t$

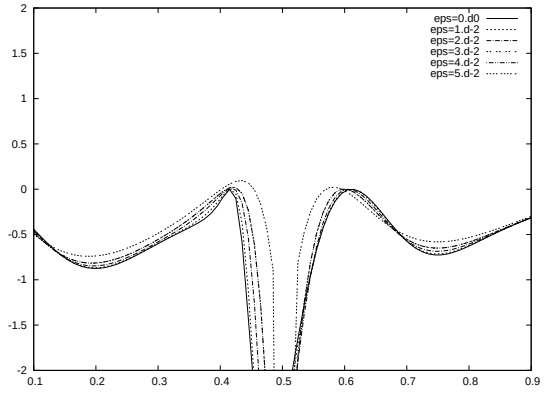

(f) $Q \times \partial_x \Theta$ at $t = 100h_t$

Figure II.3: Simulation of the hydrodynamic model (4.1)–(4.2): $h_t = 10^{-4}$, $h_x = 10^{-2}$, $\rho = 1$, $\kappa(\Theta) = \Theta^{5/2}$, $\nu = 1$

the model to capture anti-diffusive phenomena.

Acknowledgements

This research is part of a collaborative program with CEA/DAM. We thank J.-F. Clouet for many fruitful discussions and kind advices and D. Deck for allowing us to use his kinetic code. This work was also supported by Ministry of Higher Education and Research, Nord-Pas de Calais Regional Council and FEDER through the "Contrat de Projets Etat Region (CPER) 2007-2013".

Appendices

II.A Some useful properties of the linearized Landau-Fokker-Planck operator

II.A.1 On spectral properties of the linearized Landau-Fokker-Planck operator

As said in section II.2.3, the spectral properties of the linearized operator are crucial. In particular we use the Fredholm-like property (B2). However, spectral gap estimate, see (2.13), are usually not available for realistic collision kernels. Nevertheless, a fine estimate can be derived working with suitable weighted space; we refer to [1, 17, 25] for proofs, comments and applications of the following statement (see also [15] for the Boltzmann operator with soft potentials).

Lemma II.A.1 *Let us consider the linearized Landau-Fokker-Planck operator. For any* $\alpha \in [-4, 0]$*, (B2) is satisfied in* $\mathcal{D} = \left\{h : \mathbb{R}^3 \to \mathbb{R},\ \text{such that } \left\|\frac{h}{M}\right\|_D < \infty\right\}$ *where*

$$||h||_D^2 = |h|_{L^2(<v>^{-\alpha-1}M)} + |\Pi_v \nabla_v h|_{L^2(<v>^{-\alpha-1}M)} + |(Id - \Pi_v)\nabla_v h|_{L^2(<v>^{-\alpha-3}M)} + |\Pi_v \nabla_v h|_{L^2(|v|^{-\alpha-1}M)},$$

with the shorthand notation $< v >= \sqrt{1 + |v|^2}$*.*

Proof. Here and below, the norm $|.|_{L^2(w)}$ is associated to the weighted inner product

$$< \phi, \psi >_{L^2(w)} = \int \phi(v)\psi(v)w(v)\mathrm{d}v.$$

We write the problem as to find $h \in \mathcal{D}$ such that for any $g \in \mathcal{D}$ we have $a(h, g) = \int Fg\mathrm{d}v$ with

$$a(h, g) = -\left\langle (L_{\rho,\Theta} + Z_i \widetilde{C}_{ei})h, g \right\rangle_{L^2(M^{-1})},$$

and $F = |v|^\beta v M_{\rho,\Theta}(v)$ for some exponent $\beta \in \mathbb{R}$.

Firstly, we look at a coercivity estimate of the bilinear form a. Let us write

$$\begin{aligned} a(h,h) =& \frac{\Theta^{\alpha/2}}{2}\int_{\mathbb{R}^3}\int_{\mathbb{R}^3}\left|\Pi_{v-v_\star}\left(\nabla_v\frac{h}{M}-\nabla_{v_\star}\frac{h_\star}{M_\star}\right)\right|^2\frac{MM_\star \mathrm{d}v\mathrm{d}v_\star}{|v-v_\star|^{\alpha+1}} \\ &+\bar{Z}Z_i\rho_i\int_{\mathbb{R}^3}\left|\Pi_v\nabla_v\frac{h}{M}\right|^2\frac{M\mathrm{d}v}{|v|^{\alpha+1}}. \end{aligned}$$

According to [17] and to [25, Theorem 1.3], there exists $C_1>0$ with

$$\begin{aligned} &\frac{\Theta^{\alpha/2}}{2}\iint\left|\Pi_{v-v_\star}\left(\nabla_v\frac{h}{M}-\nabla_{v_\star}\frac{h_\star}{M_\star}\right)\right|^2\frac{MM_\star \mathrm{d}v\mathrm{d}v_\star}{|v-v_\star|^{\alpha+1}} \\ &\geq C_1\left(\left|\frac{h}{M}\right|_{L^2(<v>^{-\alpha-1}M)}+\left|\Pi_v\nabla_v\frac{h}{M}\right|_{L^2(<v>^{-\alpha-1}M)}+\left|(Id-\Pi_v)\nabla_v\frac{h}{M}\right|_{L^2(<v>^{-\alpha-3}M)}\right). \end{aligned}$$

Thus, there exists $C_2>0$ such that

$$a(h,h)\geq C_2\left\|\frac{h}{M}\right\|_{\mathcal{D}}^2.$$

Then, we establish the continuity of a. Remark that

$$\begin{aligned} <L_{\rho,\Theta}h,g>_{L^2(M^{-1})} =& \frac{\Theta^{\alpha/2}}{2}\iint\Pi_{v-v_\star}\left(\nabla_v\frac{h}{M}-\nabla_{v_\star}\frac{h_\star}{M_\star}\right) \\ &\cdot\Pi_{v-v_\star}\left(\nabla_v\frac{g}{M}-\nabla_{v_\star}\frac{g_\star}{M_\star}\right)\frac{MM_\star \mathrm{d}v\mathrm{d}v_\star}{|v-v_\star|^{\alpha+1}}. \end{aligned}$$

Using the Cauchy-Schwartz inequality, we write

$$\begin{aligned} |a(h,g)| \leq& \frac{\Theta^{\alpha/2}}{2}\left(\iint\left|\Pi_{v-v_\star}\left(\nabla_v\frac{h}{M}-\nabla_{v_\star}\frac{h_\star}{M_\star}\right)\right|^2\frac{MM_\star \mathrm{d}v\mathrm{d}v_\star}{|v-v_\star|^{\alpha+1}}\right)^{1/2} \\ &\times\left(\iint\left|\Pi_{v-v_\star}\left(\nabla_v\frac{g}{M}-\nabla_{v_\star}\frac{g_\star}{M_\star}\right)\right|^2\frac{MM_\star \mathrm{d}v\mathrm{d}v_\star}{|v-v_\star|^{\alpha+1}}\right)^{1/2} \\ &+\bar{n}\rho_i Z_i\left|\Pi_v\nabla_v\frac{h}{M}\right|_{L^2(|v|^{-\alpha-1}M)}\left|\Pi_v\nabla_v\frac{g}{M}\right|_{L^2(|v|^{-\alpha-1}M)}. \end{aligned}$$

We set $w=\frac{v-v_\star}{\sqrt{2}}$ and $w_\star=\frac{v+v_\star}{\sqrt{2}}$, so that

$$\begin{aligned} \iint\left|\Pi_{v-v_\star}\left(\nabla_v\frac{h}{M}-\nabla_{v_\star}\frac{h_\star}{M_\star}\right)\right|^2\frac{MM_\star \mathrm{d}v\mathrm{d}v_\star}{|v-v_\star|^{\alpha+1}} &= 2^{\frac{\alpha}{2}}\iint\left|\Pi_w\nabla_w\frac{h}{M}\right|^2\frac{e^{-\frac{|w|^2}{2}}e^{-\frac{|w_\star|^2}{2}}\mathrm{d}v\mathrm{d}v_\star}{|w|^{\alpha+1}} \\ &= 2^{\frac{\alpha}{2}}(2\pi)^{\frac{3}{2}}\left|\Pi_w\nabla_w\frac{h}{M}\right|^2_{L^2(|v|^{-\alpha-1}M)}. \end{aligned}$$

Thus, we get

$$|a(h,g)|\leq\left(2^{\frac{\alpha}{2}}(2\pi)^{\frac{3}{2}}+\bar{n}\rho_i Z_i\right)\left|\Pi_v\nabla_v\frac{h}{M}\right|_{L^2(|v|^{-\alpha-1}M)}\left|\Pi_v\nabla_v\frac{g}{M}\right|_{L^2(|v|^{-\alpha-1}M)}.$$

Eventually, we apply the Lax-Milgram theorem to conclude that the problem is well-posed. In particular the conclusion applies for $\beta=0$ and $\beta=2$. ∎

II.A.2 Proof of Lemma II.2.3

We remark that

$$\begin{aligned} L_{\rho,\Theta}G_{\rho,\Theta} &= \frac{\rho}{(2\pi\Theta)^{3/2}} v\ e^{-|v|^2/2\Theta} \\ &= \frac{\rho}{(2\pi\Theta)^{3/2}}\nabla_v \cdot \int \Theta^{\alpha/2}\frac{\Pi_{v-v_\star}}{|v-v_\star|^{\alpha+1}} \\ &\qquad (\nabla_v - \nabla_{v_\star})(G_{\rho,\Theta}(v)e^{-|v_\star|^2/2\Theta} + G_{\rho,\Theta}(v_\star)e^{-|v|^2/2\Theta})\mathrm{d}v_\star \\ &\quad + Z_i\bar{n}\rho_i\nabla_v\cdot\Big(\Theta^{\alpha/2}\frac{\Pi_v}{|v|^{\alpha+1}}\nabla_v G_{\rho,\Theta}\Big). \end{aligned}$$

Since by (2.11), $\bar{Z}\rho_i = \rho$, dividing by ρ yields

$$\begin{aligned} &\frac{1}{(2\pi\Theta)^{3/2}} v\ e^{-|v|^2/2\Theta} = Z_i\Theta^{\alpha/2}\nabla_v\cdot\Big(\frac{\Pi_v}{|v|^{\alpha+1}}\nabla_v G_{\rho,\Theta}\Big) \\ &+\frac{\Theta^{\alpha/2}}{(2\pi)^{3/2}}\nabla_v\cdot\int\frac{\Pi_{v-v_\star}}{|v-v_\star|^{\alpha+1}}\Big(\frac{v_\star}{\Theta}e^{-|v_\star|^2/2\Theta}G_{\rho,\Theta}(v) + e^{-|v_\star|^2/2\Theta}\nabla_v G_{\rho,\Theta}(v) \\ &\qquad -\frac{v}{\Theta}e^{-|v|^2/2\Theta}G_{\rho,\Theta}(v_\star) - e^{-|v|^2/2\Theta}\nabla_{v_\star}G_{\rho,\Theta}(v_\star)\Big)\ \frac{\mathrm{d}v_\star}{\Theta^{3/2}} \end{aligned}$$

which already tells us that $G_{\rho,\Theta}$ actually does not depend on ρ. We use the change of variable $v_\star/\sqrt{\Theta} \to v_\star$, and the relation $\sqrt{\Theta}(\partial_{v_k}\varphi)(v\sqrt{\Theta}) = \partial_{v_k}\big[\varphi(v\sqrt{\Theta})\big]$ so that evaluating the previous relation at $v\sqrt{\Theta}$, we are led to

$$\begin{aligned} &\frac{\Theta^{(\alpha-1)/2}}{(2\pi)^{3/2}}\nabla_v\cdot\int\frac{\Pi_{\sqrt{\Theta}(v-v_\star)}}{|\sqrt{\Theta}(v-v_\star)|^{\alpha+1}}\Big(-v_\star e^{-|v_\star|^2/2}\frac{G_{\rho,\Theta}(v\sqrt{\Theta})}{\sqrt{\Theta}} + e^{-|v_\star|^2/2}\nabla_v\Big(\frac{G_{\rho,\Theta}(v\sqrt{\Theta})}{\sqrt{\Theta}}\Big) \\ &\qquad -ve^{-|v|^2/2}\frac{G_{\rho,\Theta}(v_\star\sqrt{\Theta})}{\sqrt{\Theta}} + e^{-|v|^2/2}\nabla_{v_\star}\Big(\frac{G_{\rho,\Theta}(v_\star\sqrt{\Theta})}{\sqrt{\Theta}}\Big)\Big)\mathrm{d}v_\star \\ &\quad + Z_i\Theta^{(\alpha-1)/2}\nabla_v\cdot\Big(\frac{\Pi_{\sqrt{\Theta}v}}{|\sqrt{\Theta}v|^{\alpha+1}}\nabla_v\Big(\frac{G_{\rho,\Theta}(v\sqrt{\Theta})}{\sqrt{\Theta}}\Big)\Big) \\ &= \frac{1}{(2\pi\Theta)^{3/2}}v\sqrt{\Theta}\ e^{-|v|^2/2} = \frac{1}{(2\pi)^{3/2}}\ \frac{1}{\Theta}\ v\ e^{-|v|^2/2} \end{aligned}$$

with the property $\Pi_{\sqrt{\Theta}z} = \Pi_z$. We conclude that $\widetilde{G}(v) = \frac{G_{\rho,\Theta}}{\sqrt{\Theta}}(v\sqrt{\Theta})$ is solution of

$$L_{1,1}\widetilde{G} = \frac{1}{(2\pi)^{3/2}}\ v\ e^{-|v|^2/2}.$$

Bibliography

[1] Baranger, C., and Mouhot, C. Explicit spectral gap estimates for the linearized Boltzmann and Landau operators with hard potentials. *Rev. Mat. Iberoamericana 21* (2005), 819–841.

[2] Bers, A., and Delcroix, J.-L. *Physique des plasmas.* EDP Sciences, Paris, 2000.

[3] Besse, C., and Goudon, T. Derivation of a non-local model for diffusion asymptotics; Application to radiative transfer problems. *Commun. Comput. Phys. 8* (2010), 1139–1182.

[4] Bony, J.-M. *Méthodes mathématiques pour les sciences physiques.* Les éditions de l'école polytechnique, Paris, 2001.

[5] Bostan, M., and Goudon, T. High-electric-field limit for the Vlasov-Maxwell-Fokker-Planck system. *Ann. Inst. H. Poincaré Anal. Non linéaire 25* (2008), 1221–1251.

[6] Bostan, M., and Goudon, T. Low field regime for the relativistic Vlasov-Maxwell-Fokker-Planck system; the one and one half dimensional case. *Kinet. Relat. Models 1* (2008), 139–170.

[7] Cercignani, C. *The Boltzmann equation and its applications.* Springer-Verlag, New York, 1988.

[8] Deck, D. Documentation du code `fpelec`. Tech. rep., CEA/DAM, 2009.

[9] Decoster, A. Equations fluides et coefficients de transport des plasmas. Lecture notes, summer school, St Malo, France, GdR SPARCH-CNRS, 1994.

[10] Degond, P. From kinetic to fluid models in plasmas physics. Lecture notes, summer school, GdR SPARCH-CNRS, 1996.

[11] Degond, P., and Lemou, M. Dispersion relations for the linearized Fokker-Planck equation. *Arch. Ration. Mech. Anal. 138* (1997), 137–167.

[12] Desvillettes, L., and Golse, F. A remark concerning the Chapman-Enskog asymptotics. In *Advances in Kinetic Theory and Computing*, vol. 22, B. Perthame of *Ser. Adv. Math. Appl. Scie.* World Scientific, River Edge, NJ, 1994, pp. 191–203.

[13] DiPerna, R., and P.-L., L. Global weak solutions of Vlasov-Maxwell systems. *Commun. Pure Appl. Math. 42* (1989), 729–757.

[14] Epperlein, E. M., and Short, R. A practical nonlocal model for electron heat transport in laser plasmas. *Phys. Fluids B 3* (1991), 3092–3098.

[15] Golse, F., and Poupaud, F. Stationary solutions of the linearized Boltzmann equation in a half-space. *Math. Methods Appl. Sci. 11* (1989), 486–502.

[16] Graille, B., Mangin, T., and Massot, M. Kinetic theory of plasmas: translational energy. *Math. Models Methods Appl. Sci. 19* (2009), 527–599.

[17] Guo, Y. The Landau equation in a periodic box. *Commun. Math. Phys. 231* (2002), 391–434.

[18] Hildebrandt, A., Blossey, R., Rjasanow, S., Kohlbacher, O., and Lenhof, H.-P. Novel formulation of nonlocal electrostatics. *Physical Review Letters 93* (2004). article 108104.

[19] Hildebrandt, A., Blossey, R., Rjasanow, S., Kohlbacher, O., and Lenhof, H.-P. Electrostatic potentials of proteins in water: a structured continuum approach. *Bioinformatics 23* (2007), e99–e103.

[20] Lions, P.-L. Compactness in Boltzmann's equation via Fourier integral operator and applications III. *J. Math. Kyoto Univ. 34* (1994), 539–584.

[21] Luciani, J.-F., and Mora, P. Resummation methods of the Chapman-Enskog Expansion for a Strongly Inhomogeneous Plasma. *J. Stat. Phys. 43* (1986), 281–302.

[22] Luciani, J.-F., and Mora, P. Nonlocal electron transport in laser created plasmas. *Laser Part. Beams 12* (1994), 387–400.

[23] Luciani, J.-F., Mora, P., and Pellat, R. Quasistatic heat front and delocalized heat flux. *Phys. Fluids 28* (1985), 835–845.

[24] Molvig, K. Collisions and transport theory II: Conductivity–Spitzer Problem. Class notes, MIT, Cambridge MA, 2003.

[25] Mouhot, C. Explicit coercivity estimates for the Boltzmann and Landau operators. *Commun. Partial Differential Equations 31* (2006), 1321–1348.

[26] Natalini, R. Introduzione ai metodi numerici alle differenze finite per equazioni di evoluzione. Tech. rep., Istituto per le Applicazioni del Calcolo Mauro Picone, Consiglio Nazionale delle Ricerche, 2003.

[27] Schurtz, G. P., Nicolaï, P., and Busquet, M. A nonlocal electron conduction model for multidimensional radiation hydrodynamics codes. *Phys. Plasmas 7* (2000), 4238–4250.

[28] Spitzer, L., and Härm, R. Transport phenomena in a completely ionized gas. *Phys. Rev. 89* (1953), 977–981.

[29] Strain, R. M. The Vlasov-Maxwell-Boltzmann system in the whole space. *Commun. Math. Phys. 268* (2006), 543–567.

[30] Yang, T., and Yu, H. Global classical solutions for the Vlasov-Maxwell-Fokker-Planck system. *SIAM J. Math. Anal. 42* (2010), 459–488.

Chapitre III :

Non-Local Macroscopic Models based on Gaussian Closures for the Spitzer-Härm Regime

Résumé : Le régime de Spitzer-Härm relatif à la physique des plasmas conduit à une équation de diffusion non linéaire pour la température électronique. Dans ce travail, nous proposons une hiérarchie de modèles destinés à prendre en compte certains comportements sous-jacents à la modélisation microscopique. Ces modèles sont de type non-local. Néanmoins, aprés discrétisation en énergie, ces modèles peuvent conduire des systèmes couplés d'équations de diffusion. Nous faisons le lien entre les différents modèles en précisant certaines de leurs propriétés mathématiques. Un schéma numérique est enfin proposé pour les modèles approchés, et des simulations permettent de valider l'approche proposée.

Abstract: The Spitzer-Härm regime arising in plasma physics leads asymptotically to a nonlinear diffusion equation for the electron temperature. In this work we propose a hierarchy of models intended to retain more features of the underlying microscopic modeling. These models are of non-local type. Nevertheless, owing to energy discretization they can lead to coupled systems of diffusion equations. We make the connection between the different models precise and bring out some mathematical properties of the models. A numerical scheme is designed for the approximate models, and simulations validate the proposed approach.

Note: Ce chapitre à donné lieu a une publication dans *AIMS Kinetic and Related Models* en collaboration avec Thierry Goudon.

III.1 Introduction

The modeling of plasmas arising in Inertial Confinement Fusion leads to the following integro-differential equation

$$\partial_t F + v \cdot \nabla_x F + E \cdot \nabla_v F = C(F) \tag{1.1}$$

where the unknown $F(t,x,v)$ is interpreted as the number density of electrons in phase space. It depends on the time variable $t \geq 0$, the space variable $x \in \mathbb{R}^3$ and the velocity variable $v \in \mathbb{R}^3$. The problem is completed by an initial data

$$F_{|t=0} = F_{\text{Init}}.$$

The right hand side in (1.1) describes interactions between particles. Both electrons/electrons and ions/elec-trons collisions are embodied into the operator C, which involves certain averages with respect to the variable v. We will detail below examples of operators C that arise in the physical context which motivates this work. For the time being, let us present the crucial requirements on which our analysis is based:

Hypothesis (H1) *Mass and energy conservation:*

$$\int \begin{pmatrix} 1 \\ v^2 \end{pmatrix} C(F) \mathrm{d}v = 0.$$

Note however that we do not require the momentum conservation: indeed, for the models we are interested in the charge current is not conserved by the collision processes. It arises when assuming that F is the distribution function of electrons subject to collisions with positive charges. We adopt the simplifying assumption that the ion distribution is given. For such models mass and energy are conserved, but due to the electron/ion collision operator, the momentum is not conserved.

Hypothesis (H2) *Equilibrium: $C(F) = 0$ if and only if F is a centered Maxwellian $M_{\rho,\theta}(v) = \frac{\rho}{(2\pi\theta)^{3/2}} e^{-|v|^2/(2\theta)}$, with $\rho \geq 0$, $\theta > 0$.*

Hypothesis (H3) *Entropy dissipation:*

$$\int_{\mathbb{R}^3} C(F) \ln(F) \mathrm{d}v \leq 0,$$

and the entropy dissipation vanishes precisely when F is a Maxwellian.

To the particle distribution function $F(t,x,v)$ we associate the following macroscopic quantities

$$\begin{aligned}
&\text{Density:} && \rho(t,x) = \int_{\mathbb{R}^3} F(t,x,v)\mathrm{d}v, \\
&\text{Current } (J) \text{ and Bulk Velocity } (u): && J(t,x) = \rho u(t,x) = \int_{\mathbb{R}^3} vF(t,x,v)\mathrm{d}v, \\
&\text{Total Energy } (\mathcal{E}) \text{ and Temperature } (\theta): && 2\mathcal{E}(t,x) = \rho(t,x)|u(t,x)|^2 + 3\rho(t,x)\theta(t,x) \\
& && \quad = \int_{\mathbb{R}^3} v^2 F(t,x,v)\mathrm{d}v.
\end{aligned} \tag{1.2}$$

The definition of the field E in (1.1) that we consider is slightly unusual: E is defined as to maintain the quasi-neutrality, that is to preserve the constraint

$$\int_{\mathbb{R}^3} vF(t,x,v)\mathrm{d}v = 0. \tag{1.3}$$

To obtain the expression of E by means of the particles distribution F, we proceed as follows. Multiply (1.1) by v and integrate. Taking into account (1.3), we obtain

$$E(t,x) = \frac{1}{\rho}\left[\nabla_x \cdot \left(\int_{\mathbb{R}^3} v \otimes vF\mathrm{d}v\right) - \int_{\mathbb{R}^3} vC(F)\mathrm{d}v\right]. \tag{1.4}$$

The system (1.1), (1.4) is widely used for modeling and simulating Inertial Confinment Fusion phenomena, see e.g. [15]. We refer to [6] for a detailed derivation from the standard Vlasov-Maxwell-Fokker-Planck system in a regime of small Debye length. Note that, regardless specific difficulties related to the collision operator, the mathematical analysis of the non standard constraint (1.4) might lead to interesting questions. It involves the second order moment of the unknown, which is just controlled by the energy conservation, so that applications of average lemma techniques is not so clear, while by contrast to the Vlasov–Poisson coupling we cannot expect any regularization effect in the definition of the electric field. However existence–uniqueness issues are beyond the scope of the present work, which is rather concerned with asymptotic problems.

The simulation of Inertial Confinment Fusion devices is highly demanding in numerical resources, because the problem involves many different scales. The quasi-neutrality constraint and (1.4) constitute already a relevant simplification in comparison to the full system of electromagnetism, but solving the kinetic equation at the physical scales of interest is simply not affordable. For this reason, we are interested in designing reduced models intended to capture the main features of (1.1), (1.4) in certain asymptotic regimes. This is the objective of the present work where we are concerned with small mean free path regimes. More precisely, we are interested in the so-called Spitzer-Härm regime where the dynamics reduces to a non linear diffusion equation for the electron temperature, see [19]. However, the limiting equation, which is amenable to a quite simple numerical treatment, might fail in reproducing the behavior of the plasma with the necessary accuracy, as pointed out for instance in [3, 13, 17]. This has motivated the introduction of intermediate models. In particular, non local corrections to the Spitzer-Härm equation have been introduced in [14] with several extensions [12, 13, 3, 15, 1, 17]. In this work, we develop a different viewpoint to derive from the kinetic equation a hydrodynamic model. The system we wish to design will still depend on the scaling parameter but we expect that it can be solved with a reduced cost in comparison to kinetic simulations, with a strengthened accuracy in comparison to the asymptotic model. Our approach is inspired by the reasoning introduced by Levermore in [10] for gas dynamic equations.

This work is organized as follows. First in section III.2, we briefly review the derivation of the Spitzer-Härm regime. Next in section III.3, we discuss approximated models obtained by projection on the classical spherical harmonic basis. In particular we present variants to the classical P_N models, that can be referred to as the D_N models, [4, 10].

Such models, even if they remain of kinetic nature, already allow to substantially reduce the dimension of the variables. In Section III.4 we combine this approach to a "micro–macro decomposition" where the solution F of (1.1) is split into an equilibrium state and a remainder. It yields a new hierarchy of equations describing the evolution of the electron temperature. We explain in Section III.5 that these models can be seen as relevant generalizations of the Schurtz-Nicolaï system [17]. In Section III.5, we also investigate some mathematical properties of the hydrodynamic system we obtain by Gaussian closure and energy discretization. While additional simplifying assumptions could be useful to make the arguments tractable, the results bring out remarkable properties of the model. Section III.6 ends the paper with the presentation of numerical schemes for the approximate models and discussion of simulation results that validate the proposed equations.

III.2 Spitzer-Härm regime

The physical regime of interest is embodied into a positive parameter ε and we are led to investigate the behavior as $\varepsilon \to 0$ of the solutions $(F_\varepsilon, E_\varepsilon)$ of

$$\partial_t F_\varepsilon + \frac{1}{\varepsilon}\left(v \cdot \nabla_x F_\varepsilon + E_\varepsilon \cdot \nabla_v F_\varepsilon\right) = \frac{1}{\varepsilon^2} C(F_\varepsilon), \tag{2.1}$$

coupled with

$$E_\varepsilon(t,x) = \frac{1}{\rho_\varepsilon}\left[\nabla_x \cdot \left(\int_{\mathbb{R}^3} v \otimes v F_\varepsilon \mathrm{d}v\right) - \frac{1}{\varepsilon}\int_{\mathbb{R}^3} v C(F_\varepsilon)\mathrm{d}v\right]. \tag{2.2}$$

We refer to [6] for a thorough discussion on the scaling issues: ε is defined as the ratio of the velocity unit defined by the observation time and length scales over the thermal velocity, while assuming that the mean free path is of order ε compared to the observation length scale. We start by writing the evolution equation for the macroscopic quantities ρ_ε, u_ε and θ_ε defined by (see (1.2))

$$\rho_\varepsilon = \int_{\mathbb{R}^3} F_\varepsilon \mathrm{d}v, \quad u_\varepsilon = \frac{1}{\rho_\varepsilon}\int_{\mathbb{R}^3} v F_\varepsilon \mathrm{d}v, \quad \theta_\varepsilon = \frac{1}{3\rho_\varepsilon}\int_{\mathbb{R}^3} |v-u_\varepsilon|^2 F_\varepsilon \mathrm{d}v.$$

Multiplying (2.1) by 1, v and $|v|^2$ respectively, and integrating yield

$$\begin{cases} \partial_t \rho_\varepsilon + \dfrac{1}{\varepsilon}\nabla_x \cdot (\rho_\varepsilon u_\varepsilon) = 0, \\ \rho_\varepsilon\left(\partial_t u_\varepsilon + \dfrac{1}{\varepsilon}\left(u_\varepsilon \cdot \nabla_x\right) u_\varepsilon\right) + \dfrac{1}{\varepsilon}\nabla_x \cdot \mathsf{P}_\varepsilon = \dfrac{1}{\varepsilon^2}\displaystyle\int_{\mathbb{R}^3} v C(F_\varepsilon)\mathrm{d}v + \dfrac{1}{\varepsilon}\rho_\varepsilon E_\varepsilon, \\ \partial_t\left(3\rho_\varepsilon\theta_\varepsilon + \rho_\varepsilon u_\varepsilon^2\right) + 2\nabla_x \cdot Q_\varepsilon + \dfrac{1}{\varepsilon}\nabla_x \cdot (3\rho_\varepsilon\theta_\varepsilon u_\varepsilon + 2\mathsf{P}_\varepsilon u_\varepsilon) = -2\rho_\varepsilon E_\varepsilon \cdot u_\varepsilon - \nabla_x \cdot \left(\rho_\varepsilon |u_\varepsilon|^2 u_\varepsilon\right), \end{cases} \tag{2.3}$$

which is still coupled to (2.2). The system (2.3) is not closed since the pressure tensor P_ε and the heat flux Q_ε are defined by

$$\mathsf{P}_\varepsilon = \int_{\mathbb{R}^3} (v-u_\varepsilon) \otimes (v-u_\varepsilon) F_\varepsilon \mathrm{d}v, \qquad Q_\varepsilon = \frac{1}{2\varepsilon}\int_{\mathbb{R}^3} |v-u_\varepsilon|^2 (v-u_\varepsilon) F_\varepsilon \mathrm{d}v$$

respectively. The system also involves the distribution function through the integral term $\int_{\mathbb{R}^3} vC(F_\varepsilon)\mathrm{d}v$. These quantities cannot be expressed in general by means of ρ_ε, u_ε and θ_ε. However, the constraint (1.3) imposes $u_\varepsilon = 0$ and, thus, by using the charge conservation (the first equation in (2.3)), $\rho_\varepsilon(t,x) = \rho_\star(x)$, a fixed density defined by the initial data. Therefore (2.3) reduces to

$$3\rho_\star \partial_t \theta_\varepsilon + 2\nabla_x \cdot Q_\varepsilon = 0. \tag{2.4}$$

Based on Hilbert expansions, it is shown in [6] that the asymptotic regime $\varepsilon \to 0$ leads to the following limiting equation:

$$\begin{aligned} &F_\varepsilon(t,x,v) \to \frac{\rho_\star(x)}{(2\pi\theta(t,x))^{3/2}}\, e^{-v^2/(2\theta(t,x))}, \\ &3\rho_\star \partial_t \theta + \nabla_x \cdot Q_{SH} = 0, \\ &Q_{SH} = -\kappa\theta^{5/2}\nabla_x\theta, \end{aligned} \tag{2.5}$$

where $\kappa > 0$ is a constant depending only on the details of the collision operator, [6, Eq. (2.15)] The system (2.5) will be referred to as the Spitzer-Härm system, see [19]. We are interested in the derivation of "intermediate" models, bearing in mind the following requirements:

- We seek systems "simpler" than the mesoscopic model (2.1), (2.2), having in mind numerical purposes. Based on the fact that the limiting behavior is described by macroscopic quantities depending only on time and space variables, we can expect to reduce the dimension of the relevant variables.
- Since the models we wish to design are intended to retain some features of the non-zero ε behavior, they will still depend on the scaling parameter. However, as ε goes to 0, they should be consistent with the Spitzer-Härm equation (2.5).

Hence our approach consists in defining the approximate temperature $\tilde\theta_\varepsilon(t,x)$ and heat flux $\tilde Q_\varepsilon(t,x)$ satisfying

$$3\rho_\star \partial_t \tilde\theta_\varepsilon + 2\nabla_x \cdot \tilde Q_\varepsilon(t,x) = 0,$$

where $\tilde Q_\varepsilon$ is related to the moment of a certain quantity of mesoscopic nature $\tilde F_\varepsilon(t,x,v)$,

$$\tilde Q_\varepsilon(t,x) = \int_{\mathbb{R}^3} v\,\frac{|v|^2}{2}\,\tilde F_\varepsilon(t,x,v)\mathrm{d}v = \frac{8\pi\left(\tilde\theta_\varepsilon(t,x)\right)^3}{3}\int_0^\infty \left(\int_{\mathbb{S}^2} \Omega\ \tilde F_\varepsilon(t,x,\Omega\sqrt{2\tilde\theta_\varepsilon(t,x)\xi})\mathrm{d}\Omega\right)\xi^2\mathrm{d}\xi.$$

We use the change of variable $v \mapsto \Omega\sqrt{2\theta_\varepsilon\xi}$, with $\Omega = v/|v| \in \mathbb{S}^2$ and $\theta_\varepsilon\xi = |v|^2/2$ interpreted as an energy variable. We shall detail in the following sections possible construction of the approximate flux.

III.3 Spherical harmonics decomposition

We start by introducing a few useful notations. For $A = (A_p)_{p\in\{1,2,3\}^P}$ a tensor of order P we define recursively $A^{\otimes 2} = A \otimes A$ with $\otimes$, the Kronecker product (that is $(A^{\otimes 2})_{p=(k,l)} = A_k A_l$ a tensor of order $2P$) and $A^{\otimes n} = A \otimes A^{\otimes(n-1)}$, a tensor of order nP.

Given integers $i \leq P$, it is convenient to write the set of indices of order P as a product: $\{1,2,3\}^P = \{1,2,3\}^i \times \{1,2,3\}^{P-i}$ so that we can write accordingly the components of a tensor A of order P as $A_p = A_{jl}$ with $j \in \{1,2,3\}^i$ and $l \in \{1,2,3\}^{P-i}$. Now, let A and B be tensors of order P and Q respectively. For $i \in \mathbb{N}$, such that $2i \leq P+Q$, we define $A \overset{i}{\cdot} B$, the i-contracted product of A and B as to be the tensor of order $P+Q-2i$ defined by

$$\left(A \overset{i}{\cdot} B\right)_{jk} = \sum_{l \in \{1,2,3\}^i} A_{jl} B_{lk},$$

for $j \in \{1,2.3\}^{P-i}$ and $k \in \{1,2,3\}^{Q-i}$. For instance, when A and B are usual vectors ($P = Q = 1$), the ($i = 1$)-contracted product is nothing but the usual euclidean product; when A is a matrix and B a vector ($P = 2$, $Q = 1$), the ($i = 1$)-contracted product is nothing but the usual matrix–vector product; when A and B are matrices ($P = Q = 2$), the ($i = 1$)-contracted product is nothing but the usual matrix–matrix product while the ($i = 2$)-contracted product is what is commonly named the contracted product of A and B that is the sum of all the products of the components of A and B. By the way, in what follows when $i = 1$ we will simply note $A \cdot B$ instead of $A \overset{1}{\cdot} B$ and when $i = 2$ we will note $A : B$ instead of $A \overset{2}{\cdot} B$.

Next, we consider the spherical harmonics basis $\{Y_i,\ i \in \mathbb{N}\}$, defined by $Y_0(\Omega) = 1$ and

$$Y_i : \Omega \in \mathbb{S}^2 \longmapsto Y_i(\Omega) = \Omega^{\otimes i} - \sum_{j=0}^{i-1} P_j\left(\Omega^{\otimes i}\right) \overset{j}{\cdot} Y_j(\Omega),$$

with P_i defined by

$$P_i : f \in L^2(\mathbb{S}^2) \longmapsto P_i(f) = \left[\int_{\mathbb{S}^2} Y_i \otimes Y_i \mathrm{d}\Omega\right]^{-1} \overset{i}{\cdot} \int_{\mathbb{S}^2} f Y_i \mathrm{d}\Omega.$$

Note that Y_i is a tensor of order i and for a scalar function f, $P_i(f)$ is a tensor of order i too[1]. Given a tensor T of order j, we generalize the definition by setting $P_i(T)$ as to be the tensor of order $i+j$ defined by $\left(P_i(T)\right)_k = P_i(T_k)$ for any $k \in \{1,2,3\}^j$. The first three spherical harmonic tensors are

$$Y_0(\Omega) = 1, \qquad Y_1(\Omega) = \Omega, \qquad Y_2(\Omega) = \Omega^{\otimes 2} - \frac{Id}{3}.$$

For functions defined on $\mathbb{R}^3$, we set similarly

$$P_i(f)(|v|) = \left[\int_{\mathbb{S}^2} Y_i \otimes Y_i \mathrm{d}\Omega\right]^{-1} \overset{i}{\cdot} \int_{\mathbb{S}^2} f(|v|\Omega)\ Y_i(\Omega) \mathrm{d}\Omega$$

and, given a subset $\mathbf{n} \subset \mathbb{N}$, we define

$$P_{\mathbf{n}}^{\perp}(f)(v) = f(v) - \sum_{i \in \mathbf{n}} P_i(f)(|v|) \overset{i}{\cdot} Y_i\Big(\frac{v}{|v|}\Big).$$

[1]We warn the reader that the notation P_i has not to be confused with the ith Legendre polynomial.

This operator satisfies the following orthogonality property

$$\text{For any } i \in \mathbf{n} \text{ and a.e. } r \geq 0, \ \int_{\mathbb{S}^2} P_{\mathbf{n}}^{\perp}(f)(r\Omega) Y_i(\Omega) \mathrm{d}\Omega = 0.$$

Therefore, it makes sense to split a function $F : \mathbb{R}^3 \to \mathbb{R}$ as follows

$$\begin{aligned} &F(v) = \Pi_{\mathbf{n}}(v) + F_{\mathbf{n}}^{\perp}(v), \\ &\Pi_{\mathbf{n}}(v) = \textstyle\sum_{i\in\mathbf{n}} F_i(|v|) \overset{i}{\cdot} Y_i\Big(\dfrac{v}{|v|}\Big), \qquad F_i(|v|) = P_i(F)(|v|), \\ &F_{\mathbf{n}}^{\perp}(v) = P_{\mathbf{n}}^{\perp}(F)(v). \end{aligned}$$

We apply this decomposition to the solution of (2.1) and we denote $F_\varepsilon(t,x,v) = (\Pi_{\mathbf{n}} + F_{\mathbf{n}}^{\perp})(t,x,v)$. Accordingly, let us apply the operators P_i and $P_{\mathbf{n}}^{\perp}$ to (2.1). We obtain

$$\begin{aligned} &\partial_t F_i + \frac{1}{\varepsilon} P_i \left(\nabla_x \cdot (v F_\varepsilon) + E_\varepsilon \cdot \nabla_v F_\varepsilon \right) = \frac{1}{\varepsilon^2} P_i C\left(F_\varepsilon\right), \qquad \text{for } i \in \mathbf{n}, \\ &\partial_t F_{\mathbf{n}}^{\perp} + \frac{1}{\varepsilon} P_{\mathbf{n}}^{\perp} \left(\nabla_x \cdot (v F_\varepsilon) + E_\varepsilon \cdot \nabla_v F_\varepsilon \right) = \frac{1}{\varepsilon^2} P_{\mathbf{n}}^{\perp} C\left(F_\varepsilon\right), \end{aligned} \tag{3.1}$$

coupled with (2.2).

The first idea to design approximate models consists in simplifying the equation for the component orthogonal to $\{Y_i\}_{i\in\mathbf{n}}$, which is implicitly assumed to be small compared to the F_i's. A classical closure is obtained by truncation: the orthogonal part $F_{\mathbf{n}}^{\perp}$ is simply disregarded. It leads to the so–called $P_{\mathbf{n}}$ system where F_ε is approximated by $\Pi_{\mathbf{n}}$, the components of which are defined according to (Model III.1). Remark that the unknown depend on 1 (time) + 3 (space) + 1 ($|v|$) variables.

$$\begin{aligned} &\Pi_{\mathbf{n}}(v) = \sum_{i\in\mathbf{n}} F_i(|v|) \overset{i}{\cdot} Y_i\Big(\frac{v}{|v|}\Big), \\ &\partial_t F_i + \frac{P_i}{\varepsilon} \left[\nabla_x \cdot (v \Pi_{\mathbf{n}}) \right] + \tilde{E}_\varepsilon \cdot \frac{P_i}{\varepsilon} \nabla_v \left(\Pi_{\mathbf{n}} \right) = \frac{1}{\varepsilon^2} P_i C\left(\Pi_{\mathbf{n}} \right), \\ &\tilde{E}_\varepsilon(t,x) = \frac{1}{\rho_\star} \left[\nabla_x \cdot \left(\int_{\mathbb{R}^3} v \otimes v \Pi_{\mathbf{n}} \mathrm{d}v \right) - \frac{1}{\varepsilon} \int_{\mathbb{R}^3} v C\left(\Pi_{\mathbf{n}} \right) \mathrm{d}v \right]. \end{aligned}$$

Model III.1: $P_{\mathbf{n}}$ model.

More involved closures can be proposed, following the reasoning introduced in [9] for gas dynamics. To this end, we need further assumptions on the collision operator and the set $\mathbf{n} \subset \mathbb{N}$.

Hypothesis (H4) *The collision operator is stable on the basis $(Y_i)_{i\in\mathbf{n}}$ in the sense that for any $(F_i)_{i\in\mathbf{n}} \in \prod_{i\in\mathbf{n}} \left(L^2\left(\mathbb{R}_+\right)\right)^{3^i}$, we have*

$$P_{\mathbf{n}}^{\perp} C\left(F_i \overset{i}{\cdot} Y_i \right) = 0.$$

Hypothesis (H5) *The range of the basis* $(Y_i)_{i\in\mathbf{n}}$ *by the collision operator is orthogonal to* Y_1*: for any* $(F_i)_{i\in\mathbf{n}} \in \prod_{i\in\mathbf{n}} \left(L^2\left(\mathbb{R}_+\right)\right)^{3^i}$ *we have*

$$P_1 C\left(F_i \overset{i}{\cdot} Y_i\right) = 0.$$

These two hypothesis hold assuming that the collision operator is isotropic, in the following sense [7].

Hypothesis (H6) *The collisional operator is isotropic, which means that for any tensor–valued function* T *defined on* $\mathbb{S}^2$ *and any* $f \in L^2\left(\mathbb{R}_+\right)$ *, there exists* $\lambda : [0,\infty) \to \mathbb{R}$ *such that*

$$C\left(f\left(|v|\right) T\left(\frac{v}{|v|}\right)\right) = \lambda\left(|v|\right) T\left(\frac{v}{|v|}\right).$$

The derivation assumes that the solution F_ε of (2.1) is mainly described by the projected part $\Pi_{\mathbf{n}}$ while the remainder $F_{\mathbf{n}}^\perp$ is supposed to be of order ε compared to the leading term. Let us introduce the linearized operator

$$L_f(g) = \frac{\mathrm{d}}{\mathrm{d}s} C(f+sg)\Big|_{s=0}.$$

Then we simplify (3.1) by getting rid of the low order terms and linearizing the collision term. We are thus led to the so–called $D_{\mathbf{n}}$ model where F_ε is approached by $\tilde{F}_\varepsilon = \Pi_{\mathbf{n}} + \varepsilon F_{\mathbf{n}}^\perp$, solutions of the system in (Model III.2).

$$\begin{aligned}
&\partial_t F_i + \frac{P_i}{\varepsilon}\left[\nabla_x \cdot \left(v\left(\Pi_{\mathbf{n}} + \varepsilon F_{\mathbf{n}}^\perp\right)\right) + \tilde{E}_\varepsilon \cdot \nabla_v \left(\Pi_{\mathbf{n}} + \varepsilon F_{\mathbf{n}}^\perp\right)\right] = \frac{P_i}{\varepsilon^2} C(\Pi_{\mathbf{n}} + \varepsilon F_{\mathbf{n}}^\perp),\\
&P_{\mathbf{n}}^\perp\left[\nabla_x \cdot (v\Pi_{\mathbf{n}}) + \tilde{E}_0 \cdot \nabla_v \Pi_{\mathbf{n}}\right] = P_{\mathbf{n}}^\perp L_{\Pi_{\mathbf{n}}} F_{\mathbf{n}}^\perp = P_{\mathbf{n}}^\perp L_{\Pi_{\mathbf{n}}} P_{\mathbf{n}}^\perp F_{\mathbf{n}}^\perp,\\
&\tilde{E}_\varepsilon(t,x) = \frac{1}{\rho_\star}\left[\nabla_x \cdot \left(\int_{\mathbb{R}^3} v\otimes v\left(\Pi_{\mathbf{n}} + \varepsilon F_{\mathbf{n}}^\perp\right)\mathrm{d}v\right) - \frac{1}{\varepsilon}\int_{\mathbb{R}^3} vC\left(\Pi_{\mathbf{n}} + \varepsilon F_{\mathbf{n}}^\perp\right)\mathrm{d}v\right],\\
&\tilde{E}_0(t,x) = \frac{1}{\rho_\star}\left[\nabla_x \cdot \left(\int_{\mathbb{R}^3} v\otimes v\Pi_{\mathbf{n}}\mathrm{d}v\right) - \int_{\mathbb{R}^3} vL_{\Pi_{\mathbf{n}}}\left(F_{\mathbf{n}}^\perp\right)\mathrm{d}v\right].
\end{aligned}$$

Model III.2: $D_{\mathbf{n}}$ model.

Note that we have used the linearized operator only when approximating the equation for $F_{\mathbf{n}}^\perp$ in (3.1). Hypothesis (H4) and (H5) is used to get rid of $\mathscr{O}(\varepsilon)$ terms in the definition of the electric field. Note also that the equation for $F_{\mathbf{n}}^\perp$ can be recast as

$$P_{\mathbf{n}}^\perp\left[L_{\Pi_{\mathbf{n}}} F_{\mathbf{n}}^\perp + \frac{\nabla_v \Pi_{\mathbf{n}}}{\rho_\star}\int_{\mathbb{R}^3} wL_{\Pi_{\mathbf{n}}} F_{\mathbf{n}}^\perp(w)\mathrm{d}w\right] = P_{\mathbf{n}}^\perp\left[\nabla_x \cdot (v\Pi_{\mathbf{n}}) - \frac{1}{\rho_\star}\nabla_x \cdot \left(\int_{\mathbb{R}^3} v\otimes v\left(\Pi_{\mathbf{n}}\right)\mathrm{d}v\right)\right]$$

by taking into account the expression of $\tilde{E}_0$.
We can expect that such a model is simpler to solve numerically than the original kinetic equation. In particular, the leading unknowns F_i only depend on t, x and $|v|$, while the determination of the corrector $F_{\mathbf{n}}^\perp$ relies on the inversion of the linear operator $P_{\mathbf{n}}^\perp L_{\Pi_{\mathbf{n}}} P_{\mathbf{n}}^\perp$. This operator inherits the usual Fredholm properties satisfied by the linearized operator

$L_{\Pi_{\mathbf{n}}}$, and in some circumstances it can be explicitely inverted. However, the number of unknowns grows exponentially with the number of elements in the set $\mathbf{n}$, which restricts the applicability of this approach to the few first elements. Furthermore, the cost of 3 dimensional simulations will remain quite high, and finally, it is not clear that the $P_{\mathbf{n}}$ and $D_{\mathbf{n}}$ closures preserve the non negativity of the corresponding approximate particles distribution function $\tilde{F}$. Nevertheless, we bear in mind the spherical harmonic decomposition to derive further approximate models.

III.4 Derivation of hydrodynamic models based on micro-macro decomposition

As said in the Introduction, we wish to derive hydrodynamic models, intended to describe intermediate regimes, for small but non zero ε. According to (2.5), the leading term is a Maxwellian, and we can start by expanding

$$F_\varepsilon(t,x,v) = M_{\rho_\star,\theta_\varepsilon(t,x)}(v) + \varepsilon f_\varepsilon(t,x,v), \qquad \int_{\mathbb{R}^3}(1,v,|v|^2) f_\varepsilon \mathrm{d}v = 0$$

in the spirit of the Chapman-Enskog procedure. Here and below we denote

$$M_{\rho,\theta}(v) = \frac{\rho}{\big(2\pi\theta\big)^{3/2}} \exp\Big(-\frac{|v|^2}{2\theta}\Big).$$

By writing a relevant closure equation for the fluctuation f_ε, we will obtain an evolution equation for the approximate temperature that we denote in the sequel $\tilde{\theta}$. Indeed, we rewrite (2.1) as follows

$$\partial_t f_\varepsilon + \frac{1}{\varepsilon} v\cdot\nabla_x f_\varepsilon + \frac{1}{\varepsilon} E_\varepsilon\cdot\nabla_v f_\varepsilon + \frac{1}{\varepsilon}\Big(\partial_t + \frac{1}{\varepsilon} v\cdot\nabla_x + \frac{1}{\varepsilon} E_\varepsilon\cdot\nabla_v\Big) M_{\rho_\star,\theta_\varepsilon} = \frac{1}{\varepsilon^3} C(M_{\rho_\star,\theta_\varepsilon} + \varepsilon f_\varepsilon).$$

We can expand the right hand side, taking into account $C(M_{\rho_\star,\theta_\varepsilon}) = 0$; the leading term is

$$\frac{1}{\varepsilon^2} L_{M_{\rho_\star,\theta_\varepsilon}} f_\varepsilon.$$

We remind that integration of the equation yields, see (2.4)

$$3\rho_\star \partial_t \theta_\varepsilon + 2\nabla_x \cdot \int_{\mathbb{R}^3} v \frac{|v|^2}{2} f_\varepsilon \mathrm{d}v = 3\rho_\star \partial_t \theta_\varepsilon + 2\nabla_x \cdot Q_\varepsilon = 0.$$

We can now reproduce the manipulations of the previous section to obtain approximate equations for the fluctuation f_ε. Following the reasoning of the previous section we set $f_\varepsilon(t,x,v) = (\pi_{\mathbf{n}} + \varepsilon f^\perp_{\mathbf{n}})(t,x,v)$ with

$$\pi_{\mathbf{n}}(t,x,v) = \sum_{i\in\mathbf{n}} f_i(t,x,|v|) \overset{i}{\cdot} Y_i\Big(\frac{v}{|v|}\Big), \qquad f_i(t,x,|v|) = P_i\left(f_\varepsilon(t,x,\cdot)\right)(|v|),$$
$$f^\perp_{\mathbf{n}}(t,x,v) = P^\perp_{\mathbf{n}}\left(f_\varepsilon(t,x,\cdot)\right)(v).$$

We remind that the leading part of the particle distribution function is the Maxwellian $M_{\rho_\star,\theta_\varepsilon(t,x)}$. Therefore, reproducing the manipulations of the previous Section, we are led to

$$P_{\mathbf{n}}^{\perp}\big(\nabla_x(v(M_{\rho_\star,\theta_\varepsilon(t,x)}+\varepsilon\pi_{\mathbf{n}})+\tilde{E}_0\cdot\nabla_v(M_{\rho_\star,\theta_\varepsilon(t,x)}+\varepsilon\pi_{\mathbf{n}})\big)=\varepsilon P_{\mathbf{n}}^{\perp}L_{M_{\rho_\star,\theta_\varepsilon}}P_{\mathbf{n}}^{\perp}f_{\mathbf{n}}^{\perp}$$

which is the analog of the second equation in (Model III.2), with $\Pi_{\mathbf{n}}=M_{\rho_\star,\theta_\varepsilon(t,x)}+\varepsilon\pi_{\mathbf{n}}$. To obtain a balanced expression, we get rid of the singular term; it imposes $P_{\mathbf{n}}^{\perp}(v\cdot\nabla_x+E\cdot\nabla_v)M_{\rho_\star,\theta}=0$. Since $(v\cdot\nabla_x+E\cdot\nabla_v)M_{\rho_\star,\theta}$ is proportional to Y_1 it leads to suppose

$$1\in\mathbf{n}. \tag{4.1}$$

It is consistent with the fact that one seeks an approximation of the heat flux $Q_\varepsilon=\int_{\mathbb{R}^3}v|v|^2f_\varepsilon\mathrm{d}v$ where $v|v|^2$ is proportional to Y_1, hence the integral involves f_1. In addition we shall use analog of hypothesis (H4) for the linearized operator. We suppose that

Hypothesis (H7) *The linearized operator is stable on the basis $(Y_i)_{i\in\mathbf{n}}$: for any $(f_i)_{i\in\mathbf{n}}\in\prod_{i\in\mathbf{n}}\left(L^2\left(\mathbb{R}_+\right)\right)^{3^i}$ we have*

$$P_{\mathbf{n}}^{\perp}L_{M_{\rho,\theta}}\left(f_i\overset{i}{\cdot}Y_i\right)=0.$$

As for (H4) and (H5), these hypothesis are fulfilled when assuming the following more classical property, see [7]

Hypothesis (H8) *The linearized operator is isotropic in the sense that for any tensor–valued function T defined on $\mathbb{S}^2$ and any $f\in L^2\left(\mathbb{R}_+\right)$, there exists $\lambda:[0,\infty)\to\mathbb{R}$ such that*

$$L_{M_{\rho,\theta}}\left(f\left(|v|\right)T\left(\frac{v}{|v|}\right)\right)=\lambda\left(|v|\right)T\left(\frac{v}{|v|}\right).$$

Remark III.4.1 *This property is fulfilled by many relevant operators:*

- *BGK operator,*
- *Fokker-Planck operator in the approximation where we neglect particles with small velocity, see e.g. [18],*
- *Boltzmann operator, see e. g. [7, Annexe I.9, pp.95–103].*

We construct an approximation of F_ε having the form $\tilde{F}_\varepsilon=M_{\rho_\star,\tilde{\theta}}+\varepsilon\pi_{\mathbf{n}}+\varepsilon^2f_{\mathbf{n}}^{\perp}$. Owing to (4.1) and (H7), we can define the $D_{\mathbf{n}}$ approximation for the fluctuation. We are thus led to the model summarized in (Model III.3) where the unknowns are $\tilde{\theta}(t,x)$, $\{f_i(t,x,r),\ i\in\mathbf{n}\}$, $f_{\mathbf{n}}^{\perp}(t,x,v)$, $\tilde{E}(t,x)$.
We point out that the heat flux depends only on f_1 (which is of vectorial nature). Again, $f_{\mathbf{n}}^{\perp}$ is simply determined by inverting the linear operator $P_{\mathbf{n}}^{\perp}L_{M_{\rho_\star,\tilde{\theta}}}P_{\mathbf{n}}^{\perp}$, but the right hand side of this equation involves a term quadratic with respect to $\pi_{\mathbf{n}}$ through the second derivative of the collision operator.

$$
\begin{aligned}
&\tilde{F}_\varepsilon = M_{\rho_\star,\tilde{\theta}} + \varepsilon\pi_{\mathbf{n}} + \varepsilon^2 f_{\mathbf{n}}^\perp,\\
&3\rho_\star\partial_t\tilde{\theta} + 2\nabla_x\cdot\int_{\mathbb{R}^3} v\frac{|v|^2}{2}(\pi_{\mathbf{n}} + \varepsilon f_{\mathbf{n}}^\perp)\mathrm{d}v = 0,\\
&\partial_t f_i + \frac{P_i}{\varepsilon}(\partial_t M_{\rho_\star,\tilde{\theta}}) + \frac{P_i}{\varepsilon^2}\left(v\cdot\nabla_x\tilde{F}_\varepsilon + \tilde{E}_\varepsilon\cdot\nabla_v\tilde{F}_\varepsilon\right) = \frac{P_i}{\varepsilon^3}C\left(\tilde{F}_\varepsilon\right),\\
&P_{\mathbf{n}}^\perp L_{M_{\rho_\star,\tilde{\theta}}} P_{\mathbf{n}}^\perp f_{\mathbf{n}}^\perp = P_{\mathbf{n}}^\perp\left[\partial_t M_{\rho_\star,\tilde{\theta}} + v\cdot\nabla_x\pi_{\mathbf{n}} + \tilde{E}_0\cdot\nabla_v\pi_{\mathbf{n}} - D^2C(M_{\rho_\star,\tilde{\theta}})(\pi_{\mathbf{n}},\pi_{\mathbf{n}})\right],\\
&\tilde{E}_\varepsilon(t,x) = \frac{1}{\rho_\star}\left[\nabla_x\cdot\left(\int_{\mathbb{R}^3} v\otimes v\tilde{F}_\varepsilon\mathrm{d}v\right) - \frac{1}{\varepsilon}\int_{\mathbb{R}^3} vC(\tilde{F}_\varepsilon)\mathrm{d}v\right],\\
&\tilde{E}_0(t,x) = \frac{1}{\rho_\star}\left[\nabla_x\cdot\left(\int_{\mathbb{R}^3} v\otimes vM_{\rho_\star,\tilde{\theta}}\mathrm{d}v\right) - \int_{\mathbb{R}^3} vL_{M_{\rho_\star,\tilde{\theta}}}(\pi_{\mathbf{n}})\mathrm{d}v\right]
\end{aligned}
$$

Model III.3: $D_{\mathbf{n}}$ model for fluctuations.

III.4.1 Intermediate hydro-kinetic models

In this Section we take advantage of the fact that the heat flux involves the component f_1 of the spherical harmonic expansion only. Therefore, we wish to derive a relevant approximation of f_1. From now on we restrict to the simple case where we choose $\mathbf{n} = \{1\}$. For the sake of concreteness, we replace the collision operator by a BGK–like approximation defined as follows: for any $F \in L^2(\mathbb{R}^3)$ expanded on the spherical harmonic basis $F = \sum_{i\in\mathbb{N}} F_i \overset{i}{\cdot} Y_i$, we set

$$
C(F) = \frac{M_{\rho_\star,\tilde{\theta}}}{\tau_0} - \sum_{i\in\mathbb{N}}\frac{F_i \overset{i}{\cdot} Y_i}{\tau_i}, \tag{4.2}
$$

with $\tau_i(\rho_\star,\tilde{\theta},|v|)\in\mathbb{R}$, the relaxation time associated to Y_i. From now on we work with this operator, which can be seen as a reasonable approximation of more realistic collision operators. In particular, it satisfies (H8). In addition, the second derivative satisfies this property too, so its contribution in (Model III.3) vanishes. Let us remark that the following identities hold:

$$
\begin{aligned}
\nabla_x\cdot\Big(v\left(f_1(|v|)\cdot Y_1(v/|v|)\right)\Big) &= \sum_{i,j} r\partial_{x_i}\left(f_1\right)_j(r)\Omega_i\Omega_j\\
&= \frac{r}{3}\nabla_x\cdot f_1(r)Y_0(\Omega) + r\nabla_x f_1(r) : Y_2(\Omega),\\
\nabla_v\cdot\Big(\tilde{E}_\varepsilon f_1(|v|)\cdot Y_1(v/|v|)\Big) &= \sum_{i,j}\Big(\Omega_i\Omega_j\partial_r(f_1)_j(r)\tilde{E}_i + [\delta_{ij}-\Omega_i\Omega_j]\Big(\frac{(f_1)_j(r)}{r}\tilde{E}_i\Big)\Big)\\
&= \Big(\frac{\partial_r f_1(r)\cdot\tilde{E}_\varepsilon}{3} + \frac{2f_1(r)\cdot\tilde{E}_\varepsilon}{3r}\Big)Y_0(\Omega)\\
&\quad + \Big(\partial_r f_1(r)\otimes\tilde{E}_\varepsilon - \frac{f_1(r)\otimes\tilde{E}_\varepsilon}{r}\Big) : Y_2(\Omega),
\end{aligned}
$$

with $v = r\Omega$, $r = |v|$ and $\Omega = v/|v|$. Therefore, the equation for f_1 casts as

$$
\partial_t f_1 + P_1\left(\nabla_x\cdot\left(vf_{\{1\}}^\perp\right) + \tilde{E}_\varepsilon\cdot\nabla_v f_{\{1\}}^\perp\right) + \frac{r}{\varepsilon^2}\left(\nabla_x\tilde{M} - \frac{\tilde{M}}{\tilde{\theta}}\tilde{E}_\varepsilon\right) = -\frac{f_1}{\varepsilon^2\tau_1}. \tag{4.3}
$$

On the same token, the equation for $f^{\perp}_{\{1\}}$ reads

$$\begin{aligned} P^{\perp}_{\{1\}} L_{M_{\rho_\star,\tilde\theta}}\left(f^{\perp}_{\{1\}}\right) = &\left(\partial_t M_{\rho_\star,\tilde\theta} + \frac{\partial_r f_1 \cdot \tilde E_0}{3} + \frac{2 f_1 \cdot \tilde E_0}{3r} + \frac{r}{3}\nabla_x \cdot f_1\right) Y_0 \\ &+ \left(\partial_r f_1 \otimes \tilde E_0 - \frac{f_1 \otimes \tilde E_0}{r} + r\nabla_x f_1\right) : Y_2 \end{aligned} \tag{4.4}$$

where the right hand side has only components on Y_0 and Y_2. Of course, the time derivative of $M_{\rho_\star,\tilde\theta}$ can be computed by using the equation for $\tilde\theta$. Using (4.2), we arrive at

$$\begin{aligned} f^{\perp}_{\{1\}}(t,x,v) &= \widetilde{f_0}(t,x,r) Y_0(\Omega) + \widetilde{f_2}(t,x,r) : Y_2(\Omega), \\ \widetilde{f_0} &= -\tau_0 \left(\frac{r}{3}\nabla_x \cdot f_1 + \frac{\tilde E_0}{3}\cdot\left(\partial_r f_1 + \frac{2 f_1}{r}\right) - \frac{4\pi}{9\rho_\star}\left(\frac{r^2}{2\tilde\theta} - \frac{3}{2}\right)\frac{M_{\rho_\star,\tilde\theta}}{\tilde\theta}\nabla_x \cdot \int_0^\infty r^5 f_1 \mathrm{d}r\right) \\ \widetilde{f_2} &= -\tau_2\left(r\nabla_x f_1 + \tilde E_0 \otimes \left(\partial_r f_1 - \frac{f_1}{r}\right)\right) \end{aligned} \tag{4.5}$$

We can summarize the model we have derived so far: the approximate particle distribution function reads $\tilde F_\varepsilon = M_{\rho_\star,\tilde\theta} + \varepsilon f_1 \cdot Y_1 + \varepsilon^2\left(\tilde f_0 Y_0 + \tilde f_2 : Y_2\right)$ where the unknowns are governed by the equations in (Model III.4). (Here $\overset{3}{\cdot}$ is the 3−contracted product of a

$$\begin{aligned} 3\rho_\star \partial_t \tilde\theta =& -\frac{4\pi}{3}\nabla_x \cdot \int_0^\infty r^5 f_1 \mathrm{d}r, \\ \partial_t f_1 + \frac{f_1}{\varepsilon^2\tau_1} =& -r\nabla_x \widetilde{f_0} - \partial_r \widetilde{f_0}\tilde E_0 - 2\widetilde{f_2}\cdot\tilde E_0 - \frac{r}{\varepsilon^2}\left(\nabla_x M_{\rho_\star,\tilde\theta} - \frac{M_{\rho_\star,\tilde\theta}}{\tilde\theta}\tilde E_\varepsilon\right) \\ &- \frac{3}{4\pi}\int_{\mathbb{S}^2} Y_2 \otimes Y_2 \mathrm{d}\Omega \overset{3}{\cdot} \left(r\nabla_x \widetilde{f_2} + \tilde E_\varepsilon \otimes \left(\partial_r \widetilde{f_2} - \frac{2\widetilde{f_2}}{r}\right)\right), \\ \tilde E_\varepsilon(t,x) =& \frac{1}{\rho_\star}\left[\frac{4\pi}{3}\nabla_x \int_{\mathbb{R}} r^4\left(M_{\rho_\star,\tilde\theta} + \varepsilon^2\tilde f_0\right)\mathrm{d}r + \varepsilon^2\int_{\mathbb{S}^2} Y_2 \otimes Y_2 \mathrm{d}\Omega \vdots \nabla_x \int_{\mathbb{R}} r^4 \tilde f_2 \mathrm{d}r \right. \\ &\left. + \frac{4\pi}{3}\int_{\mathbb{R}} \frac{r^3 f_1(t,x,r)}{\tau_1}\mathrm{d}r\right], \\ \tilde E_0(t,x) =& \frac{1}{\rho_\star}\left[\frac{4\pi}{3}\nabla_x \int_{\mathbb{R}} r^4 M_{\rho_\star,\tilde\theta}\mathrm{d}r + \frac{4\pi}{3}\int_{\mathbb{R}} \frac{r^3 f_1(t,x,r)}{\tau_1}\mathrm{d}r\right], \\ &\widetilde{f_0} \text{ and } \widetilde{f_2} \text{ defined by (4.5).} \end{aligned}$$

Model III.4: D_1 model for fluctuations.

tensor a order 4 with a tensor of order 3.)

We still wish to derive simpler models, fully of hydrodynamic nature. Proceeding with a naive Chapman-Enskog expansion might lead to ill-posed problems. Nevertheless, we shall introduce a relevant expansion of the solution, which will lead to interesting generalization of the non-local models proposed in the physics literature. For the next step, it is convenient to introduce the change of variable $r = \sqrt{2\xi\tilde{\theta}(t,x)}$, and to define $\frac{2\pi}{3} r^5 f_1(t,x,r)\mathrm{d}r = \mathcal{Q}(t,x,\xi)\mathrm{d}\xi$. In other words we set

$$\mathcal{Q}(t,x,\xi) = \frac{16\pi}{3}\tilde{\theta}^3(t,x)\xi^2 \; f_1\Big(t,x,\sqrt{2\xi\tilde{\theta}(t,x)}\Big). \tag{4.6}$$

The new variable ξ can be interpreted as the ratio between the kinetic energy of the particle $\frac{1}{2}r^2$ and the thermal energy $\tilde{\theta}$. Consequently, for the heat flux we have

$$\tilde{Q}(t,x) = \frac{2\pi}{3}\int_0^\infty r^5 f_1(t,x,r)\mathrm{d}r = \int_0^\infty \mathcal{Q}(t,x,\xi)\mathrm{d}\xi$$

while the current constraint becomes

$$0 = \int_{\mathbb{R}^3} v f_1(t,x|v|)\cdot Y_1(v/|v|)\mathrm{d}v = \frac{4\pi}{3}\int_0^\infty r^3 f_1(t,x,r)\mathrm{d}r = \frac{1}{\tilde{\theta}(t,x)}\int_0^\infty \frac{\mathcal{Q}(t,x,\xi)}{\xi}\mathrm{d}\xi.$$

Let us now check the consistency of the model (Model III.4). We expand the field $\tilde{E}_\varepsilon$ as follows:

$$\tilde{E}_\varepsilon = E_0 + \varepsilon E_1 + \varepsilon^2\tilde{\mathscr{E}}.$$

Identifying the leading order terms in the equation for the deviation f_1 leads to

$$\begin{aligned} f_1 \simeq f_{1,0} &= -r\tau_1\left(\nabla_x M_{\rho_\star,\tilde{\theta}} - \frac{M_{\rho_\star,\tilde{\theta}}}{\tilde{\theta}}E_0\right) \\ &= -r\tau_1 M_{\rho_\star,\tilde{\theta}}\left(\frac{\nabla_x\rho_\star}{\rho_\star} + \left(\frac{v^2}{2\tilde{\theta}} - \frac{3}{2}\right)\frac{\nabla_x\tilde{\theta}}{\tilde{\theta}} - \frac{E_0}{\tilde{\theta}}\right). \end{aligned} \tag{4.7}$$

Hence the quasi-neutrality constraint

$$\int_0^\infty r^3 f_1^0(t,x,r)\mathrm{d}r = 0$$

yields

$$E_0 = \tilde{\theta}\,\frac{\displaystyle\int_0^\infty r^4\tau_1 e^{-r^2/(2\tilde{\theta})}\left(\nabla_x\ln\rho_\star + \left(\frac{r^2}{2\tilde{\theta}} - \frac{3}{2}\right)\nabla_x\ln\tilde{\theta}\right)\mathrm{d}r}{\displaystyle\int_0^\infty r^4\tau_1 e^{-r^2/(2\tilde{\theta})}\mathrm{d}r}, \tag{4.8}$$

by integration of (4.7). Continuing further the expansion and identifying terms arising with the same power with respect to ε, we get

$$E_1 = 0$$

and

$$\begin{aligned}\tilde{\mathscr{E}} =&\frac{1}{\varepsilon^2}\left(\frac{\nabla_x\left(\rho_\star\theta_\varepsilon\right)}{\rho_\star} - E_0 + \frac{4\pi}{3\rho_\star}\int_{\mathbb{R}_+}\frac{r^3}{\tau_1}f_1\mathrm{d}r\right)\\ &+\frac{1}{\rho_\star}\left(\frac{4\pi}{3}\int_{\mathbb{R}_+} r^4\nabla_x\widetilde{f}_0\mathrm{d}r + \int_{\mathbb{S}^2} Y_2\otimes Y_2\mathrm{d}\Omega \overset{3}{\cdot}\int_{\mathbb{R}_+} r^4\nabla_x\widetilde{f}_2\mathrm{d}r\right).\end{aligned} \tag{4.9}$$

Coming back to the heat flux, we obtain at leading order

$$\begin{aligned}\mathcal{Q}(t,x,\xi)\simeq\mathcal{Q}_0(t,x,\xi) &= \frac{16\pi}{3}\tilde{\theta}^3(t,x)\ \xi^2 f_{1,0}\big(t,x,\sqrt{2\xi\tilde{\theta}(t,x)}\big)\\ &= -\frac{4\sqrt{2}}{3\sqrt{\pi}}\rho_\star\tilde{\theta}(t,x)\ \tau_1\\ &\quad\times\xi^{5/2}\left(\xi-\tfrac{3}{2}-\frac{\displaystyle\int_0^\infty\zeta^{3/2}\left(\zeta-\frac{3}{2}\right)\tau_1 e^{-\zeta}\mathrm{d}\zeta}{\displaystyle\int_0^\infty\zeta^{3/2}\tau_1 e^{-\zeta}\mathrm{d}\zeta}\right)e^{-\xi}\ \nabla_x\tilde{\theta}(t,x).\end{aligned} \tag{4.10}$$

We keep in mind in all these expressions that τ_1 depends on $\big(\rho_\star(x),\tilde{\theta}(t,x),\sqrt{2\xi\tilde{\theta}(t,x)}\big)$. If we stop the expansion at this order, we recover the classical Spitzer-Härm heat flux after integration with respect to the variable ξ:

$$3\rho_\star\partial_t\theta = 2\nabla_x\cdot\int_0^\infty\mathcal{Q}_0(t,x,\xi)\mathrm{d}\xi = \nabla_x\cdot(\kappa\theta^{5/2}\nabla_x\theta) \tag{4.11}$$

with κ as in (2.5). The model we wish to design now can be seen as a correction of this equation, depending on ε.

$$3\rho_\star\partial_t\tilde{\theta} = 2\nabla_x\cdot\int_0^\infty(\mathcal{Q}_0+\varepsilon\tilde{\mathcal{Q}})(t,x,\xi)\mathrm{d}\xi = \nabla_x\cdot(\kappa\tilde{\theta}^{5/2}\nabla_x\tilde{\theta}) + 2\varepsilon\nabla_x\cdot\int_0^\infty\tilde{\mathcal{Q}}(t,x,\xi)\mathrm{d}\xi$$

where the corrective term, which formally appears at order $\mathscr{O}(\varepsilon^2)$, is obtained by taking into account the perturbation on the equation (4.3).

Using the notation introduced above, we can go back to (4.3), which, by using (4.6), recasts as

$$\partial_t\mathcal{Q} + \frac{\mathcal{Q}}{\varepsilon^2\tau_1} - \mathscr{D}_x(\mathcal{Q}) + \mathscr{T}(\mathcal{Q}) - \frac{4\rho_\star\tilde{\theta}}{3\sqrt{\pi}}\xi^{5/2}e^{-\xi}\tilde{\mathscr{E}} = \frac{\mathcal{Q}_0}{\varepsilon^2\tau_1}, \tag{4.12}$$

with $\mathscr{D}_x$ the second order differential operator defined by

$$\begin{aligned}\mathscr{D}_x\left(\mathcal{Q}\right) =&\nabla_x\left[\frac{2\tilde{\theta}}{3}\tau_0\xi\nabla_x\cdot\mathcal{Q} - \frac{8\tilde{\theta}}{9\sqrt{\pi}}\tau_0\xi^{5/2}\left(\xi-\frac{3}{2}\right)e^{-\xi}\nabla_x\cdot\int_0^\infty\mathcal{Q}(t,x,\zeta)\mathrm{d}\zeta\right]\\ &+\nabla_x\cdot\left[\frac{3\tilde{\theta}}{2\pi}\tau_2\xi\int_{\mathbb{S}^2}Y_2\otimes Y_2\mathrm{d}\Omega:\nabla_x\mathcal{Q}\right],\end{aligned} \tag{4.13}$$

(with : the 2−contracted product $\overset{2}{\cdot}$ between a tensor of order 4 and a matrix, as defined in Section III.3) and $\mathscr{T}$ is a pseudo-differential operator with respect to the variable ξ and a first order differential operator with respect to the space variable

$$\mathscr{T}(\mathcal{Q}) = \sum_{k=0}^{1}\sum_{j=1}^{3} \partial_{x_j}^k \int_0^\infty a_j^k(t,x,\xi,\zeta)\widehat{\mathcal{Q}}(t,x,\zeta)\; e^{i\xi\zeta}\mathrm{d}\zeta \tag{4.14}$$

where $\widehat{\mathcal{Q}}$ stands for the Fourier transform of $\mathcal{Q}$ and the kernels a_j^k depend on the field $\tilde{E}_\varepsilon$ (the derivation of their expression is tedious and the detailed formula is unexciting).

This term in (4.14) appears as a serious numerical bottleneck because its numerical approximation would require many discretization points of the energy variable, computations of integrals, and inversion of non–sparse matrices. Motivated by numerical purposes, the model we propose is now based on the following approximations:

- We replace $\mathscr{T}(\mathcal{Q}) = \mathscr{T}(\mathcal{Q}_0+\varepsilon\tilde{\mathcal{Q}})$ by $\mathscr{T}(\mathcal{Q}_0)$. (Note that we have already neglected some terms of order $\mathscr{O}(\varepsilon)$ in equation (4.12).) The advantage is that the dependence of $\mathscr{T}(\mathcal{Q}_0)$ with respect to ξ is simple and explicit and $\mathscr{T}(\mathcal{Q}_0)$ is only a first order differential operator with respect to the space variable, the coefficients of which can be evaluated by computing a couple of simple integrals.
- We account for this modification in the definition of the field that comes from the current constraint, bearing in mind (4.8).

We are thus led to the set of equations collected in (Model III.5).

The system (Model III.5) is still not purely hydrodynamic because it involves the energy variable ξ. The final step relies on energy-discretization.

$$\begin{aligned}
&3\rho_\star\partial_t\tilde{\theta}+2\nabla_x\cdot\int_0^\infty \mathcal{Q}\mathrm{d}\xi = 0,\\
&\partial_t\mathcal{Q}+\frac{\mathcal{Q}}{\varepsilon^2\tau_1} - \mathscr{D}_x(\mathcal{Q}) - \frac{4\rho_\star\tilde{\theta}}{3\sqrt{\pi}}\xi^{5/2}e^{-\xi}\tilde{\mathscr{E}} = \frac{\mathcal{Q}_0}{\varepsilon^2\tau_1} - \mathscr{T}(\mathcal{Q}_0),\\
&\tilde{\mathscr{E}} = \frac{1}{\rho_\star\tilde{\theta}}\int_0^\infty \frac{1}{\xi}\left[\frac{\mathcal{Q}-\mathcal{Q}_0}{\varepsilon^2\tau_1} - \mathscr{D}_x(\mathcal{Q}) + \mathscr{T}\left(\mathcal{Q}_0\right)\right]\mathrm{d}\xi,\\
&\qquad \text{with } \mathcal{Q}_0, \mathscr{D}_x, \mathscr{T} \text{ given respectively by (4.10), (4.13) and (4.14).}
\end{aligned}$$

Model III.5: Approximate D_1 model for fluctuations: formulation with the generalized heat flux.

III.4.2 Towards hydrodynamic models: energy discretization

Since the hydrodynamic equation (4.11) involves an integral over the energy variable, we are going to approximate the heat flux by using Gaussian quadrature. Proceeding

that way, we shall obtain a system of coupled hydrodynamic equations. To this end we consider $g \in \mathbb{N} \setminus \{0\}$ and for any $i \in \{1, ..., g\}$, $\alpha > -1$, we define $(\xi_1, ..., \xi_g)$ as to be the zeroes of the gth Laguerre generalized polynomials

$$\mathscr{L}_g^{(\alpha)}(\xi) = \sum_{i=1}^{g} (-1)^i \binom{g+\alpha}{g-i} \frac{\xi^i}{i!}.$$

We shall see below how the parameter α can be chosen depending on the collision operator. Therefore, assuming enough regularity on the function $\xi \mapsto \mathcal{Q}(\xi)$ we have the following Gaussian quadrature formula

$$\int_0^\infty \mathcal{Q}(\xi) \mathrm{d}\xi = \sum_{i=1}^{g} \omega_i \mathcal{Q}(\xi_i) + \frac{g!\Gamma(g+\alpha+1)}{(2g)!} \partial_\xi^{2g} \left(\mathcal{Q}(\xi) \xi^{-\alpha} e^{\xi} \right)(c),$$

with $c \geq 0$ and weight ω_i associated to the point ξ_i defined by

$$\omega_i = \frac{\Gamma(g+\alpha)\xi_i}{g!(g+\alpha) \left(\mathscr{L}_{g-1}^{(\alpha)}(\xi_i) \right)^2} \xi_i^{-\alpha} e^{\xi_i}.$$

Based on this formula we are going to use a discrete model where only evaluations of $\mathcal{Q}$ at the quadrature points appear, replacing $\xi-$integrals by the corresponding weighted sums. Implicitly, using such a discretization presumes the regularity of the solution $\mathcal{Q}(t, x, \xi)$. Considering regimes close to the Spitzer-Härm regime, where the dynamics is determined by a (non–linear) diffusion equation, such a regularity assumption might look reasonable (we also refer to the regularity analysis of solutions close to equilibrium [8]). Furthermore, we are interested in a macroscopic description, which means that we accept to disregard the local details of the behavior of the solution with respect to the energy variable. Eventually, we write the hydrodynamic model by considering (Model III.5) at the quadrature points ξ_i, see (Model III.6) below.

Let us discuss the choice of the quadrature weight. To this end, let us assume that

Hypothesis (H9) *The coefficient τ_1 is given by*

$$\tau_1 \left(\rho_\star, \tilde{\theta}, r = \sqrt{2\xi\tilde{\theta}} \right) = \bar{\tau}_1 \frac{r^3}{\rho_\star} = \bar{\tau}_1 \frac{\left(2\tilde{\theta}\xi \right)^{3/2}}{\rho_\star},$$

with $\bar{\tau}_1 > 0$, a constant.

This assumption is physically relevant, in particular as far as we are concerned with the homogeneity with respect to the energy variable. Indeed, we remind that, coming back to physical quantities, the relaxation time for ion-electron collision has the form $\tau_{ei} = \frac{m^2}{4\pi c^4 \ln \Lambda} \frac{r^3}{\rho_\star}$, with m, the electron mass, c, the electron charge and $\ln \Lambda$, the Coulomb logarithm. Within this framework (4.10) becomes

$$\begin{aligned} &\mathcal{Q}_0 = -\tilde{\kappa}(\xi) \nabla_x \tilde{\theta}, \\ &\tilde{\kappa}(t, x, \xi) = \tfrac{16\bar{\tau}_1}{3\sqrt{\pi}} \xi^4 (\xi - 4) e^{-\xi} \tilde{\theta}^{5/2}(t, x). \end{aligned} \tag{4.15}$$

$$
\begin{aligned}
&3\rho_\star \partial_t \tilde{\theta} + 2\nabla_x \cdot \sum_{j=1}^{g} \omega_j \mathcal{Q}_j = 0,\\
&\partial_t \mathcal{Q}_j + \frac{\mathcal{Q}_j}{\varepsilon^2 \mu_j} - \mathscr{D}_j\left((\mathcal{Q}_k)_{k\in[\![1,g]\!]}\right) - \frac{4\rho_\star \tilde{\theta}}{3\sqrt{\pi}} \xi_j^{5/2} e^{-\xi_j} \tilde{\mathscr{E}}\\
&\qquad = -\frac{\kappa_j}{\varepsilon^2 \mu_j} \nabla_x \tilde{\theta} - \mathscr{T}_j\left(-\tilde{\kappa} \nabla_x \tilde{\theta}\right),\\
&\tilde{\mathscr{E}} = \frac{1}{\rho_\star \tilde{\theta}} \sum_{j=1}^{g} \frac{\omega_j}{\xi_j} \left[\frac{\mathcal{Q}_j - \mathcal{Q}_0(\xi_j)}{\varepsilon^2 \mu_j} - \mathscr{D}_j\left((\mathcal{Q}_k)_{k\in[\![1,g]\!]}\right) + \mathscr{T}_j\left(-\tilde{\kappa}\nabla_x \tilde{\theta}\right)\right],\\
&\mathscr{D}_j\left((\mathcal{Q}_k)_{k\in[\![1,g]\!]}\right) = \nabla_x \left[\nu_j^1 \nabla_x \cdot \mathcal{Q}_j - \nu_j^2 \nabla_x \cdot \sum_{k=1}^{g} \omega_k \mathcal{Q}_k\right]\\
&\qquad\qquad + \nabla_x \cdot \left[\nu_j^3 \int_{\mathbb{S}^2} Y_2 \otimes Y_2 \mathrm{d}\Omega : \nabla_x \mathcal{Q}_j\right],\\
&\mathscr{T}_j(\mathcal{Q}) = \sum_{k=0}^{1} \sum_{l=1}^{3} \partial_{x_l}^k \int_0^\infty a_l^k(t,x,\xi_j,\zeta) \mathcal{Q}(t,x,\zeta)\ e^{i\xi_j\zeta} \mathrm{d}\zeta,
\end{aligned}
$$

with for any $j \in [\![1,g]\!]$, $\mathcal{Q}_j(t,x) = \mathcal{Q}(t,x,\xi_j)$,

$$
\begin{aligned}
&\kappa_j(t,x) = \frac{4\sqrt{2}}{3\sqrt{\pi}} \rho_\star(x) \tilde{\theta}(t,x) \tau_1(t,x,\xi_j) \xi_j^{5/2}\\
&\qquad \times \left(\xi_j - \frac{3}{2} - \frac{\displaystyle\int_0^\infty \zeta^{3/2}\left(\zeta - \frac{3}{2}\right)\tau_1(t,x,\zeta) e^{-\zeta}\mathrm{d}\zeta}{\displaystyle\int_0^\infty \zeta^{3/2}\tau_1(t,x,\zeta)e^{-\zeta}\mathrm{d}\zeta}\right) e^{-\xi_j},\\
&\mu_j(t,x) = \tau_1(t,x,\xi_j),\\
&\nu_j^1(t,x) = \frac{2\tilde{\theta}(t,x)}{3} \xi_j \tau_0(t,x,\xi_j),\\
&\nu_j^2(t,x) = \frac{8\tilde{\theta}(t,x)}{9\sqrt{\pi}} \xi_j^{5/2}\left(\xi_j - \frac{3}{2}\right) e^{-\xi_j} \tau_0(t,x,\xi_j),\\
&\nu_j^3(t,x) = \frac{3\tilde{\theta}(t,x)}{2\pi} \xi_j \tau_2(t,x,\xi_j).
\end{aligned}
$$

Model III.6: Hydrodynamic system based on energy discretization and quadrature approximation.

Similarly, the electric field (4.8) reads

$$
\tilde{E}_0 = \tilde{\theta}\left(\nabla_x \ln(\rho_\star) + \frac{5}{2}\nabla_x \ln(\tilde{\theta})\right).
$$

With these formulae we can compute the Spitzer-Härm flux

$$Q_{SH} = \int_0^\infty \mathcal{Q}_0 \mathrm{d}\xi = -\kappa \nabla_x \tilde{\theta},$$

where

$$\kappa(t,x) = \int_0^\infty \tilde{\kappa}(t,x,\xi)\mathrm{d}\xi = \frac{128\bar{\tau}_1}{\sqrt{\pi}}\tilde{\theta}^{5/2}(t,x).$$

Then, we can distinguish two relevant choices for the parameter α :

- From a numerical point of view, we want the quadrature formula as exact as possible for a reduced number of discretization points. According to (4.15) and with $\alpha = 4$, we recover the Spitzer-Härm flux when $g \geq 1$.

- From a physical point of view, we would like to preserve the quasi-neutrality constraint (1.3). Bearing in mind the relation

  $$\rho_\star u = \frac{1}{\tilde{\theta}} \int_0^\infty \frac{\mathcal{Q}}{\xi}\mathrm{d}\xi,$$

  at the leading order we are led to

  $$0 = \int_0^\infty \frac{\mathcal{Q}_0}{\xi}\mathrm{d}\xi = \frac{16\bar{\tau}_1}{3\sqrt{\pi}} \int_0^\infty \xi^3 \left(\xi - 4\right) e^{-\xi}\mathrm{d}\xi \; \tilde{\theta}^{5/2}\nabla_x\tilde{\theta}.$$

  With $\alpha = 3$, we recover the constraint when $g \geq 1$. However, since we also wish to recover the Spitzer-Härm heat flux, we will need $g \geq 2$.

III.5 Nonlocal (Schurtz-Nicolaï) model revisited

The purpose of this Section is two–fold. First, we shall see that (Model III.6) generalizes the non-local model introduced by Schurtz and Nicolaï [17]. Second, adopting further simplifications, we will discuss some mathematical properties of the model, that can be reasonably expected to extend to the complete system.

III.5.1 The Schurtz-Nicolaï model

The Schurtz-Nicolaï system is obtained from (Model III.6) with the following manipulations:

a) The field deviation $\tilde{\mathscr{E}}$ is neglected,

b) The operator $\mathscr{T}$ is disregarded,

c) The second order operator $\mathscr{D}_x$ is replaced by a mere Laplacian,

d) The time derivative is neglected in the equation for the generalized fluxes $\mathcal{Q}_j$.

$$3\rho_\star \partial_t \tilde{\theta} + 2\nabla_x \cdot \sum_{j=1}^{g} \omega_j \mathcal{Q}_j = 0,$$
$$\mathcal{Q}_j - \varepsilon^2 \tilde{\nu}_j \Delta_x \mathcal{Q}_j = -\kappa_j \nabla_x \tilde{\theta}.$$

Model III.7: Schurtz-Nicolaï model.

Therefore, we are led to (Model III.7), with $\kappa_j(t,x) = \tilde{\kappa}(t,x,\xi_j)$ and ν_j a coefficient coming from the approximation of $\mathscr{D}_x$.

This model has been studied in the specific case $g = 1$ in [6] where well-posedness and maximum principle are established. A numerical scheme is also proposed which preserves these fundamental properties of the model. However, the model (Model III.7) suffers several drawbacks. Since the current is defined as $\sum_{i=1}^{g} \frac{\omega_i \mathcal{Q}_i}{\xi_i}$, the quasi-neutrality constraint cannot be satisfied with only one energy group ($g = 1$) in the case $\alpha = 4$, or the model lead to the trivial relation $\mathcal{Q}_1 = 0$ in the case $\alpha = 3$. However, dealing with $g > 1$ quadrature points might lead to ill-posed problems since $\widetilde{\kappa}(\xi)$ takes negative values as it has been argued in view of severe instabilities reported in numerical simulations, see [13], [17, Section III.C], [3, Section III].

For this reason, Schurtz and Nicolaï have suggested to replace $\widetilde{\kappa}$ by $\frac{16\bar{\tau}_1}{3\sqrt{\pi}}\xi^4 e^{-\xi}\tilde{\theta}^{5/2}$. This quantity is non negative and its integral over $(0,\infty)$ coincides with the integral of $\tilde{\kappa}$. This rough approximation looks highly questionable. In particular the quasineutrality constraint is not satisfied whatever the choice of the integration method and on a physical point of view, this approximation means that all particles are moving with the same orientation.

III.5.2 Nonlocal models with flux defined by evolution equations

The path we propose consists in going back to the system (Model III.6), where we use the simplifications a) and b), but we keep the time derivative in the flux equation. In order to match better with the derivation, we also slightly generalize the simplified second order operator which approaches $\mathscr{D}_x$ in c). It leads to (Model III.8), where we have set $\kappa_j(t,x) = \tilde{\kappa}(t,x,\xi_j)$. We shall see that this is crucial to restore the expected properties of the model.

To start with, we observe that the model has remarkable dissipation properties.

Proposition III.5.1 *Assume that for any $j \in [\![1,g]\!]$, the coefficients μ_j, ν_j and κ_j are positive and constant. We introduce the following entropy functional $\mathcal{H} = \frac{1}{2}\left(\frac{3\rho_\star}{2}\tilde{\theta}^2 + \varepsilon^2 \sum_{j=1}^{g} \frac{\omega_j \mu_j}{\kappa_j} |\mathcal{Q}_j|^2\right)$. This quantity is dissipated by the system (Model III.8)*

$$\frac{\mathrm{d}}{\mathrm{d}t}\int_{\mathbb{R}^3} \mathcal{H}\mathrm{d}x \leq 0$$

$$3\rho_\star\partial_t\tilde{\theta}+2\nabla_x\cdot\sum_{j=1}^{g}\omega_j\mathcal{Q}_j=0,$$
$$\partial_t\mathcal{Q}_j+\frac{\mathcal{Q}_j}{\varepsilon^2\mu_j}-\nabla_x\left(\nu_j\nabla_x\cdot\mathcal{Q}_j\right)=-\frac{\kappa_j}{\varepsilon^2\mu_j}\nabla_x\tilde{\theta}.$$

Model III.8: Hydrodynamic model with evolution equation on the heat flux.

Proof. We have

$$\frac{\mathrm{d}}{\mathrm{d}t}\int_{\mathbb{R}^3}\mathcal{H}\mathrm{d}x=\int_{\mathbb{R}^3}\left[\frac{3\rho_\star}{2}\tilde{\theta}\partial_t\tilde{\theta}+\varepsilon^2\sum_{j=1}^{g}\frac{\omega_j\mu_j}{\kappa_j}\mathcal{Q}_j\cdot\partial_t\mathcal{Q}_j\right]\mathrm{d}x.$$

Using (Model III.8), we obtain

$$\frac{\mathrm{d}}{\mathrm{d}t}\int_{\mathbb{R}^3}\mathcal{H}\mathrm{d}x=-\sum_{j=1}^{g}\int_{\mathbb{R}^3}\left[\tilde{\theta}\nabla_x\cdot(\omega_j\mathcal{Q}_j)+\nabla_x\tilde{\theta}\cdot(\omega_j\mathcal{Q}_j)+\frac{\omega_j}{\kappa_j}\left|\mathcal{Q}_j\right|^2-\varepsilon^2\frac{\omega_j\mu_j\nu_j}{\kappa_j}\mathcal{Q}_j\nabla_x\left(\nabla_x\cdot\mathcal{Q}_j\right)\right]\mathrm{d}x.$$

Integrating by part yields

$$\frac{\mathrm{d}}{\mathrm{d}t}\int_{\mathbb{R}^3}\mathcal{H}\mathrm{d}x=-\sum_{j=1}^{g}\omega_j\int_{\mathbb{R}^3}\left[\frac{1}{\kappa_j}\left|\mathcal{Q}_j\right|^2+\varepsilon^2\frac{\mu_j\nu_j}{\kappa_j}\left|\nabla_x\cdot\mathcal{Q}_j\right|^2\right]\mathrm{d}x\leq 0.$$

■

However, the hypothesis of Proposition (III.5.1) are not satisfied with the coefficients $\kappa_j=\widetilde{\kappa}(t,x,\xi_j)$ obtained according to the derivation detailed above. Indeed for small ξ, the function $\xi\mapsto\widetilde{\kappa}(\xi)$ is non positive. In what follows we are interested in the well-posedness and stability issues for (Model III.8), in the one-dimension framework. For the sake of simplicity we suppose that the coefficients κ_j,ν_j,μ_j and $\rho_\star$ are constant. The coefficients κ_j are not supposed to be non negative, but we assume that they satisfy

$$\sum_{j=1}^{g}\omega_j\kappa_j>0. \tag{5.1}$$

This property is natural because it corresponds to the fact that the integral of the function $\xi\mapsto\tilde{\kappa}(\xi)$ is positive. It turns out that (5.1) is the crucial property guaranteeing the well–posedness of the Spitzer-Härm regime. We start by rewriting (Model III.8) as the following reaction, advection, diffusion system

$$\partial_t X+RX+A\partial_x X-D\partial_x^2 X=0, \tag{5.2}$$

where the unknown is the vector–valued function

$X(t,x) = \big(\tilde\theta(t,x), \mathcal{Q}_1(t,x), ..., \mathcal{Q}_g(t,x)\big) \in \mathbb{R}^{g+1}$ and the matrices R, A, D are defined by

$$R = \left(\begin{array}{c|ccc} 0 & 0 & \dots & 0 \\ \hline \vdots & \ddots & 0 & 0 \\ 0 & 0 & \dfrac{1}{\varepsilon^2\mu_j} & 0 \\ \vdots & 0 & 0 & \ddots \end{array}\right), \qquad A = \left(\begin{array}{c|ccc} 0 & \dots & \dfrac{2\omega_j}{3\rho_\star} & \dots \\ \hline \vdots & 0 & \dots & 0 \\ \dfrac{\kappa_j}{\varepsilon^2\mu_j} & \vdots & \ddots & \vdots \\ \vdots & 0 & \dots & 0 \end{array}\right), \quad D = \left(\begin{array}{c|ccc} 0 & \dots & 0 & \dots \\ \hline \vdots & \ddots & 0 & 0 \\ 0 & 0 & \nu_j & 0 \\ \vdots & 0 & 0 & \ddots \end{array}\right).$$

Let us introduce a few notations which are needed to derive a well–posedness statement. We set $\alpha_0^0 = 1$, $\beta_0^0 = 0$ and

$$\begin{aligned}
&\forall i \in [\![1,g]\!],\ \forall m \in [\![0,i]\!], && \alpha_i^m = \sum_{\substack{k_1,\dots,k_i \\ k_\alpha \neq k_\beta}}^{[\![1,g]\!]} \left[\prod_{l=1}^{m} \nu_{k_l}\right] \left[\prod_{l=m+1}^{i} \frac{1}{\varepsilon^2\mu_{k_l}}\right], \\
&\forall m \in [\![0,g+1]\!], && \alpha_{g+1}^m = 0, \\
&\forall i \in [\![1,g+1]\!], && \beta_i^0 = 0, \qquad \beta_i^i = 0, \\
&\forall i \in [\![1,g+1]\!],\ \forall m \in [\![1,i-1]\!], && \beta_i^m = \sum_{\substack{k_1,\dots,k_{i-1} \\ k_\alpha \neq k_\beta}}^{[\![1,g]\!]} \frac{2\omega_{k_{i-1}}\kappa_{k_{i-1}}}{3\varepsilon^2\rho_\star\mu_{k_{i-1}}} \left[\prod_{l=1}^{m-1} \nu_{k_l}\right] \left[\prod_{l=m}^{i-2} \frac{1}{\varepsilon^2\mu_{k_l}}\right].
\end{aligned} \tag{5.3}$$

We next define the sequence $\gamma_n^m(i)$ by

- for any $i \in [\![0, \lfloor \frac{g+1}{2} \rfloor]\!]$, $m \in [\![0, M_0(i) = 2i]\!]$, we set $\gamma_0^m(i) = \alpha_{2i}^m + \beta_{2i}^m$,
- for any $i \in [\![0, \lfloor \frac{g}{2} \rfloor]\!]$, $m \in [\![0, M_1(i) = 2i+1]\!]$, we set $\gamma_1^m(i) = \alpha_{2i+1}^m + \beta_{2i+1}^m$,
- and finally, for any $n \in [\![0, g-1]\!]$, $i \in [\![0, \lfloor \frac{g-1-n}{2} \rfloor]\!]$, $m \in [\![0, M_{n+2}(i) = \max\left(M_n(0) + M_{n+1}(i+1), M_n(i+1) + M_{n+1}(0)\right))]\!]$, we have the iteration formula

$$\gamma_{n+2}^m(i) = \sum_{\substack{l_1=0 \\ l_2+l_1=m}}^{M_{n+1}} \sum_{l_2=0}^{M_n} \begin{vmatrix} \gamma_{n+1}^{l_1}(0) & \gamma_{n+1}^{l_1}(i+1) \\ \gamma_n^{l_2}(0) & \gamma_n^{l_2}(i+1) \end{vmatrix}. \tag{5.4}$$

Theorem III.5.1 *We assume that*

Hypothesis (H10) *For any $n \in [\![0, g+1]\!]$, and $m \in [\![0, M_n(0)]\!]$, the coefficients $\gamma_n^m(0)$ are non negative and there exists an index $m \in [\![0, M_n(0)]\!]$ such that $\gamma_n^m(0) > 0$,*

Hypothesis (H11) *The coefficients μ_i, $i \in [\![1,g]\!]$, are positive, pairwise distinct, and there holds $\sum_{i=1}^g \omega_i\kappa_i > 0$,*

Hypothesis (H12) *The coefficients ν_i, $i \in [\![1,g]\!]$, are positive, pairwise distinct, and there holds $\sum_{i=1}^g \frac{\omega_i\kappa_i\nu_i}{\varepsilon^2\mu_i} > 0$.*

Then, (5.2) is well-posed in $L_2(\mathbb{R})$*: there exists a constant* $C > 0$ *such that, for any initial data* $X_0 \in \big(L_2(\mathbb{R})\big)^{g+1}$*, the problem (5.2) has a unique solution* $X = \Big(\tilde{\theta}, \mathcal{Q}_1, ..., \mathcal{Q}_g\Big) \in C^0\big([0,\infty), \big(L_2(\mathbb{R})\big)^{g+1}\big)$ *which verifies the following stability estimate for any* $t \geq 0$

$$\|X(t)\|_{L^2} \leq C\|X_0\|_{L^2}.$$

Furthermore, $\lim_{t\to\infty} \|X(t)\|_{L^2} = 0$.

The proof is inspired from arguments introduced by Liu and Zeng [11, Chapter 6], even though it is definitely not a direct application of Theorem 6.2 in [11]. Indeed, the system (5.2) does not admit a symmetric form: we cannot find a symmetric matrix S such that SA and SD are symmetric. By using the Fourier Transform, the solution of (5.2) can be cast as

$$X(t,x) = \mathscr{F}^{-1}\big(\Gamma(t,\xi)\mathscr{F}X(0)\big)$$

where

$$\Gamma(t,\xi) = \exp(-t(R + i\xi A + \xi^2 D)).$$

Therefore the stability estimate will appear as a consequence of the spectral properties of the matrix $\Lambda(\xi) = -R - i\xi A - \xi^2 D$. To this end, we remind the following classical statements.

Lemma III.5.1 (Lyapounov stability estimate) *Let* $\mathcal{A}$ *be a bounded subset of* $\mathcal{M}_n(\mathbb{C})$*. Pick* $\delta > 0$*. We suppose that for any* $A \in \mathcal{A}$ *and for any eigenvalue* λ *of* A*, we have* $\mathrm{Re}(\lambda) \leq -\delta$*. Then, there exists* $c > 0$ *such that for any* $t > 0$ *and any* $A \in \mathcal{A}$*,*

$$\|e^{tA}\| \leq \frac{1}{c}e^{-ct}.$$

Lemma III.5.2 (Routh-Hurwitz stability criterion) *Let* P *be a polynomial function with real coefficients. Let* Q *be a polynomial function the zeroes of which are the sum of two zeroes of* P*. The coefficients of* P *and* Q *are positive iff the real part of the zeroes of* P *is negative.*

The proof of this claim can be found in [16]. We shall use these basic statements to investigate the spectral properties of the system (5.2). We consider the characteristic polynomial of the matrix $\Lambda(\xi)$

$$P_g(\lambda,\xi) = \det\big(\lambda\mathbb{I} + R + i\xi A + \xi^2 D\big) = \begin{vmatrix} \lambda & i\dfrac{2\omega_1}{3\rho_\star}\xi & \dots & \dots & i\dfrac{2\omega_g}{3\rho_\star}\xi \\ i\dfrac{\kappa_1}{\varepsilon^2\mu_1}\xi & \lambda + \dfrac{1}{\varepsilon^2\mu_1} + \nu_1\xi^2 & 0 & \dots & 0 \\ \vdots & 0 & \ddots & \ddots & \vdots \\ \vdots & \vdots & \ddots & \ddots & 0 \\ i\dfrac{\kappa_g}{\varepsilon^2\mu_g}\xi & 0 & \dots & 0 & \lambda + \dfrac{1}{\varepsilon^2\mu_g} + \nu_g\xi^2 \end{vmatrix}.$$

This determinant can be evaluated by expanding from the last line and the last column. We obtain the recursion formula

$$P_g(\lambda,\xi) = \left(\lambda + \frac{1}{\varepsilon^2\mu_g} + \nu_g\xi^2\right) P_{g-1}(\lambda,\xi) + \frac{2\omega_g\kappa_g}{3\varepsilon^2\rho_\star\mu_g}\xi^2 \prod_{k=1}^{g-1}\left[\lambda + \frac{1}{\varepsilon^2\mu_k} + \nu_k\xi^2\right].$$

Observe that $P_1(\lambda,\xi) = \lambda^2 + \left(\frac{1}{\varepsilon^2\mu_1} + \nu_1\xi^2\right)\lambda + \frac{2\omega_1\kappa_1}{3\varepsilon^2\rho_\star\mu_1}\xi^2$. Then, we are going to discuss the behavior of the eigenvalues depending whether $|\xi|$ is large or small while an estimate can be derived for the intermediate regimes.

Lemma III.5.3 *Let assumption (H11) in Theorem III.5.1 be fulfilled. Then, $\Lambda(0) = -R$ has $g+1$ distinct eigenvalues: 0 and g real and negative eigenvalues. When $\xi \neq 0$ lies in a sufficiently small neighborhood of 0, $\xi \mapsto \Lambda(\xi)$ admits $g+1$ distinct eigenvalues, which are holomorphic functions of ξ; all those eigenvalues have a negative real part and the eigenvalue which tends to 0 as ξ goes to 0 is asymptotically equivalent to $-\frac{2}{3\rho_\star}\sum_{j=1}^g \omega_j\kappa_j\xi^2$. More precisely, in this neighborhood of 0 we have*

$$\Gamma(t,\xi) = e^{-\frac{2}{3\rho_\star}\sum_{j=1}^g \omega_j\kappa_j\xi^2 t + \mathscr{O}(\xi^3 t)}\mathcal{P}_0(\xi) + \sum_{j=1}^g e^{-\frac{t}{\varepsilon^2\mu_j} + \mathscr{O}(\xi t)}\mathcal{P}_j(\xi),$$

where $\mathcal{P}_j(\xi)$ are the eigenprojectors of $\Lambda(\xi)$.

Proof. Let us set $P_g(\lambda,\xi) = \sum_{k=0}^{g+1} a_k^g(\xi)\lambda^{g+1-k}$. The induction formula for P_g yields an induction formula for the a_k^g's. More precisely we have

$$\begin{aligned}
a_0^g &= a_0^{g-1}\\
a_1^g &= a_1^{g-1} + a_0^{g-1}\left(\frac{1}{\varepsilon^2\mu_g} + \nu_g\xi^2\right)\\
a_2^g &= a_2^{g-1} + a_1^{g-1}\left(\frac{1}{\varepsilon^2\mu_g} + \nu_g\xi^2\right) + \frac{2\omega_g\kappa_g}{3\varepsilon^2\rho_\star\mu_g}\xi^2\\
a_i^g &= a_i^{g-1} + a_{i-1}^{g-1}\left(\frac{1}{\varepsilon^2\mu_g} + \nu_g\xi^2\right) + \frac{2\omega_g\kappa_g}{3\varepsilon^2\rho_\star\mu_g}\xi^2 \sum_{\substack{k_1,\dots,k_{i-2}\\ k_\alpha\neq k_\beta}}^{[\![1,g-1]\!]} \prod_{l=1}^{i-2}\left[\frac{1}{\varepsilon^2\mu_{k_l}} + \nu_{k_l}\xi^2\right] \qquad \forall i \in [\![3,g]\!],\\
a_{g+1}^g &= a_g^{g-1}\left(\frac{1}{\varepsilon^2\mu_g} + \nu_g\xi^2\right) + \frac{2\omega_g\kappa_g}{3\varepsilon^2\rho_\star\mu_g}\xi^2 \prod_{l=1}^{g-1}\left[\frac{1}{\varepsilon^2\mu_l} + \nu_l\xi^2\right],
\end{aligned}$$

with $a_0^1 = 1$, $a_1^1 = \frac{1}{\varepsilon^2\mu_1} + \nu_1\xi^2$ and $a_2^1 = \frac{2\omega_1\kappa_1}{3\varepsilon^2\rho_\star\mu_1}\xi^2$. We seek an expression of a_i^g as a polynomial with respect to the variable ξ. We can check that a_i^g is defined for any $i \in [\![1,g+1]\!]$ by $a_i^g = \sum_{m=0}^i (\alpha_i^m + \beta_i^m)\xi^{2m}$ and (5.3) satisfies the induction formula. Then, for $|\xi| \ll 1$, we seek an expansion of the zeroes $\lambda(\xi)$ of $\lambda \mapsto P_g(\lambda,\xi)$ as $\lambda(\xi) = \sum_{i=0}^\infty \lambda_i\xi^i$:

- Of course, we have

$$P_g(\lambda,0) = \sum_{i=0}^g \alpha_i^0\lambda^{g+1-i} = \lambda\sum_{i=1}^g \sum_{\substack{k_1,\dots,k_i\\ k_\alpha\neq k_\beta}}^{[\![1,g]\!]} \prod_{l=1}^i \frac{1}{\varepsilon^2\mu_{k_l}}\lambda^{g-i} = \lambda\prod_{i=1}^g\left(\lambda + \frac{1}{\varepsilon^2\mu_i}\right).$$

Therefore, as $\xi \to 0$ it is clear that the eigenvalues of $\Lambda(\xi)$ tend to the eigenvalues of $-R$ which are $\{0, -\frac{1}{\varepsilon^2\mu_1}, ..., -\frac{1}{\varepsilon^2\mu_g}\}$. It defines the leading term λ_0. However, because 0 belongs to the spectrum of R, we need to describe more precisely the asymptotic behavior of the eigenvalues $\lambda(\xi)$ for small ξ's.

- At first order, we have

$$\lim_{\xi\to 0} \xi^{-1} P_g\left(\lambda(\xi), \xi\right) = \left(\alpha_g^0 + \beta_g^0\right)\lambda_1 = \prod_{i=1}^{g} \frac{1}{\varepsilon^2\mu_i}\lambda_1 = 0.$$

Thus we get $\lambda_1 = 0$.

- At next order, we have

$$\lim_{\xi\to 0} \xi^{-2} P_g\left(\lambda(\xi), \xi\right) = \left(\alpha_g^0 + \beta_g^0\right)\lambda_2 + \left(\alpha_{g+1}^1 + \beta_{g+1}^1\right) = \prod_{i=1}^{g} \frac{1}{\varepsilon^2\mu_i}\lambda_2 + \frac{2}{3\rho_\star}\sum_{j=1}^{g} \frac{\omega_j\kappa_j}{\varepsilon^2\mu_j} \prod_{\substack{i=1\\ i\neq j}}^{g} \frac{1}{\varepsilon^2\mu_i}.$$

Thus we get $\lambda_2 = -\frac{2}{3\rho_\star}\sum_{j=1}^{g} \omega_j\kappa_j$, which is negative by (5.1). ∎

Lemma III.5.4 *Let assumption (H12) in Theorem III.5.1 be fulfilled. There exists $K > 0$ such that for any ξ verifying $|\xi| \geq K$, $\Lambda(\xi)$ admits $g+1$ distinct eigenvalues, which are holomorphic functions of ξ, all having a negative real part: the smallest eigenvalue is asymptotically equivalent to $\frac{2}{3\rho_\star}\sum_{j=1}^{g} \frac{\omega_j\kappa_j\nu_j}{\varepsilon^2\mu_j}$ while the others behave like $-\nu_j\xi^2$. More precisely, for $|\xi| \geq K$ we have*

$$\Gamma(t,\xi) = e^{-\frac{2}{3\rho_\star}\sum_{j=1}^{g} \frac{\omega_j\kappa_j\nu_j}{\varepsilon^2\mu_j}t + \mathscr{O}(t/\xi)}\mathcal{P}_0(\xi) + \sum_{j=1}^{g} e^{-\nu_j\xi^2 t + \mathscr{O}(\xi t)}\mathcal{P}_j(\xi),$$

where $\mathcal{P}_j(\xi)$ are the eigenprojectors of $\Lambda(\xi)$.

Proof. We use the notation introduced in the proof of Lemma III.5.3. We are now interested in the asymptotic behavior for large ξ's. As $|\xi|$ goes to infinity we remark that $\Lambda(\xi)$ is equivalent to $-\xi^2 D$. Since 0 is a (simple) eigenvalue of D we need to investigate more precisely the asymptotic behavior of the spectrum of $\Lambda(\xi)$ in order to prevent the occurrence of an eigenvalue with positive real part. We remark that, as a function of ξ, $P_g(\lambda, \xi)$ involves only even powers of ξ, with highest degree $2g$. We have

$$\lim_{|\xi|\to\infty} \xi^{-2g} P_g\left(\lambda, \xi\right) = \left(\alpha_g^g + \beta_g^g\right)\lambda + \left(\alpha_{g+1}^g + \beta_{g+1}^g\right) = \prod_{i=1}^{g} \nu_i\lambda + \frac{2}{3\rho_\star}\sum_{j=1}^{g} \frac{\omega_j\kappa_j}{\varepsilon^2\mu_j} \prod_{\substack{i=1\\ i\neq j}}^{g} \nu_i.$$

It determines the behavior of the last eigenvalue of $\Lambda(\xi)$ as to given by $\lambda_\infty = -\frac{2}{3\rho_\star}\sum_{j=1}^{g} \frac{\omega_j\kappa_j\nu_j}{\varepsilon^2\mu_j} < 0$ when $|\xi|$ goes to ∞. ∎

It remains to study the behavior of the spectrum for intermediate $|\xi|$.

Lemma III.5.5 *Let assumption (H10) in Theorem III.5.1 be fulfilled. Then, for any $\bar{\xi} > 0$ there exists $\bar{\lambda} > 0$ such that for any $\bar{\xi} \leq |\xi| \leq \frac{1}{\bar{\xi}}$, the eigenvalues $\lambda(\xi)$ of $\Lambda(\xi)$ satisfy*

$$\mathrm{Re}\left(\lambda(\xi)\right) \leq -\bar{\lambda}$$

Proof. This is a direct application of Lemma III.5.2. For any $\xi \neq 0$, the coefficients of the polynomial function $\lambda \mapsto P_g(\lambda, \xi)$ are real positive. We are led to construct a polynomial Q the zeroes of which are the sum of two zeroes of $P_g(\cdot, \xi)$. Such a construction is well–established, and we shall use a practical criterion. Let us introduce for any $n \in [\![0, g+1]\!]$ and $i \in [\![0, \lfloor \frac{g+1-n}{2} \rfloor]\!]$

$$R_n(i)(\xi) = \frac{\displaystyle\sum_{m=0}^{M_n(i)} \gamma_n^m(i) \xi^{2m}}{\displaystyle\prod_{k=0}^{n-1} \left(R_k(0)(\xi)\right)^{F_{n-k}}},$$

where the $F(j)$'s are the Fibonacci numbers (defined by the recursion $F_0 = 0$, $F_1 = 1$ and $F_{n+2} = F_n + F_{n+1}$) and γ_n^m and M_n are given in (5.4). The coefficients R_n are the elements of the Routh array (see [16]). Then assumption (H10) implies that all $g+2$ elements $R_n(0)$, $n \in [\![0, g+1]\!]$, of the first column of the Routh array are positive. We deduce that for any $\xi \neq 0$ fixed, the zeroes of $\lambda \mapsto P_g(\lambda, \xi)$ have negative real parts. We conclude by a continuity argument. ∎

Then we are ready to end the proof of Theorem III.5.1.

Proof of Theorem III.5.1. We start by using Lemma III.5.3 and Lemma III.5.4: we can find $0 < \tilde{\lambda}_0 \leq \frac{2}{3\rho_\star} \sum_{j=1}^g \omega_j \kappa_j$, $0 < \tilde{\lambda}_\infty \leq \frac{2}{3\rho_\star} \sum_{j=1}^g \frac{\omega_j \kappa_j \nu_j}{\varepsilon^2 \mu_j}$ and $\bar{\xi} > 0$ such that for any $|\xi| \leq \bar{\xi}$ (resp. $|\xi| \geq \frac{1}{\bar{\xi}}$) $\Lambda(\xi)$ is diagonalizable and the eigenvalues satisfy $\mathrm{Re}\,\lambda(\xi) \leq -\tilde{\lambda}_0 \xi^2$ (resp. $\mathrm{Re}\,\lambda(\xi) \leq -\tilde{\lambda}_\infty$). In addition, by using Lemma III.5.5 and the Lyapounov stability Lemma III.5.1, there exists $\tilde{\lambda} > 0$ satisfying for any $\bar{\xi} < |\xi| < \frac{1}{\bar{\xi}}$, $|\Gamma(t, \xi)| \leq \frac{1}{\tilde{\lambda}} e^{-\tilde{\lambda} t}$ (but for such ξ the matrix $\Lambda(\xi)$ might admit Jordan blocks). Then we shall use these estimates to evaluate the Green function

$$\mathscr{G}(t, x) = \frac{1}{2\pi} \lim_{r \to \infty} \int_{-r}^{r} \Gamma(t, \xi) e^{i\xi x} \mathrm{d}\xi,$$

the limit being understood in the Schwartz class $\mathscr{S}'(\mathbb{R})$. We introduce the following approximate Green kernel

$$\mathscr{G}^\star(t, x) = \frac{1}{\sqrt{4\pi \sum_{j=1}^g \omega_j \kappa_j t}} e^{-\frac{x^2}{4 \sum_{j=1}^g \omega_j \kappa_j t}} \mathcal{P}_0(0) + e^{-\frac{2}{3\rho_\star} \sum_{j=1}^g \frac{\omega_j \kappa_j \nu_j}{\varepsilon^2 \mu_j} t} \delta_{x=0} \lim_{\zeta \to \infty} \mathcal{P}_0(\zeta).$$

It corresponds, by using the Inverse Fourier Transform, to the leading terms of Γ, associated to the eigenvalue 0. It remains to evaluate the remainder $\mathscr{R} = \mathscr{G} - \mathscr{G}^\star$. Following [11, Chapters 5– 6, sp. Lemma 5.5, 5.6 & 5.7], we show that the remainder is a function and there exists $C > 0$ such that for any $x \in \mathbb{R}$ and $t > 0$,

$$|\mathscr{R}(t, x)| \leq C \left(t + 1\right)^{-\frac{1}{2}} t^{-\frac{1}{2}} e^{-\frac{x^2}{Ct}}.$$

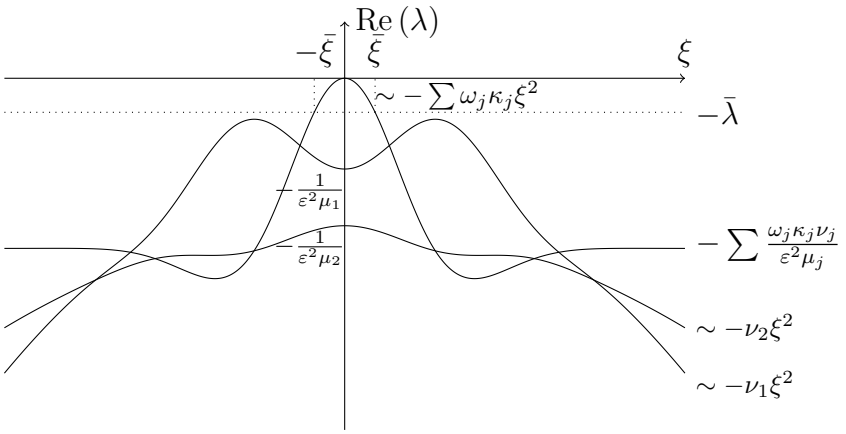

Figure III.1: Example of real part of eigenvalues of Λ in function of ξ for two quadrature points.

We conclude by writing the solution as a convolution product between the Green function and the initial condition. Qualitatively, as time becomes large, the solution mainly behaves like the solution of the heat equation with diffusion coefficient $\sum_{j=1}^{g} \omega_j \kappa_j$. ∎

Remark III.5.1 *The set of assumptions in Theorem III.5.1 might look quite complicated. However, we can readily perform a computer-assisted check-up to determine whether or not the model is well-posness. For $g = 1$ we need to assume $(\kappa_1, \mu_1, \nu_1) \in \left(\mathbb{R}_+^*\right)^3$. For $g = 2$ the Theorem applies when assuming $\mu_{1,2} \in \left(\mathbb{R}_+^*\right)^2$ with $\mu_1 \neq \mu_2$, $\nu_{1,2} \in \left(\mathbb{R}_+^*\right)^2$ with $\nu_1 \neq \nu_2$, and $\kappa_{1,2} \in \mathbb{R}^2$, with*

$$\begin{cases} \omega_1\kappa_1 + \omega_2\kappa_2 > 0, \\ \dfrac{\omega_1\kappa_1\nu_1}{\mu_1} + \dfrac{\omega_2\kappa_2\nu_2}{\mu_2} > 0, \\ \dfrac{2}{3\rho_\star}\left(\dfrac{\omega_1\kappa_1}{\mu_1^2} + \dfrac{\omega_2\kappa_2}{\mu_2^2}\right) \geq -\dfrac{\mu_1\nu_1 + \mu_2\nu_2 + 2\varepsilon^2\mu_1\mu_2\left(\nu_1 + \nu_2\right)}{\varepsilon^2\mu_1^2\mu_2^2}. \end{cases}$$

Anyway, assuming $\sum_{i=1}^{g} \omega_i\kappa_i > 0$ is very natural because it corresponds to the condition of well-possness of the asymptotic model obtained by letting ε go to 0. It is also consistent with the definition of the classical diffusion coefficient in the Spitzer-Härm model. The coefficients $(\mu_i)_{i\in[\![1,g]\!]}$ are values of the isotropic relaxation time evaluated at the Gauss-Laguerre quadrature points. Thus they are naturally positive.

III.6 Numerical schemes for the reduced models

We propose a numerical scheme to solve simplified models as introduced in Section III.5. The simulation will validate the interest of the new evolution models we have proposed in the previous Section. Dealing with the one dimension framework and with a single energy quadrature point, the model (Model III.7) has been numerically investigated in

[6], where stability issues of the proposed scheme are discussed in details. Here we wish to study on numerical grounds the models (Model III.7) or (Model III.8) in the case where we consider many energy quadrature points. By contrast to the situation investigated in [6], it is likely there is no maximum principle for (Model III.8). Hence, we do not care of the L^∞ stability of the scheme. According to the modeling viewpoint, we are interested in solutions that verify the constraint (1.3). In discrete form, it casts as

$$\sum_{j=1}^{g} \frac{\omega_j \mathcal{Q}_j}{\xi_j} = 0, \tag{6.1}$$

and the scheme will be addressed to satisfy this constraint. Therefore, we need to reintroduce a field $\mathscr{E}$, and we are finally led to simulate the system

$$3\rho_\star \partial_t \theta + 2\sum_{j=1}^{g} \omega_j \nabla_x \cdot \mathcal{Q}_j = S(t,x), \tag{6.2}$$

$$\partial_t \mathcal{Q}_j + \frac{\mathcal{Q}_j}{\varepsilon^2 \mu_j} - \nabla_x \left(\nu_j \nabla_x \cdot \mathcal{Q}_j\right) - \eta_j \mathscr{E} = -\frac{\kappa_j}{\varepsilon^2 \mu_j} \nabla_x \theta, \tag{6.3}$$

with $\mathscr{E}$ associated to the constraint (6.1). Defining physically relevant initial data $(\theta^0, Q_1^0, ..., Q_g^0)$ for such a reduced model is far from clear, because there is no natural initialization for the generalized heat flux. In order to observe relevant evolution, we can start form a global equilibrium where θ^0 is constant and $\mathcal{Q}_j^0 = 0$, but the system is perturbed by the action of the source term $S(t,x) \neq 0$ in (6.2).

III.6.1 Discretization

Here we adopt the Finite Difference point of view. Hence we work on a cartesian homogeneous grid: we assume that the space variable is d-dimensional, we denote by $h_i > 0$ the space step in the i-th direction and we set $\mathbf{H} = \mathrm{diag}(h_1, ..., h_d)$, $h_x = \max(h_1, ..., h_d)$. Let $h_t > 0$ be the time step. Given $\mathbf{k} = (k_1, ..., k_d) \in \mathbb{Z}^d$, the unknowns $\theta_{\mathbf{k}}^n$ are intended to be approximations of $\theta(nh_t, \mathbf{Hk})$. Since the density $\rho_\star$ is given, we denote $\rho_{\mathbf{k}} = \rho_\star(\mathbf{Hk})$. Following the ideas introduced in [6], the generalized heat fluxes are evaluated on a staggered grid, see Fig. III.2: let $\mathbf{e}^i$ be the ith element of the canonic basis in $\mathbb{R}^d$, then for any $j \in \{1, ..., g\}$, $Q_{j,i}\big|_{\mathbf{k}+\frac{1}{2}\mathbf{e}^i}^n$ is intended to be an approximation of the ith component of the vector $Q_j \in \mathbf{R}^d$, evaluated at time nh_t and position $\mathbf{H}(\mathbf{k} + \frac{1}{2}\mathbf{e}^i)$. Dealing with such a regular grid in certainly not appropriate for physically realistic simulations where, due to the combination with mesh refinements strategies, unstructured meshes are used. We will go back to the design of adapted Finite Volume schemes for such kind of situations elsewhere [5].

It is convenient to introduce the following operators:

- grad^D acts on scalar unknowns and returns a flux quantity: given $\left(\psi_{\mathbf{k}}\right)_{\mathbf{k}\in\mathbb{Z}^d}$, we define the vector with components

$$\mathrm{grad}^D_{\mathbf{k}+\frac{1}{2}\mathbf{e}^i}(\psi) = \frac{\psi_{\mathbf{k}+\mathbf{e}^i} - \psi_{\mathbf{k}}}{h_i},$$

  It is intended to approximate the gradient $\nabla_x \psi\big(\mathbf{H}(\mathbf{k} + \frac{1}{2}\mathbf{e}^i)\big)$.

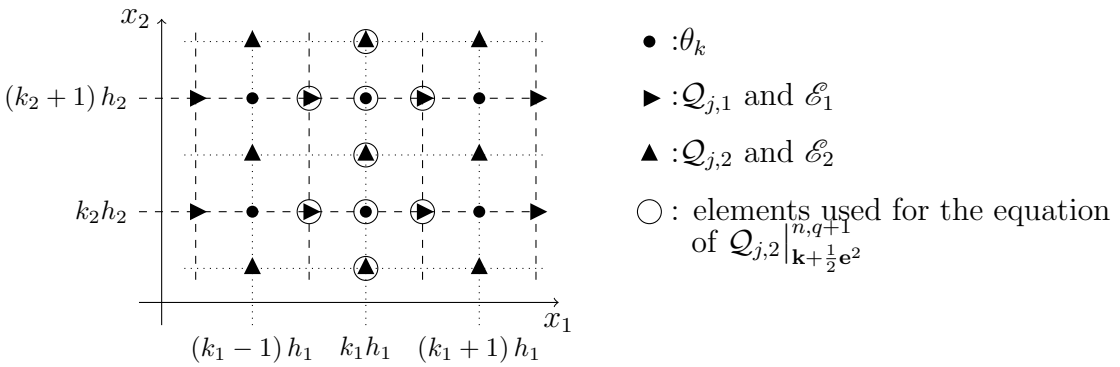

Figure III.2: Staggered grids in dimension 2 ($\mathcal{Q}_j = (\mathcal{Q}_{j,1}, \mathcal{Q}_{j,2})$).

- div^D acts of discrete fluxes and returns a scalar quantity: given $\left(\phi_{1,\mathbf{k}+\frac{1}{2}\mathbf{e}^1}, ..., \phi_{d,\mathbf{k}+\frac{1}{2}\mathbf{e}^d}\right)_{\mathbf{k}\in\mathbb{Z}^d} \in \mathbf{R}^d$, we have

$$\mathrm{div}^D_{\mathbf{k}}(\phi) = \sum_{i=1}^{d} \frac{\phi_{i,\mathbf{k}+\frac{1}{2}\mathbf{e}^i} - \phi_{i,\mathbf{k}-\frac{1}{2}\mathbf{e}^i}}{h_i}.$$

  It is intended to approximate the divergence $\nabla_x \cdot \phi(\mathbf{Hk})$.

In this framework, given $0 \le \tau \le 1$, (6.2) is approximated by

$$\theta^{n+1}_{\mathbf{k}} = \theta^n_{\mathbf{k}} - \frac{2h_t}{3\rho_{\mathbf{k}}} \sum_{j=1}^{g} \omega_j \mathrm{div}^D_{\mathbf{k}} \left(\tau \mathcal{Q}^n_j + (1-\tau)\mathcal{Q}^{n+1}_j\right) + h_t S^{n+1}_{\mathbf{k}}. \tag{6.4}$$

Similarly, the evolution of the generalized flux obeys, in discrete form,

$$\begin{aligned} &\frac{\mathcal{Q}_{j,i}\big|^{n+1}_{\mathbf{k}+\frac{1}{2}\mathbf{e}^i} - \mathcal{Q}_{j,i}\big|^{n}_{\mathbf{k}+\frac{1}{2}\mathbf{e}^i}}{h_t} + \frac{\tau \mathcal{Q}_{j,i}\big|^{n+1}_{\mathbf{k}+\frac{1}{2}\mathbf{e}^i} + (1-\tau)\,\mathcal{Q}_{j,i}\big|^{n}_{\mathbf{k}+\frac{1}{2}\mathbf{e}^i}}{\varepsilon^2 \mu_j^{n+\tau}\big|_{\mathbf{k}+\frac{1}{2}\mathbf{e}^i}} \\ &\quad -\mathrm{grad}^D_{\mathbf{k}+\frac{1}{2}\mathbf{e}^i}\left(\nu_j^{n+\tau}\mathrm{div}^D\left(\tau\mathcal{Q}^{n+1}_j + (1-\tau)\,\mathcal{Q}^n_j\right)\right) - \eta_j\big|^{n+\tau}_{\mathbf{k}+\frac{1}{2}\mathbf{e}^i}\mathscr{E}_i\big|^{n+\tau}_{\mathbf{k}+\frac{1}{2}\mathbf{e}^i} \\ &\quad = -\frac{\kappa_j\big|^{n+\tau}_{\mathbf{k}+\frac{1}{2}\mathbf{e}^i}}{\varepsilon^2\mu_j\big|^{n+\tau}_{\mathbf{k}+\frac{1}{2}\mathbf{e}^i}}\mathrm{grad}^D_{\mathbf{k}+\frac{1}{2}\mathbf{e}^i}\left(\tau\theta^{n+1} + (1-\tau)\,\theta^n\right). \end{aligned} \tag{6.5}$$

Eventually the field $\mathscr{E}\big|^{n,n+1}_{\mathbf{k}+\frac{1}{2}\mathbf{e}^i}$ has to be defined so that the following discrete form of the constraint (6.1):

$$\sum_{j=1}^{g} \frac{\omega_j \mathcal{Q}_{j,i}\big|^{n+1}_{\mathbf{k}+\frac{1}{2}\mathbf{e}^i}}{\xi_j} = 0 \tag{6.6}$$

is fulfilled. With $\tau = 0$ the scheme is explicit. But, according to the analysis in [6] we are led in this case to a stability constraint of parabolic type, $h_t = \mathscr{O}(h_x^2)$ which makes the computational cost prohibitive, especially for multi-dimensional simulations. Hence, using $0 < \tau \le 1$ makes the scheme implicit and improves the stability properties.

The coefficients in (6.5) are thus defined as follows. First we define by interpolation the temperature on the staggered grid, by setting

$$\theta^n_{\mathbf{k}+\frac{1}{2}\mathbf{e}^i} = \frac{\theta^n_{\mathbf{k}} + \theta^n_{\mathbf{k}+\mathbf{e}^i}}{2}.$$

Then, we set

$$\begin{aligned}
\mu_j\big|^{n+\tau}_{\mathbf{k}+\frac{1}{2}\mathbf{e}^i} &= \mu_j\left(\tau\theta^{n+1}_{\mathbf{k}+\frac{1}{2}\mathbf{e}^i} + (1-\tau)\,\theta^n_{\mathbf{k}+\frac{1}{2}\mathbf{e}^i}\right),\\
\kappa_j\big|^{n+\tau}_{\mathbf{k}+\frac{1}{2}\mathbf{e}^i} &= \kappa_j\left(\tau\theta^{n+1}_{\mathbf{k}+\frac{1}{2}\mathbf{e}^i} + (1-\tau)\,\theta^n_{\mathbf{k}+\frac{1}{2}\mathbf{e}^i}\right),\\
\eta_j\big|^{n+\tau}_{\mathbf{k}+\frac{1}{2}\mathbf{e}^i} &= \eta_j\left(\tau\theta^{n+1}_{\mathbf{k}+\frac{1}{2}\mathbf{e}^i} + (1-\tau)\,\theta^n_{\mathbf{k}+\frac{1}{2}\mathbf{e}^i}\right),\\
\nu_j\big|^{n+\tau}_{\mathbf{k}} &= \nu_j\left(\tau\theta^{n+1}_{\mathbf{k}} + (1-\tau)\,\theta^n_{\mathbf{k}}\right).
\end{aligned}$$

In order to treat the non linear system (6.4)-(6.6), we proceed iteratively. Knowing the numerical unknowns at time nh_t, we set $\left(\theta^{n,0}_{\mathbf{k}}, \mathcal{Q}_{j,i}\big|^{n,0}_{\mathbf{k}+\frac{1}{2}\mathbf{e}^i}\right) = \left(\theta^n_k, \mathcal{Q}_{j,i}\big|^{n}_{\mathbf{k}+\frac{1}{2}\mathbf{e}^i}\right)$. Then, we define the following coefficients

$$\begin{aligned}
\theta\big|^{n,q}_{\mathbf{k}+\frac{1}{2}\mathbf{e}^i} &= \frac{\theta^{n,q}_{\mathbf{k}} + \theta^{n,q}_{\mathbf{k}+\mathbf{e}^i}}{2},\\
\mu_j\big|^{n,q}_{\mathbf{k}+\frac{1}{2}\mathbf{e}^i} &= \mu_j\left(\tau\theta\big|^{n,q}_{\mathbf{k}+\frac{1}{2}\mathbf{e}^i} + (1-\tau)\,\theta^n_{\mathbf{k}+\frac{1}{2}\mathbf{e}^i}\right),\\
\kappa_j\big|^{n,q}_{\mathbf{k}+\frac{1}{2}\mathbf{e}^i} &= \kappa_j\left(\tau\theta\big|^{n,q}_{\mathbf{k}+\frac{1}{2}\mathbf{e}^i} + (1-\tau)\,\theta^n_{\mathbf{k}+\frac{1}{2}\mathbf{e}^i}\right),\\
\eta_j\big|^{n,q}_{\mathbf{k}+\frac{1}{2}\mathbf{e}^i} &= \eta_j\left(\tau\theta\big|^{n,q}_{\mathbf{k}+\frac{1}{2}\mathbf{e}^i} + (1-\tau)\,\theta^n_{\mathbf{k}+\frac{1}{2}\mathbf{e}^i}\right),\\
\nu_j\big|^{n,q}_{\mathbf{k}} &= \nu_j\left(\tau\theta\big|^{n,q}_{\mathbf{k}} + (1-\tau)\,\theta^n_{\mathbf{k}}\right),\\
\tilde{\mu}_j\big|^{n,q}_{\mathbf{k}+\frac{1}{2}\mathbf{e}^i} &= \frac{\tau h_t \mu_j\big|^{n,q}_{\mathbf{k}+\frac{1}{2}\mathbf{e}^i}}{\varepsilon^2\mu_j\big|^{n,q}_{\mathbf{k}+\frac{1}{2}\mathbf{e}^i} + \tau h_t},\\
\tilde{\kappa}_j\big|^{n,q}_{\mathbf{k}+\frac{1}{2}\mathbf{e}^i} &= \frac{\tau h_t \kappa_j\big|^{n,q}_{\mathbf{k}+\frac{1}{2}\mathbf{e}^i}}{\varepsilon^2\mu_j\big|^{n,q}_{\mathbf{k}+\frac{1}{2}\mathbf{e}^i} + \tau h_t},\\
\tilde{r}_j\big|^{n,q}_{\mathbf{k}+\frac{1}{2}\mathbf{e}^i} &= \frac{\varepsilon^2\mu_j\big|^{n,q}_{\mathbf{k}+\frac{1}{2}\mathbf{e}^i} - (1-\tau)\,h_t}{\varepsilon^2\mu_j\big|^{n,q}_{\mathbf{k}+\frac{1}{2}\mathbf{e}^i} + \tau h_t}.
\end{aligned} \tag{6.7}$$

Now, we define $\left(\mathcal{Q}_{j,i}\big|^{n,q+1}_{\mathbf{k}+\frac{1}{2}\mathbf{e}^i}, \mathscr{E}_i\big|^{n,q+1}_{\mathbf{k}+\frac{1}{2}\mathbf{e}^i}\right)$ as to be the solution of the *linear* system

$$\begin{aligned}
&\mathcal{Q}_{j,i}\big|^{n,q+1}_{\mathbf{k}+\frac{1}{2}\mathbf{e}^i} - \varepsilon^2\tilde{\mu}_j\big|^{n,q}_{\mathbf{k}+\frac{1}{2}\mathbf{e}^i}\mathrm{grad}^D_{\mathbf{k}+\frac{1}{2}\mathbf{e}^i}\left(\nu_j^{n,q}\mathrm{div}^D\mathcal{Q}_j\big|^{n,q+1}\right)\\
&\quad -\frac{2}{3}\tilde{\kappa}_j\big|^{n,q}_{\mathbf{k}+\frac{1}{2}\mathbf{e}^i}\tau h_t\ \mathrm{grad}^D_{\mathbf{k}+\frac{1}{2}\mathbf{e}^i}\left(\frac{1}{\rho}\mathrm{div}^D\sum_{l=1}^{g}\omega_l\mathcal{Q}_l\big|^{n,q+1}\right) - \varepsilon^2\tilde{\mu}_j\big|^{n,q}_{\mathbf{k}+\frac{1}{2}\mathbf{e}^i}\eta_j\big|^{n,q}_{\mathbf{k}+\frac{1}{2}\mathbf{e}^i}\mathscr{E}_i\big|^{n,q+1}_{\mathbf{k}+\frac{1}{2}\mathbf{e}^i}\\
&\qquad = -\frac{\tilde{\kappa}_j\big|^{n,q}_{\mathbf{k}+\frac{1}{2}\mathbf{e}^i}}{\tau}\mathrm{grad}^D_{\mathbf{k}+\frac{1}{2}\mathbf{e}^i}\left(\theta^n+\tau h_t S^{n+1}\right) + \tilde{r}_j\big|^{n,q}_{\mathbf{k}+\frac{1}{2}\mathbf{e}^i}\mathcal{Q}_{j,i}\big|^{n}_{\mathbf{k}+\frac{1}{2}\mathbf{e}^i}\\
&\qquad\quad +\varepsilon^2\tilde{\mu}_j\big|^{n,q}_{\mathbf{k}+\frac{1}{2}\mathbf{e}^i}\frac{1-\tau}{\tau}\mathrm{grad}^D_{\mathbf{k}+\frac{1}{2}\mathbf{e}^i}\left(\nu_j^{n,q}\mathrm{div}^D\mathcal{Q}_j\big|^{n}\right)\\
&\qquad\quad +\frac{2}{3}\tilde{\kappa}_j\big|^{n,q}_{\mathbf{k}+\frac{1}{2}\mathbf{e}^i}(1-\tau)\,h_t\ \mathrm{grad}^D_{\mathbf{k}+\frac{1}{2}\mathbf{e}^i}\left(\frac{1}{\rho}\mathrm{div}^D\sum_{l=1}^{g}\omega_l\mathcal{Q}_l\big|^{n}\right),\\
&\sum_{j=1}^{g}\frac{\omega_j\mathcal{Q}_j\big|^{n,q+1}_{\mathbf{k}+\frac{1}{2}\mathbf{e}^i}}{\xi_j} = 0.
\end{aligned} \tag{6.8}$$

Note that, unfortunately, this linear system is non-symmetric in general. Finally the temperature is obtained by solving

$$\theta^{n,q+1}_{\mathbf{k}} = \theta^n_{\mathbf{k}} - \frac{2h_t}{3\rho_{\mathbf{k}}}\sum_{l=1}^{g}\omega_l\mathrm{div}^D_{\mathbf{k}}\left(\tau\mathcal{Q}_l\big|^{n,q+1} + (1-\tau)\,\mathcal{Q}_l\big|^{n}\right) + h_t S^{n+1}_{\mathbf{k}}. \tag{6.9}$$

The updated quantities $\left(\theta^{n+1}_{\mathbf{k}}, \mathcal{Q}_j\big|^{n+1}_{\mathbf{k}+\frac{1}{2}\mathbf{e}^i}, \mathscr{E}_i\big|^{n+1}_{\mathbf{k}+\frac{1}{2}\mathbf{e}^i}\right)$, solution of the non-linear system (6.4)–(6.6) are seen as the limit when q goes to infinity of $\left(\theta^{n,q}_{\mathbf{k}}, \mathcal{Q}_j\big|^{n,q}_{\mathbf{k}+\frac{1}{2}\mathbf{e}^i}, \mathscr{E}_i\big|^{n,q}_{\mathbf{k}+\frac{1}{2}\mathbf{e}^i}\right)$. In practice, we stop the iteration when the relative error between the two last iterates is below a certain threshold. Usually, a few iterations are enough to construct the fixed point. The performances of the scheme are discussed below through a series of numerical experiments in the one dimension framework.

Remark III.6.1 *The method might appear as too costly for the purposes of industrial simulations, because we have to solve a coupled system of $g+1$ vectorial equations (fluxes and field) at each position. A relevant simplification consists in uncoupling the definition of the heat fluxes. To this end we can make use of Jacobi methods where coupling terms are treated explicitly: only terms involving the current energy group are treated implicitly. It greatly reduces the complexity of the underlying linear system to be solved when updating the fluxes. In this approach, the constraint needs to be evaluated explicitly. Summing over the quadrature points in* (6.8) *after having multiplied it by $\frac{\omega_j}{\xi_j}$, yields an expression of $\mathscr{E}\big|^{n,q+1}_{\mathbf{k}+\frac{1}{2}\mathbf{e}^i}$. Then, by inserting it in the implicit equations of the generalized heat flux we write g linear systems of vectorial equations (fluxes) at each position. These linear systems are independent, so the resolution could easily be parallelized. Eventually, we estimate the temperature using* (6.9)*. The mean field perturbation does not need to be estimated at each iteration. This adaptation has been introduced in the code* `Aladin` *developed by CEA/DAM: two-dimensional simulations and further comparisons with a kinetic P_1 code (see (Model III.1)) look promising but modeling efforts are still necessary to define correctly many physical parameters.*

III.6.2 Asymptotic consistency

We start by investigating the behavior of the scheme (6.7)–(6.9) as the parameter ε vary. The test case we propose is quite close to the simulation performed in [6]. The problem is set on the slab $(0,1)$ endowed with periodic boundary conditions. As an initial condition we consider $\theta^0(x) = f(x - [x])$ with, for any $x \in (0,1)$

$$f(x) = \frac{3}{2} + \frac{1}{2}\sin\left(\frac{2x}{2\delta}\frac{\pi}{2}\right)\mathbb{1}_{[0,\frac{1}{2}-\delta]} + \frac{1}{2}\sin\left(\frac{1-2x}{2\delta}\frac{\pi}{2}\right)\mathbb{1}_{]\frac{1}{2}-\delta,\frac{1}{2}+\delta[} + \frac{1}{2}\sin\left(\frac{2\,(x-1)}{2\delta}\frac{\pi}{2}\right)\mathbb{1}_{[\frac{1}{2}+\delta,1]}$$

and $\delta = 0.01$. The generalized heat flux vanish initially $\mathcal{Q}_j^0(x) = 0$ (note that the initialisation of $\mathcal{Q}_j$ is physically not realistic) and we do not bring any energy to the system $S(t,x) = 0$. We assume an homogeneous density $\rho_\star = 1$. The number of energy groups is $g = 5$, and $\alpha = 3$. The relaxation times are defined as $\tau_0 = 5.10^2$ and τ_1 is given by (H9) with $\bar{\tau}_1 = 1$. We use the scheme (6.7)–(6.9) with $\tau = 1$ (fully implicit version), the space step $h_1 = 1/500$, and the time step $h_t = 10^{-6}$.

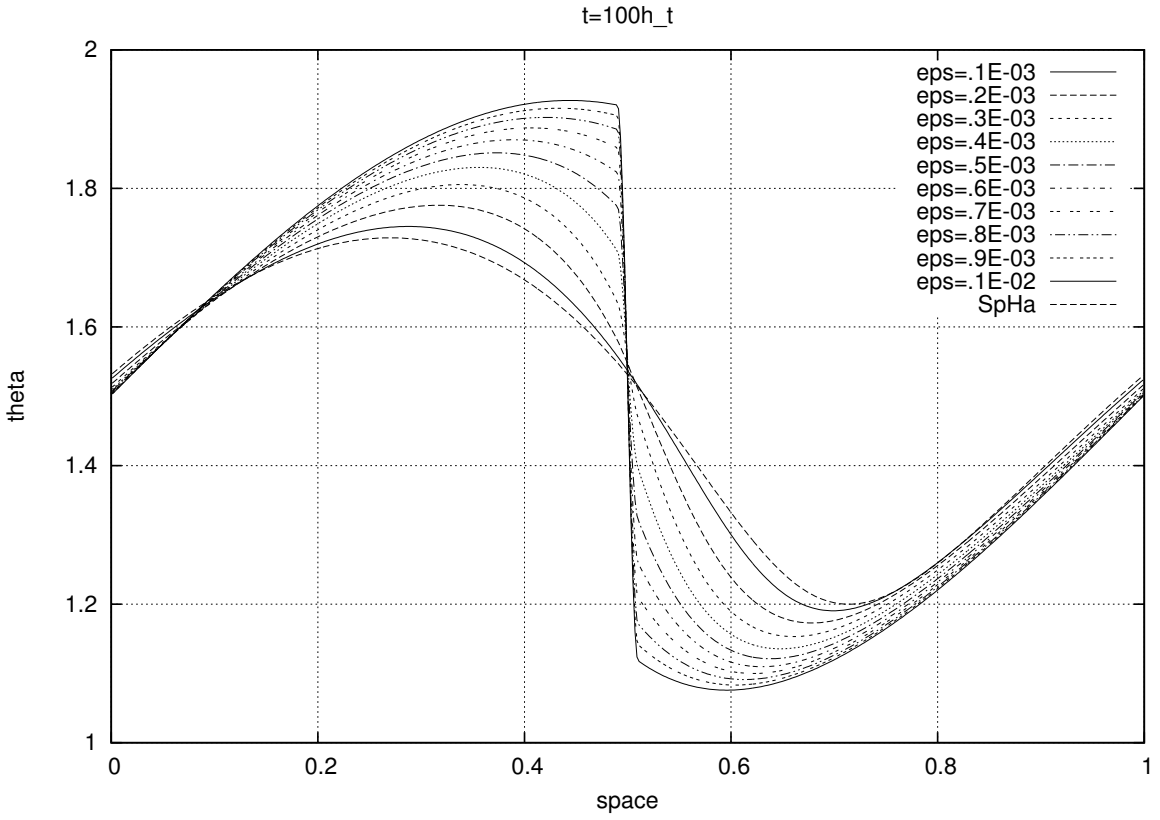

Figure III.3: Asymptotic consistency: Temperature profile for different values of ε at time $t = 10^{-4}$.

Formally, as ε goes to 0 the system (6.1)–(6.3) tends to the the Spitzer-Härm equation. As ε goes to infinity, the flux equation degenerates to

$$\partial_t \mathcal{Q}_j - \nabla_x\left(\nu_j \nabla_x \cdot \mathcal{Q}_j\right) - \eta_j \mathscr{E} = 0,$$

Initializing the generalized heat flux by $\mathcal{Q}_j^0(x) = 0$, we are led to the trivial solution is $\mathcal{Q}_j(t,x) = 0$.
Fig. III.3 shows the solutions of (6.7)–(6.9), at a fixed time, for several values of ε. As ε decreases we observe that the discontinuity smears out, and the solution tends to the one given by the Spitzer-Härm model. This numerical experiment confirms that the model is consistent with the Spitzer-Härm regime as $\varepsilon \to 0$.

III.6.3 Simulations of relaxation

Here we wish to compare, for a fixed value of ε (here $\varepsilon = 10^{-4}$), the solutions provided by several models we have discussed so far. Precisely, we compare the solution of (6.1)-(6.3) to the solution of the model (Model III.7). To this end, we use the same scheme than for solving (6.7)–(6.9) but we drop the terms corresponding to the time derivative, as well as the terms associated to the constraint. Furthermore, since the problem is unstable (and likely ill-posed) when the coefficients $\tilde{\kappa}$ take negative values, we use the correction proposed in (2.18). Fig. III.6.3 displays the solutions, compared to the Spitzer-Härm model that corresponds to the asymptotic case $\varepsilon = 0$.

On this simulation, the temperature profiles are very similar. As said above, the initial condition is not physically realistic but its impact on the results becomes negligible after a few time steps. Indeed, the profiles of the heat flux become similar as time increases. Nevertheless the initial temperature profile is constructed so that the temperature gradient varies brutally, which brings out the delocalization effects: the non-local models capture the so–called "antidiffusive effect", as presented in [3]: for time $t = h_t$ and $t = 10h_t$, the direction of the heat flux is not necessarily dictated by the temperature gradient and $Q \cdot \nabla_x \theta$ might change sign. However, with the model (Model III.7) the current does not vanish: on the contrary, it is far from negligible in the area of delocalization where we observe discrepancies in the temperature profiles provided by the different models. By contrast (6.1)–(6.3) preserves a vanishing current due to the numerical constraint (6.6).

III.6.4 Simulation of laser beam

The next simulation is physically more relevant: we start from the global equilibrium, $\theta^0 = 1$ and $\mathcal{Q}_j^0 = 0$, but we bring locally some energy in the system through the source term $S \neq 0$. More precisely we set

$$S(t,x) = 10^5 \exp\left(-\frac{|x-1/2|^2}{10^{-3}}\right) \mathbb{1}_{t \leq 2.10^{-6}}.$$

This source could be interpreted as a simple modeling of a laser beam in the plan orthogonal to the x direction. The other parameters are the same as in the previous simulations. As shown in Fig. III.6.4, the temperature profiles are steeper with the non-local models, especially for short times. We also observe sensible differences in the amplitude of the heat fluxes. Note also that the model (6.1)–(6.3) produces steeper profiles than (Model III.7). Like for the relaxation test case, the current does not vanish with (Model III.7) whereas it is exactly zero for (6.1)–(6.3).

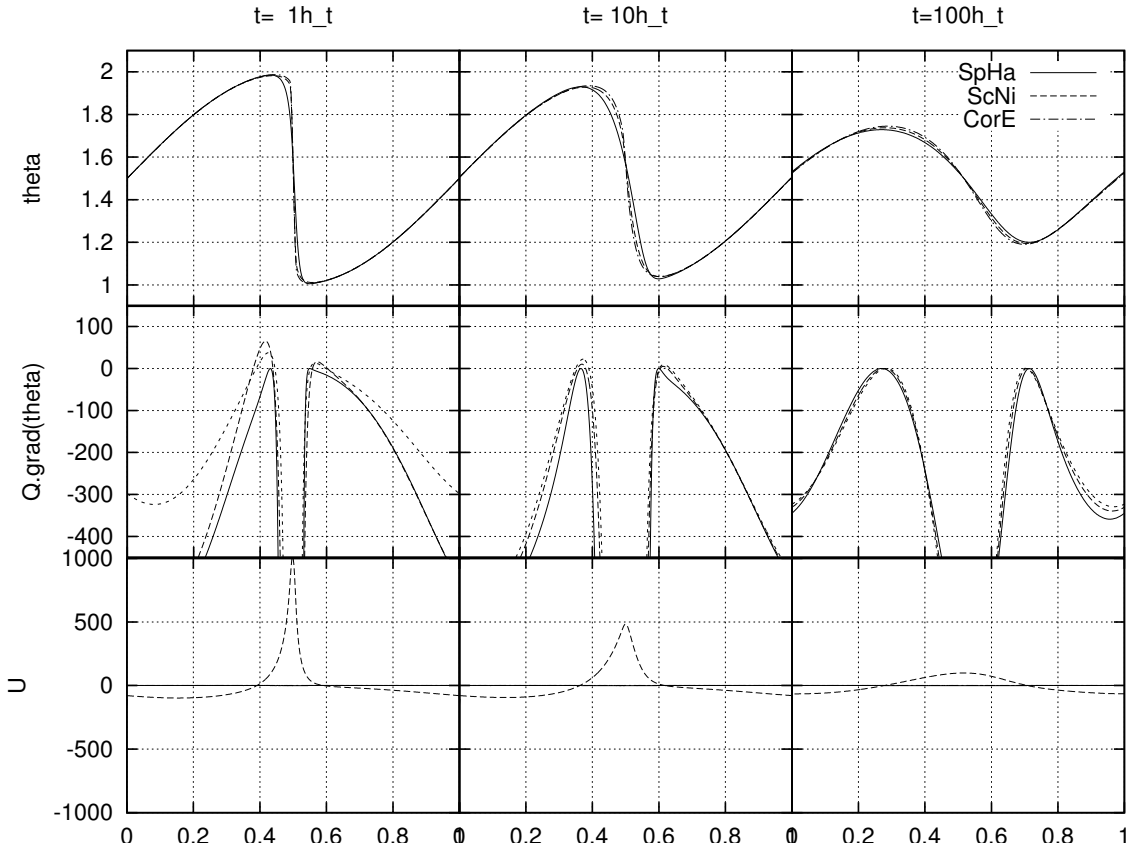

Figure III.4: Relaxation test case. `SpHa` curves are performed with the Spitzer-Härm model, `ScNi` curves are performed with the Schurtz-Nicolaï model (Model III.7) and `CorE` curves are performed with the scheme (6.7)–(6.9): Temperature profiles (Up), scalar product between the heat flux and the temperature gradient (Middle), and current profiles (Bottom).

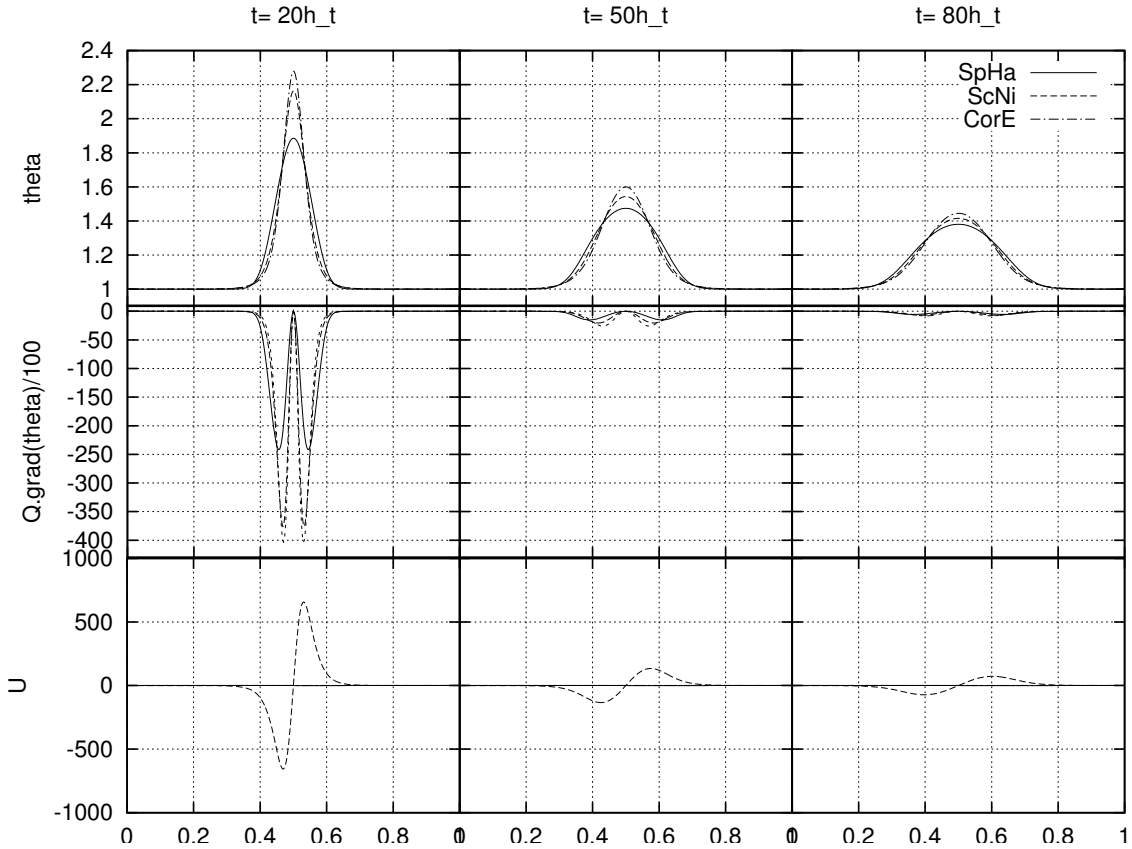

Figure III.5: Simulation of a laser beam. `SpHa` curves are performed with the Spitzer-Härm model, `ScNi` curves are performed with the Schurtz-Nicolaï model (Model III.7) and `CorE` curves are performed with the scheme (6.7)–(6.9): Temperature profiles (Up), scalar product between the heat flux and the temperature gradient (Middle), and current profiles (Bottom).

Conclusion

We have revisited the derivation of the Spitzer-Härm regime in plasma physics and bring out a hierarchy of intermediate models. In particular, we have introduced a new class of non–local models which generalizes the Schurtz–Nicolaï models. By defining the generalized heat fluxes with evolution equations, we have shown that well–posedness and stability properties of the model are restored, without introducing spurious truncation of the coefficients. Furthermore, the physical constraint on the current can be readily incorporated in the system. A numerical scheme of Finite Difference type has been introduced to solve the non-local models, and we have checked on numerical grounds the consistency of the new model with the Spitzer-Härm regime and its ability in capturing anti–diffusive effects.

Acknowledgments

This work is supported by CEA/DAM. We thank J.-F. Clouet, D. Deck and J.-F. Coulombel for kind encouragements and fruitful advices.

Appendices

III.A Extension to the generalized Schurtz-Nicolaï Model

We propose to expend properties presented in [6] on the Schurtz-Nicolaï model introduced in [17] to the case of parameter depend on internal energy. Indeed the Schurtz-Nicolaï model could be presented as a simplification of the Model (III.6), derived in III.4.1 with some simplifications as :

a) The field deviation $\tilde{\mathscr{E}}$ is neglected,

b) The operator $\mathscr{T}$ is disregarded,

c) The second order operator $\mathscr{D}_x$ is replaced by a mere Laplacian,

d) The time derivative is neglected in the equation for the generalized fluxes $\mathcal{Q}_\xi$.

It lead to the following system

$$\begin{aligned} &3\rho_\star \partial_t \tilde{\theta} + 2\nabla_x \cdot \int \mathcal{Q}_\xi \mathrm{d}\xi = 0, \\ &\mathcal{Q}_\xi - \varepsilon^2 \nu_\xi \Delta_x \mathcal{Q}_\xi = -\tilde{\kappa}_\xi \nabla_x \tilde{\theta}, \end{aligned} \tag{1.1}$$

with ν_ξ and $\tilde{\kappa}_\xi$ are coefficients coming from the derivation depend on the internal energy ξ. System (1.1) is a continuous version of model (III.7) in internal energy variable and is a generalized version of [6, equation (3.2)]. Note that since the field deviation $\tilde{\mathscr{E}}$ is neglected, the model does not satisfy the constrain of vanishing current. In this part, we adapt proof of [6, Theorem (3.1), Proposition (3.2)] to write similar properties for system (1.1).

Theorem III.A.1 *Let ν_ξ and $\tilde{\kappa}_\xi$ be constant in time and space variable with ν_ξ positive and for any $0 < a \leq 1$ the inequalities*

$$\int_{\mathbb{R}_+} \frac{\tilde{\kappa}_\xi}{\varepsilon^2 \nu_\xi} \mathrm{d}\xi \geq 0, \qquad \text{and} \qquad \int_{\mathbb{R}_+} \frac{\tilde{\kappa}_\xi}{\varepsilon^4 \nu_\xi^2} a^{1/\sqrt{\nu_\xi}} \mathrm{d}\xi \geq 0$$

holds. Furthermore suppose that $\rho_\star(x) \geq \underline{\rho} > 0$. Let $\tilde{\theta}_0 \in L^\infty(\mathbb{R}^3)$ be a non negative function such that $\rho_\star \tilde{\theta}_0 \in L^1(\mathbb{R}^3)$. There exists a unique function such that $\rho_\star \tilde{\theta} \in C^1\left([0, +\infty[; L^1(\mathbb{R}^3)\right)$ solution of the system (1.1) with $\tilde{\theta}_0$ as initial condition. In addition, $\tilde{\theta}$ satisfies the maximum principle: for any $t \geq 0$ and a.e. $x \in \mathbb{R}^3$,

$$0 \leq \min_{z \in \mathbb{R}^3} \tilde{\theta}_0(z) \leq \tilde{\theta}(t, x) \leq \max_{z \in \mathbb{R}^3} \tilde{\theta}_0(z). \tag{1.2}$$

Proof. We denote by $\mathcal{F}$ the Fourier transform and by $\mathcal{F}^{-1}$ the inverse Fourier transform

$$\mathcal{F}(\psi)(w) = \int_{\mathbb{R}^3} \psi(x) e^{-ix\cdot w} \mathrm{d}x, \qquad \mathcal{F}^{-1}(\phi)(x) = \left(\frac{1}{2\pi}\right)^3 \int_{\mathbb{R}^3} \phi(w) e^{ix\cdot w} \mathrm{d}w,$$

with w the Fourier space variable. We start by rewriting the system (1.1) in the Fourier space. Since

$$\mathcal{F}\mathcal{Q}_\xi(w) = \tilde{\kappa}_\xi \frac{iw}{1 + \varepsilon^2 \nu_\xi w^2} \mathcal{F}\left(\tilde{\theta}\right),$$

we get

$$\partial_t \mathcal{F}\left(\rho\tilde{\theta}\right) = \frac{2}{3} iw \mathcal{F} \int_{\mathbb{R}_+} \mathcal{Q} \mathrm{d}\xi = -\frac{2}{3} \int_{\mathbb{R}_+} \frac{\tilde{\kappa}_\xi}{\varepsilon^2 \nu_\xi} \left(1 + \frac{1}{1 + \varepsilon^2 \nu_\xi w^2}\right) \mathrm{d}\xi \mathcal{F}\left(\tilde{\theta}\right).$$

Back to the real space, it becomes:

$$\rho \partial_t \tilde{\theta} = -\frac{2}{3} \int_{\mathbb{R}_+} \frac{\tilde{\kappa}_\xi}{\varepsilon^2 \nu_\xi} \left(\tilde{\theta} - W_\xi \star \tilde{\theta}\right) \mathrm{d}\xi, \qquad \text{with} \qquad W_\xi = \mathcal{F}^{-1}\left(\frac{1}{1 + \varepsilon^2 \nu_\xi w^2}\right). \tag{1.3}$$

We have the following expression for the convolution kernel, see [2, Section 6.5] ,

$$W_\xi(x) = \frac{1}{4\pi\varepsilon^2 \nu_\xi |x|} \, e^{-|x|/\varepsilon\sqrt{\nu_\xi}}.$$

This kernel is positive and unitary in the sense that

$$W_\xi \geq 0 \qquad \text{and} \qquad W_\xi \star 1 = \frac{1}{4\pi\varepsilon^2 \nu_\xi} \int_{\mathbb{R}^3} \frac{e^{-|x|/\varepsilon\sqrt{\nu_\xi}}}{|x|} \mathrm{d}x = \frac{1}{\varepsilon^2 \nu_\xi} \int_0^\infty z \, e^{-z/\varepsilon\sqrt{\nu_\xi}} \mathrm{d}z = 1$$

holds. Let us consider the auxiliary problem

$$\begin{cases} \rho \partial_t u + Lu = g, \\ u(t = 0) = \tilde{\theta}_0, \end{cases} \tag{1.4}$$

with $L > 0$ and $\rho g \in C^0\left([0,+\infty[; L^1(\mathbb{R}^3)\right)$. With a standard contraction argument, we show that there exists a unique solution u of (1.4) with $\rho u \in C^1\left([0,+\infty[; L^1(\mathbb{R}^3)\right)$. Let $\left(u_n\right)_{n\in\mathbb{N}}$ be the sequence defined by $u_0(t,x) = \tilde{\theta}_0(x)$ and

$$\begin{cases} \rho\partial_t u_{n+1} + \dfrac{2}{3}\displaystyle\int_{\mathbb{R}_+} \frac{\tilde{\kappa}_\xi}{\varepsilon^2\nu_\xi}\mathrm{d}\xi u_{n+1} = \frac{2}{3}\int_{\mathbb{R}_+} \frac{\tilde{\kappa}_\xi}{\varepsilon^2\nu_\xi} W_\xi \mathrm{d}\xi \star u_n, \\ u_{n+1}(t=0,x) = \tilde{\theta}_0(x). \end{cases} \tag{1.5}$$

This sequence is well-defined because u_{n+1} is solution of (1.4) with $L = \frac{2}{3}\int_{\mathbb{R}_+} \frac{\tilde{\kappa}_\xi}{\varepsilon^2\nu_\xi}\mathrm{d}\xi > 0$ and $g = \frac{2}{3}\int_{\mathbb{R}_+} \frac{\tilde{\kappa}_\xi}{\varepsilon^2\nu_\xi} W_\xi \mathrm{d}\xi \star u_n$. So, we have, for any n, $\rho u_n \in C^1\left([0,+\infty[; L^1(\mathbb{R}^3)\right)$. Let compare two iterations. We have

$$\rho\partial_t\left(u_{n+1} - u_n\right) + L\left(u_{n+1} - u_n\right) = \frac{2}{3}\int_{\mathbb{R}_+} \frac{\tilde{\kappa}_\xi}{\varepsilon^2\nu_\xi} W_\xi \mathrm{d}\xi \star \left(u_n - u_{n-1}\right).$$

We set

$$\mathrm{sg}(x) = \begin{cases} 1 & \text{if } x \geq 0, \\ -1 & \text{else.} \end{cases}$$

Then we get

$$\begin{aligned} \rho\partial_t\left(u_{n+1} - u_n\right)\mathrm{sg}\left(u_{n+1} - u_n\right) + L\left(u_{n+1} - u_n\right)\mathrm{sg}\left(u_{n+1} - u_n\right) \\ = \frac{2}{3}\int_{\mathbb{R}_+} \frac{\tilde{\kappa}_\xi}{\varepsilon^2\nu_\xi} W_\xi \mathrm{d}\xi \star \left(u_n - u_{n-1}\right)\mathrm{sg}\left(u_{n+1} - u_n\right). \end{aligned}$$

Since $L = \int_{\mathbb{R}_+} \frac{\tilde{\kappa}_\xi}{\varepsilon^2\nu_\xi}\mathrm{d}\xi$ is positive we have $L\left(u_{n+1} - u_n\right)\mathrm{sg}\left(u_{n+1} - u_n\right) \geq 0$. In addition, since for any $0 < a \leq 1$ we have

$$\int_{\mathbb{R}_+} \frac{\tilde{\kappa}_\xi}{\varepsilon^4\nu_\xi^2} a^{1/\sqrt{\nu_\xi}}\mathrm{d}\xi \geq 0,$$

we write

$$\begin{aligned} &\int_{\mathbb{R}^3}\left|\frac{1}{6\pi}\int_{\mathbb{R}^3}\int_{\mathbb{R}_+} \frac{\tilde{\kappa}_\xi}{\varepsilon^4\nu_\xi^2}\left(e^{-|y|/\varepsilon}\right)^{1/\sqrt{\nu_\xi}}\mathrm{d}\xi \frac{u_n(x-y) - u_{n-1}(x-y)}{|y|}\mathrm{d}y\ \mathrm{sg}\left(u_{n+1} - u_n\right)\right|\mathrm{d}x \\ &\quad\leq \int_{\mathbb{R}^3}\frac{1}{6\pi}\int_{\mathbb{R}^3}\int_{\mathbb{R}_+} \frac{\tilde{\kappa}_\xi}{\varepsilon^4\nu_\xi^2}\left(e^{-|y|/\varepsilon}\right)^{1/\sqrt{\nu_\xi}}\mathrm{d}\xi \frac{|u_n(x-y) - u_{n-1}(x-y)|}{|y|}\mathrm{d}y\mathrm{d}x \\ &\quad\leq \frac{2}{3}\int_{\mathbb{R}_+} \frac{\tilde{\kappa}_\xi}{\varepsilon^2\nu_\xi}\int_{\mathbb{R}^3} W_\xi \star |u_n - u_{n-1}|\,\mathrm{d}x\mathrm{d}\xi. \end{aligned}$$

Finally, since W_ξ is unitary, we get

$$\int_{\mathbb{R}^3} \rho|u_{n+1} - u_n|(t,x)\mathrm{d}x \leq \frac{L}{\underline{\rho}}\int_0^t\int_{\mathbb{R}^3} \rho|u_n - u_{n-1}|(s,x)\mathrm{d}x\mathrm{d}s.$$

We deduce that

$$\|\rho(u_{n+1} - u_n)(t,\cdot)\|_{L^1(\mathbb{R}^3)} \leq \frac{(Lt/\underline{\rho})^{n+1}}{(n+1)!}\sup_{s\in[0,t]}\|\rho(u_1 - u_0)(s,\cdot)\|_{L^2(\mathbb{R}^3)}$$

holds. Since the series $\sum_n \frac{(Lt/\rho)^{n+1}}{(n+1)!}$ converges, it implies that the sequence $\left(u_n\right)_{n\in\mathbb{N}}$ satisfies the Cauchy criterion and thus it has a limit $\tilde{\theta}$ with $\rho\tilde{\theta} \in C^0\left([0,+\infty[;L^1(\mathbb{R}^3)\right)$. Passing to the limit in (1.5) we observe that $\tilde{\theta}$ satisfies (1.3) with initial data $\tilde{\theta}_0$.
It remains to discuss the maximum principe. Of course, the initial guess verifies $u_0(t,x) = \tilde{\theta}_0(x) \leq M$. Let us now assume that $\max_{x\in\mathbb{R}^3}\ u_n(t,x) \leq M$ holds. Since W_ξ is unitary, we have $W_\xi \star M = M$. Therefore, we can write

$$\rho\partial_t\left(u_{n+1}-M\right) + L\left(u_{n+1}-M\right) = \frac{2}{3}\int_{\mathbb{R}_+}\frac{\tilde{\kappa}_\xi}{\varepsilon^2\nu_\xi}W_\xi \star \left(u_n - M\right)\mathrm{d}\xi.$$

We use the function

$$(\psi)_+ = \left| \begin{array}{ll} \psi & \text{if } \psi > 0, \\ 0 & \text{else.} \end{array} \right.$$

Then we have

$$\begin{aligned}\rho\partial_t\left(u_{n+1}-M\right)\left(u_{n+1}-M\right)_+ + L\left(u_{n+1}-M\right)\left(u_{n+1}-M\right)_+ \\ = \frac{2}{3}\int_{\mathbb{R}_+}\frac{\tilde{\kappa}_\xi}{\varepsilon^2\nu_\xi}W_\xi \star \left(u_n - M\right)\mathrm{d}\xi\left(u_{n+1}-M\right)_+.\end{aligned}$$

Since $L > 0$, we observe that $L\left(u_{n+1}-M\right)\left(u_{n+1}-M\right)_+ \geq 0$, and, since for any $0 < a \leq 1$ we have

$$\int_{\mathbb{R}_+}\frac{\tilde{\kappa}_\xi}{\varepsilon^4\nu_\xi^2}a^{1/\sqrt{\nu_\xi}}\mathrm{d}\xi \geq 0, \qquad \text{we write} \qquad \frac{2}{3}\int_{\mathbb{R}_+}\frac{\tilde{\kappa}_\xi}{\varepsilon^2\nu_\xi}W_\xi \star \left(u_n - M\right)\mathrm{d}\xi\left(u_{n+1}-M\right)_+ \leq 0.$$

It follows that

$$\frac{\mathrm{d}}{\mathrm{d}t}\int_{\mathbb{R}^3}\rho\left(u_{n+1}-M\right)_+^2(t,x)\mathrm{d}x \leq 0.$$

Since initially $\left(u_{n+1}(0,x)-M\right) = \left(\tilde{\theta}_0(x) - M\right) \leq 0$, we conclude that $u_{n+1}(t,x) \leq M$. With similar arguments, we treat the bound from below and we finally obtain, for any $n \in \mathbb{N}$,

$$\min_{z\in\mathbb{R}^3}\tilde{\theta}_0(z) \leq u_n(t,x) \leq \max_{z\in\mathbb{R}^3}\tilde{\theta}_0(z).$$

Passing to the limit achieves the expected result. ∎

Remark III.A.1 *Results of* **Theorem III.A.1** *could be extend to coefficient $\tilde{\kappa}_\xi$ function of the temperature. The demonstration need to introduce a cut-off of the linearity as it is presented in [6, Theorem (3.1)]. Remark that positive coefficients $\tilde{\kappa}_\xi$ and ν_ξ satisfy the condition of* **Theorem III.A.1**. *It pointing out that $\tilde{\kappa}_\xi$ could admit negative value. In particular coefficients given by*

$$\tilde{\kappa}_\xi = C_1\xi^4\left(\xi-4\right)e^{-\xi}\theta^{5/2}, \qquad \textit{and} \qquad \nu_\xi = C_2\sqrt{\xi},$$

with $C_1 > 0$ and $C_2 > 0$ satisfy same results announced in **Theorem III.A.1**.

Proposition III.A.1 *Suppose that $\nu_\xi(t,x,\xi)$ and $\kappa_\xi(t,x,\xi)$ are positives for any $(t,x,\xi) \in \mathbb{R}_+ \times \mathbb{R}^3 \times \mathbb{R}_+$. Then, the following entropy dissipation holds*

$$\frac{\mathrm{d}}{\mathrm{d}t}\int_{\mathbb{R}^3} \rho_\star |\tilde{\theta}|^2 \mathrm{d}x \leq 0 \tag{1.6}$$

Proof. The energy conservation follows directly by integration. Next, we rewrite the equations introducing the generalized temperature $\tilde{\theta}_\xi$ as

$$\begin{aligned}
&3\rho_\star \partial_t \tilde{\theta}_\xi + 2\nabla_x \cdot \mathcal{Q}_\xi = 0,\\
&\mathcal{Q}_\xi - \varepsilon^2 \nu_\xi \Delta_x \mathcal{Q}_\xi = -\tilde{\kappa}_\xi \nabla_x \tilde{\theta},\\
&\tilde{\theta} = \int_{\mathbb{R}_+} \tilde{\theta}_\xi \mathrm{d}\xi,\\
&\tilde{\theta}_\xi(t=0) = \tilde{\theta}(t=0) e^{-\xi}.
\end{aligned}$$

Remark that $\tilde{\theta}_\xi(t,x,\xi)$ is not necessary positive. However, the generalized temperature is well-defined since the temperature $\tilde{\theta}$ is well-defined. Then, we multiply the equation on the generalized temperature by the temperature $\tilde{\theta}$ and the equation on the generalized heat flux by the generalized heat flux. It lead

$$\begin{aligned}
&3\int_{\mathbb{R}^3} \rho_\star \tilde{\theta} \partial_t \tilde{\theta}_\xi \mathrm{d}x - 2\int_{\mathbb{R}^3} \mathcal{Q}_\xi \cdot \nabla_x \tilde{\theta} \mathrm{d}x = 0,\\
&\int_{\mathbb{R}^3} \frac{|\mathcal{Q}_\xi|^2}{\tilde{\kappa}_\xi} \mathrm{d}x + \varepsilon^2 \int_{\mathbb{R}^3} \frac{\nu_\xi \left|\nabla_x \cdot \mathcal{Q}_\xi\right|^2}{\tilde{\kappa}_\xi} \mathrm{d}x = -\int_{\mathbb{R}^3} \mathcal{Q}_\xi \cdot \nabla_x \tilde{\theta} \mathrm{d}x.
\end{aligned}$$

Eventually, we replace in the first equation the expression of $\int \mathcal{Q}_\xi \cdot \nabla_x \tilde{\theta} \mathrm{d}x$ and we integrate on ξ variable. We have

$$\begin{aligned}
\partial_t \int_{\mathbb{R}^3} \rho_\star |\tilde{\theta}|^2 \mathrm{d}x &= -\frac{2}{3}\int_{\mathbb{R}^3}\int_{\mathbb{R}_+} \frac{|\mathcal{Q}_\xi|^2 + \varepsilon^2 \nu_\xi \left|\nabla_x \cdot \mathcal{Q}_\xi\right|^2}{\tilde{\kappa}_\xi} \mathrm{d}\xi \mathrm{d}x\\
&\leq 0.
\end{aligned}$$

∎

Bibliography

[1] Alouani Bibi, F., and Matte, J.-P. Nonlocal electron heat transport and electron-ion energy transfer in the presence of strong collisional heating. *Laser Part. Beams 22* (2004), 103–108.

[2] Bony, J.-M. *Méthodes mathématiques pour les sciences physiques.* Les éditions de l'école polytechnique, Paris, 2001.

[3] Epperlein, E. M., and Short, R. A practical nonlocal model for electron heat transport in laser plasmas. *Phys. Fluids B 3* (1991), 3092–3098.

[4] Frank, M., Levermore, D., and Shäfer, M. Diffusive corrections to $\mathbb{P}_N$ approximations. *SIAM Multiscale Model. Simul. 9* (2011), 1–28.

[5] Goudon, T., and Parisot, M. Finite Volume Schemes on Unstructured Grids for Generalized Non-Local Spitzer-Härm Models. Tech. rep., INRIA, 2011. in preparation.

[6] Goudon, T., and Parisot, M. On the Spitzer-Härm regime and Non-Local Approximations: modeling, analysis and numerical simulations. *SIAM Multiscale Model. Simul. 9* (2011), 568–600.

[7] Graille, B. *Modélisation de mélanges gazeux réactifs ionisés dissipatifs.* PhD thesis, Ecole Polytechnique, 2004.

[8] Guo, Y. The Landau equation in a periodic box. *Commun. Math. Phys. 231* (2002), 391–434.

[9] Levermore, D. Boundary conditions for moment closures. *IPAM KT2009, UCLA, CA* (2009).

[10] Levermore, D. Kinetic theory, Gaussian moment closures, and fluid approximations. *IPAM KT2009, Culminating retreat, Lake Arrowhead, CA* (2009).

[11] Liu, T.-P., and Zeng, Y. Large time behavior of solutions for general quasilinear hyperbolic-parabolic systems of conservation laws. *Mem. Amer. Math. Soc. 125*, 599 (1997), viii+120.

[12] Luciani, J.-F., and Mora, P. Resummation methods of the Chapman-Enskog Expansion for a Strongly Inhomogeneous Plasma. *J. Stat. Phys. 43* (1986), 281–302.

[13] Luciani, J.-F., and Mora, P. Nonlocal electron transport in laser created plasmas. *Laser Part. Beams 12* (1994), 387–400.

[14] Luciani, J.-F., Mora, P., and Pellat, R. Quasistatic heat front and delocalized heat flux. *Phys. Fluids 28* (1985), 835–845.

[15] Nicolaï, P., Feugeas, J.-L., and Schurtz, G. A practical nonlocal model for heat transport in magnetized laser plasmas. *Phys. Plasmas 13* (2006), 032701+13.

[16] Routh, E. J. *A treatise on the stability of a given state of motion.* Macmillan and Co., 1877.

[17] Schurtz, G. P., Nicolaï, P., and Busquet, M. A nonlocal electron conduction model for multidimensional radiation hydrodynamics codes. *Phys. Plasmas 7* (2000), 4238–4250.

[18] Shkarofsky, I. P. Cartesian tensor expansion of the Fokker-Planck equation. *Can. J. Phys. 41* (1963), 1753–1775.

[19] Spitzer, L., and Härm, R. Transport phenomena in a completely ionized gas. *Phys. Rev. 89* (1953), 977–981.

Chapitre IV :

Finite Volume Schemes on Unstructured Grids for Generalized Non-Local Spitzer-Härm Models

Résumé : Au régime de Spitzer-Härm, les équations de la physique des plasmas se reduisent par une équation parabolique non-linéaire pour la température électronique. En revenant sur la dérivation de cette équation asymptotique et par des arguments de limites hydrodynamiques, nous sommes amenés à construire une hiérarchie de modèles où le flux de chaleur est défini à l'aide d'une relation non-locale, pouvant être réinterprétée en introduisant des équations de diffusion couplées. Nous abordons la question de la conception de méthodes numériques permettant de résoudre ces équations. La contrainte de base sur le schéma est d'être asymptotiquement consistant avec le régime de Spitzer-Härm. Par ailleurs, les simulations de physique réaliste rendent l'utilisation de maillages non-structurés inévitable. Nous développons un schéma volumes finis, basée sur la discrétisation Vertex-Based, qui atteint ces objectifs. Nous discutons du point de vue numérique de l'efficacité de la méthode, et de la capacité des modèles généralisés à capter les phénomènes pertinents manqué par le problème asymptotique.

Abstract: In the so-called Spitzer-Härm regime, equations of plasma physics reduce to a non linear parabolic equation for the electronic temperature. Coming back to the derivation of this limiting equation through hydrodynamic regime arguments, one is led to construct a hierarchy of models where the heat fluxes are defined through a non-local relation which can be reinterpreted as well by introducing coupled diffusion equations. We address the question of designing numerical methods to simulate these equations. The basic requirement for the scheme is to be asymptotically consistent with the Spitzer-Härm regime. Furthermore, the constraints of physically realistic simulations make the use of unstructured meshes unavoidable. We develop a Finite Volume scheme, based on Vertex-Based discretization, which reaches these objectives. We discuss on numerical grounds the efficiency of the method, and the ability of the generalized models in capturing relevant phenomena missed by the asymptotic problem.

IV.1 Introduction

The evolution of a plasma can be described by the Vlasov-Maxwell-Fokker-Planck system which is a set of coupled PDEs satisfied by the distribution of charged particles in phase space and the electromagnetic fields. The numerical simulation of such a system is highly challenging. Source of numerical difficulties are related on the one hand to the high dimensionality of the unknowns, and on the other hand to the presence of stiff terms in many situations of practical interest. Indeed, working with distributions of particles in phase space means that the unknown depends not only on time and space variables, but also on the velocity variable. Discretizing this additional variable and the corresponding (differential and integral) operators increases the size of the numerical unknowns. Next, from the physical properties of the plasma a set of dimensionless parameters can be defined, which govern the stability of the simulation. In many situations, like for instance for the simulation of ICF devices which has motivated the present work, the stiffness induced by the values of the parameters can be highly demanding in numerical resources and computational time. Hence, based on specific behavior of the parameters and using asymptotic arguments, we can find reduced models. In particular when the particles distributions functions are driven to equilibrium (for instance due to the collisions mechanisms) we are led to models where the unknowns depend only on the time and space variables. The Spitzer-Härm regime discussed in the seminal work [17] is one of those regimes. The asymptotic discussion is embodied into a single parameter, that we denote from now on by $0 < \varepsilon \ll 1$. It turns out that as ε goes to 0, which corresponds roughly speaking to assume that the Debye length and the mean free path are small compared to the observation units, the dynamics of the plasma is entirely described by the evolution of the electron temperature $\theta(t, X)$ which obeys

$$\begin{cases} \partial_t \theta + \dfrac{2}{3\rho} \nabla_X \cdot Q = S, \\ Q = -\kappa_{SH}(\theta) \nabla_X \theta. \end{cases} \tag{1.1}$$

In (1.1), $X \mapsto \rho(X) > 0$ and $S(t, X)$ are God-given density and source term respectively. The diffusion coefficient $\theta \mapsto \kappa_{SH}(\theta) > 0$ keeps track of the microscopic description since its expression depends on the details of the interparticles collisions. The scaling issues and the derivation of (1.1) from the kinetic framework are detailed in [7, 8], which also contains further references. Another important feature of the Spitzer-Härm regime is the fact that it imposes a vanishing current

$$J = 0 \tag{1.2}$$

where $J(t, X)$ is the first order moment of the electrons distribution function. Note that this constraint is used in many models, even when working at the kinetic level, as a definition of the electric field, [15].

Of course the limiting equation (1.1) is quite simple, and it can be solved numerically by using many efficient methods. However, it turns out that it misses some phenomena that should be inherited form the kinetic modeling, see [5]. Hence, one is interested in completing the model, through $\varepsilon-$dependent terms, bearing in mind to describe a more complex physics, but remaining accessible to a cheap numerical

treatment. To this end models based on "delocalized heat fluxes" have been proposed in the literature since the pioneering work of Luciani, Mora and Virmont [14], see [13, 11, 12, 16]. The derivation of such non-local models has been revisited recently in [8] where the following system has been introduced as an alternative to the Spitzer-Härm equation:

$$\begin{cases} \partial_t \theta + \dfrac{2}{3\rho} \nabla_X \cdot Q = S, \\ Q(t,X) = \displaystyle\int_0^\infty \mathcal{Q}(t,X,\xi)\,\mathrm{d}\xi, \\ \partial_t \mathcal{Q} + \dfrac{\mathcal{Q}}{\varepsilon^2 \mu} - \nabla_X \left(\nu \nabla_X \cdot \mathcal{Q}\right) - \eta \mathcal{E} = -\dfrac{\kappa}{\varepsilon^2 \mu} \nabla_X \theta. \end{cases} \tag{1.3}$$

The additional variable $\xi \geq 0$ can be interpreted as an internal energy and $\mathcal{Q}(t,X,\xi)$ appears as to be a generalized heat flux, as already introduced by Schurtz and Nicolaï in [16]. The coefficients μ, ν, κ, η depend on both the energy variable ξ and the temperature θ, hence making the model non-linear (but they are supposed independent on the scaling parameter ε). Their expressions again depend on the collision processes; for our purposes, it is important to keep in mind that

$$\mu(\xi,\theta) > 0, \qquad \nu(\xi,\theta) > 0, \qquad \kappa(\xi,\theta) \in \mathbb{R}, \qquad \eta(\xi,\theta) \in \mathbb{R}$$

holds. It is convenient to define the electric field as

$$E = E_{SH} + \varepsilon^2 \mathcal{E}, \qquad E_{SH} = \theta \left(\nabla_X \ln \rho - \frac{5}{2} \nabla_X \ln \theta \right),$$

and the perturbation $\mathcal{E}$ is defined in connection to the constraint (1.2), which now takes the form (see [8] for details)

$$J(t,X) = \frac{1}{\theta} \int_0^\infty \frac{\mathcal{Q}(t,X,\xi)}{\xi}\,\mathrm{d}\xi = 0. \tag{1.4}$$

The problem (1.3)-(1.4) is completed with initial condition

$$\theta(0,X) = \theta^0(X), \qquad \mathcal{Q}(0,X,\xi) = \mathcal{Q}^0(X,\xi), \tag{1.5}$$

where $\mathcal{Q}^0(X,\xi)$ is assumed to satisfy the constraint (1.4). The problem is set on a smooth bounded domain Ω; on the boundary $\partial\Omega$ it is natural to use the Neumann condition

$$\mathcal{Q}(t,X,\xi) \cdot n_{\partial\Omega} = 0, \tag{1.6}$$

with $n_{\partial\Omega}$ the unit outward normal. As ε goes to 0, we formally recover (1.1), endowed with Neumann boundary condition, from (1.3), once we have said that

$$\kappa_{SH}(\theta) = \int_0^\infty \kappa(\xi,\theta)\,\mathrm{d}\xi > 0.$$

We point out that the integral is positive while $\kappa(\xi,\theta)$ changes sign to be able to satisfy (1.4) at the asymptotic regime $\varepsilon \to 0$.

The system (1.3) is not strictly of macroscopic type because it still involves the internal energy variable $\xi \geq 0$. The approach devised in [8] consists in replacing the continuous equations (1.3) by a discrete version where the generalized heat flux is evaluated at a reduced set of quadrature points $\xi_1, ..., \xi_g$, for some $g \in \mathbb{N} \setminus \{0\}$. This is motivated by the fact that the important quantities are defined by integrals of the generalized heat flux. To be more specific, we use a Gauss-Laguerre quadrature approximation : given $\alpha > -1$, and $g \in \mathbb{N} \setminus \{0\}$, we set $\xi_1, ..., \xi_g$ as to be the zeroes of the gth Laguerre generalized polynomials:

$$Ł_g^{(\alpha)}(\xi) = \sum_{j=1}^{g} (-1)^j \binom{g+\alpha}{g-j} \frac{\xi^j}{j!}$$

For any smooth function $\xi \mapsto \mathcal{Q}(\xi)$ the following Gaussian quadrature formula

$$\int_0^\infty \mathcal{Q}(\xi)\,\mathrm{d}\xi = \sum_{j=1}^{g} \omega_j \mathcal{Q}(\xi_j) + \frac{g!\Gamma(g+\alpha+1)}{(2g)!} \partial_\xi^{2g} \left(\mathcal{Q}(\xi) \frac{e^\xi}{\xi^\alpha} \right)(c),$$

holds for some $c \geq 0$ where the weight ω_j is associated to ξ_j by

$$\omega_j = \frac{\Gamma(g+\alpha)\xi_j}{g!(g+\alpha)\left(\mathscr{L}_{g-1}^{(\alpha)}(\xi_j)\right)^2} \frac{e^{\xi_j}}{\xi_j^\alpha}.$$

We obtain now a purely macroscopic model by introducing $\mathcal{Q}_1(t,X), ..., \mathcal{Q}_g(t,X)$, intended to be approximation of $\mathcal{Q}(t,X,\cdot)$ at the quadrature points $\xi_1, ..., \xi_g$. The discrete model obtained that way reads

$$\begin{cases} \partial_t \theta + \dfrac{2}{3\rho} \nabla_X \cdot Q = S, \\ Q = \displaystyle\sum_{j=1}^{g} \omega_j \mathcal{Q}_j, \\ \partial_t \mathcal{Q}_j + \dfrac{\mathcal{Q}_j}{\varepsilon^2 \mu_j} - \nabla_X \left(\nu_j \nabla_X \cdot \mathcal{Q}_j \right) - \eta_j \mathcal{E} = -\dfrac{\kappa_j}{\varepsilon^2 \mu_j} \nabla_X \theta, \end{cases} \tag{1.7}$$

where the coefficients are simply given by evaluating the original coefficients at the quadrature points:

$$\mu_j(\theta) = \mu(\xi_j, \theta), \qquad \nu_j(\theta) = \nu(\xi_j, \theta), \qquad \kappa_j(\theta) = \kappa(\xi_j, \theta).$$

The constraint (1.4) becomes

$$\sum_{j=1}^{g} \frac{\omega_j \mathcal{Q}_j}{\xi_j} = 0. \tag{1.8}$$

For the boundary condition, we get

$$\mathcal{Q}_j \cdot n_{\partial\Omega} = 0. \tag{1.9}$$

The model (1.7) is derived and analyzed in [8]. By contrast to other non local models where usually fluxes are solutions of stationary equations, like for instance the Shurtz-Nicolaï system, (1.7) do not need any artificial cut-off of the coefficients to be well-posed and to satisfy basic stability estimates. Hence, (1.7) can be a valuable alternative to delocalized models in plasmas simulations. As a first attempt a numerical scheme on cartesian grids is proposed in [8], which allows to validate the relevancy of the reduced model. However, most applications need more elaborate discretizations based on unstructured meshes, because of complex geometries or coupling of the plasma equations with other physical effects, as the resolution of the dynamic of ions with Lagrangian method. This is also unavoidable if the simulation is coupled to mesh refinement strategies. This is the question we address in this work: we propose a scheme of Finite Volume type to simulate the system (1.7)-(1.9). Of course numerical schemes for the Spitzer-Härm equation (1.1) are quite standard, so that a natural requirement is to construct the scheme for (1.7)-(1.9) in such a way it degenerates as $\varepsilon \to 0$ to one of those simple scheme for (1.1). A difficulty consists in avoiding unnecessary spreading of the numerical stencil: proceeding naively would lead to update fluxes and temperature at a given point by using a large number of neighbors. In turn, it would increase the complexity of the underlying linear system and thus would impact negatively the numerical efficiency, creating also spurious diffusion effects and ambiguities for treating boundary terms.
The method has also some flexibility and it can be readily adapted to treat similar problems like the simulation of electrostatic potentials as arising in the modeling of the dielectric properties of water [9, 10].

The paper is organized as follows. In section IV.2, we use a simple time discretization and define a relevant space discretization which allows to reach our objectives. From a mesh made of triangles, the temperature is evaluated at the vertices of the meshing (Vertex Based Method) while the heat fluxes are evaluated on the interfaces of the corresponding control volumes. In this construction gradients are simply approximated by using $\mathbb{P}_1$ interpolations in triangles. In section IV.3, we present a coupling strategy which allows to use the Spitzer-Härm limit in a part of the computational domain and the generalized Spitzer-Härm model everywhere else. We are able to couple the models thanks to the consistency of the generalized Spitzer-Härm scheme to the Spitzer-Härm scheme. Section IV.4 is devoted to a series of numerical tests which bring out the numerical performances of the scheme and show the ability of the model (1.7)-(1.9) in capturing new effects. A more elaborate time discretization is discussed in Section IV.5.2: by using an iterative procedure, which is reminiscient of the Jacobi method, we uncouple the resolution of the heat fluxes equation, which substantially improves the performances of the scheme in terms of computational time.

IV.2 A Vertex-Based Finite Volume Scheme

IV.2.1 Discretization

Time Discretization

To start with let us discuss the time discretization. Let $h_t > 0$ denote the time step. Integrating

$$\partial_t \theta + \frac{2}{3\rho} \nabla_X \cdot Q = S, \qquad Q = \sum_{j=1}^{g} \omega_j \mathcal{Q}_j(t, X) \tag{2.1}$$

over $[nh_t, (n+1)h_t]$ we obtain

$$\theta((n+1)h_t, X) - \theta(nh_t, X) = \int_{nh_t}^{(n+1)h_t} S(t, X)\, \mathrm{d}t - \frac{2}{3\rho} \nabla_X \cdot \sum_{j=1}^{g} \omega_j \int_{nh_t}^{(n+1)h_t} \mathcal{Q}_j \, \mathrm{d}t.$$

The source term S is known, and we denote

$$S^{n,n+1}(X) = \frac{1}{h_t} \int_{nh_t}^{(n+1)h_t} S(t, X)\, \mathrm{d}t.$$

For the fluxes the integral $\int_{nh_t}^{(n+1)h_t} \mathcal{Q}_j \, \mathrm{d}t$ is approximated by interpolating between the values of $\mathcal{Q}_j$ at time nh_t and $(n+1)h_t$. Given a parameter $0 \leq \tau \leq 1$, we are thus led to the following semi-discrete version of (2.1)

$$\frac{\theta^{n+1} - \theta^n}{h_t} = \; S^{n,n+1} - \frac{2}{3\rho} \nabla_X \cdot \sum_{j=1}^{g} \omega_j (\tau \mathcal{Q}_j^{n+1} + (1-\tau) \mathcal{Q}_j^n). \tag{2.2}$$

Proceeding similarly with the fluxes equations yields

$$\begin{aligned} \frac{\mathcal{Q}_j^{n+1} - \mathcal{Q}_j^n}{h_t} + \frac{\tau \mathcal{Q}_j^{n+1} + (1-\tau)\, \mathcal{Q}_j^n}{\varepsilon^2 \mu_j^{n+\tau}} - \nabla_X \left(\nu_j^{n+\tau} \nabla_X \cdot \left(\tau \mathcal{Q}_j^{n+1} + (1-\tau)\, \mathcal{Q}_j^n \right) \right) \\ - \eta_j^{n+\tau} \left(\tau \mathcal{E}^{n+1} + (1-\tau)\, \mathcal{E}^n \right) = - \frac{\kappa_j^{n+\tau}}{\varepsilon^2 \mu_j^{n+\tau}} \nabla_X \left(\tau \theta^{n+1} + (1-\tau)\, \theta^n \right). \end{aligned} \tag{2.3}$$

The coefficients are defined by

$$\begin{aligned} \mu_j^{n+\tau} &= \mu_j \left(\tau \theta^{n+1} + (1-\tau)\, \theta^n \right) \\ \nu_j^{n+\tau} &= \nu_j \left(\tau \theta^{n+1} + (1-\tau)\, \theta^n \right), \\ \kappa_j^{n+\tau} &= \kappa_j \left(\tau \theta^{n+1} + (1-\tau)\, \theta^n \right). \end{aligned}$$

The field $\mathcal{E}^n$ is defined as to maintain the constraint

$$\sum_{j=1}^{g} \frac{\omega_j \mathcal{Q}_j^n}{\xi_j} = 0. \tag{2.4}$$

In the sequel, we shall use the shorthand notation

$$\theta^{n+\tau} = \tau \theta^{n+1} + (1-\tau)\, \theta^n, \quad \mathcal{Q}_j^{n+\tau} = \tau \mathcal{Q}_j^{n+1} + (1-\tau)\, \mathcal{Q}_j^n, \quad \mathcal{E}^{n+\tau} = \tau \mathcal{E}^{n+1} + (1-\tau)\, \mathcal{E}^n.$$

It can be interpreted as an approximation of the corresponding unknowns at time $(n+\tau)\,h_t$. The parameter τ allows to tune how much the scheme is made implicit, in connection to stability and accuracy issues. As $\tau = 0$, the scheme is fully explicit. But, according to the analysis in [7] it is likely that the stability of the scheme is constrained by a condition of parabolic type, where the time step have to be in order of the square of the space step, which makes the computational cost prohibitive, especially for multi-dimensional simulations. Hence, using $0 < \tau \leq 1$ makes the scheme implicit and improves the stability properties. However, due to the fact that the coefficients depend on θ, the system (2.2)-(2.4) is non linear for $\tau > 0$.

To deal with the nonlinearities, we proceed iteratively. Knowing the unknowns at time nh_t, we construct a sequence $\left(\theta^{n,r}, \mathcal{Q}_1^{n,r}, ..., \mathcal{Q}_g^{n,r}\right)_{r\in\mathbb{N}}$ the limit of which as $r \to \infty$ will define θ^{n+1} and the $\mathcal{Q}_j^{n+1}$'s. We set $\theta^{n,0} = \theta^n$, $\mathcal{Q}_j^{n,0} = \mathcal{Q}_j^n$ and we define iteratively $\theta^{n,r}$ and $\mathcal{Q}_1^{n+\tau,r}, ..., \mathcal{Q}_g^{n+\tau,r}$ by solving the linear system

$$\begin{cases} \mathcal{Q}_j^{n+\tau,r+1} - \varepsilon^2 \tilde{\mu}_j^{n+\tau,r} \nabla_X \left(\nu_j^{n+\tau,r} \nabla_X \cdot \mathcal{Q}_j^{n+\tau,r+1} \right) - \dfrac{2}{3} \tilde{\kappa}_j^{n+\tau,r} \tau h_t \nabla_X \left(\dfrac{1}{\rho} \nabla_X \cdot \displaystyle\sum_{l=1}^{g} \omega_l \mathcal{Q}_l^{n+\tau,r+1} \right) \\ \qquad - \varepsilon^2 \tilde{\mu}_j^{n+\tau,r} \eta_j^{n+\tau,r} \mathcal{E}^{n+\tau,r+1} = \dfrac{\varepsilon^2 \tilde{\mu}_j^{n+\tau,r}}{\tau h_t} \mathcal{Q}_j^n - \tilde{\kappa}_j^{n+\tau,r} \nabla_X \left(\theta^n + \tau h_t S^{n,n+1} \right) \\ \displaystyle\sum_{j=1}^{g} \frac{\omega_j \mathcal{Q}_j^{n+\tau,r+1}}{\xi_j} = 0, \\ \theta^{n+\tau,r+1} = \theta^n + \tau h_t S^{n,n+1} - \dfrac{2\tau h_t}{3\rho} \nabla_X \cdot \displaystyle\sum_{j=1}^{g} \omega_j \mathcal{Q}_j^{n+\tau,r+1}, \end{cases} \tag{2.5}$$

where we have set

$$\begin{aligned} &\mu_j^{n+\tau,r}(\theta) = \mu_j\left(\theta^{n+\tau,r}\right), \qquad && \tilde{\mu}_j^{n+\tau,r}(\theta) = \frac{\mu_j^{n+\tau,r}(\theta)\,\tau h_t}{\varepsilon^2 \mu_j^{n+\tau,r}(\theta) + \tau h_t}, \\ &\nu_j^{n+\tau,r}(\theta) = \nu_j\left(\theta^{n+\tau,r}\right), \\ &\eta_j^{n+\tau,r}(\theta) = \eta_j\left(\theta^{n+\tau,r}\right), \\ &\kappa_j^{n+\tau,r}(\theta) = \kappa_j\left(\theta^{n+\tau,r}\right), \qquad && \tilde{\kappa}_j^{n+\tau,r}(\theta) = \frac{\kappa_j^{n+\tau,r}(\theta)\,\tau h_t}{\varepsilon^2 \mu_j^{n+\tau,r}(\theta) + \tau h_t}. \end{aligned} \tag{2.6}$$

In practice, a few iterations are sufficent to obtain a good approximation of the limit of the iterative process. We are thus led to solve a system of elliptic equations and we are going to discuss in the following section the space discretization of (2.5) based on a Finite Volume formulation of the problem.

Finite Volume Discretization

For the sake of simplicity, we restrict the presentation to the two-dimension framework. We give some hints for the generalization to the 3D case in Section IV.5.1 below. Since

solutions of (1.3) are expected to converge to those of (1.1) in the Spitzer-Härm regime $\varepsilon \to 0$, we start by writing a scheme for the limit equation.

We can rewrite the problem as a single equation for the temperature θ

$$3\rho\partial_t\theta - 2\nabla_X \cdot (\kappa_{SH}\nabla_X\theta) = S \tag{2.7}$$

According to the discussion in Section IV.2.1, we are led to consider the following semi-discrete problem

$$\theta^{n+\tau,r+1} - \frac{2\tau h_t}{3\rho}\nabla_X \cdot \left(\kappa_{SH}^{n+\tau,r}\nabla_X\left(\theta^{n+\tau,r+1}\right)\right) = \theta^n + \tau h_t S^{n,n+1}, \tag{2.8}$$

with $\kappa_{SH}^{n+\tau,r} = \sum_{j=1}^{g}\kappa_j^{n+\tau,r}$. Adopting the Finite Volume viewpoint, the numerical unknown will be intended to approximate the mean value of the temperature over some control volume, and we will need to introduce a suitable definition of the gradient of the temperature on the interfaces of the control volume.

In this work we consider a tessellation of the computational domain Ω , noted $\mathbb{T}$, made of conforming and isotropic triangles. It constitutes the so-called primal mesh.The temperature is estimated at the vertices of the mesh. Let k stand for a vertex. We denote by $\mathscr{C}_k$ the associated control volume. As shown in Figure (IV.1), it is obtained by joining the centroids of all the triangles having k as a vertex and the midpoint of the edges of these triangles. The segments of this polygonal curve containing $\mathscr{C}_k$ are called the faces of the control volume, and $|\mathscr{C}_k| = \int_{\mathscr{C}_k} \mathrm{d}X$ stands for the surface (volume in dimension 3) of the domain $\mathscr{C}_k$. The set of the control volumes defines another tessellation of Ω, named the dual mesh. Finally, we denote by $\mathbb{F}_{\mathscr{C}_k}$, the set of the faces of $\mathscr{C}_k$ which do not belong to $\partial\Omega$. Faces lying on $\partial\Omega$ can be disregarded due to the Neumann boundary condition (1.9).

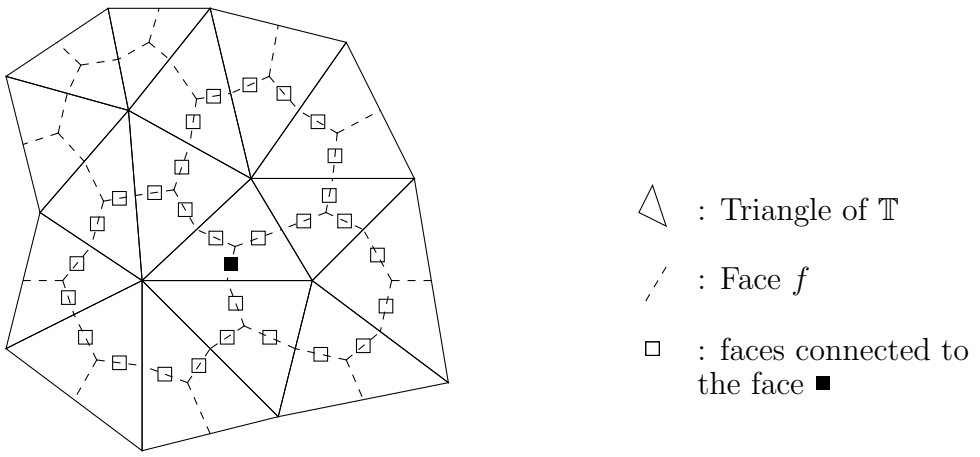

Figure IV.1: Example of control volume $\mathscr{C}_k$ and connectivity.

Let us integrate (2.8) over a control volume $\mathscr{C}_k$. By using the Stokes formula, we obtain

$$\begin{aligned}\frac{1}{|\mathscr{C}_k|}\int_{\mathscr{C}_k}\rho\theta^{n+\tau,r+1}\,\mathrm{d}X-\frac{2\tau h_t}{3|\mathscr{C}_k|}\sum_{f\in\mathbb{F}_{\mathscr{C}_k}}\int_f\left(\kappa_{SH}^{n+\tau,r}\nabla_X\left(\theta^{n+\tau,r+1}\right)\right)\,\mathrm{d}\sigma\cdot\frac{N_{\mathscr{C}_k}^f}{|f|}\\ =\frac{1}{|\mathscr{C}_k|}\int_{\mathscr{C}_k}\rho\theta^n\,\mathrm{d}X+\tau h_t\frac{1}{|\mathscr{C}_k|}\int_{\mathscr{C}_k}\rho S^{n,n+1}\,\mathrm{d}X,\end{aligned}\tag{2.9}$$

where $N_{\mathscr{C}_k}^f$ is the normal to the face f outward of the volume $\mathscr{C}_k$ with norm $|N_{\mathscr{C}_k}^f|=|f|=\int_f\mathrm{d}\sigma$, the length of the face. We set

$$\rho_k=\frac{1}{|\mathscr{C}_k|}\int_{\mathscr{C}_k}\rho\,\mathrm{d}X,\qquad S_k^{n,n+1}=\frac{1}{\rho_k|\mathscr{C}_k|}\int_{\mathscr{C}_k}\rho S^{n,n+1}\,\mathrm{d}X.$$

The numerical unknown $\theta_k^{n+\tau,r+1}$ is intended to approximate the mean value $\frac{1}{|\mathscr{C}_k|}\int_{\mathscr{C}_k}\theta^{n+\tau,r+1}\,\mathrm{d}X$. The scheme will be defined by mimicking relation (2.9). To this end we need to define the numerical flux on the faces of $\mathscr{C}_k$ which relies on constructing the gradient of the temperature on the faces. The idea consists is using the three vertices of the triangle containing the considered interface to define a $\mathbb{P}_1$ approximation of the temperature, then taking its derivative to obtain the gradient. Such a construction already appears in fluid mechanics when dealing with non homogeneous incompressible viscous flows [3]. It can be compared to DDFV construction which are usually based on Cell Center discretization see [2, 4] and the references therein. More precisely, the construction proceeds as follows. Let K be the cardinal of the set of vertices of the mesh. Given $\psi\in\mathbb{R}^K$, we set

$$\mathscr{P}\left[\psi\right](X)=\sum_{T\in\mathbb{T}}\left(\nabla_T\left[\psi\right]\cdot\left(X-\frac{\sum_{k\in\mathbb{V}_T}X_k}{3}\right)+C_T\left[\psi\right]\right)\mathbf{1}_T,\tag{2.10}$$

where $\mathbb{V}_T$ is the set of the vertices of the triangle T and X_k is the vector of coordinates of the vertex k. The definition is completed by imposing

$$\mathscr{P}\left[\psi\right](X_k)=\psi_k.$$

In other words we consider the piecewise $\mathbb{P}_1$ function having its values at the vertices prescribed by the ψ_k's. We have

$$\left(\nabla_T\left[\psi\right]\right)_i=\frac{\det\left(W^i\right)}{\det\left(V\right)},\qquad C_T\left[\psi\right]=\frac{\sum_{k\in\mathbb{V}_T}\psi_k}{3},$$

with V the 2×2 matrix with coefficients $V_{j,k}=\left(X_{l_k}-X_{l_3}\right)_j$ while $(l_i)_{1\le i\le3}$ are indices of vertices of triangle T. W^i is obtained from V by replacing its i^{th} column by the column vector $\left(\psi_{l_1}-\psi_{l_3},\psi_{l_2}-\psi_{l_3}\right)^t$. The definition makes sense because $\det\left(V\right)$ vanishes iff the surface of T vanishes, and for a given mesh this quantity is bounded from below. Observe that $\mathscr{P}\left[\psi\right]$ is continuous on Ω. Going back to the numerical scheme, we write

$$\theta_k^{n+\tau,r+1}-\frac{2\tau h_t}{3\rho_k|\mathscr{C}_k|}\sum_{f\in\mathbb{F}_{\mathscr{C}_k}}\kappa_{SH,f}^{n+\tau,r}\nabla_{T_f}\left[\theta^{n+\tau,r+1}\right]\cdot N_{\mathscr{C}_k}^f=\theta_k^n+\tau h_tS_k^{n,n+1},\tag{2.11}$$

where T_f is the triangle which contains the face f, $\kappa_{SH,f} = \kappa_{SH}^{n+\tau,r}\left(\mathscr{P}\left[\theta\right](X_f)\right)$ and X_f being the centroid of the face f.

We shall use the scheme just derived for (1.1) as a starting point to develop a numerical method for the more involved model (1.3). To this end, it is convenient to introduce the vectorial quantity, naturally associated to faces f of the control volumes,

$$Q_{SH,f}^{n+\tau,r+1} = -\kappa_{SH,f}^{n+\tau,r}\nabla_{T_f}\left[\theta^{n+\tau,r+1}\right]. \tag{2.12}$$

It can be interpreted as an approximation of the heat flux in the direction of the normal to the face f at time $(n+\tau)\,h_t$, that is

$$\frac{1}{|f|}\int_f Q_{SH}\left((n+\tau)\,h_t,\sigma\right)\,\mathrm{d}\sigma.$$

Remark that $\psi \in \mathbb{R}^K \mapsto \mathscr{P}[\psi]$ is a linear operator. We replace $\theta^{n+\tau,r+1}$ in (2.12) by is expression given in (2.11) to obtain

$$\begin{aligned} Q_{SH,f}^{n+\tau,r+1} - \frac{2\kappa_{SH,f}^{n+\tau,r}\tau h_t}{3}\nabla_{T_f}\left[\frac{1}{\rho|\mathscr{C}|}\sum_{f^\star\in\mathbb{F}_{\mathscr{C}_k}} Q_{SH,f^\star}^{n+\tau,r+1}\cdot N_{\mathscr{C}}^f\right] \\ = -\kappa_{SH,f}^{n+\tau,r}\nabla_{T_f}\left[\theta^n + \tau h_t S_k^{n,n+1}\right], \end{aligned} \tag{2.13}$$

$$\theta_k^{n+\tau,r+1} = \theta_k^n + \tau h_t S_k^{n,n+1} - \frac{2\tau h_t}{3\rho_k|\mathscr{C}_k|}\sum_{f\in\mathbb{F}_{\mathscr{C}_k}} Q_{SH,f}^{n+\tau,r+1}\cdot N_{\mathscr{C}_k}^f.$$

Obviously (2.13) defines the same sequence θ_k^n as (2.11). However, as a numerical scheme it is not relevant to make use of (2.13) because it involves more unknowns and the linear system to be inverted has a larger stencil and loses some advantageous proporties as symmetry, Figure (IV.1). Nevertheless, formula (2.13) is interesting because it provides a natural way to evaluate the consistency of a scheme for (1.3) with the Spitzer-Härm regime $\varepsilon \to 0$: letting ε go to 0 in the definition of the flux for (1.3) we should recover (2.13). As already noticed, the heat flux in (2.12) is naturally discretized on the faces of the control volumes. Therefore, the new numerical unknown for (1.3) $\mathcal{Q}_{j,f}^{n+\tau,r+1}$ is interpreted as an approximation of the mean value of $\mathcal{Q}_j^{n+\tau,r+1}$ on the face f. Remark we do not associate a control volume to the discrete unknown $\mathcal{Q}_{j,f}^{n+\tau,r+1}$. However, we are able to define discrete second order differential operators on the generalized heat fluxes on the faces, need to the resolution of (1.3). To this end, we first remark that for any $Q : \mathbb{R}^2 \to \mathbb{R}^2$ smooth enough vector function, the integration of the Jacobian matrix $\nabla_X Q$ on a bounded surface could be estimated using a Stokes formulae by its mean value on the boundary of the surface. In particular, on a control volume k, we have

$$\int_{\mathscr{C}_k}\nabla_X Q\,\mathrm{d}X = \int_{\partial\mathscr{C}_k} Q\otimes n\,\mathrm{d}\sigma = \sum_{f\in\mathbb{F}_{\mathscr{C}_k}}\frac{1}{|f|}\int_f Q\,\mathrm{d}\sigma\otimes N_{\mathscr{C}_k}^f,$$

with n the outward normal to the boundary $\partial\mathscr{C}_k$. Mimicking this formulae, we proceed into two steps.

1. Let $q = (q_1, ..., q_M)$ be a given set of M vectors in $\mathbb{R}^2$, with M the number of faces of the mesh. Hence each q_j is associated to a unique face of the dual mesh. We associate to q the piecewise constant matrix-valued function which is defined of each volume control by

$$\mathscr{G}_k[q] = \frac{1}{|\mathscr{C}_k|} \sum_{f \in \mathbb{F}_{\mathscr{C}_k}} q_f \otimes N^f_{\mathscr{C}_k}. \tag{2.14}$$

   This quantity is intended to define the (discrete) mean derivative of a function on a control volume from the values on the faces.

2. The previous step defines $\mathscr{G}_1[q], ..., \mathscr{G}_K[q]$, associating to each vertex k of the primal mesh. Then we can use the operator $\mathscr{P}$ to construct a function which is $\mathbb{P}_1$ on each triangle $T \in \mathbb{T}$ and next consider $\nabla_{T_f}[\mathscr{G}[q]]$ for each face of the dual mesh.

Coming back to the equations under consideration, Step 1 defines $\mathrm{Tr}\big(\mathscr{G}_k\big[\mathcal{Q}_j^{n+\tau,r+1}\big]\big)$: on each control volume $\mathscr{C}_k$, this quantity is intended to approximate $\frac{1}{|\mathscr{C}_k|}\int_{\mathscr{C}_k} \nabla_X \cdot \mathcal{Q}_j^{n+\tau,r+1}\,\mathrm{d}X$. Then using the reconstruction by triangle $\mathscr{P}$, we are able to define on each $T \in \mathbb{T}$ an approximation of the second order derivative of the generalized heat fluxes with $\nabla_T\big[\mathrm{Tr}\big(\mathscr{G}\big[\mathcal{Q}_j^{n+\tau,r+1}\big]\big)\big]$. With these notations, we arrive at the following definition of the scheme: for any face f and $k \in \{1, ..., K\}$ we have

$$\begin{aligned}
&\mathcal{Q}_{j,f}^{n+\tau,r+1} - \varepsilon^2 \tilde{\mu}_{j,f}^{n+\tau,r} \nabla_{T_f}\left[\nu_j^{n+\tau,r}\,\mathrm{Tr}\big(\mathscr{G}\big[\mathcal{Q}_j^{n+\tau,r+1}\big]\big)\right] \\
&\quad - \frac{2\tilde{\kappa}_{j,f}^{n+\tau,r}\tau h_t}{3}\nabla_{T_f}\left[\frac{1}{\rho}\,\mathrm{Tr}\left(\mathscr{G}\left[\sum_{l=1}^{g}\omega_l \mathcal{Q}_l^{n+\tau,r+1}\right]\right)\right] - \varepsilon^2 \tilde{\mu}_{j,f}^{n+\tau,r}\eta_{j,f}^{n+\tau,r}\mathcal{E}_f^{n+\tau,r+1} \\
&\qquad = \frac{\varepsilon^2 \tilde{\mu}_{j,f}^{n+\tau,r}}{\tau h_t}\mathcal{Q}_{j,f}^{n} - \tilde{\kappa}_{j,f}^{n+\tau,r}\nabla_{T_f}\left[\theta^n + \tau h_t S_k^{n,n+1}\right], \\
&\theta_k^{n+\tau,r+1} = \theta_k^n + \tau h_t S_k^{n,n+1} - \frac{2\tau h_t}{3\rho_k}\,\mathrm{Tr}\left(\mathscr{G}\left[\sum_{j=1}^{g}\omega_j \mathcal{Q}_j^{n+\tau,r+1}\right]\right).
\end{aligned} \tag{2.15}$$

The field $\mathcal{E}_f^{n+\tau,r+1}$ is associated to the constraint $\displaystyle\sum_{j=1}^{g}\frac{\omega_j \mathcal{Q}_{j,f}^{n+\tau,r+1}}{\xi_j} = 0$, and the coefficients are given by

$$\begin{aligned}
&\tilde{\mu}_{j,f}^{n+\tau,r} = \frac{1}{|f|}\int_f \tilde{\mu}_j^{n+\tau,r}\left(\mathscr{P}[\theta](X)\right)\mathrm{d}\sigma, \quad \tilde{\kappa}_{j,f}^{n+\tau,r} = \frac{1}{|f|}\int_f \tilde{\kappa}_j^{n+\tau,r}\left(\mathscr{P}[\theta](X)\right)\mathrm{d}\sigma, \\
&\eta_{j,f}^{n+\tau,r} = \frac{1}{|f|}\int_f \eta_j^{n+\tau,r}\left(\mathscr{P}[\theta](X)\right)\mathrm{d}\sigma, \quad \nu_{j,k}^{n+\tau,r} = \frac{1}{|\mathscr{C}_k|}\int_{\mathscr{C}_k}\nu_j^{n+\tau,r}(\theta_k)\,\mathrm{d}X = \nu_j^{n+\tau,r}(\theta_k).
\end{aligned} \tag{2.16}$$

Remark that the Neumann boundary condition is naturally taken into account by imposing

$$\mathcal{Q}_{j,f}^{n+\tau,r+1} \cdot N^f_{\mathscr{C}_k} = 0 \quad \text{when } f \in \partial\Omega$$

and k is the index of the volume which admit f as a face. Accordingly, the boundary terms are also incorporated in the summation over the faces.

Remark IV.2.1 *We observe that the quantity* $\mathrm{Tr}\big(\mathscr{G}\,[q]\,\big)$ *depends only on the inner products* $q_f \cdot N^f_{\mathscr{C}_k}$. *Precisely, we have*

$$\mathrm{Tr}\big(\mathscr{G}\,[q]\,\big)\big|_{\mathscr{C}_k} = \frac{1}{|\mathscr{C}_k|}\sum_{f\in\mathbb{F}_{\mathscr{C}_k}} q_f \cdot N^f_{\mathscr{C}_k}.$$

Therefore it appears clearly that $\mathcal{Q}^{n+\tau,r}_{j,f} \cdot N^f_{\mathscr{C}_k}$ *is the only relevant variable to be used in the numerical scheme* (2.15). *It means that the unknowns reduce to a scalar quantity associated to each vertex of the primal mesh and* g *scalar quantities associated to each face of the dual mesh.*
Moreover, it is worth pointing out that the strategy, with the operators $\mathscr{P}$ *and* $\mathscr{G}$, *can be used to treat more general non-local equations, involving more complicated second order derivatives of the heat fluxes, see [8]. For instance* $\nabla_X \cdot \nabla_X \mathcal{Q}_j^{n+\tau,r+1}$ *becomes in the scheme*

$$\mathrm{Tr}\big(\nabla_{T_f}\left(\mathscr{G}\left[\mathcal{Q}_j^{n+\tau,r+1}\right]\right)\big).$$

Let us discuss what the scheme (2.15) does when ε goes to 0. Formally we obtain

$$\begin{aligned}
&\mathcal{Q}^{n+\tau,r+1}_{j,f} - \frac{2\kappa^{n+\tau,r}_{j,f}\tau h_t}{3}\nabla_{T_f}\left[\frac{1}{\rho}\,\mathrm{Tr}\left(\mathscr{G}\left[\sum_{l=1}^{g}\omega_l\mathcal{Q}_l^{n+\tau,r+1}\right]\right)\right] \\
&\qquad = -\kappa^{n+\tau,r}_{j,f}\nabla_{T_f}\left[\theta^n + \tau h_t S_k^{n,n+1}\right], \qquad (2.17)\\
&\theta_k^{n+\tau,r+1} = \theta_k^n + \tau h_t S_k^{n,n+1} - \frac{2\tau h_t}{3\rho_k}\,\mathrm{Tr}\left(\mathscr{G}\left[\sum_{j=1}^{g}\omega_j\mathcal{Q}_j^{n+\tau,r+1}\right]\right).
\end{aligned}$$

Since the operator $\mathscr{P}$ is linear, we can rewrite the first equation using the second and we get $\mathcal{Q}^{n+\tau,r+1}_{j,f} = -\kappa^{n+\tau,r}_{j,f}\nabla_{T_f}[\theta^{n+\tau,r+1}]$. Finally we replace $\mathcal{Q}^{n+\tau,r+1}_{j,f}$ in the equation for the temperature by its expression and we arrive at (2.11).

IV.2.2 Schurtz-Nicolaï Model

The Schurtz-Nicolaï model has been introduced in [16] as a relevant simplified model for ICF simulation. It can be recovered from (1.3) by neglecting the time derivative and the perturbation $\mathcal{E}$ in the equation for the heat fluxes. Therefore, the Schurtz-Nicolaï model reads

$$\begin{cases}
\partial_t\theta + \dfrac{2}{3\rho}\nabla_X\cdot Q = S,\\
\mathcal{Q} - \varepsilon^2\mu\nabla_X\left(\nu\nabla_X\cdot\mathcal{Q}\right) = -\kappa\nabla_X\theta, \qquad (2.18)\\
Q = \displaystyle\int_0^\infty \mathcal{Q}\,\mathrm{d}\xi.
\end{cases}$$

Remark that the constraint (1.4) is not satisfied anymore. Furthermore it has been noticed that negative values of the coefficient κ might lead to instabilities (which is not the case for the time evolution problem, as shown in [8]), see [12], [5, Section III]. However, (2.18) is widely used in ICF codes, usually at the price of truncating κ in order to keep positive values only [16, Section III.C]. The delocalized operator is simplified and it makes the divergence of the generalized heat flux appear. Hence it is convenient to

introduce the new scalar quantity $\tilde{\theta}\,(t,x,\xi) = \nabla_X \cdot \mathcal{Q}(t,x,\xi)$. It can be interpreted as the contribution to the evolution of the temperature of the generalized heat flux with a given internal energy ξ. We obtain a closed system involving the new variable by applying the divergence operator to the generalized heat flux equation. We are led to the following 2×2 system:

$$\begin{cases} \partial_t \theta + \dfrac{2}{3\rho} \displaystyle\int_0^\infty \tilde{\theta}\, \mathrm{d}\xi = S, \\ \tilde{\theta} - \varepsilon^2 \nabla_X \cdot \left(\mu \nabla_X \left(\nu \tilde{\theta} \right) \right) = -\nabla_X \cdot \left(\kappa \nabla_X \theta \right), \end{cases}$$

We derive a numerical scheme for this problem by following the reasoning proposed for the classical Spitzer-Härm equation. It yields

$$\begin{aligned} &\tilde{\theta}_{j,k}^{n+\tau,r+1} - \frac{\varepsilon^2}{|\mathscr{C}_k|} \sum_{f \in \mathbb{F}_{\mathscr{C}_k}} \mu_{j,f}^{n+\tau,r} \nabla_{T_f} \left[\nu_j^{n+\tau,r} \tilde{\theta}_j^{n+\tau,r+1} \right] \cdot N_{\mathscr{C}_k}^f \\ &\quad - \frac{1}{|\mathscr{C}_k|} \sum_{f \in \mathbb{F}_{\mathscr{C}_k}} \frac{2\kappa_{j,f}^{n+\tau,r} \tau h_t}{3} \nabla_{T_f} \left[\frac{1}{\rho} \sum_{l=1}^{g} \omega_l \tilde{\theta}_l^{n+\tau,r+1} \right] \cdot N_{\mathscr{C}_k}^f \\ &\qquad = -\frac{1}{|\mathscr{C}_k|} \sum_{f \in \mathbb{F}_{\mathscr{C}_k}} \kappa_{j,f}^{n+\tau,r} \nabla_{T_f} \left[\theta^n + \tau h_t S_k^{n,n+1} \right] \cdot N_{\mathscr{C}_k}^f, \\ &\theta_k^{n+\tau,r+1} = \theta_k^n + \tau h_t S_k^{n,n+1} - \frac{2\tau h_t}{3\rho_k} \sum_{j=1}^{g} \omega_j \tilde{\theta}_{j,k}^{n+\tau,r+1}. \end{aligned} \tag{2.19}$$

On the same token, it is worthwhile showing that the scheme (2.15) adapts readily to treat (2.18). Since we neglect the time derivative of the generalized heat flux, we obtain

$$\begin{aligned} &\mathcal{Q}_{j,f}^{n+\tau,r+1} - \varepsilon^2 \mu_{j,f}^{n+\tau,r} \nabla_{T_f} \left[\frac{\nu_j^{n+\tau,r}}{|\mathscr{C}|} \sum_{f^\star \in \mathbb{F}_{\mathscr{C}}} \mathcal{Q}_{j,f^\star}^{n+\tau,r+1} \cdot N_{\mathscr{C}_k}^f \right] \\ &\quad - \frac{2\kappa_{j,f}^{n+\tau,r} \tau h_t}{3} \nabla_{T_f} \left[\frac{1}{\rho |\mathscr{C}|} \sum_{f^\star \in \mathbb{F}_{\mathscr{C}}} \sum_{l=1}^{g} \omega_l \mathcal{Q}_{l,f^\star}^{n+\tau,r+1} \cdot N_{\mathscr{C}_k}^f \right] \\ &\qquad = -\kappa_{j,f}^{n+\tau,r} \nabla_{T_f} \left[\theta^n + \tau h_t S_k^{n,n+1} \right], \\ &\theta_k^{n+\tau,r+1} = \theta_k^n + \tau h_t S_k^{n,n+1} - \frac{2\tau h_t}{3\rho_k |\mathscr{C}_k|} \sum_{f \in \mathbb{F}_{\mathscr{C}_k}} \sum_{j=1}^{g} \omega_j \mathcal{Q}_{j,f}^{n+\tau,r+1} \cdot N_{\mathscr{C}_k}^f. \end{aligned} \tag{2.20}$$

We remark that (2.20) leads to (2.19) when summing the flux equations over the faces of the control volume $\mathscr{C}_k$ and defining the discrete version of the new variable $\tilde{\theta}$ as to be $\tilde{\theta}_{j,k}^{n+\tau,r+1} = \sum_{f^\star \in \mathbb{F}_{\mathscr{C}}} \mathcal{Q}_{j,f^\star}^{n+\tau,r+1} \cdot N_{\mathscr{C}_k}^f$. In practice the formulation (2.19) has to be preferred over (2.20) for simulating the Schurtz-Nicolaï model because the corresponding linear system is symmetric, and, for a given mesh, it has both a smaller size and a smaller stencil. The method adapts to more complicated delocalized operators, as presented in [8]. For instance we can introduce as a new unknown the jacobian of the generalized heat flux $\tilde{\Theta}\,(t,x,\xi) = \nabla_X \mathcal{Q}(t,x,\xi)$ or its discrete version $\tilde{\Theta}_{j,k}^{n+\tau,r+1} = \mathscr{G}\left[\mathcal{Q}_j^{n+\tau,r+1}\right] = \frac{1}{|\mathscr{C}_k|} \sum_{f \in \mathbb{F}_{\mathscr{C}_k}} \mathcal{Q}_{j,f}^{n+\tau,r+1} \otimes N_f$. Then the previous construction can be repeated to define a

numerical scheme. However, the new variable is now a matrix and it is not clear that the resulting scheme is more effective than a version of (2.20) with a discretization of the complete delocalized operator.

IV.3 Coupling of models: domain decomposition approach

For many applications, for instance for ICF computations and the design of devices of energy deposit by laser beams, the asymptotic Spitzer-Härm approximation is valid on a large part of the simulation domain. As discussed above, the Spitzer-Härm model is quite simple, and it can be numerically treated for a reasonable cost. However, the zones where the Spitzer-Härm model does not apply are precisely located at places where discrepancies can have a major impact on the studied physics. A simulation based on the generalized model on the full domain is certainly unnecessarily costly. For these reasons, we explain now how we can combine the two modeling, just using the complex model where it is needed, through a coupling strategy. Since the scheme (2.15) is asymptotically consistent to the scheme (2.11) for the Spitzer-Härm equation, we do not need too much additional numerical tools. The discussion relies on the definition of coupling conditions and on finding a practical method to detect where the interface has to be placed. We propose an "a priori" estimator to decide where the asymptotic Spitzer-Härm equation has to be used.

IV.3.1 Coupling strategy

Let us first suppose that the scheme is well-defined on each triangle of the mesh. We note by Ω_{SH} the part of the domain where the Spitzer-Härm model is valid and Ω_{SHG} the remainder of the computational domain. We suppose that the interface Σ between the two subdomains Ω_{SH} and Ω_{SHG} is made of a set of vertices of triangles of the primal mesh $\mathbb{T}$. Obviously, far from the interface Σ, we do not modify the models. However, close to the interface, the updating of the numerical unknowns from one subdomain depends on the values on the complementary subdomain. Hence, we need to adapt the definition of the operator $\mathscr{G}$. Remark that with the scheme (2.11), the numerical unknowns depend on their direct neighbors.

Depending whether a given volume belongs to Ω_{SH} or Ω_{SHG} we apply the scheme (2.11) or (2.15). We are now interested in the definition of the scheme on the interfaces. First we slightly generalize the operator $\mathscr{G}$ so that we can approach gradient on control volumes involved by the interface. We split the summation in (2.14) according to the two subdomains. Coming back to (2.17), $\mathcal{Q}_{j,f}^{n+1,r+1}$ becomes $-\kappa_{j,f}^{n+1,r+1}\nabla_{T_f}\left[\theta^{n+\tau,r+1}\right]$ in the subdomain Ω_{SH}. We define

$$\begin{aligned}\mathscr{G}_k^\star\left[\mathcal{Q}_j^{n+\tau,r+1}\right] = \frac{1}{|\mathscr{C}_k|}\Big(&\sum_{f\in\mathbb{F}_{\mathscr{C}_k}\cap\Omega_{SHG}} \mathcal{Q}_{j,f}^{n+\tau,r+1}\otimes N_{\mathscr{C}_k}^f \\ &- \sum_{f\in\mathbb{F}_{\mathscr{C}_k}\cap\Omega_{SH}} \kappa_{j,f}^{n+\tau,r}\nabla_{\mathbb{T}_f}\left[\theta^{n+\tau,r+1}\right]\otimes N_{\mathscr{C}_k}^f\Big).\end{aligned} \tag{3.1}$$

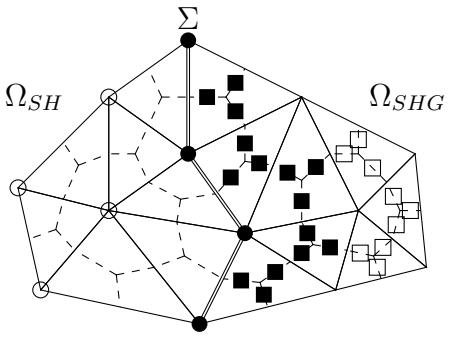

$=$: Interface Σ

Numerical unknowns

- $\circ$: $\theta_k^{n+1,r+1}$ on Ω_{SH}
- $\bullet$: $\theta_k^{n+1,r+1}$ depending values on Ω_{SHG}
- $\square$: $\mathcal{Q}_{j,f}^{n+1,r+1}$ on Ω_{SHG}
- $\blacksquare$: $\mathcal{Q}_{j,f}^{n+1,r+1}$ depending values on Ω_{SH}

Figure IV.2: Numerical discretization near to the interface.

Remark that $\kappa_{j,f}^{n+\tau,r+1}$ is well defined even in the subdomain Ω_{SH} since κ depends on ξ and θ only. Then we are able to define the same operator on the hydrodynamic heat flux which appears in (2.11). Since $\mathscr{G}_k^\star$ is a linear operator, we have

$$\begin{aligned}\mathscr{G}_k^\star\left[Q^{n+\tau,r+1}\right] \;=\; \frac{1}{|\mathscr{C}_k|}\Big(&\sum_{f\in\mathbb{F}_{\mathscr{C}_k}\cap\Omega_{SHG}}\sum_{j=1}^{g}\omega_j\mathcal{Q}_{j,f}^{n+\tau,r+1}\otimes N_{\mathscr{C}_k}^f\\ &-\sum_{f\in\mathbb{F}_{\mathscr{C}_k}\cap\Omega_{SH}}\kappa_{SH,f}^{n+\tau,r}\nabla_{\mathbb{T}_f}\left[\theta^{n+\tau,r+1}\right]\otimes N_{\mathscr{C}_k}^f\Big).\end{aligned}\tag{3.2}$$

The coupled scheme summarizes as follows

$$\begin{cases}\theta_k^{n+\tau,r+1}+\frac{2\tau h_t}{3\rho_k}\operatorname{Tr}\left(\mathscr{G}^\star\left[Q^{n+\tau,r+1}\right]\right)=\theta_k^n+\tau h_t S_k^{n,n+1}, & \text{for any } k\in\Omega_{SH},\\ \mathcal{Q}_{j,f}^{n+\tau,r+1}-\varepsilon^2\tilde{\mu}_{j,f}^{n+\tau,r}\nabla_{T_f}\left[\nu_j^{n+\tau,r}\operatorname{Tr}\left(\mathscr{G}^\star\left[\mathcal{Q}_j^{n+\tau,r+1}\right]\right)\right]\\ \quad-\frac{2\tilde{\kappa}_{j,f}^{n+\tau,r}\tau h_t}{3}\nabla_{T_f}\left[\frac{1}{\rho}\operatorname{Tr}\left(\mathscr{G}^\star\left[Q^{n+\tau,r+1}\right]\right)\right]-\varepsilon^2\tilde{\mu}_{j,f}^{n+\tau,r}\eta_{j,f}^{n+\tau,r}\mathcal{E}_f^{n+\tau,r+1}\\ \quad=\frac{\varepsilon^2\tilde{\mu}_{j,f}^{n+\tau,r}}{\tau h_t}\mathcal{Q}_{j,f}^n-\tilde{\kappa}_{j,f}^{n+\tau,r}\nabla_{T_f}\left[\theta^n+\tau h_t S^{n,n+1}\right], & \text{for any } f\in\Omega_{SHG},\end{cases}\tag{3.3}$$

and furthermore

$$\theta_k^{n+\tau,r+1}=\theta_k^n+\tau h_t S_k^{n,n+1}-\frac{2\tau h_t}{3\rho_k}\operatorname{Tr}\left(\mathscr{G}^\star\left[Q^{n+\tau,r+1}\right]\right),\qquad\text{for any } k\in\Omega_{SHG}\setminus\Sigma.$$

Remark that the evaluation of the temperature on $\Omega_{SHG}\setminus\Sigma$ can be performed explicitly having at hand the quantities determined by solving the system (3.3).

IV.3.2 "A priori" estimator

We wish now to discuss a relevant definition of the interface Σ. A rough method simply consists in splitting the domain once for all at the beginning of the simulation according to

the knowledge of experimental data. The subdomain Ω_{SH} corresponds to a region where the perturbation are expected to remain small, with small variation of the temperature θ: the asymptotic Spitzer-Härm model is likely accurate enough. However, this method does not adapt to numerical results and leads to make use of a subdomain Ω_{SHG} larger than needed. A more refined method defines dynamically the subdomains by using a local estimate of the variation of the heat flux. The subdomains can be defined at each iteration or after a fixed number of time iterations, in order to keep a number of numerical unknowns as small as possible in the scheme (2.15).

Let us denote $\Omega_{SH}^{n,r}$ and $\Omega_{SHG}^{n,r}$ the subdomains at iteration (n,r). We know the solution $\theta^{n+\tau,r}$ on the subdomain $\Omega_{SH}^{n+1,r}$ and $\mathcal{Q}_{j,f}^{n+\tau,r}$ on the subdomain $\Omega_{SHG}^{n+1,r}$. We now construct an "a priori" estimator $E_T^{n+1,r+1}$ which will be used to update the new subdomain $\Omega_{SH}^{n+1,r+1}$ and $\Omega_{SHG}^{n+1,r+1}$. Note that since the subdomains change from one iteration to another, we shall need to define the value of $\mathcal{Q}_{j,f}^{n,r}$ in the subdomain $\Omega_{SH}^{n+1,r} \cap \Omega_{SHG}^{n+1,r+1}$. We start by expanding the definition of the generalized heat flux to the subdomain $\Omega_{SH}^{n+1,r}$ by equating it to the asymptotic value of $\mathcal{Q}_{j,f}^{n+\tau,r}$ as ε goes to 0. Using (2.17), we write

$$\mathcal{Q}_{j,f}^{n+\tau,r} = -\kappa_{j,f}^{n+1,r-1} \nabla_{T_f} \left[\theta^{n+\tau,r}\right], \qquad \text{for any } f \in \Omega_{SH}. \tag{3.4}$$

Obviously the perturbation of the field vanishes on $\Omega_{SH}^{n+1,r}$. Since ε is not vanishing, the generalized heat flux $\mathcal{Q}_{j,f}^{n+\tau,r}$ on $\Omega_{SH}^{n+1,r}$ is not solution of (2.15). Then we compare in any triangle, the solution of the two schemes. Using (2.15), we are able to compare the solution of (2.15) to its asymptotic value given by (3.4), it yields

$$\begin{aligned} &\left|\mathcal{Q}_{j,f}^{n+\tau,r+1} + \kappa_{j,f}^{n+\tau,r} \nabla_T \left[\theta^{n+\tau,r+1}\right]\right| \\ &\quad = \varepsilon^2 \tilde{\mu}_{j,f}^{n+\tau,r+1} \left| \frac{\mathcal{Q}_{j,f}^{n} + \kappa_{j,f}^{n+\tau,r} \nabla_T \left[\theta^{n+\tau,r+1}\right]}{\tau h_t} \right. \\ &\qquad \left. + \nabla_T \left[\nu_j^{n+\tau,r} \operatorname{Tr}\left(\mathscr{G}\left[\mathcal{Q}_j^{n+\tau,r+1}\right]\right)\right] + \eta_{j,f}^{n+\tau,r} \mathcal{E}_f^{n+\tau,r+1} \right|, \end{aligned} \tag{3.5}$$

where we used the definition (2.6) of coefficients to compare the diffusion coefficients of the two models, i.e. $\kappa_{j,f}^{n+1,r} - \tilde{\kappa}_{j,f}^{n+1,r} = \frac{\varepsilon^2 \tilde{\mu}_{j,f}^{n+1,r} \kappa_{j,f}^{n+1,r}}{\tau h_t}$. Eventually, we define the following estimator function, $E_T^{n+1,r+1}$, stepwise constant on any triangle of the whole domain Ω,

$$\begin{aligned} E_T^{n+1,r+1} = &\varepsilon^2 \max_{\substack{f \in T \\ j \in [\![1,g]\!]}} \tilde{\mu}_{j,f}^{n+\tau,r+1} \left| \frac{\mathcal{Q}_{j,f}^{n} + \kappa_{j,f}^{n+\tau,r} \nabla_T \left[\theta^{n+\tau,r+1}\right]}{\tau h_t} \right. \\ &\left. + \nabla_T \left[\nu_j^{n+\tau,r} \operatorname{Tr}\left(\mathscr{G}\left[\mathcal{Q}_j^{n+\tau,r+1}\right]\right)\right] + \eta_{j,f}^{n+\tau,r} \mathcal{E}_f^{n+\tau,r+1} \right|. \end{aligned} \tag{3.6}$$

Since the generalized heat flux $\mathcal{Q}_{j,f}^{n+\tau,r}$ on $\Omega_{SH}^{n+1,r}$ obtained by using formulae (3.4) is not solution of the scheme (2.15), the equality (3.5) does not hold in the subdomain $\Omega_{SH}^{n+1,r}$. The estimator function vanishes on a triangle iff the solution of the scheme (2.15) estimated in the whole domain corresponds to the solution of the scheme (2.11).

However, we cannot use directly this definition because it depends on the unknown at iteration $(n+\tau, r+1)$, which has not yet be estimated. However, according to [8, Theorem 5.1], the solution can be expected to have some regularity. Thus, the estimator

at the previous iteration $E^{n+1,r}$ is an effective approximation to define the subdomains. Eventually we fix a threshold $0 < \delta \ll 1$, and for any $T \in \mathbb{T}$ we set

$$T \in \left| \begin{array}{ll} \Omega_{SH}^{n+1,r+1}, & \text{if } E^{n+1,r} \leq \delta, \\ \Omega_{SHG}^{n+1,r+1}, & \text{otherwise.} \end{array} \right.$$

This method will be further discussed in Section IV.4.3.

IV.4 Numerical Results

In this section, first we check numerically the stability and consistency properties of the scheme (2.15). Then we perform simulations illustrating some kinetic effects not taken into account by the Spitzer-Härm equation. For all the simulations, the linear systems are inverted using the `MUMPS` library [1].

IV.4.1 Validation of the Scheme

Consistency

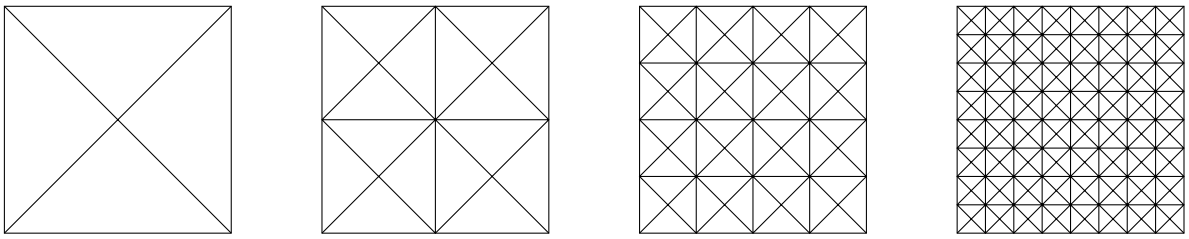

Struc 1: $h = \frac{\sqrt{2}}{2}$, Struc 2: $h = \frac{\sqrt{2}}{4}$, Struc 3: $h = \frac{\sqrt{2}}{8}$, Struc 4: $h = \frac{\sqrt{2}}{16}$.

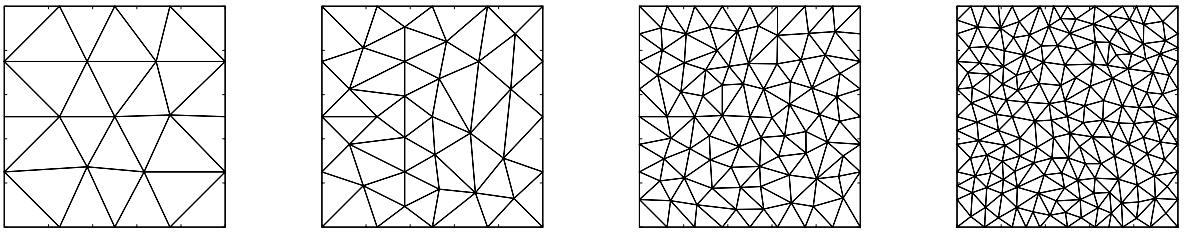

Unstruc 1: $h \approx 0.25$, Unstruc 2: $h \approx 0.156$, Unstruc 3: $h \approx 0.09$, Unstruc 4: $h \approx 0.062$.

Figure IV.3: Examples of mesh used to estimate the consistence. In the first line, structured meshes obtained with iterative process, Struc n is the union of four Struc $n-1$ scaled by $1/2$. In the second line, unstructured meshes obtained by Delaunay triangulation using the mesh generator *Triangle*.

In order to validate the scheme and to investigate its consistency properties we start with a simple situation where all coefficients are constants. Precisely, we set

$$\rho = \mu = \nu = \eta = 1, \qquad \kappa(\xi) = \frac{\xi^4 (\xi - 4)}{24}, \qquad \kappa_{SH} = \int_{\mathbb{R}_+} \kappa \, \mathrm{d}\xi = 1.$$

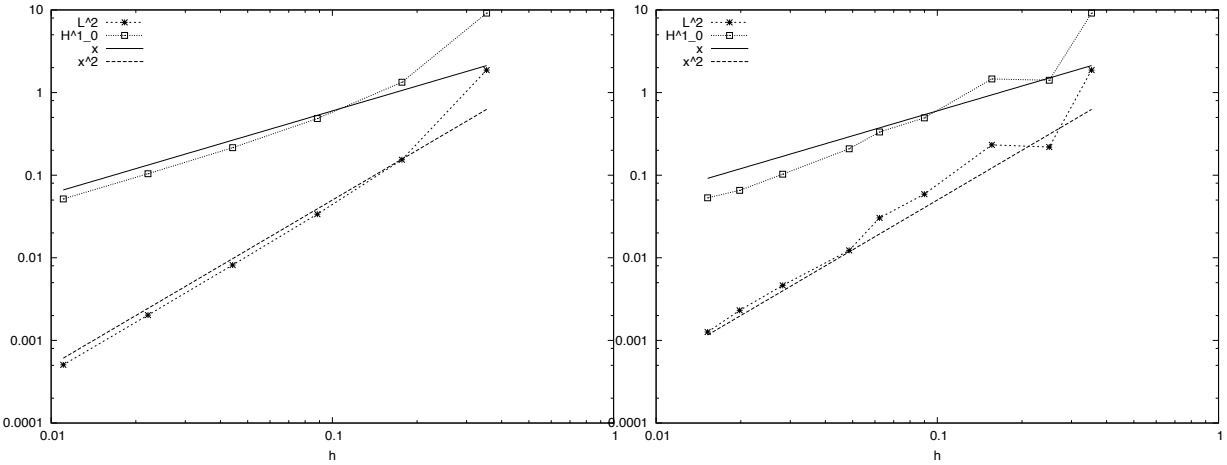

Structured meshes. Unstructured meshes.

Figure IV.4: Errors in the L^2 norm and in the H_0^1 norm between the numerical and the analytical results.

As time goes to ∞, we can expect that the solution of (1.3) tends to an asymptotic profile determined by the following system

$$\begin{cases} \displaystyle\int_\Omega \theta^\infty \,\mathrm{d}X = \int_\Omega \theta^0 \,\mathrm{d}X + \int_0^\infty \int_\Omega S \,\mathrm{d}X \,\mathrm{d}t, \\ \dfrac{2}{3\rho}\nabla_X \cdot Q^\infty = S, \\ Q^\infty - \varepsilon^2 \mu \nabla_X \left(\nu \nabla_X \cdot Q^\infty\right) = -\kappa_{SH} \nabla_X \theta^\infty, \\ \mathcal{E}^\infty = 0. \end{cases} \tag{4.1}$$

The computational domain is the square $\Omega = [0,1]^2$ and the initial condition is $\theta^0(X) = 100$ and $\mathcal{Q}_j^0(X) = 0$. We work with the following source term

$$S(x_1, x_2) = \frac{4\left(2\pi\right)^2 \kappa_{SH}}{3\rho} \cos\left(2\pi x_1\right) \cos\left(2\pi x_2\right). \tag{4.2}$$

We can easily check that the corresponding solution of (4.1) is given by

$$\theta^\infty(x_1, x_2) = \int_\Omega \theta^0 \,\mathrm{d}X + \left(1 + 2\varepsilon^2 \left(2\pi\right)^2 \mu\nu\right) \cos\left(2\pi x_1\right) \cos\left(2\pi x_2\right).$$

We perform two set of simulation, in a stuctured grid presented in the first line of Figure IV.3, and in a unstructured grid shown for some value of h, the size of the smallest edge of the mesh. We denote θ_h^∞ the solution produced by the scheme (2.15) with a mesh characterized by h. We estimate the error $\theta^\infty - \theta_h^\infty$ with both the $L^2\left(\mathbb{T}\right)$ norm and the $H_0^1\left(\mathbb{T}\right)$ norm, the discrete norms being defined by

$$|\theta_h^n - \theta^\infty|_{L^2(\mathbb{T})} = \left(\sum_{\mathscr{C}_k \in \mathbb{C}} |\mathscr{C}_k| |\theta_k^n - \theta^\infty\left(X_k\right)|^2\right)^{1/2}, \qquad |\theta_h^n - \theta^\infty|_{H_0^1(\mathbb{T})} = \left(\sum_{T \in \mathbb{T}} |T| \left|\nabla_T \left[\theta^n - \theta^\infty\right]\right|^2\right)^{1/2}. \tag{4.3}$$

The simulations are performed using $g = 2$ points in the energy discretization with $\alpha = 3$. The time step is set to 1 and we use $\tau = 1$ (fully implicit scheme) while ε is set to 10^{-1}. Figure IV.4 shows that the numerical scheme (2.15) reaches second order accuracy for the $L^2(\mathbb{T})$ norm and first order for the $H_0^1(\mathbb{T})$ norm. Further tests show that this conclusion remains unaffected by making ε vary.

Influence of the Energy Discretization

g		2	3	4
N inc		36864	49152	61440
Stencil		45	75	107
α	0	101.812	103.642	103.647
	1	101.535	103.674	103.666
	2	103.766	103.729	103.708
	3	103.806	103.774	103.751
	4	103.825	103.804	103.784

Number of unknowns, stencil and L^∞ norm.

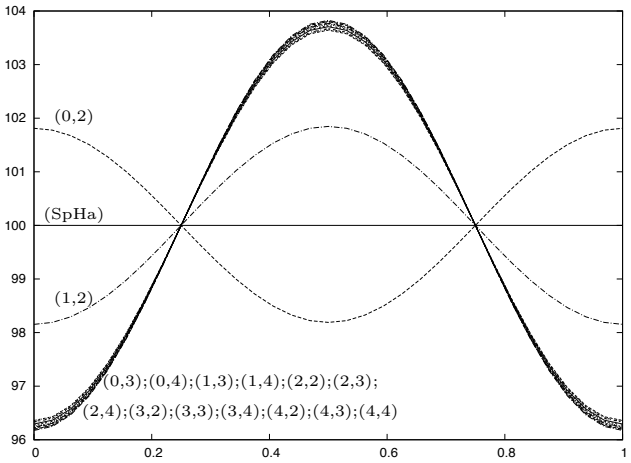

Numerical solutions on $y = 0.5$ for several value (α, g).

Figure IV.5: Numerical results for several value of (α, g). The left tabular is the L^∞ norm of the solution. The right figure is the temperature profile on the hyperplan $x_2 = 0.5$.

We now wish to investigate on numerical grounds the influence of the energy discretization, embodied into the fitting parameters α and g. We specify how the coefficients μ, ν, η, κ depend on the energy variable ξ as follows

$$\begin{aligned} \mu &= \frac{2^{3/2}\tau_1}{\rho}\xi^{3/2}\theta^{3/2}, & \nu &= \frac{2\tau_0}{3}\xi\theta \\ \kappa &= \frac{16\tau_1}{3\sqrt{\pi}}\xi^4(\xi-4)\,e^{-\xi}\theta^{5/2}, & \eta &= \frac{4\rho}{3\sqrt{\pi}}\xi^{5/2}e^{-\xi}\theta, \end{aligned} \tag{4.4}$$

where we set $\tau_0 = 200$ and $\tau_1 = 1$. These parameters can be interpreted as relaxation time respectively in the isotropic and anisotropic direction. Such expressions can be derived from the kinetic modeling dealing with a BGK-like collision operator, see [8].

The density ρ is still assumed to be constant ($\rho(X) = 1$). The initial condition and the source term we are using are still defined by (4.2). Again we work with the structured mesh presented in Figure IV.3; the space step is $h = \frac{\sqrt{2}}{64}$, the time step is $h_t = 10^{-5}$ and the scheme is used in the fully implicit version $\tau = 1$. Finally we set $\varepsilon = 10^{-2}$.

Figure IV.5 shows the numerical results on the hyperplane $x_2 = 0.5$ for several

values of g, the number of points in the energy discretization, and several value of α. The figure shows that the solution could be very bad when the number of points and the weight mismatch. For instance the results with $(\alpha, g) = (0, 2)$ are unphysical and it is worth pointing out that these parameters are violating hypothesis of [8, theorem 5.1] during the iteration process: we have at some moment $\kappa_{1,f}^{n,r} + \kappa_{2,f}^{n,r} < 0$. We also observe that the amplitude of the solution is slightly modified by the weight of the Laguerre quadrature method. The amplitude is an appropriate indicator of the impact of the non-local model. Defining the L^∞ norm of the solution by

$$|\theta_h^n|_{L^\infty(\mathbb{T})} = \max_{\mathscr{C}_k \in \mathbb{C}} \theta_k^n,$$

results are displayed at the last line of Figure IV.5. The convergence rate and the appropriate weight are not clearly identifiable. Thorough investigations with a larger number of points in the energy discretization are needed. However such simulations are quite expensive both in terms of CPU time and memory storage requirements. In particular, the stencil of the linear systems and thus the CPU time of the simulation increase with the number of points in the energy discretization, while they do not depend on the weight of the Laguerre polynomials. The first line in Figure IV.5 gives the number of unknowns of the linear system to be inverted. Obviously it is proportional to $g + 1$ (generalized heat fluxes + field perturbation). The second line is the mean stencil, that is the ratio between the number of non-zero element of the linear system by the number of lines. This result shows that the stencil increases proportionally to the number of points in the energy discretization. Then it becomes prohibitive to use a large number of quadrature points. Anyway, it seems appropriate to use parameter α which exactly estimates the asymptotic Spitzer-Härm regime with just 2 points, i.e $\alpha \in \{2, 3, 4\}$, while the parameter of delocalization ε is not too large.

IV.4.2 Relaxation Profile and Kinetic Effect

The following test case is closer to the simulation of plasma in practical situations. Indeed it has been reported that the Spitzer-Härm model (1.1) is marginally valid for ICF plasmas [5]. As said above this remark has motivated the development of richer reduced models that include some delocalization effects. The relevancy of such models is evaluated by their ability in reproducing "antidiffusive effects" which are typical of the kinetic simulation: in some circumstances, the inner product between the heat flux and the temperature gradient is not necessarily negative, a feature that cannot be captured by the Spitzer-Härm equation (1.1) because $Q_{SH} \cdot \nabla_X \theta_{SH} = -\kappa_{SH} |\nabla_X \theta_{SH}|^2$ is always negative.

Hence, we consider data that produce a strong gradient initially, like

$$\theta^0(x_1, x_2) = \frac{3 + 7\cos(\pi x_1) e^{-100|X - X_c|^2}}{2}, \qquad \mathcal{Q}_j^0(X) = 0,$$

where X_c is the centroid of the computational domain. Like in the previous section, the parameters are set as follows: $\tau_0 = 200$, $\tau_1 = 1$, $\rho(X) = 1$, $h_t = 10^{-5}$, $\tau = 1$, $(\alpha, g) = (2, 2)$ and we use a structured mesh with a space step $h = \frac{\sqrt{2}}{1024}$. The results we

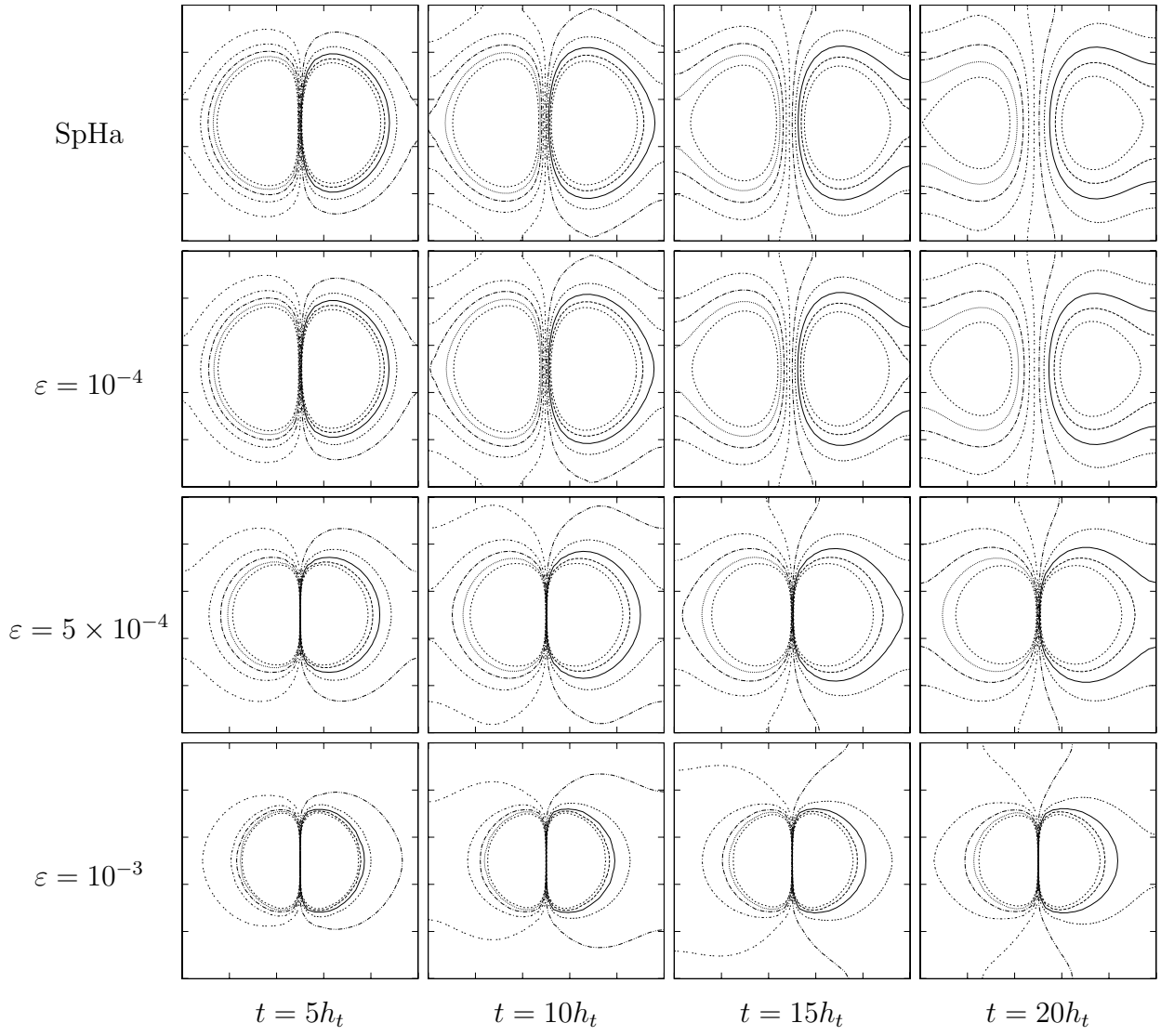

Figure IV.6: Temperature isoline (from 1.491 to 1.509 every 2×10^{-3}) with (2.11) (first line) and for several value of ε with (2.15) at some time iterations.

discuss below are qualitatively interesting, but they should be considered with caution because on the one hand the non-linear definition of the coefficients highly depends on the physical context and they can influence the shape of the solution, and on the other hand the initialization of the heat flux we have chosen is unphysical; definitely finding relevant initial values for the $\mathcal{Q}_j$ is a difficulty when using this kind of hydrodynamic models.

Figure IV.6 shows the temperature contour lines for several values of ε. As ε goes to 0, the solution of (2.15) (first line in Figure IV.6) goes to the solution of (2.11) (second and fourth lines of Figure IV.6). For ε as small as 10^{-4}, the numerical discrepancies between the two solutions are not significant. In addition, we clearly identify that the spreading of temperature with the non local model (1.3) is reduced significantly as ε increases.

This effect is more important in areas with large temperature gradients. Simulation with $\varepsilon = 5 \times 10^{-4}$ in Figure IV.6 illustrates this remark. When temperature gradients are smaller, the solution looks like the solution of the classical Spitzer-Härm model, yet the large gradient area ($X = .5$) is preserved.

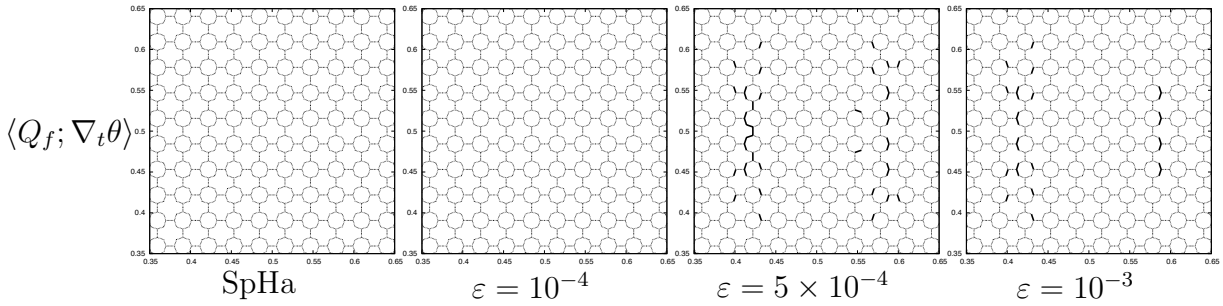

Figure IV.7: Product $\langle Q_f; \nabla_t \theta \rangle$ defined by (4.5) with (2.11) (first figure) and with (2.15) for several value of ε (second and fourth figure) zoomed on the central area at $t = 5h_t$. Dotted lines are faces with $\langle Q_f; \nabla_t \theta \rangle \leq 0$ and full lines are faces with $\langle Q_f; \nabla_t \theta \rangle > 0$.

In [7, 8], simulations in one dimension have shown that (1.3) can reproduce "antidiffusive effects". Here, a difficulty comes from the fact that the numerical scheme (2.15) does not estimate the heat flux but rather its projection to the normal direction to the faces of the control volume (see Remark IV.2.1: the numerical unknown for the fluxes is actually $\mathcal{Q}_{j,f}^{n,r} \cdot N_{\mathscr{C}_k}^f$). Hence the definition of the inner product between the heat flux and temperature gradient at the discrete level is ambiguous. Therefore, we consider the following quantity, evaluated on the faces of the dual mesh

$$\langle Q_f; \nabla_{T_f} \theta \rangle = \left(\sum_{j=1}^{g} \omega_j \mathcal{Q}_{j,f}^n \cdot N_{\mathscr{C}_k}^f \right) \left(\nabla_{T_f} \theta^n \cdot N_{\mathscr{C}_k}^f \right). \tag{4.5}$$

For the Spizer-Härm equation this quantity becomes, see (2.12), $Q_{SH,f}^n \cdot N_{\mathscr{C}_k}^f \times \nabla_t \theta_{SH}^n \cdot N_{\mathscr{C}_k}^f = -\kappa_{SH} \left(\nabla_t \theta_{SH}^n \cdot N_{\mathscr{C}_k}^f \right)^2$. Figure IV.7 shows that the product (4.5) can become positive when running (2.15) with $\varepsilon > 0$: on the faces marked with full lines in Figure IV.7 the heat flux goes in the opposite direction compared to the Spitzer-Härm flux. As expected these effects are very localized in regions of large temperature gradients. Nevertheless the impact of such effects in applications can be important because it generally occurs precisely where the main part of energy is deposited by the source (Laser Beam).

IV.4.3 Domain decomposition impact

Let us point out that using (1.3) in the whole domain could be needlessly expensive. In view of the numerical results it is likely relevant to adopt a domain decomposition approach, using the standard Spitzer-Härm equation (1.1) in the main domain and the more involved system (1.3) in regions where large temperature gradients are observed, as it is described in Section IV.3.2. We remind that, for most applications we are aware of, such regions are very localized.

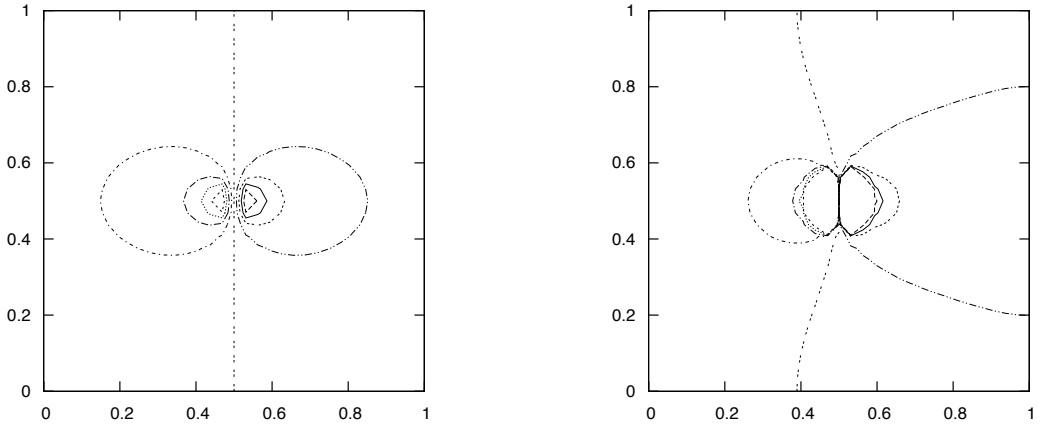

Numerical solution of scheme (2.11).

Numerical solution of scheme (2.15)

Figure IV.8: Isoline of the numerical solutions for the two different models (1.1) (scheme (2.11), left) and (1.3) (scheme (2.15), right) from 9.992 to 10.008 every 0.002.

To illustrate the accuracy of the coupling strategy, we now perform a test case with a very localized source term. More precisely we set

$$S(x_1, x_2) = 10^7 \cos(\pi x_1)\, e^{-1000|X - X_c|^2}$$

where X_c is the centroid of the computational domain. Note that the average of the source term over the whole domain vanishes. Then we estimate the solution provided by the schemes at equilibrium. The parameters are set as follows: $\tau_0 = 200$, $\tau_1 = 1$, $\rho(X) = 1$, $\tau = 1$, $(\alpha, g) = (2, 2)$ and we use a structured mesh with a space step $h = \frac{\sqrt{2}}{512}$.

Figure IV.8 shows the solution of the simulation with the models (1.1) (scheme (2.11), left figure) and (1.3) (scheme (2.15), right figure), respectively. The diffusion of the temperature is less important for the generalized Spitzer-Härm model and the temperature remains larger in the region of the source term. Figure IV.9 shows the accuracy of the coupling strategy. On the left part of the figure, we plot the error in the L_2-norm and H_0^1-norm between the solutions obtained with the coupled scheme (3.3) and the solution obtained with the non-local model (2.15) used everywhere in the domain, for several values of the threshold parameter δ. For a small enough value of δ ($< 10^{-4}$), the coupling strategy leads exactly to the same result than the scheme (2.15). This has to be compared with the right part of the figure where we plot informations about the linear systems like the number of unknowns and the stencil of the coupling resolution for several values of the threshold parameter δ. Remark that for small values of δ ($< 10^{-4}$), the linear system is the same than the one of the scheme (2.15), and for large values of δ ($\geq 10^4$), it is the same than the one of the scheme (2.11).

In the intermediate range $10^{-2} \leq \delta \leq 1$, the coupling strategy leads to results quite close to the solution of (2.15) and the linear system is substantially smaller in number of

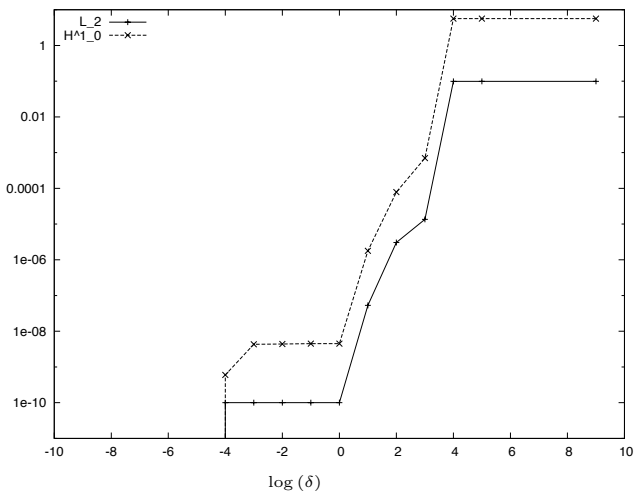

Errors in the L^2 norm and in the H_0^1 norm.

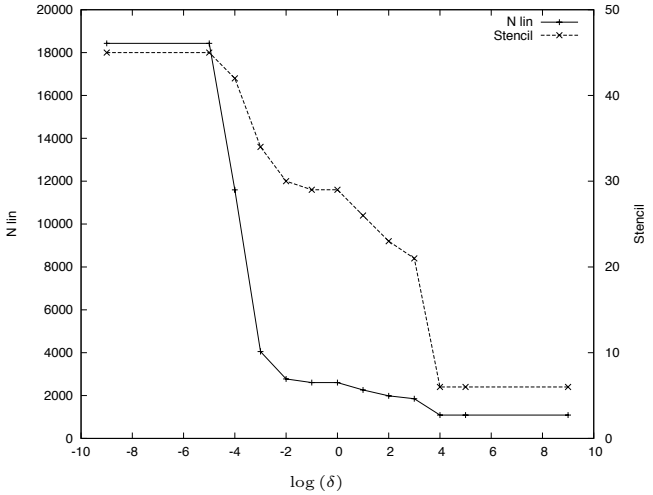

Nombre of unknowns (N lin) and mean stencil of the linear system of the scheme (3.3).

Figure IV.9: Comparison between the numerical results of the coupling strategy (3.3) and the scheme (2.15) in the whole domain.

unknowns and in stencil than when using (2.15). In addition, the linear system can be organized block–wise, according to the sub-domain Ω_{SH}, with symmetric blocks. This remark makes the use of parallelization strategies very appealing to solve the linear system. Eventually, note that for $10^{-4} < \delta < 10^{-2}$, the iterative process needed to estimate the non-linearity and the sub-domains converges with some difficulties. It is due to the fact that the space variation of the estimator (define in (3.6)) is small in a large region where the value of the estimator is close to δ. The iterative process needs more iterations to determine the sub-domain interface and the efficiency of the strategy is limited. Figure IV.10 shows the sub-domain interfaces for several values of the parameter δ. For $10^{-4} \leq \delta \leq 10^{-2}$, the sub-domains are not symmetric according to the axes $y = 0.5$, as the solution needs to be. The sub-domains interfaces oscillate from close contours. For larger values of δ, these oscillations do not appear and the convergence of the iterative process is quite fast.

IV.5 Generalizations and Comments

IV.5.1 Higher Dimensions and General Meshes

The scheme presented in Section IV.2.1 can be generalized to the three dimensions framework. In this context, the mesh is composed by tetrahedrons which replace the triangles used in two dimensions. The numerical unknowns corresponding to the temperature are still stored at the vertices of the mesh. The control volume of a given vertex k is the set of points in $\mathbb{R}^3$ limited by an assembly of triangular facets, where each facet is formed by connecting edge midpoints, element centroids and face centroids in the primal mesh, in such a way that only the node k is contained within the dual mesh cell, see [6]. The

generalized heat fluxes are thus stored at the centroids of the faces of the volume control (hence they are 12 values per tetrahedron instead of 3 per triangle in two dimensions). Since tetrahedrons have four vertices, we can build the $\mathscr{P}$ operator as we did in two dimensions, it now defines a piecewise $\mathbb{P}_1$ function depending on the three space coordinates. Remark that the Matrix operator $\mathscr{G}$ is well defined in any dimension and for any bounded control volume. The scheme can be generalized as well to meshes made of elements more complex than triangles or tetrahedrons. Indeed the key issue relies on the construction of the $\mathscr{P}$ operator on the elements which are determined by $d+1$ vertices and faces. When the problem becomes overdetermined, well-documented approximation techniques can be used, e. g. least squares methods or projections, see [2, 4].

IV.5.2 Uncoupling the Generalized Heat Fluxes

The system (2.5) is macroscopic, but it is made of $(g+1)$ coupled equations; the resolution could be expensive, especially in multi-dimensional frameworks, for cases where the heat fluxes are vectorial unknowns (see Remark IV.2.1). Indeed, in (2.15), the number of unknowns and the stencil of the linear system are proportional to the number of points used in the energy discretization, as it is illustrated in Figure IV.5. In this Section we present a decoupling strategy so that (2.15) is replaced by an iterative process, which relies on solving g uncoupled equations at each iteration. This decoupling strategy can be interpreted as a block-Jacobi method applied to the linear system (2.15), where the blocks are defined by the index of the energy variable. In this approach, the field needs to be estimated explicitly by means of the other unknowns. To this end we multiply the equations for the heat fluxes in (2.5) by $\frac{\omega_j}{\xi_j}$ and we sum over $j \in \{1, ..., g\}$. It yields

$$\mathcal{E}^{n+\tau,r+1} = -\frac{\displaystyle\sum_{j=1}^{g}\left[\frac{\omega_j\tilde{\mu}_j^{n+\tau,r}}{\xi_j}\left(\frac{\mathcal{Q}_j^n}{\tau h_t} + \nabla_X\left(\nu_j^{n+\tau,r}\nabla_X\cdot\left(\mathcal{Q}_j^{n+\tau,r+1}\right)\right)\right)\right]}{\displaystyle\sum_{j=1}^{g}\left[\frac{\omega_j\tilde{\mu}_j^{n+\tau,r}\eta_j^{n+\tau,r}}{\xi_j}\right]}. \tag{5.1}$$

Then we replace $\mathcal{E}^{n,r+1}$ in the equation on the generalized heat fluxes in (2.5) by its expression given by (5.1). At this step, we have written a coupled system of g (generalized heat fluxes) vectorial equations, without any approximation from (2.5). In particular, the scheme satisfies exactly the constraint (2.4). Next, we approximate the generalized heat fluxes at the quadrature point j, $\mathcal{Q}_j^{n,r+1}$, by $\hat{\mathcal{Q}}_j^{n,r+1}$, within all generalized heat fluxes at other quadrature points are estimating at the known iteration in the iterative process (2.5) (same iteration number that the one used to solve non-linearities). $\hat{\mathcal{Q}}_j^{n,r+1}$ are now

defined using

$$\begin{aligned}
&\hat{\mathcal{Q}}_j^{n+\tau,r+1} - \varepsilon^2 \hat{\mu}_j^{n+\tau,r} \nabla_X \left(\nu_j^{n+\tau,r} \nabla_X \cdot \hat{\mathcal{Q}}_j^{n+\tau,r+1} \right) - \frac{2}{3} \tilde{\kappa}_j^{n+\tau,r} \tau h_t \nabla_X \left(\frac{1}{\rho} \nabla_X \cdot \omega_j \hat{\mathcal{Q}}_j^{n+\tau,r+1} \right) \\
&\quad = \frac{\varepsilon^2 \hat{\mu}_j^{n+\tau,r}}{\tau h_t} \hat{\mathcal{Q}}_j^n - \tilde{\kappa}_j^{n,r} \nabla_X \left(\hat{\theta}^n + \tau h_t S^{n,n+1} \right) + \frac{2}{3} \tilde{\kappa}_j^{n+\tau,r} \tau h_t \nabla_X \left(\frac{1}{\rho} \nabla_X \cdot \sum_{\substack{l=1 \\ l \neq j}}^{g} \omega_l \hat{\mathcal{Q}}_l^{n+\tau,r} \right) \\
&\qquad - \frac{\varepsilon^2 \tilde{\mu}_j^{n+\tau,r} \eta_j^{n+\tau,r}}{\sum_{l=1}^{g} \left[\dfrac{\omega_l \tilde{\mu}_l^{n+\tau,r} \eta_l^{n+\tau,r}}{\xi_l} \right]} \sum_{\substack{l=1 \\ l \neq j}}^{g} \left[\frac{\omega_l \tilde{\mu}_l^{n+\tau,r}}{\xi_l} \left(\frac{\hat{\mathcal{Q}}_l^n}{\tau h_t} + \nabla_X \left(\nu_l^{n+\tau,r} \nabla_X \cdot \left(\hat{\mathcal{Q}}_l^{n+\tau,r} \right) \right) \right) \right]
\end{aligned} \tag{5.2}$$

where we have set

$$\hat{\mu}_j^{n,r} = \left(1 - \frac{\dfrac{\omega_j \tilde{\mu}_j^{n,r} \eta_j^{n,r}}{\xi_j}}{\sum_{l=1}^{g} \left[\dfrac{\omega_l \tilde{\mu}_l^{n,r} \eta_l^{n,r}}{\xi_l} \right]} \right) \tilde{\mu}_j^{n,r}.$$

The differential operators in (5.2) have the same structure than the differential operators in (2.5). Finally, we write the numerical scheme following the discretization introduced in (IV.2.1). We write

$$\begin{aligned}
&\hat{\mathcal{Q}}_{j,f}^{n+\tau,r+1} - \varepsilon^2 \hat{\mu}_{j,f}^{n+\tau,r} \nabla_{T_f} \left[\frac{\nu_j^{n+\tau,r}}{|\mathscr{C}|} \sum_{f^\star \in \mathbb{F}_{\mathscr{C}}} \hat{\mathcal{Q}}_{j,f^\star}^{n+\tau,r+1} \cdot N_{\mathscr{C}_k}^{f^\star} \right] - \frac{2}{3} \omega_j \tilde{\kappa}_{j,f}^{n+\tau,r} \tau h_t \nabla_{T_f} \left[\frac{1}{\rho |\mathscr{C}|} \sum_{f^\star \in \mathbb{F}_{\mathscr{C}}} \hat{\mathcal{Q}}_{j,f^\star}^{n+\tau,r+1} \cdot N_{\mathscr{C}_k}^{f^\star} \right] \\
&\quad = \frac{\varepsilon^2 \hat{\mu}_{j,f}^{n+\tau,r}}{\tau h_t} \hat{\mathcal{Q}}_{j,f}^n - \tilde{\kappa}_{j,f}^{n+\tau,r} \nabla_{T_f} \left[\hat{\theta}^n + \tau h_t S_k^{n,n+1} \right] + \frac{2}{3} \tilde{\kappa}_{j,f}^{n+\tau,r} \tau h_t \nabla_{T_f} \left[\frac{1}{\rho |\mathscr{C}|} \sum_{f^\star \in \mathbb{F}_{\mathscr{C}}} \sum_{\substack{l=1 \\ l \neq j}}^{g} \omega_l \hat{\mathcal{Q}}_{l,f^\star}^{n+\tau,r} \cdot N_{\mathscr{C}_k}^{f^\star} \right] \\
&\qquad - \frac{\varepsilon^2 \tilde{\mu}_{j,f}^{n+\tau,r} \eta_{j,f}^{n+\tau,r}}{\sum_{l=1}^{g} \left[\dfrac{\omega_l \tilde{\mu}_{l,f}^{n+\tau,r} \eta_{l,f}^{n+\tau,r}}{\xi_l} \right]} \sum_{\substack{l=1 \\ l \neq j}}^{g} \left[\frac{\omega_l \tilde{\mu}_{l,f}^{n+\tau,r}}{\xi_l} \left(\frac{\hat{\mathcal{Q}}_l^n}{\tau h_t} + \nabla_{T_f} \left[\frac{\nu_j^{n+\tau,r}}{|\mathscr{C}|} \sum_{f^\star \in \mathbb{F}_{\mathscr{C}}} \hat{\mathcal{Q}}_{j,f^\star}^{n+\tau,r} \cdot N_{\mathscr{C}_k}^{f^\star} \right] \right) \right] \\
&\hat{\theta}_k^{n+\tau,r+1} = \hat{\theta}_k^n + \tau h_t S_k^{n,n+1} - \frac{2\tau h_t}{3\rho_k |\mathscr{C}_k|} \sum_{f \in \mathbb{F}_{\mathscr{C}_k}} \sum_{j=1}^{g} \omega_j \hat{\mathcal{Q}}_{j,f}^{n+\tau,r+1} \cdot N_{\mathscr{C}_k}^f,
\end{aligned} \tag{5.3}$$

with $\hat{\theta}_k^n$ an approximation of $\frac{1}{|\mathscr{C}_k|} \int_{\mathscr{C}_k} \hat{\theta}^n \, \mathrm{d}X$, $\hat{\mathcal{Q}}_{j,f}^{n+\tau,r}$ an approximation of $\frac{1}{|f|} \int_f \hat{\mathcal{Q}}_j^{n+\tau,r} \, \mathrm{d}\sigma$ and

$$\hat{\mu}_{j,f}^{n,r} = \left(1 - \frac{\dfrac{\omega_j \tilde{\mu}_{j,f}^{n,r} \eta_{j,f}^{n,r}}{\xi_j}}{\sum_{l=1}^{g} \left[\dfrac{\omega_l \tilde{\mu}_{l,f}^{n,r} \eta_{l,f}^{n,r}}{\xi_l} \right]} \right) \tilde{\mu}_{j,f}^{n,r}.$$

In summary, we replace (2.15) which requires, at each iteration of fixed point, to solve implicitly one system of $g+1$ unknowns (generalized heat fluxes plus field perturbation) at each face of the control volume by (5.3) where we have to solve implicitly g (approximated generalized heat fluxes (5.2)) equations at each face of the control volume. In (5.3), the size and the stencil of the linear systems do not depend of the number of points in the energy discretization. In addition, since the computation of the heat fluxes (5.2)

are totally independent, the method can be easily parallelized, the resolution using as many processors as the number of points in the energy discretization. Note that this strategy can be used in combination with the domain decomposition approach presented in IV.3.2, using at least one processor for the sub-domain Ω_{SH} and as many processors as the number of the energy discretization for the sub-domain Ω_{SHG}.
However, the method has some drawbacks. In particular, now the constraint (2.4) is not exactly satisfied at each iteration, even though it holds at convergence of the iterative process.

Conclusion

This paper is concerned with non-local versions of heat transfer equations arising in plasma physics. The heat flux is obtained by solving a coupled system of parabolic-like equations, constrained by a condition of vanishing current. The model we investigate generalizes the Schurtz-Nicolaï system, which is quite popular in the ICF community. In this paper, we have introduced a Vertex-Based finite volume scheme for solving the generalized non-local Spitzer-Härm equations on multidimensional unstructured grids. Numerical experiments validate the accuracy and the asymptotic consistency of the scheme, and demonstrate the possible occurrence of anti-diffusive effects. We also discuss adaptations of the method that are relevant from a practical viewpoint.

Acknowledgements. This work is partly supported by CEA/DAM. We are gratefully indebted to J.-F. Clouet and D. Deck for many fruitful discussions and their constant encouragements.

Bibliography

[1] Amestoy, P., Duff, I., and L'Excellent, J.-Y. MUMPS MUltifrontal Massively Parallel Solver version 2.0. Tech. rep., CERFACS, 1998.

[2] Andreianov, B., Boyer, F., and Hubert, F. Discrete duality finite volume schemes for Leray-Lions type elliptic problems on general 2D meshes. *Numerical Methods for PDEs 23* (2007), 145–195.

[3] Calgaro, C., Creusé, E., and Goudon, T. An Hybrid Finite Volume - Finite Element method for Variable Density Incompressible Flows. *J. Comput. Phys. 227* (2008), 4671–4696.

[4] Coudière, Y., and Hubert, F. A 3D discrete duality finite volume method for nonlinear elliptic equation. *SIAM J. Sci. Comp.* (2010).

[5] Epperlein, E. M., and Short, R. A practical nonlocal model for electron heat transport in laser plasmas. *Phys. Fluids B 3* (1991), 3092–3098.

[6] Evans, B., Hassan, O., Jones, J., Morgan, K., and Remaki, L. Simulating Steady State and Transient Aerodynamic Flows Using Unstructured Meshes and Parallel Computers. *Computational Fluid Dynamic Review 2010* (2010), 1–27.

[7] Goudon, T., and Parisot, M. On the Spitzer-Härm regime and Non-Local Approximations: modeling, analysis and numerical simulations. *SIAM Multiscale Model. Simul. 9* (2011), 568–600.

[8] Goudon, T., and Parisot, M. Non-Local Macroscopic Models based on Gaussian Closures for the Spitzer-Härm Regime. *AIMS' Journals* (2012). to appear.

[9] Hildebrandt, A., Blossey, R., Rjasanow, S., Kohlbacher, O., and Lenhof, H.-P. Novel formulation of nonlocal electrostatics. *Physical Review Letters 93* (2004). article 108104.

[10] Hildebrandt, A., Blossey, R., Rjasanow, S., Kohlbacher, O., and Lenhof, H.-P. Electrostatic potentials of proteins in water: a structured continuum approach. *Bioinformatics 23* (2007), e99–e103.

[11] Luciani, J.-F., and Mora, P. Resummation methods of the Chapman-Enskog Expansion for a Strongly Inhomogeneous Plasma. *J. Stat. Phys. 43* (1986), 281–302.

[12] Luciani, J.-F., and Mora, P. Nonlocal electron transport in laser created plasmas. *Laser Part. Beams 12* (1994), 387–400.

[13] Luciani, J.-F., Mora, P., and Pellat, R. Quasistatic heat front and delocalized heat flux. *Phys. Fluids 28* (1985), 835–845.

[14] Luciani, J.-F., Mora, P., and Virmont, J. Nonlocal Heat Transport Due to Steep Temperature Gradients. *Phys. Rev. Lett. 51* (1983), 1664–1667.

[15] Nicolaï, P., Feugeas, J.-L., and Schurtz, G. A practical nonlocal model for heat transport in magnetized laser plasmas. *Phys. Plasmas 13* (2006), 032701+13.

[16] Schurtz, G. P., Nicolaï, P., and Busquet, M. A nonlocal electron conduction model for multidimensional radiation hydrodynamics codes. *Phys. Plasmas 7* (2000), 4238–4250.

[17] Spitzer, L., and Härm, R. Transport phenomena in a completely ionized gas. *Phys. Rev. 89* (1953), 977–981.

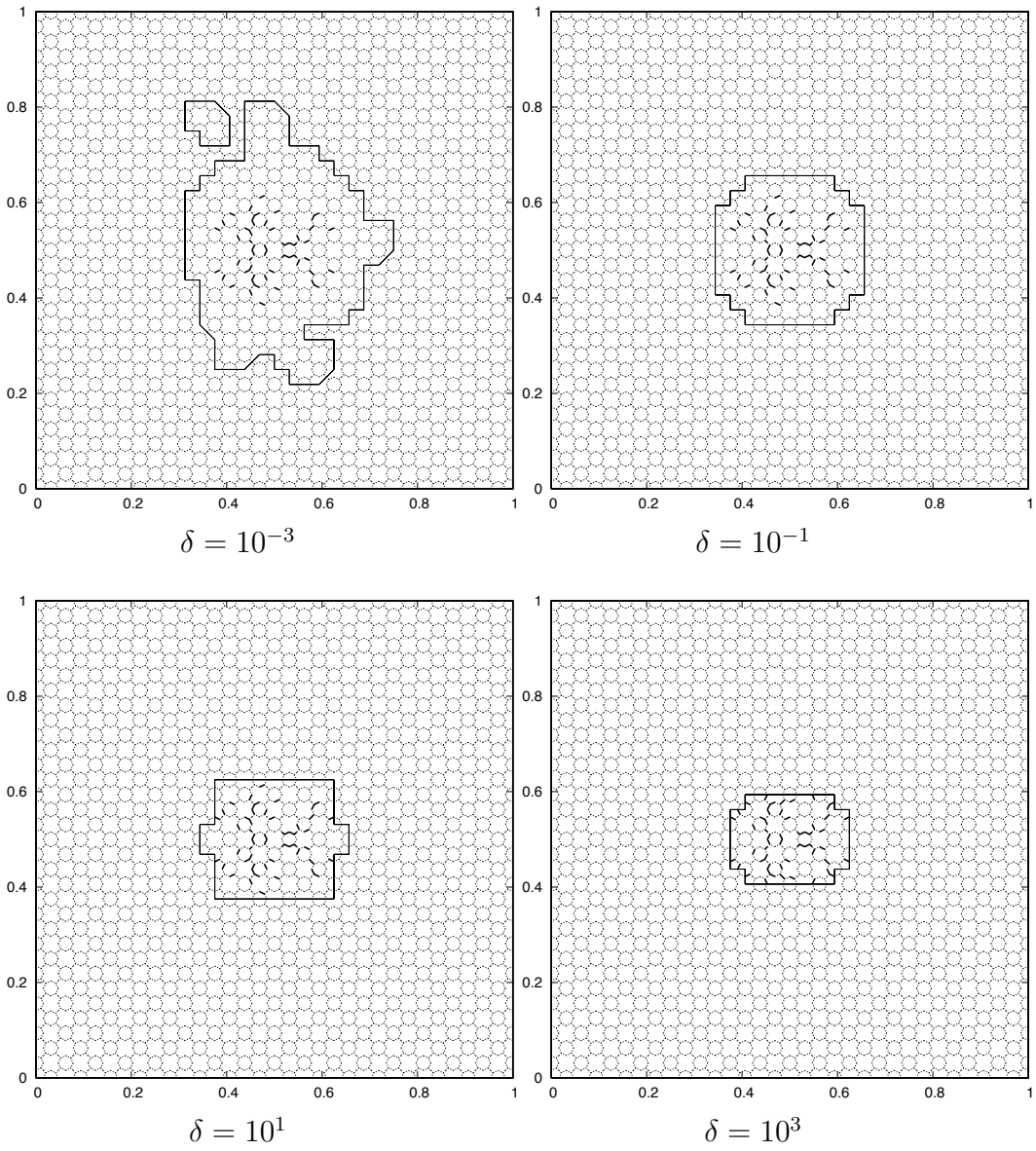

Figure IV.10: Product $\langle Q_f; \nabla_t \theta \rangle$ defined by (4.5) and sub-domains interface for several value of δ. Dotted lines are faces with product $\langle Q_f; \nabla_t \theta \rangle$ negative, thick plain lines are faces with product $\langle Q_f; \nabla_t \theta \rangle$ positive and thin plain lines are sub-domains interface.

Chapitre V :

Hybrid Model for the coupling of an Asymptotic Preserving Scheme with the Asymptotic Limit Model: the one dimension case

Résumé : Dans cet article, une stratégie est étudiée pour le couplage spatial d'un schéma préservant l'asymptotique avec le modèle limite asymptotique, associé à un problème elliptique, singulièrement perturbé et fortement anisotrope. Cette stratégie de couplage semble être très avantageuse du point de vue numérique par rapport au modèle de perturbation singulière initiale ou comparé au schéma préservant l'asymptotique dans le domaine complet introduit dans des travaux antérieurs. Le modèle abordé dans ce document est bien adapté pour la simulation d'un plasma en présence d'un champ magnétique dont l'intensité peut varier considérablement dans le domaine de la simulation.

Abstract: In this paper a strategy is investigated for the spatial coupling of an asymptotic preserving scheme with the asymptotic limit model, associated to a singularly perturbed, highly anisotropic, elliptic problem. This coupling strategy appears to be very advantageous as compared with the numerical discretization of the initial singular perturbation model or the purely asymptotic preserving scheme introduced in previous works. The model problem addressed in this paper is well suited for the simulation of a plasma in the presence of a magnetic eld, whose intensity may vary considerably within the simulation domain.

Note: Ce chapitre à donné lieu a un proceeding dans *ESAIM: proceedings* en collaboration avec Pierre Degond, Fabrice Deluzet, Dario Maldarella, Jacek Narski et Claudia Negulescu.

V.1 Introduction

This paper is devoted to the development of an efficient numerical method for strongly magnetized plasmas, such as the ones occurring in a tokamak. Due to the large magnetic field, the medium is highly anisotropic, and numerous models require the resolution of an anisotropic elliptic equation (see [2, 6]). In this framework, the anisotropy ratio is related to the reciprocal of the dimensionless cyclotron frequency. The model problem addressed in the present paper is for example well suited for the investigation of the Euler-Lorentz system in the drift limit (see [2, 6]), the computation of the momentum component aligned with the magnetic field requiring the resolution of an anisotropic elliptic equation, in which the dominant part of the operator is supplemented with either Neumann or Periodic boundary conditions. The purpose is then to develop a numerical scheme to compute accurately and rapidly the solution of this anisotropic elliptic problem for considerably varying anisotropy values. Indeed, the anisotropy is assumed large in some sub-regions of the simulation domain, elsewhere of magnitude one. The final goal is to propose a coupling strategy between an Asymptotic-Preserving reformulation of the initial problem, used in the regions where the anisotropy is not too large, and the limit model for very large anisotropies. This Limit model is obtained from the AP-formulation by letting the anisotropic parameter, defined as the reciprocal of the anisotropy ratio, tend to zero.
The paper is then organized as follows. The singularly perturbed model problem is stated in section V.2 for a simplified one dimensional configuration. An Asymptotic Preserving (AP) reformulation, introduced in a previous work (see [3, 5]), is then detailed. This AP-method combines a discretization of the singular perturbation problem for intermediate values of the anisotropy and a discretization of the limit problem for vanishing anisotropic parameter, being thus accurate independently on the intensity of the anisotropy. Note that these Asymptotic Preserving techniques have been first introduced in [7]. The coupling strategy with the Limit model is then addressed in section V.3 and detailed for both the singular perturbation problem and the AP-method. Finally the numerical schemes are briefly presented and first numerical experiments are discussed in section V.4. The coupling strategy for the general multidimensional problem, as well as the detailed mathematical and numerical analysis, shall be the objective of the forthcoming work [4].

V.2 The one dimensional model problem and its Asymptotic Preserving formulation

V.2.1 The singular perturbation problem

The aim of this paper is the study of the following one-dimensional model problem. Let $\Omega_z = [-1, 1]$ be the computational domain, z being the space variable. The singular

perturbation problem (P-model) reads then

$$(P)\begin{cases} -\partial_z\left(\dfrac{1}{\varepsilon(z)}\partial_z u_\varepsilon\right)+u_\varepsilon=f, & z\in\Omega_z \\ \dfrac{1}{\varepsilon(1)}\partial_z u_\varepsilon(1)=g^+, & \dfrac{1}{\varepsilon(-1)}\partial_z u_\varepsilon(-1)=g^-, \end{cases} \tag{2.1}$$

where $u_\varepsilon:\Omega_z\to\mathbb{R}$ is the unknown of the problem and ε is a given regular and positive function with large variations on the computational domain. In the rest of this document, the system (2.1) will be referred to as the Singular Perturbation model (P-model), its weak formulation is precised by

Theorem V.2.1 *Let $f\in L^2(\Omega_z)$ and $\varepsilon\in L^\infty(\Omega_z)$ such that $0<\varepsilon(z)<1$ for almost all $z\in\Omega_z$. Then there exist a unique solution $u_\varepsilon\in H^1(\Omega_z)$ of the P-model, verifying the weak form*

$$(P)\quad \int_{\Omega_z}\varepsilon^{-1}\partial_z u_\varepsilon\partial_z\psi\mathrm{d}z+\int_{\Omega_z}u_\varepsilon\psi\mathrm{d}z=\int_{\Omega_z}f\psi\mathrm{d}z+g^+\psi(1)-g^-\psi(-1),\qquad\forall\psi\in H^1(\Omega_z). \tag{2.2}$$

Note that a straight discretization of the system (2.2) for $0<\varepsilon\ll 1$ produces a linear system with a large conditioning number. Indeed, assuming formally $\varepsilon=0$ in the whole domain, system (2.1) leads to

$$\begin{cases} \partial^2_{zz}u=0, & \text{in } \Omega_z, \\ \partial_z u=0, & \text{in } \partial\Omega_z. \end{cases} \tag{2.3}$$

This system has an infinite amount of solutions since it is verified by all the constants. For this reason the discretized system (2.1) is expected to have a conditioning number that blows up with vanishing values of ε. To circumvent this difficulty an asymptotic preserving scheme has been introduced in [3, 5]. The guidelines for the construction of this AP-scheme are briefly sketched here, and we refer to the above articles for the full details.

V.2.2 Asymptotic preserving reformulation of the problem

The AP-scheme is obtained by reformulating the system (2.1) in such a manner, that the limit $\varepsilon\to 0$ becomes regular. It relies on a decomposition of the solution into its mean part corrected by a fluctuation as defined by

$$u_\varepsilon=\bar{u}_\varepsilon+u'_\varepsilon,\qquad \bar{u}_\varepsilon=\frac{1}{L_z}\int_{\Omega_z}u_\varepsilon\mathrm{d}z,\qquad L_z=mes(\Omega_z).$$

The fluctuating part of the solution has a zero mean value, a fundamental property for the AP-scheme. Integrating now (2.1) along the anisotropy direction gives an equation for the mean part, for all ε-values :

$$\bar{u}_\varepsilon=\bar{f}+\frac{g^+-g^-}{L_z}. \tag{2.4}$$

The equation verified by the fluctuating component can be obtained by taking the difference of equations (2.1) and (2.4), leading to

$$\begin{cases} -\partial_z\left(\varepsilon^{-1}\partial_z u'_\varepsilon\right) + u'_\varepsilon = f' - \dfrac{g^+ - g^-}{L_z}, & \text{in } \Omega_z, \\ \varepsilon^{-1}(1)\,\partial_z u'_\varepsilon(1) = g^+, \qquad \varepsilon^{-1}(-1)\,\partial_z u'_\varepsilon(-1) = g^-, \\ \displaystyle\int_{\Omega_z} u'_\varepsilon \mathrm{d}z = 0. \end{cases} \tag{2.5}$$

This system has a unique solution for all values of ε. The AP-method is composed of equations (2.4) and (2.5), providing respectively the mean and the fluctuating parts of the solution. A Lagrangian multiplier is introduced in the weak formulation of the AP-formulation, in order to cope with the constraint $\bar{u}' = 0$.

Theorem V.2.2 *There exist a unique solution* $(u'_\varepsilon, \bar{u}_\varepsilon, \lambda) \in H^1(\Omega_z) \times \mathbb{R} \times \mathbb{R}$ *of the Asymptotic Preserving reformulation (AP-model)*

$$\bar{u}_\varepsilon = \frac{1}{L_z}\int_{\Omega_z} f \mathrm{d}z + \frac{g^+ - g^-}{L_z}, \tag{2.6a}$$

$$\begin{cases} \displaystyle\int_{\Omega_z} \varepsilon^{-1}\partial_z u'_\varepsilon \partial_z \psi \mathrm{d}z + \int_{\Omega_z} u'_\varepsilon \psi \mathrm{d}z = \\ \qquad\qquad \displaystyle\int_{\Omega_z}\left(f' - \frac{g^+ - g^-}{L_z}\right)\psi \mathrm{d}z + g^+\psi(1) - g^-\psi(-1), \qquad \forall \psi \in H^1(\Omega_z) \\ \displaystyle\int_{\Omega_z} u'_\varepsilon \mathrm{d}z = 0. \end{cases} \tag{2.6b}$$

Moreover, $u_\varepsilon := \bar{u}_\varepsilon + u'_\varepsilon$ *is the unique solution of the (P)-problem* (2.1) *and* $\lambda = 0$.

The results of this section are obvious implications of the results obtained in [3, 5].

V.3 The coupling strategy

Let us now assume that the anisotropy function is very small in one sub-domain and of magnitude one in the rest of the domain. The aim shall be to couple two different models, associated with the two sub-regions, the coupling strategy being based on Dirichlet-to-Neumann interface conditions. Let for this $\Omega_z = \Omega_z^+ \cup \Omega_z^-$ with $\Omega_z^- = [-1, 0]$, $\Omega_z^+ = [0, 1]$, $L_z^- = mes(\Omega_z^-)$, $L_z^+ = mes(\Omega_z^+)$ and let the function ε verify $\varepsilon(z) = \delta\chi(z), \forall z \in \Omega_z^-$ with $0 < \delta \ll 1$ and $0 < \chi(z) < 1, \forall z \in \Omega_z^-$. For simplicity reasons, we shall omit here the ε index of the solution u_ε of the (P)-model, but shall denote it by u^+ in Ω_z^+ resp. u^- in Ω_z^-. The P-problem can thus be rewritten in Ω_z^- as

$$\begin{cases} -\partial_z\left(\chi^{-1}\partial_z u^-\right) + \delta u^- = \delta f, \qquad z \in \Omega_z^-, \\ \chi^{-1}(-1)\,\partial_z u^-(-1) = \delta g^-. \end{cases}$$

The limit regime in the sub-domain Ω_z^- can be investigated by letting $\delta \to 0$, which yields $\partial_z u^-(-1) = 0$ in Ω_z^-. The solution u^- in this limit regime is constant and totally determined by its value at the interface $z = 0$,

$$u^-(z) = u^-(0), \qquad \forall z \in \Omega_z^-. \tag{3.1}$$

This is the big advantage of the coupling strategy : the solution in the small ε-region does not depend on the coordinate aligned with the anisotropy. Its computation is then provided by a simplified system of equations as compared to the original problem, leading thus to considerable gain in simulation time.
A boundary condition at the sub-domain interface has to be provided for the computation of the solution in Ω_z^+, ensuring by this mean the coupling of the two models. In this aim the equation (2.1) is integrated on Ω_z^- giving, thanks to property (3.1)

$$L_z^- u^-(0) - \varepsilon^{-1}(0)\,\partial_z u^-(0) = \int_{\Omega_z^-} f(z)\,\mathrm{d}z - g^-.$$

Due to continuity arguments, the computation of the solution in Ω_z^+ is then approximated by the following problem

$$(P-L)\begin{cases} -\partial_z\left(\varepsilon^{-1}\partial_z u^-\right) + u^- = f, & z \in \Omega_z^+, \\ \varepsilon^{-1}(1)\,\partial_z u^+(1) = g^+, & \\ -\varepsilon^{-1}(0)\,\partial_z u^-(0) + L_z^- u^-(0) = \displaystyle\int_{\Omega_z^-} f(z)\,\mathrm{d}z - g^-, & \end{cases} \tag{3.2}$$

with $u^-(z) = u^+(0)$ in Ω_z^-. The weak formulation of the coupled P-L model (P-model coupled to the Limit model) is given by : Find $(u^+, u^-) \in H^1(\Omega_z^+) \times H^1(\Omega_z^-)$, such that

$$\begin{aligned} \int_{\Omega_z^+} \varepsilon^{-1}\partial_z u^+ \partial_z \phi \mathrm{d}z + \int_{\Omega_z^+} u^+\phi \mathrm{d}z &= \int_{\Omega_z^+} f\phi \mathrm{d}z + g^+\phi(1) \\ &- L_z^- u^-(0)\,\phi(0) + \left(\int_{\Omega_z^-} f(z)\,\mathrm{d}z - g^-\right)\phi(0), \qquad \forall \phi \in H^1(\Omega_z^+) \end{aligned} \tag{3.3a}$$

$$u^-(z) = u^+(0), \qquad \forall \phi \in H^1(\Omega_z^-) \tag{3.3b}$$

Comparable computations allow the derivation of the coupling strategy for the AP-formulation with the Limit-model. First, as a consequence of the property (3.1), we have $u^{-'}(z) = u^{+'}(0), z \in \Omega_z^-$. The zero mean property of the fluctuation can then be transformed into :

$$\int_{\Omega_z^+} u^{+'}(z)\,\mathrm{d}z = -L_z^- u^{+'},$$

Finally the AP-formulation coupled to the limit system reads :

$$(AP-L)\begin{cases} -\partial_z\left(\varepsilon^{-1}\partial_z u^{+'}\right) + u^{+'} = f' - \dfrac{g^+ - g_-}{L_z}, & \text{in } \Omega_z^+, \\ \varepsilon^{-1}(1)\,\partial_z u^{+'}(1) = g^+, & \\ L_z^- u^{+'}(0) - \varepsilon^{-1}(0)\,\partial_z u^{+'}(0) = \displaystyle\int_{\Omega_z^-} f'\mathrm{d}z - \frac{L_z^-}{L_z}\left(g^+ - g^-\right) - g^-, & \\ \displaystyle\int_{\Omega_z^+} u^{+'}(z)\,\mathrm{d}z = -L_z^- u^{+'}(0), & \end{cases}$$

where $u^{-'}(z) = u^{+'}(0), \forall z \in \Omega_z^-$ and $\bar{u}$ is computed thanks to equation (2.4). The weak formulation of this system is given by : Find $\left(u^{+'}, u^{-'}, \bar{u}, \lambda\right) \in H^1(\Omega_z^+) \times H^1(\Omega_z^-) \times \mathbb{R} \times \mathbb{R}$ solution of the AP-L model (AP formulation coupled to the Limit model)

$$\bar{u} = \frac{1}{L_z}\int_{\Omega_z} f\mathrm{d}z + \frac{g^+ - g^-}{L_z}, \tag{3.4a}$$

$$\begin{cases} \displaystyle\int_{\Omega_z^+} \varepsilon^{-1}\partial_z u^{+'}\partial_z\phi \mathrm{d}z + \int_{\Omega_z^+} u^{+'}\phi \mathrm{d}z + \lambda\int_{\Omega_z^+}\phi \mathrm{d}z = \int_{\Omega_z^+} f'\phi \mathrm{d}z - \frac{g^+ - g^-}{L_z}\int_{\Omega_z^+}\phi \mathrm{d}z \\ + g^+\phi(1) + \left(\displaystyle\int_{\Omega_z^-} f'\phi \mathrm{d}z - \frac{L_z^-}{L_z}\left(g^+ - g^-\right) - g^- - L_z u^{+'}(0)\right)\phi(0), \qquad \forall\phi \in H^1\left(\Omega_z^+\right), \\ \displaystyle\int_{\Omega_z^+} u^{+'}\mathrm{d}z = -L_z^- u^{+'}(0), \end{cases} \tag{3.4b}$$

$$u^{-'}(z) = u^{+'}(0), \qquad \forall z \in \Omega_z^- \tag{3.4c}$$

V.4 Numerical methods and experiments

A discretization based on the finite element method is briefly sketched, before presenting the results of some numerical computations.
The domain Ω_z is descretized via a cartesian mesh defined by $(z_i)_{i\in[\![-N,N]\!]}$, where N is the number of unknowns in half of the computational domain. The weak formulations associated to the P-model (2.2) and its AP-formulation (2.6) as well as the coupled P-L model (3.3) and the coupled AP-L formulation (3.4) are discretized using the classical $\mathbb{P}_1$ finite element approximation. Two types of quadrature formulae are used for the integral approximations : Newton-Côtes with 1 to 5 points and Legendre-Gauss with 2 to 5 points. The linear systems obtained after discretization are solved thanks to the same direct method (MUMPS [1]).
To study the numerical results obtained via the presented four methods, an analytical solution is constructed, defined by

$$u(z) = 10 + \varepsilon(z)\cos(\pi z), \qquad z \in \Omega_z. \tag{4.1}$$

This function verifies the boundary conditions. The anisotropy function ε is given by

$$\varepsilon(z) = \varepsilon_0 \exp(p(z-1)), \qquad z \in \Omega_z, \tag{4.2}$$

where p and ε_0 are two real parameters, the former being a positive value providing the variations of ε, the latter representing the maximal value of ε_0 in the domain. This expression of the function ε allows to address large variations of the anisotropy.
The first simulation is run for a uniform anisotropy $\varepsilon(z) = \varepsilon_0, (p = 0)$. The L^2-error, computed between the exact analytic solution (4.1) and the four numerical solutions is displayed on figure V.1(a), as a function of ε_0. The discretized P-model is observed to produce accurate approximations for large and intermediate ε_0 values, but the error rapidly increases for values smaller than 10^{-5}. This feature has already been mentioned in precedent works [3, 5]. It can be explained by the conditioning of the discretized P-model which blows up with vanishing ε_0. The AP-formulation produces comparable accurate approximations as the P-model, on the range of large ε_0-values. However, the accuracy of the AP-scheme is preserved on the whole range of ε_0-values, and decreases even linearly until a plateau is reached for $\varepsilon_0 \sim 10^{-10}$. Below this value the error remains constant for smaller anisotropies. The approximation error for the AP scheme can be decomposed in two parts : the error approximation for the mean and the fluctuating parts of the solution. The mean part computation accuracy is only explained by the quadrature formula used to approximate the mean part of f. This error is related to h_z^m and will be denoted as $\mathcal{O}(h_z^m)$, where h_z is the mesh interval and m is a positive integer.

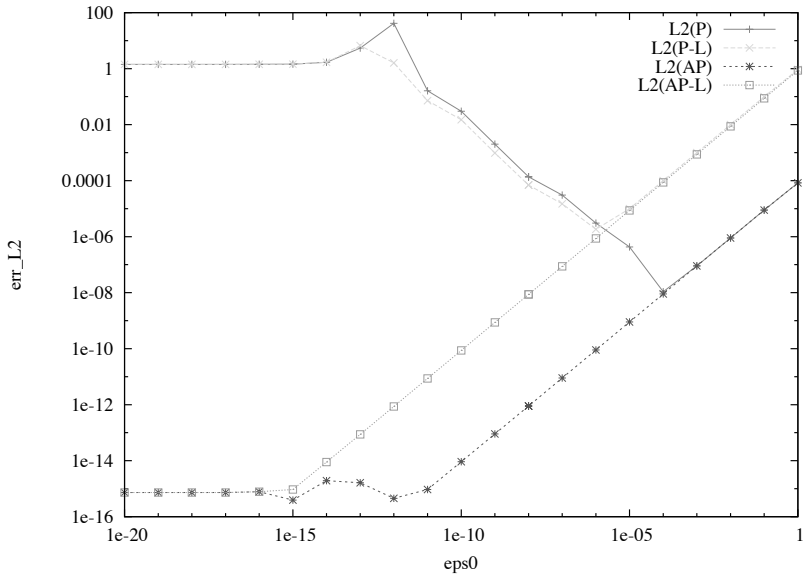

(a) Error in L^2-norm, as a function of ε_0 for $p = 0$ (in log-scales)

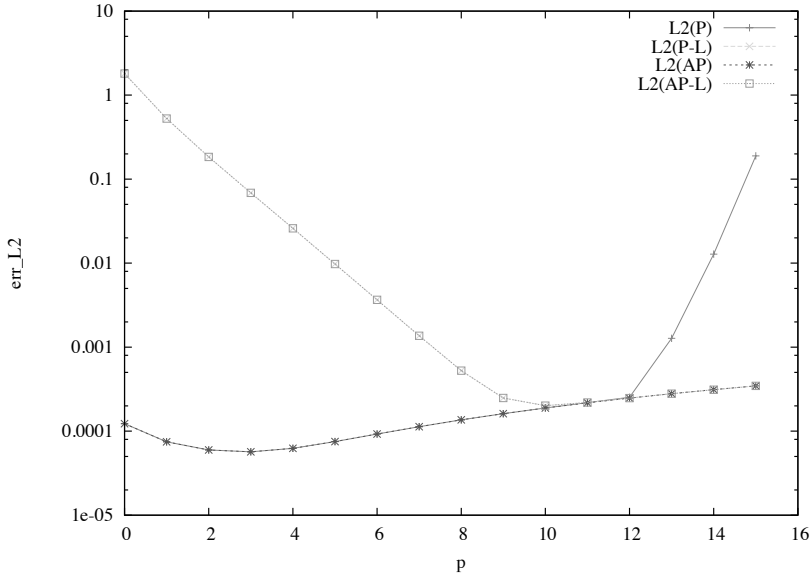

(b) Error in L^2-norm, as a function of p for $\varepsilon_0 = 1$ (in log-scales)

Figure V.1: Relative error L^2-norm for an anisotropy $\varepsilon(z) = \varepsilon_0 \exp(p(z-1))$ between the exact solution and the numerical approximations. Four approaches are compared (P), resp. (AP) : Perturbation model, resp. Asymptotic Preserving formulation, on the whole domain, (P-L) resp. (AP-L) : the singular Perturbation model, resp. the Asymptotic Preserving formulation, on the right half space coupled with the limit model on the left half space (AP-L). The computations are carried out on a mesh with 200 cells.

For the fluctuating part, a differential equation is solved with a $\mathbb{P}_1$ finite element scheme, providing an approximation precise up to $\mathcal{O}(h_z^2)$ if the error is measured with the L^2-

norm. More precisely, the fluctuating part of the solution scaling as ε_0, the approximation error of the numerical scheme is comparable to $\varepsilon_0\mathcal{O}\left(h_z^2\right)$. For the AP-scheme the global error can then be defined as $\varepsilon_0\mathcal{O}\left(h_z^2\right) + \mathcal{O}\left(h_z^m\right)$. For the numerical experiments carried out here, the quadrature formulae provide an estimation of the integral terms with a precision much higher than the second order ($m > 2$). This explains the AP-scheme total error linear decrease with vanishing ε_0, for large and intermediate ε_0-values. In this range of ε_0-values, the global error is totally dominated by the fluctuating part approximation error ($\varepsilon_0\mathcal{O}\left(h_z^2\right)$). For the smallest ε_0-values, the global error is dominated by the error approximation of the mean part and remains constant independently of the ε_0-values, explaining the plateau observed on figure V.1(a) for $\varepsilon_0 < 10^{-10}$. The analysis is quite the same for the AP-L scheme, but in this case an error due to the model has also to be taken into account. Indeed in one sub-domain, the fluctuating part of the solution is dropped, which translates into an error proportional to ε_0. The total error for the AP-L scheme is thus given by $\mathcal{O}\left(h_z^m\right) + \varepsilon_0\mathcal{O}\left(h_z^2\right) + \varepsilon_0$. The mesh interval h_z being small compared to 1, the total error is totally dominated by ε_0 for the largest values of the anisotropy range. A linear decrease of the error, with vanishing ε_0, is thus also observed, until the contribution of the term $\mathcal{O}\left(h_z^m\right)$ becomes signficant. The efficiency of the coupling strategy is demonstrated by these first experiments. Indeed, for small values of ε_0 the AP-scheme coupled with the limit model produces very accurate results for the solution. Not surprisingly, for intermediate and large values of ε_0 the precision of this approximation is poor compared with that of the AP-formulation used on the whole simulation domain, since it is computed with an approximated limit model on half of the computational domain. Note that the advantage of the coupling strategy consists of a signficant computational time gain, since, in the limit regime, the solution has one degree of freedom less. However, this coupling strategy is expected to be efficient in cofigurations where the anisotropy ratio is large in one part of the simulation domain, while being small in the other. Finally a second simulation is carried out with a non uniform anisotropy. The error as a function of the parameter p is displayed on figure V.1(b). These simulations are performed with $\varepsilon_0 = 1$. The approximations computed thanks to either the (P-L) or the (AP-L) formulations are accurate for the largest p-values. For small values of this parameter, the anisotropy variations are not large enough to obtain small ε in the sub-domain where the limit problem is used. This explains the poor quality of the approximations for vanishing values of p. The singular perturbation problem is observed to suffer from a signficant lack of accuracy for large variations of the anisotropy. Note that the coupling strategy allows to fix this issue, since the (P-L) approximation is accurate for the largest value of the parameter. Finally the AP-scheme furnish accurate computations on the whole range of p values, its accuracy being comparable to the singular perturbation model for moderate anisotropies while being comparable to the hybrid model on the other part of the p-values range. All this should be investigated further in the forthcoming work [4].

V.5 Conclusion and perspectives

The results presented in this work concern a coupling strategy between an Asymptotic-Preserving reformulation of a Singular Perturbation problem, with the associated Asymptotic Limit model. The coupling is performed via Dirichlet-to-Neumann interface condi-

tions. The aim is to accelerate the resolution of a highly anisotropic elliptic equation, as compared to the entirely AP-resolution introduced in previous works. The first numerical results are presented in a simplfied 1D cofiguration. The detailed study (mathematical and numerical) of a general 3D framework will be the objective of the future work [4].

Bibliography

[1] Amestoy, P., Duff, I., and L'Excellent, J.-Y. MUMPS MUltifrontal Massively Parallel Solver version 2.0. Tech. rep., CERFACS, 1998.

[2] Brull, S., Degond, P., and Deluzet, F. Degenerate anisotropic elliptic problems and magnetized plasma simulations. *Commun. Comput. Phys.* (2011). to appear.

[3] Degond, P., Deluzet, F., Lozinski, A., Narski, J., and Negulescu, C. Duality based Asymptotic-Preserving Method for highly anisotropic diffusion equations. *Commun. Math. Sci.* (2011). to appear.

[4] Degond, P., Deluzet, F., Narski, J., Negulescu, C., Maldarella, D., and Parisot, M. Hybrid Model for the Coupling of an Asymptotic Preserving Scheme with the Asymptotic Limit Model. in preparation.

[5] Degond, P., Deluzet, F., and Negulescu, C. An Asymptotic Preserving scheme for strongly anisotropic elliptic problems. *SIAM Multiscale Model. Simul. 8* (2010), 645–666.

[6] Degond, P., Deluzet, F., Sangam, A., and Vignal, M.-H. An asymptotic preserving scheme for the Euler equations in a strong magnetic field. *J. Comput. Phys. 228* (2009), 3540–3558.

[7] Jin, S. Efficient Asymptotic-Preserving (AP) Schemes For Some Multiscale Kinetic Equations. *SIAM J. Sci. Comp. 21* (1999), 441–454.

Chapitre VI :

Conclusion générale

La modélisation du transport des électrons peut se faire à plusieurs échelles, premettant soit de tenir compte d'effets à très petite échelle, soit de simuler le comportement moyen d'un plasma d'électrons sur des échelles de temps comparables à celles des expérimentations physiques. Dans ce travail de thèse, nous apportons une première réponse à la simulation numérique en régime intermédiaire, c'est-à-dire permettant de réaliser des simulations à des échelles de temps relativement importantes, tout en tenant compte de certains effets cinétiques. L'ensemble des aspects nécessaire à l'établissement de simulations fiables et pratiques est abordé depuis l'établissement des équations modélisant le système, jusqu'à sa résolution au moyen d'outils informatiques en passant par une étude des propriétés de la solution. Nous rappellons ici les principaux résultats énoncés dans ce manuscript puis nous finirons par proposer quelques perspectives qui pourraient être étudiées par la suite sur ce sujet.

Apports de la thèse

Une première étape de l'étude a consisté à établir pour une classe relativement large d'opérateurs de collisions que le régime de Spitzer-Härm peut être obtenu à partir des équations de Vlasov-Fokker-Plank-Maxwell à l'aide d'un développement de Hilbert. L'expression du coefficient de diffusion est établie de manière implicite en fonction de l'opérateur de collisions.

Le principal apport de ce travail est l'établissement d'une hiérarchie de modèle découlant les uns des autres à partir des équations de Vlasov-Fokker-Plank-Maxwell jusqu'aux équations de Spitzer-Härm. Ces modèles établis à l'aide d'une méthode inspirée des travaux de Levermore tiennent notamment compte de la contrainte de courant nul, négligée dans la plupart des modèles intermédiaires proposés jusqu'alors. Le modèle le plus remarquable modélise l'évolution de la température électronique à l'aide de deux équations : la conservation de l'énergie d'une part, et une équation d'évolution non-locale du flux thermique généralisé; fonction du temps, de la position et de l'énergie interne locale. Un terme de correction du champ moyen, pouvant être comparé à une méthode de Lagrangien augmenté, permet d'assurer au système la contrainte de courant nul. L'expression des coefficients de ce modèle est donnée par une formule implicite en fonction de l'opérateur de collisions, et une expression plus pratique

est proposée à partir d'un opérateur de collisions généralisant l'opérateur de BGK.

L'analyse mathématique du modèle ainsi mis en équations semblait difficile de part la nature intégro-différentielle et non-linéaire du système. Nous nous sommes alors intéressés aux propriétés de modèles similaires dans leurs structures mais dont certains termes ont été simplifiés.

Le modèle de Schurtz et Nicolaï peut être interprété comme une simplification du modèle de Spitzer-Härm généralisé dans le cas d'un flux thermique stationnaire. Ce modèle présente un principe du maximum et est entropique.

Un second modèle est étudié à partir d'une simplification de l'opérateur de collisions du modèle de Spitzer-Härm généralisé. Dans le cas 1D, linéaire et en négligeant la correction du champ moyen, nous énonçons dans ce travail un théorème d'existence et d'unicité. Le principal avantage de la démonstration est qu'elle ne nécessite pas que les coefficients de diffusion thermique soient tous positifs. Dans le cas contraire, il ne serait pas possible d'assurer la contrainte de courant nul.

Le dernier point de la thèse porte sur la mise en place de méthodes numériques performantes permettant de simuler le comportement d'un plasma mis dans les conditions relatives à la dérivation du modèle. Ce travail a été réalisé en gardant en vue la partie industrielle du projet.

Un premier schéma basé sur l'approche des différences finies ne permettait pas de satisfaire toutes les contraintes de la simulation de plasmas réalistes. Cependant, cette étape a permis de valider la discrétisation en temps et de mettre en avant que certaines propriétés obtenues au niveau continu sont préservées au niveau discret, notamment la stabilité et la dissipation d'entropie. Le principe du maximum pour le modèle de Schurtz-Nicolaï est également préservé sous une condition originale sur le pas de temps.

Pour les besoins des applications multiphysiques, un schéma d'ordre deux sur des maillages non structurés basé sur les volumes finis est également mis en place. Ce schéma permet de prendre en compte des opérateurs de délocalisation relativement généraux. L'avantage majeur de ce modèle est d'être consistant avec un modèle classique permettant de résoudre les équations du régime asymptotique de Spitzer-Härm.

Le schéma ainsi obtenu reste relativement complexe autant en nombre d'inconnues qu'en structure du système à résoudre. Dans un premier temps une stratégie de couplage spatial entre le schéma et le régime asymptotique de Spitzer-Härm est mise en place permettant de réduire efficacement la taille et la complexité du système. Enfin une stratégie de découplage des groupes d'énergie est proposée en appliquant aux équations semi-discrétisées en temps une méthode de Jacobi.

Perspectives

Nous présentons maintenant quelques pistes de réflexion nous paraissant intéressantes pour la suite de l'étude.

La modélisation du transport électronique est la principale œuvre à retenir de ce travail. Cependant quelques points peuvent encore être étudiés. En particulier, l'étude ne traite pas ici les différents types de conditions limites. En effet, la traduction de con-

ditions limites cinétiques sur les variables hydrodynamiques sont en général un véritable enjeu et nécessite une étude à part entière.

La dérivation repose en grande partie sur l'hypothèse de courant nul. Cette hypothèse ne reflète pas un comportement réaliste du plasma. Elle pourrait être levée en supposant une distribution ionique donnée, pas nécessairement froide, et en conservant l'hypothèse de neutralité électrique. Le modèle ainsi étudié serait posé sur la totalité des inconnues hydrodynamiques, à savoir la densité de particule et la quantité de mouvement des ions ainsi que la température électronique.

De plus, le modèle de Spitzer-Härm généralisé présente un certain nombre de paramètres; fonction de la densité, de la température (certainement de la quantité de mouvement) et de l'énergie interne. L'expression de ces coefficients n'est établie que de manière implicite ou pour un opérateur de collisions peu réaliste. La dérivation d'un modèle similaire à partir d'un opérateur de collisions plus réaliste (type Boltzmann ou Landau) semble peu accessible. Cependant une étude paramètrique à partir de cas tests significatifs en prenant comme référence les résultats d'un code cinétique pourrait permettre d'expliciter les coefficients.

Pour valider le modèle dont la dérivation n'est que formelle, il faudrait écrire une estimation d'erreur entre la solution du modèle de Vlasov-Fokker-Plank-Maxwell et le modèle de Spitzer-Härm généralisé dans le cadre de la dérivation. Une erreur d'ordre du carré du libre parcours moyen est attendue et permettrait de conclure sur la fiabilité du modèle pour décrire un écoulement d'électrons.

En ce qui concerne l'étude mathématique du modèle, l'essentiel du travail reste à faire. En effet le théorème d'existence énoncé ne porte que sur un modèle excessivement simplifié. Une analyse dans le cadre multi-dimensionnel et non-linéaire est encore à réaliser. De plus, la démonstration est très calculatoire et pose problème dans le cas de l'opérateur de délocalisation complet (estimation d'un déterminant d'une matrice pleine). Enfin la contrainte de courant nul devrait être prise en compte ajoutant une condition de type Lagrangien augmenté.

Un autre point, plus original et certainement très intéressant du point de vue physique serait de montrer pour un certain type de conditions initiales qu'un principe du maximum sur la température électronique peut être formulé pour le modèle de Spitzer-Härm généralisé. En effet on ne peut pas espérer que ce principe soit vérifié pour toutes conditions initiales, puisque le flux thermique initial influence fortement la solution dans les premiers instants. Cependant, ce principe est vérifié par le modèle de Schurtz et Nicolaï qui néglige l'influence du flux initial. On peut donc espérer que pour un flux thermique initial "cohérent" avec le profil de température initial, le principe du maximum se vérifie.

Résumé : Ce travail est consacré à l'étude d'un problème issu de la physique des plasmas : le transfert thermique des électrons dans un plasma proche de léquilibre Maxwellien.

Dans un premier temps, le régime asymptotique de Spitzer-Härm est étudié. Un modèle proposé par Schurtz et Nicolaï est situé dans le contexte des limites hydrodynamiques hors du cadre strictement asymptotique et analysé. Le lien avec les modèles non-locaux de Luciani et Mora est établi, ainsi que des propriétés mathématiques comme le principe du maximum et la dissipation d'entropie.

Ensuite, une dérivation formelle à partir des équations de Vlasov est proposée. Une hiérarchie de modèles intermédiaires entre les équations cinétiques et la limite hydrodynamique est décrite. Notamment, un nouveau système hydrodynamique, de nature intégro-différentielle, est proposé. Le système de Schurtz et Nicolaï apparaît comme une simplification du système issu de la dérivation. L'existence et l'unicité de la solution du système non stationnaire sont établies dans un cadre simplifié.

La dernière partie est consacrée à la mise en oeuvre d'un schéma numérique spécifique pour résoudre ces modèles. On propose une approche par volumes finis pouvant être efficace sur des maillages non-structurés. La précision de ce schéma permet de capturer des effets spécifiques de nature cinétique, qui ne peuvent être reproduits par le modèle asymptotique de Spitzer-Härm. La consistance de ce schéma avec celui de l'équation de Spitzer-Härm est mise en évidence, ouvrant la voie à des stratégies de couplage entre les deux modélisations.

Mots-clé : Physique des plasmas, Équations cinétiques, Limite hydrodynamique, Régime de Spitzer-Härm, Modèles non-locaux, Schémas volumes finis, Maillages non structurés.

Abstract : This work is devoted to the study of a problem resulting from plasma physics: heat transfer of electrons in a plasma close to Maxwellian equilibrium.

Firstly, the asymptotic regime of Spitzer-Harm is studied. A model proposed by Schurtz and Nicolai is analyzed and located in the context of hydrodynamic limits outside of the strictly asymptotic. The link to non-local models of Luciani and Mora is established, as well as the mathematical properties such as the principle of maximum and entropy dissipation.

Then, a formal derivation from the Vlasov equations is proposed. A hierarchy of intermediate models between the kinetic equations and the hydrodynamic limit is described. In particular, a new system hydrodynamics, integro-differential in nature, is proposed. The system Schurtz and Nicolai appears as a simplification of the system resulting from the diversion. The existence and uniqueness of the solution of the nonstationary system are established in a simplified framework.

The last part is devoted to the implementation of a specific numerical scheme for solving these models. We propose a finite volume approach can be effective on unstructured grids. The accuracy of this scheme to capture specific effects such as kinetic, which may not be reproduced by the asymptotic Spitzer-Harm model. The consistency of this pattern with that of the Spitzer-Harm equation is highlighted, paving the way for a strategy of coupling between the two models.

Key-words: Plasma physics, Kinetic equations, Hydrodynamic limit, Spitzer-Härm Regime, Non-local models, Finite volume scheme, Unstructured grids.